An Attempt to Date Fluid Inclusions in Quartz:

Implications for the $^{40}Ar/^{39}Ar$ Method

Sarah A. W. Lundberg

Department of Earth and Environmental Science

New Mexico Institute of Mining and Technology

Socorro, New Mexico

Submitted in partial fulfillment of the requirements for the degree of

Master of Science in Geochemistry

May, 1999

ACKNOWLEDGEMENTS

I would like to thank my advisor Dr. Andrew Campbell for his patience and most of all perseverance. I would also like to thank the rest of my committee Dr. Nelia Dunbar, Dr. Matthew Heizler and Dr. William McIntosh. I am truly appreciative of their time and effort, in brainstorming sessions and for going above and beyond the call of duty, both with committee meetings and revisions.

The Department of Earth and Environmental Science, the Minority fellowship from the office of the graduate dean, The Bureau of Mines and Mineral Resources, specifically the microprobe lab and the New Mexico Geochronology Research Laboratory have provided support, in the form of teaching assistantships and research assistantships during the course of my study, which is very much appreciated.

This work was partially funded through National Science Foundation grant EAR-9526642 to Dr. Andrew Campbell, Dr. Matthew Heizler and Dr. Nelia Dunbar.

Kingsley Burlinson was kind enough to run two samples in his decrepitometry laboratory, which resulted in the decrepigrams shown in Figure 19

I would also like to thank Rich Esser and Lisa Peters for all their assistance in the Argon Lab, and with my countless computer problems.

Dr. William Wilson served as a consultant on the argon properties of steel, chrome plating, and 3-D plane fitting.

Additional thank yous go to all my family and friends, especially Shari Bauman and Erik Munroe, who helped me find a needle in a haystack.

A special thanks to my husband Stephen, who taught me to rise and shine, and most of all to laugh at myself.

Finally, this work is dedicated to my dad, without whom I never would have found my song bird in winter.

You gain strength, courage, and confidence
by every experience in which you really stop
to look fear in the face.
You must do the thing which
you think you cannot do.

-Eleanor Roosevelt

TABLE OF CONTENTS

TABLE OF CONTENTS con.

LIST OF FIGURES

LIST OF TABLES

LIST OF APPENDICES

This thesis is accepted on behalf of the faculty

of the Institute by the following committee

Andrew Campbell

Advisor

Willis C. McCutchen

Nelia W. Dunbar

June 14 1999

Date

I release this document to the New Mexico Institute of Mining and Technology.

Sarah Lundberg 6-14-99

Student's Signature Date

ABSTRACT

The primary aim of this work was to investigate the possibility of dating fluid inclusions in quartz veins from the Capitan Pluton, south-central New Mexico with the $^{40}Ar/^{39}Ar$ method. Because quartz is such an abundant vein mineral, the ability to use the $^{40}Ar/^{39}Ar$ method to date quartz would allow a wide range of ore deposit systems to be dated. Vein quartz from Capitan is considered to be deposited from primary magmatic waters and is cogenetic with vein adularia, which provides a tight constraint on the age of the quartz veins. The fluid inclusion populations are exceptionally well-characterized. The inclusions have been shown to be remarkably abundant, highly saline, and relatively large. Samples of different grain sizes from several prospect pits were analyzed using furnace, laser and in vacuo crushing as argon extraction methods. $^{40}Ar/^{39}Ar$ age spectra from vein adularia show argon loss profiles. The plateau ages obtained from the adularia range from 25.80 ± 0.22 to 31.60 ± 2.00 Ma, which agree well with the known age of the pluton. Ages determined from $^{40}Ar/^{39}Ar$ analysis of quartz exhibit a wide range of behavior. In addition to anomalous old ages typical of samples containing excess ^{40}Ar ($^{40}Ar_E$), anomalously young ages were observed in 7 samples. The young ages were measured at the high temperature degassing steps, which implies they are a result of material contained within the quartz, rather than some form of contamination. *In vacuo* crushing of the quartz released up to 83% of the ^{39}Ar. A substantial part of the $^{40}Ar_E$ was removed, but some remained in the samples after crushing. The remaining $^{40}Ar_E$ in the samples, measured by post *in vacuo* crush step-heating, resulted in ages older than the emplacement age of the pluton. The $^{40}Ar_E$ appears to be distributed throughout the quartz, not associated with one phase in particular and was very difficult to quantify. As

a result of the distribution of the $^{40}Ar_E$, the quartz yielded releatively high precision plateau ages in the high temperature steps, which are as old as 81.7 ± 4.1 Ma. The Cl/K ratios measured during $^{40}Ar/^{39}Ar$ analysis are remarkably homogeneous and agree well with the results from crush-leach analysis, obtained for the vein quartz (Campbell et al., 1995) which implies that the bulk quartz, as opposed to sylvite or feldspar is being measured during $^{40}Ar/^{39}Ar$ analysis. Quartz was thought to be a neutral substrate, which would not contribute to the argon budget of the inclusions. This was not the case. The quartz was found to be heterogeneous on the micron level, containing many small solid inclusions of salts and other K-bearing phases. Complexity of K and Ar distribution in the quartz prohibits reliable dating of the fluid inclusions in Capitan quartz.

1. INTRODUCTION

Understanding the timing of ore deposition is critical to understanding ore genesis. This basic knowledge would enable many advances in our ability to produce models for mineral exploration. Unfortunately, very few analytical methods allow direct determination of mineral deposition age. Historically, ages have been estimated using the fundamental concepts of cross cutting relationships and stratigraphic superposition. Radioisotope methods of dating have become increasingly useful, although some minerals that are spatially related to ore deposits can be radioisotopically dated, most are not necessarily temporally related to the formation of the ore. For example K-feldspars formed during potassic alteration can be dated using the $^{40}Ar/^{39}Ar$ system, but may pre-date the ore. In addition to the fundamental problem that the dateable mineral may not be the same age as the related ore, radioisotopic systems typically suffer from low abundance of the parent isotope and/or incomplete knowledge of the concentrations of initial isotopes. For example, the $^{40}Ar/^{39}Ar$ isotopic system typically has an initial atmospheric ratio of $^{40}Ar/^{36}Ar$ equal to 295.5. However, in some cases there is a significantly higher amount of trapped ^{40}Ar than is associated with atmosphere. This additional component is referred to as excess ^{40}Ar ($^{40}Ar_E$). Unless the excess component can be quantitatively removed, the apparent age of the sample will be older than the true age of the deposit.

In some cases ore minerals themselves can be successfully dated using radioisotopic techniques, although these methods have not been commonly applied. Exceptions include sphalerites from Mississippi Valley Type (MVT) deposits, which

have been dated using the Rb-Sr method (Brannon et al., 1991; Nakai et al., 1993). Sm-Nd has also been used to directly date fluorites in MVT deposits (Chesley et al., 1994; Chesley et al., 1991). Additionally, molybdenite has a significantly high concentration of Re which can be used to date deposits using the Re-Os method, unless hydrothermal alteration has disturbed the system (McCandless et al., 1993). Pb ages have been calculated for galena but have been found to be incorrect (Gulson and Porritt, 1987; Jones et al., 1977). Pb has also been used to date cassiterite (Gulson, 1992),

The ideal solution to the problem of dating ore deposits would be to find a datable mineral that is present in many different types of deposits and is cogenetic with ore deposition. Quartz is very common in mineralization assemblages and is typically deposited penecontemporaneously with the ore. Unfortunately, quartz has very low concentrations of any radioactive isotope than can be detected by known analytical methods. However, fluid inclusions within the quartz can contain significant amounts of K, and may provide a means of dating the deposition of quartz using the $^{40}Ar/^{39}Ar$ method. Therefore, the ability to date fluid inclusions in quartz would be valuable to the understanding of the timing of ore deposition. Other attempts to date fluid inclusions have been made using Rb-Sr methods (Petke and Diamond, 1996; Shepherd and Darbyshire, 1981), but typically fluid inclusions do not have large enough concentrations of these elements to make use of this method.

Fluid inclusions in ore deposits contain valuable information about composition of fluids, and temperatures and pressures of formation of host minerals. Observational non-destructive methods, such as measuring homogenization and freezing temperatures, allow information to be obtained about the chemical and physical conditions at the time

of formation of the fluid inclusions. Additionally, destructive methods such as crushing or decrepitation for chemical analysis, or stable isotope analysis can provide supplementary information about the composition and source of the fluid. Analyzing the radioactive isotopes in the fluid to obtain the dates of formation is a natural extension of these destructive methods. This information could provide another piece to the picture of how the deposits formed.

This work describes an attempt to use the $^{40}Ar/^{39}Ar$ method to date fluid inclusions in quartz. ^{40}K present in fluid inclusions as sylvite daughter minerals and ions dissolved in the inclusion fluid will decay over time to ^{40}Ar. To maximize the argon signal and provide concentrations of argon isotopes above initial levels, fluid inclusions should be old, large, abundant, and have high salinity and high K/Na ratios. The host quartz should also be free of contaminating K-rich phases, to ensure that the only source of argon is the fluid inclusions. This is essential because, even in the ideal situations, the amount of argon measured from fluid inclusions is small; and even sub-micron K-rich phases in the quartz could swamp the fluid inclusion argon signal. To optimize these conditions the quartz used in this study is from the Capitan pluton, south-central New Mexico. Capitan vein quartz is known for its large, abundant, high salinity fluid inclusions. The populations of fluid inclusions present, their source, and the microthermometry have been described in detail (Campbell et al., 1995). Because of the thorough characterization of the deposit and the ideal nature of the inclusions, these samples should provide unique insight into the argon systematics, and allow investigation of the prospects of $^{40}Ar/^{39}Ar$ dating fluid inclusions in quartz. Capitan was also chosen

because the veins have abundant cogenetic adularia, which has been used to determine the age of the vein quartz.

To further the goal of using exceptionally well characterized pure samples, doubly polished chips were analyzed by electron microprobe to identify and characterize any sources of contamination, such as adhered adularia or Fe-stained weathered areas. K-bearing phases contained within the quartz lattice, such as adularia, sylvite, or K-glass, were also found and characterized to determine any potential effects they might have on the age results. A variety of heating and crushing experiments on multiple size fractions of quartz, and multiple splits of the same sample were used to understand how reproducible the results would be on samples from other locations where less was known about the samples.

2. PREVIOUS WORK

Rama and Hart (1965) first suggested that ^{40}Ar in fluid inclusions, produced by radioactive decay of ^{40}K, could provide the absolute timing of formation of mineral deposits. Many attempts to date fluid inclusions in quartz using $^{40}Ar/^{39}Ar$ have been made since (Kelley et al., 1986; Turner and Bannon, 1988; Turner, 1988; Turrin et al., 1988; Turner and Bannon, 1992; Qiu, 1996) but have met with limited or no success. Even though certain dates appear to be correct, or at least approach the known age of the deposit, the samples contained other minerals in addition to quartz. Kelley et al. (1986), Turner and Bannon (1988), and Turner et al. (1988), Turner and Bannon (1992) Qiu (1996), were probably all dating minerals included in the quartz, such as mica and/or trace amounts of K-bearing minerals, possibly feldspar, and not the fluid inclusions within the quartz.

In addition to problems with contaminating minerals, large amounts $^{40}Ar_E$ associated with fluids both in quartz and feldspar continue to cause difficulty (Rama and Hart, 1965; Kelley et al., 1986; Turner et al., 1988; Turner and Bannon, 1992; Turner and Wang, 1992; Harrison et al., 1993, 1994; Qiu, 1996). $^{40}Ar_E$ prohibits reliable dating because the radiogenic portion of ^{40}Ar ($^{40}Ar^*$) cannot be calculated. $^{40}Ar_E$ must be liberated from the fluid inclusions prior to analysis, or must be quantifiable. Previous $^{40}Ar/^{39}Ar$ studies have suggested $^{40}Ar_E$ may be directly proportional to the amount of Cl in the sample (Harrison et al., 1993, 1994; Kelley et al., 1986; Qiu, 1996; Turner and Bannon, 1992; Turner and Wang, 1992; Turner et al., 1988). Turner et al. (1988, 1992) and Kelly et al. (1986) have made extensive use of three-dimensional diagrams, known as

CAKE diagrams (Cl, Atmospheric, Potassium K, Excess) to understand the argon budget contained within the fluid inclusion bearing samples. The CAKE diagram attempts to show relationships among the Cl correlated component of ^{40}Ar, the radiogenic K-correlated component, and the atmospheric component; all of which contribute to the measured concentration of ^{40}Ar in the analyzed sample. Turner et al. (1988, 1992) and Kelly et al. (1986) subsequently used the intercepts of the various axis in the same way they are used in 2-D isotope correlation diagrams to identify the non-radiogenic portion of the ^{40}Ar, and to determine information about the source of the fluid. Harrison et al. (1993) found a method to quantify and remove Cl-correlated excess Ar in K-feldspars. They used two successive heating steps at the same temperature, called isothermal duplicate heating steps, to separate the Cl-correlated component of the ^{40}Ar from the $^{40}Ar^*$. Their studies showed the potential of physically separating $^{40}Ar_E$ from $^{40}Ar^*$ or correcting for $^{40}Ar_E$ by correlation techniques. Thus our initial hypothesis was that $^{40}Ar_E$ could be released by crushing the quartz *in vacuo*, separated by using isothermal duplicates, or correlated to chlorine in the sample, and thus be quantifiable.

3. GEOLOGY AND MINERALIZATION

The Capitan pluton is the largest of several Tertiary igneous complexes in south-central New Mexico. The shallowly emplaced pluton was formed during a single intrusive event and shows evidence of fractional crystallization (Allen and McLemore, 1991). A biotite K-Ar age of 26.5 Ma, has been reported for the pluton (Allen, 1988). More recently, Campbell et al. (1994) dated both K-feldspar and adularia using $^{40}Ar/^{39}Ar$, and determined an age of 28.3 ± 0.1 Ma. This date was interpreted to approximate the age of the Capitan pluton.

Mineralized quartz veins were formed from hydrous fluids, exsolved from the magma, which were injected into fractured or brecciated zones in the outer carapace of the pluton (Dunbar et al., 1996; Phillips, 1990; Phillips et al., 1991). The veins, which range in size from millimeters to meters in width and are up to 300 m in length, contain quartz, adularia, and minor amounts of allanite, hematite, titanite and thorite, in addition to fluorite and calcite in some of the prospects (Phillips, 1990). The vein quartz and adularia samples used in this study were obtained from mine and prospect pits within the pluton. Figure 1 is a map of Capitan pluton showing sample locations. Hydrogen and oxygen stable isotope values obtained from fluid inclusions within vein quartz suggest that the fluids are magmatic (Campbell et al., 1995).

Fluid inclusions from Capitan quartz are remarkably abundant and relatively large. Several fluid inclusion types are present, but over 90% of the inclusions in these quartz samples are type 1 inclusions. Type 1 inclusions are high salinity inclusions containing liquid, vapor and several daughter minerals. Temperature of homogenization,

bulk salinity and the number of measurements for type 1 fluid inclusions in quartz (Campbell et al., 1995) are given in Table 1. Fluid inclusion salinity for the various prospects, along with the K, Na, and Cl concentrations from crush-leach analysis and the bulk Cl/K are given in Table 2.

The high temperature of homogenization and high salinity, stable isotope data and the occurrence of veins within the pluton all suggest that the mineralization formed from magmatic fluids as the Capitan granite was cooling. This information is important to this study because in combination with the ages obtained from the pluton adularia may provide an absolute age for the veins. The high salinity, abundance and large size of the inclusions provide a significant source of K in the quartz. In this study, bulk extraction methods were used. All of the fluid inclusions in a given quartz grain were analyzed. If multiple generations of fluid inclusions were present, and those generations had multiple ages, we would not obtain geologically relevant ages for both populations. Instead, one homogenized age would be obtained. Because the fluid inclusions from Capitan are > 90% type 1 inclusions, we were able to use bulk sampling methods such as step heating and crushing.

Table 1. Microthermometry data from Capitan type 1 fluid inclusions

T_h (°C)[1]	Bulk Salinity[2]	K/Na Ratios[2]	Number of Measurements
398-600	65.8-83.6	0.16-0.32	280

1 Homogenization of Type 1 inclusions in quartz by halite dissolution.
2 As determined by halite and sylvite dissolution temperatures.
Notes: Data from Campbell et al. (1995)

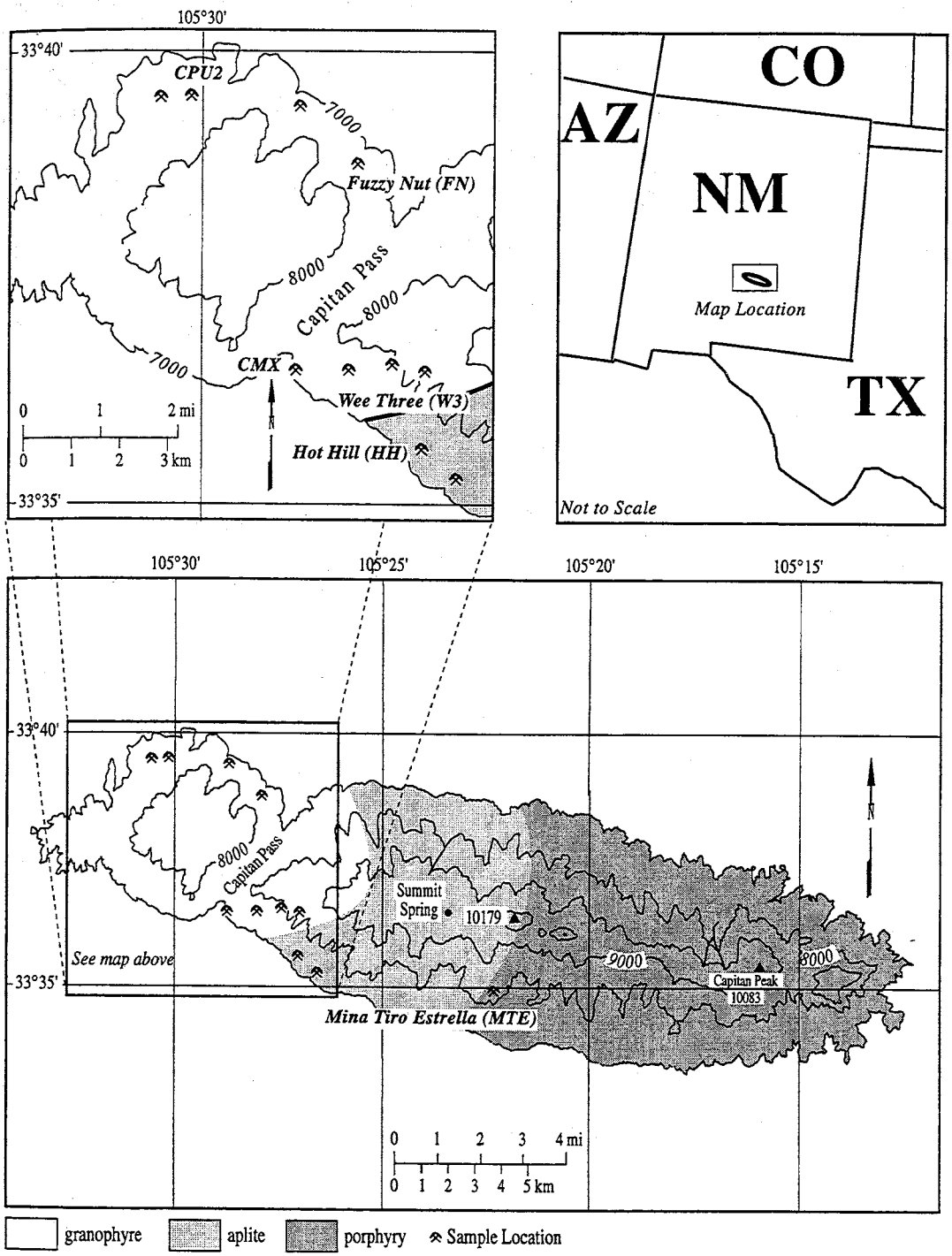

Figure 1 Map of Capitan pluton, showing sample locations. Modified from Dunbar et al. (1996).

Table 2. Salinity, Na, K, and Cl concentrations and Cl/K ratios from crush leach analysis of Capitan quartz.

Sample	MTE	W3	CPU	CMX	FN
Salinity wt % NaCl + KCl	78.5± 4.8	74.4± 2.2	N/A[2]	78.2±2.8	73.9±3.1
Na ppm.[1]	178632	199935	182438	195717	173686
K ppm[1]	74868	71017	61409	65409	68902
Cl ppm[1]	429504	443416	398937	425248	402066
Cl/K	5.74	6.24	6.5	6.54	5.84

1 Selected element from reconstructed fluid inclusion composition from crush leach data

2 N/A = not analyzed

Notes: Charge balance for all elements originally analyzed MTE = 1.04, W3 = 1.03, CPU = 1.05, CMX = 1.02, FN = 1.03 Data from Campbell et al. (1995)

4. EXPERIMENTAL METHODS

4.1. Argon Sample Preparation

Quartz samples were prepared for argon analysis in two ways. The first method was used to obtain high purity bulk quartz grain separates and the second method to prepare polished chips with a high density of fluid inclusions. In the first method, quartz was separated from the vein using a hammer and chisel to remove the outermost tips of the drusey quartz in the veins. The base of the quartz crystals were typically adhered to vein adularia or the pluton wall. Vein adularia was avoided to achieve the high purity of quartz required to ensure that only inclusions bearing quartz, was being analyzed. The grains were sieved to size. Multiple size splits of the same sample were prepared to determine what effects, if any, grain size had on the results. Single grains that weighed from 5-200 mg were prepared. Additionally, some grains were crushed to a fine powder and two sizes were analyzed, (< 53μm, and 53-63μm) to determine the effects of breaking the inclusions prior to irradiation. Because of the large number of splits and sample types, the sample size, irradiation and the method of analysis are summarized in Table 3. After the initial $^{40}Ar/^{39}Ar$ results were obtained from these samples it was established that the number of inclusions in the quartz was highly variable and decreased close to the tip of the quartz. Since most of the quartz was initially obtained from the tips of crystals, we hoped to increase the density of inclusions by sampling the quartz closer to the base. The increased density of inclusions should yield a higher argon signal because the amount of K and Cl in the quartz would be substantially higher. Doubly

polished chips were prepared to allow observation electron microprobe analysis of the inclusions and prior to $^{40}Ar/^{39}Ar$ analysis.

Several splits of six samples (MTE, CMX2, W3-3, HH, FN, and CPU2) were prepared for $^{40}Ar/^{39}Ar$ analysis using the first method to obtain bulk grain separates. Samples were initially prepared with light crushing, and sieving. Pure quartz grains were hand-picked from crushed vein material. The adularia and quartz grains were very similar in appearance due to the cloudy nature of the quartz, and the small size of the grains used. The quartz grain separates were washed in distilled water and dried in a low-temperature (<100° C) oven. Acetone, other solvents, and acids were avoided to minimize the effect of any unknown precipitant that could contaminate the quartz.

Separation of quartz from adularia was accomplished using magnetic separation. The dielectric nature of quartz proved to be an excellent property to facilitate quartz/feldspar separation. The two channel tray of a Franz magnetic separator was angled, < 5°, slightly inclined toward the magnet. Small grains of quartz (14 - 30 mesh) were loaded in the high channel, away from the magnet. Relatively high currents in the magnet repelled the quartz keeping it in the high channel. Feldspars, which are only very weakly attracted to the magnet, dropped into the low channel.

Following magnetic separation and hand-picking, the grains were examined using a binocular microscope to eliminate grains that contained adhered adularia or surface iron contamination. Multiple grain sizes were prepared including large, approximately 150 mg pieces, small grains of approximately 5 mg, and fine grained crushed splits of 63 μm - 53 μm, and less than 53 μm. The two splits smaller than 63 μm were obtained using an agate mortar and pestle to crush larger grains and subsequently were dry sieved to the

appropriate size. Because static electricity caused the particles to stick together the reported grain sizes are approximate.

As will be shown in the argon results section (5.2), many of the results using grains prepared by the first method had low Ar signal sizes and did not yield the expected Cl/K ratios. This was thought to be a result of low fluid inclusion density and contamination by micron sized solid inclusions of K-bearing phases. Thus, the sample number was reduced to three (CMX, MTE, W3) and the second method (polished sections) was used to further constrain variables such as fluid inclusion density and the presence of small solid inclusions in the quartz. Billets were cut from hand samples of the vein quartz, using a slow speed fluid inclusion saw. Water was used as much as possible instead of oil as a sawing and polishing lubricant to reduce hydrocarbon contamination. The chips were carefully examined to determine the relative amount of several variables and photographed prior to analysis. The results of these examinations are detailed in Section 5.1. The chips were examined with a microscope to select areas that contained a high density of fluid inclusions. The electron microprobe was used to further examine the chips for adhered adularia and for included K-bearing phases.

Adularia samples were obtained from the same veins as the quartz. They were chipped from the vein with a hammer and chisel. Approximately 15 mg samples of the largest grains present were chosen by hand picking. Hand-picking also helped to eliminate grains that were obviously weathered, or stained with iron, although in some cases iron staining was unavoidable. The adularia grains were milky white, peach, or pink in color. MTEADL was the purest sample with large euhedral white to pink grains. FNADL and HHADL were the most Fe stained. Less material was available from FN

and HH prospects, because the veins were smaller than the other locations. The adularia grain separates were washed in distilled water and dried in a low temperature (<100° C) oven.

Table 3 Summary of sample type and method of analysis.

Sample	Irradiation	Weight[3]	Material	Method	Cl/K
CPU<5353	53-TB[1]	~200	Crushed prior to irradiation	Step heat	0.09
CPU>5353	53-TB[1]	~50	Crushed prior to irradiation	Step heat	0.10
MTE<5353	53-TB[1]	~200	Crushed prior to irradiation	Step heat	0.20
MTE>5353	53-TB[1]	~200	Crushed prior to irradiation	Step heat	0.53
MTEE53	53-TB[1]	179.6	Single large grain	Step heat	6.5
MTELF1	53-TB[1]	5.8	Single small grain	Laser Fusion	25.6
MTELF2	53-TB[1]	5.1	Single small grain	Laser Fusion	20.9
MTELF3	53-TB[1]	6.1	Single small grain	Laser Fusion	11.5
MTELF4	53-TB[1]	6.1	Single small grain	Laser Fusion	12.6
MTELF5	53-TB[1]	4.6	Single small grain	Laser Fusion	10.1
MTELF6	53-TB[1]	7.1	Single small grain	Laser Fusion	7.8
MTELF7	53-TB[1]	5.0	Single small grain	Laser Fusion	9.0
MTELF8	53-TB[1]	5.4	Single small grain	Laser Fusion	13.8
MTELF9	53-TB[1]	5.1	Single small grain	Laser Fusion	8.2
MTELF10	53-TB[1]	4.8	Single small grain	Laser Fusion	6.7
MTELF11	53-TB[1]	4.7	Single small grain	Laser Fusion	6.6
MTELF12	53-TB[1]	5.5	Single small grain	Laser Fusion	5.6
MTELF13	53-TB[1]	4.4	Single small grain	Laser Fusion	6.8
MTELF14	53-TB[1]	5.6	Single small grain	Laser Fusion	28.9
MTELF15	53-TB[1]	4.6	Single small grain	Laser Fusion	7.1
MTELF16	53-TB[1]	4.1	Single small grain	Laser Fusion	6.9
MTELF17	53-TB[1]	4.4	Single small grain	Laser Fusion	11.1
MTELF18	53-TB[1]	4.8	Single small grain	Laser Fusion	6.1
MTELF19	53-TB[1]	4.7	Single small grain	Laser Fusion	9.6
MTELF20	53-TB[1]	6.9	Single small grain	Laser Fusion	10.0
MTELF21	53-TB[1]	4.4	Single small grain	Laser Fusion	6.0
MTELF22	53-TB[1]	5.5	Single small grain	Laser Fusion	8.0
MTELF23	53-TB[1]	5.1	Single small grain	Laser Fusion	2.7
MTELF24	53-TB[1]	5.2	Single small grain	Laser Fusion	8.6
MTELF25	53-TB[1]	5.0	Single small grain	Laser Fusion	6.2
MTELF26	53-TB[1]	4.7	Single small grain	Laser Fusion	10.3
MTELF27	53-TB[1]	5.3	Single small grain	Laser Fusion	13.1
MTELF28	53-TB[1]	5.7	Single small grain	Laser Fusion	5.0
MTELF29	53-TB[1]	7.9	Single small grain	Laser Fusion	10.3
MTELF30	53-TB[1]	5.9	Single small grain	Laser Fusion	30.0
MTELF31	53-TB[1]	5.2	Single small grain	Laser Fusion	13.8
MTELF32	53-TB[1]	4.0	Single small grain	Laser Fusion	13.5
MTELF33	53-TB[1]	5.9	Single small grain	Laser Fusion	8.6
MTELF34	53-TB[1]	4.8	Single small grain	Laser Fusion	1.9
W353	53-TB[1]	178.2	Six large grains	Step heat	0.20
CPU2FF1	53-TR[2]	8.0	Single small grain	Furnace Fusion	5.9
CMX2FF1	53-TR[2]	6.2	Single small grain	Furnace Fusion	6.1
CMX2FF2	53-TR[2]	6.7	Single small grain	Furnace Fusion	4.2

Table 3 con.

Sample	Irradiation	Weight[3]	Material	Method	Cl/K
CMX2FF3	53-TR[2]	4.9	Single small grain	Furnace Fusion	6.9
CMX53	53-TR[2]	183.4	Large grains	Step heat	0.90
CPU253	53-TR[2]	163.2	Large grains	Step heat	0.10
HH53	53-TR[2]	167.4	Large grains	Step heat	3.0
W3ADL	53-TR[2]	14.9	Vein Adularia	Step heat	0.01
W3FF1	53-TR[2]	5.2	Single small grain	Furnace Fusion	6.5
W3FF2	53-TR[2]	5.8	Single small grain	Furnace Fusion	4.4
W3FF3	53-TR[2]	5.2	Single small grain	Furnace Fusion	4.5
W3FF4	53-TR[2]	6.6	Single small grain	Furnace Fusion	6.4
W3FF5	53-TR[2]	6.0	Single small grain	Furnace Fusion	5.9
W3FF6	53-TR[2]	20.8	Single medium grain	Furnace Fusion	.13
W3FF7	53-TR[2]	18.0	Single medium grain	Furnace Fusion	5.6
W3FF8	53-TR[2]	20.8	Single medium grain	Furnace Fusion	6.4
MTEADL	53-TR[2]	15.45	Vein Adularia	Step heat	0.004
CPU2ADL	53-TR[2]	15.6	Vein Adularia	Step heat	0.004
HHADL	53-TR[2]	11.0	Vein Adularia	Step heat	0.003
FNADL	53-TR[2]	14.8	Vein Adularia	Step heat	0.003
ADADL	53-TR[2]	14.3	Pluton Adularia	Step heat	0.005
CMX2ADL	53-TR[2]	15.1	Vein Adularia	Step heat	0.033
MTE64	53-TR[2]	101.5	Large grains	Step Heat	5.0
MTEC64	64-TR[2]	204.2	Large grains	In vacuo	4.6
MTEC64T	64-TR[2]	204.2	Total of MTEC64 and MTEPC64	Combo[5]	4.7
MTEPC64	64-TR[2]	197.5	*In vacuo* crushed	Step heat	4.9
W364	64-TR[2]	97.0	Large grains	Step heat	5.7
W364FF1	64-TR[2]	7.8	Single small grain	Furnace Fusion	2.1
W364FF2	64-TR[2]	7.3	Single small grain	Furnace Fusion	2.6
W364FF3	64-TR[2]	4.9	Single small grain	Furnace Fusion	5.5
W364FF4	64-TR[2]	14.0	Single medium grain	Furnace Fusion	5.3
W364FF5	64-TR[2]	15.1	Single medium grain	Furnace Fusion	1.1
W364FF6	64-TR[2]	21.1	Single medium grain	Furnace Fusion	5.9
W364FF7	64-TR[2]	10.8	Single small grain	Furnace Fusion	9.7
W364FF8	64-TR[2]	14.5	Single small grain	Furnace Fusion	1.6
W3C64	64-TR[2]	297.2	Large grains	In vacuo	4.5
W3C64T	64-TR[2]	297.2	Combination of W3C64 and	Combo[5]	4.5
W3PC64	64-TR[2]	144.4	*In vacuo* crushed	Step heat	6.3
CMXA	91-TB[1]	62.3	Polished chip	Step heat	5.9
CMXB	91-TB[1]	45.4	Polished chip	Step heat	6.7
CMXC	91-TB[1]	73.1	Polished chip	Isothermal[6]	6.5
CMXD	91-TB[1]	105.5	Polished chip	Step heat	5.4
CMXE	91-TB[1]	104.0	Polished chip	In vacuo	5.2
CMXEC	91-TB[1]	104.0	*In vacuo* crushed	Step heat	5.7
CMXET	91-TB[1]	104.0	Total of CMXEC and CMXE	Combo[5]	6.6
MTEB	91-TB[1]	31.5	Polished chip	AB[4] Step heat	6.9
MTEC-1	91-TB[1]	6.4	Small portion of polished chip	AB[4] Step heat	2.1
MTEC-2	91-TB[1]	78.4	Large portion of polished chip	Step heat	6.5
MTED	91-TB[1]	104.0	Polished chip	Step heat	6.4
MTEE	91-TB[1]	137.5	Polished chip	In vacuo	6.9
MTEELC	91-TB[1]	80.3	*In vacuo* crushed – Large split	Step heat	7.1
MTEESC	91-TB[1]	50.1	*In vacuo* crushed – Small split	Step heat	6.9
MTEET	91-TB[1]	137.5	Total MTEEC, MTEELC,	Combo[5]	7.3
W3A	91-TB[1]	31.4	Polished chip	AB[4] Step heat	7.1

Table 3 con.

Sample	Irradiation	Weight[3]	Material	Method	Cl/K
W3CD	91-TB[1]	112.5	Polished chip	Isothermal[6]	5.0
W3E	91-TB[1]	56.7	Polished chip	Step heat	5.1
W3F	91-TB[1]	93.2	Polished chip	In vacuo	5.0
W3FC	91-TB[1]	58.9	*In vacuo* crushed	Step heat	5.3
W3FT	91-TB[1]	58.9	Total of W3F and W3FC	Combo[5]	6.1
W3G	91-TB[1]	95.2	Polished chip	Step heat	6.0

1 TB = Tube, samples were irradiated, wrapped in foil in an evacuated tube
2 TR = Tray, samples were irradiated in an Al tray, in an evacuated tube
3 Sample weight prior to analysis in mg
4 AB = Abbreviated heating schedule used for small samples to maximize signal size in any given step
5 Combo = A combination of separate analysis for purpose of combining crushing and post-crushing step heating of same sample
6 Isothermal = isothermal duplicate step heating schedule, two steps at each temperature

4.2. Irradiation

Crushed material was wrapped in Cu foil and packed in evacuated silica tubes for irradiation. Medium grain sizes were loaded in Al trays that were subsequently sealed in evacuated silica tubes. Very large grains were packed loose in the silica tubes. All of the adularia was loaded into Al trays. Fish Canyon sanidine (FCS), 27.84 Ma relative to an age of 520.4 Ma on Mmhb-1 hornblende (Cebula et al., 1986; Samson and Alexander, 1987) was used to monitor the neutron flux. Loose grains of FCS were packed in separate holes in the covered Al trays and Al wrapped grains of FCS were packed between the Cu packages, or grains in the tubes. The height of the packages from the base of the tubes was recorded to allow J factors to be calculated for the grains in between the monitors. Samples were irradiated in 3 separate irradiation packages (NM-53, NM-64, and NM-91) at the University of Michigan, Ford reactor. They were irradiated underwater for 24 hours in position L67 with no shielding and had J values of ≈ 0.003. Actual J values, and sample sizes are listed in Appendix A. The Ford reactor was chosen to minimize the temperature the samples were exposed to during irradiation and

to produce $^{38}Ar_{Cl}$. The samples returned without evidence of the inner quartz tubes breaking, which would be indicative of possible wetting or other contamination. The large outer tube containing the Al trays did break in irradiation NM-53, possibly during return shipping.

4.3. Argon Analysis

Samples were analyzed at New Mexico Geochronology Research Laboratory (NMGRL). Three methods of argon extraction are used, a standard double vacuum Mo resistance furnace, CO_2 laser, and an *in vacuo* crusher. All three extraction lines are low volume and connected to a MAP 215-50 mass spectrometer. Furnace gas reacts with three SAES GP-50 getters and a tungsten filament. Laser or crusher gas reacts only with two GP-50 getters and tungsten filament. The mass spectrometer is operated in static mode and gas is measured on an electron multiplier. The sensitivity was determined by analyzing a biotite standard of known composition and the discrimination was determined using a series of air aliquots. The sensitivities are equal to 1.0×10^{-13}, 1.5×10^{-13}, and 5.0×10^{-14} moles/nA for the furnace, crusher, and laser extraction lines, respectively. Discrimination values for each analysis are given in the appendices.

4.3.1. Furnace Analysis

Samples were incrementally heated from 300 - 1800° C or fused at 1750° C in the furnace. Furnace temperatures were measured using a thermocouple attached to the bottom of the crucible. Prior to analysis, an additional thermocouple was mounted inside the crucible to determine the temperature offset (complete results are given in Appendix B). During analysis, only the thermocouple on the outside of the crucible is used. By

measuring the actual temperature inside the crucible prior to analysis, a more accurate measure of the temperature inside the crucible can be obtained. The offset ranged from -39°C at 300° C to -8°C at 1500°C. This offset, (from the lower thermocouple, outside the crucible, to the upper thermocouple, inside the crucible) in most cases was outweighed by temperature perturbations caused by the samples themselves. It was noted that the extreme topography, caused by large quartz grains produced a substantial temperature gradient within the crucible. Therefore, temperatures stated can only be used as an approximation of the actual furnace temperature. The thermocouples were calibrated by observing the melting of Cu foil, which melts at 1083° C. Heating duration generally lasted 10 minutes but slightly longer heating steps were used at lower temperatures to allow the furnace to equilibrate. In some runs, low temperature steps were added to the heating schedule to accommodate large amounts of gas evolving at temperatures under 500° C. Abbreviated heating schedules, with as few as four steps, were used to maximize the signal size of small samples. Isothermal duplicate heating steps were used to determine if a non-radiogenic component of ^{40}Ar, related to the decrepitation of fluid inclusions, could be liberated in the first step, leaving a higher proportion of $^{40}Ar^*$ in the second step. Due to the low signal size of the duplicate steps, they provided no additional information, and will not be discussed further. However, the complete data tables and age spectra are given in Appendix C.

4.3.2. Laser Analysis

To investigate the argon concentration homogeneity of the quartz, approximately 5 mg pieces of irradiated quartz were fused using the CO_2 laser. Samples were loaded

into a Cu tray and placed under vacuum. Quartz proved difficult to quantitatively fuse. As the grains began to melt, the sample would sputter onto the cover, thereby making it difficult to deliver the laser power to the sample. As a result, some samples did not totally fuse, and therefore their argon may have not totally degassed.

4.3.3. Crusher Analysis

An *in vacuo* crusher was developed to release argon trapped in the inclusion fluid, but allow the lattice gas associated with the quartz and sylvite daughter minerals to remain. Lattice gas is the argon held within the mineral structure, as opposed to the gas held within the fluid. Gas in the inclusion fluid should escape as a result of crushing. In sylvite daughter minerals, the gas in the lattice should only be from the radioactive decay of ^{40}K to ^{40}Ar.

For initial testing of the crusher, FCS was crushed to determine the proportion of gas coming from exterior sources, such as leaks, or evolving from the steel (commonly cast in a pure Ar atmosphere) as opposed to that coming from the sample. This standard (FCS) was chosen as an initial testing material because the argon isotope composition is very well known. Initial crushing of FCS (age spectra and data tables are given in Appendix D) showed that significant atmospheric argon was being evolved from the steel, thus the *in vacuo* mortar and pestle were chrome plated. This substantially reduced the blank.

The mortar and pestle style *in vacuo* crusher proved very effective for degassing the sample. During our initial trial, 60 % of the predicted yield of radiogenic gas was released from FCS. This compares to much smaller (0.1 – 4.8%) release by other

crushing systems. (Harrison et al., 1993; Turner and Wang, 1992). Turner and Wang (1992) suggest argon released during crushing is either a result of recoil or from voids. Harrison et al. (1993) suggested argon is sited in inclusions and at grain boundaries. Sanidine has a very coherent crystal structure and therefore few defects. It is highly unlikely that the amount of gas released in the crusher trials is due to Ar adhered to edges or defects. Therefore the gas must be coming from the crystal lattice of the sanidine. Thus, the source of the argon released from quartz *in vacuo* crushing may not be limited to fluid inclusion gas.

The largest quartz chip from each sample location was crushed *in vacuo* prior to step heating in the furnace. The samples were crushed 7-25 times with each crush increasing in intensity. No method of quantitatively measuring the intensity of the crushing was available, due to the style of the crusher. The pestle was held above the sample during evacuation on a brace. On the first crush, the pestle was simply lowered onto the chip, thereby breaking it. The chip was subsequently ground until a fine powder remained. One sample, MTEE, was sieved after crushing to separate the fraction larger than 168 μm (100 mesh) from the smaller fraction. The size fractions were subsequently step-heated individually. Samples were crushed until the amount of signal obtained from each crush began to decrease significantly.

4.3.4. Data Reduction

Data was reduced using standard methods of correcting for interfering reactions, discrimination, and sensitivity as described below. Molar quantities were used for all of the diagrams presented in this work with the exception of isochrons. A summary table of

the molar quantities of Ar isotopes and calculated elemental abundances is given in Appendix E. The values for molar quantities were determined by correcting the signal acquired by the mass spectrometer for sensitivity and discrimination. Corrections determined using K-glass and CaF_2 were as follows: The Ca/K ratio was divided by1.96 and multiplied by the moles of $^{39}Ar_K$ to obtain moles of $^{37}Ar_{Ca}$. The Cl/K ratio was divided by 0.277 and multiplied by the moles of $^{39}Ar_K$ to obtain moles of $^{38}Ar_{Cl}$. Complete tables of the $^{40}Ar/^{39}Ar$ data from polished chips can be found Appendix F. The factors used to correct for ^{40}Ar formed from the ^{40}K during irradiation ($^{40}Ar_K/^{39}Ar_K$) were 0.0270, 0.0250 and 0.0265 for irradiations NM-53, NM-64, and NM-91, respectively.

4.4. Electron Microprobe Sample Preparation

Samples of quartz and adularia were prepared in one inch round grain mounts using a thermally cured epoxy. The grains were chosen from the same material that was used for argon analysis. The epoxy rounds were polished using Gridabrade™ diamond impregnated discs, attached to a magnetic lap wheel. The samples were ground using the 168 μm grit wheel until the excess epoxy was removed and a substantial amount of sample was exposed. The samples were then ground on the 63, 30, 15 μm wheels for approximately 1 minute each. For the final polish, loose diamond powder suspended in deionized water, was used on dedicated pads for 6, 2, and < 1 μm size. Samples were polished for 3 minutes on each lap and cleaned ultrasonically in between grit sizes.

Doubly polished quartz chips were mounted on double stick carbon tape on a one inch round glass slide and carbon coated. The polishing was performed prior to mounting in the same manner as above.

4.5. Electron Microprobe Analysis

The Cameca SX-100 electron microprobe at New Mexico Bureau of Mines and Mineral Resources (NMBMMR) was used to examine the quartz and phases included in the quartz. Back Scatter Electron (BSE) and Secondary Electron (SE) images, along with X-ray maps of the quartz and adularia were collected. Quantitative analysis of the quartz, adularia and included phases were performed, with the latter being limited by the difficulty of analyzing small volatile phases. An accelerating voltage of 15 kV was used, with beam currents ranging from 100 pA for the SE imaging, to 20 nA for the BSE imaging, x-ray maps and quantitative analysis.

5. RESULTS

5.1. Characterization of the Samples

5.1.1. Optical Examination Results

5.1.1.1. Adularia

Petrographic examination of thin sections of the adularia revealed minimal clay alteration, although the samples appear to be turbid (Parsons et al., 1988). The tubidity is thought to represent abundant microstructures, such as micropores. Microstructures, have been invoked to help explain argon kinetics in K-feldspars (Burgess et al., 1992; Fitzgerald and Harrison, 1993; Foland, 1994; Parsons et al., 1988). Kaolinite or other clays may be present in small amounts, but there is a distinct absence of fine grained micas in thin section.

5.1.1.2. Quartz

Extensive characterization of the quartz crystals was performed prior to $^{40}Ar/^{39}Ar$ analysis. The chips were examined using the transmitted light microscopy and a number of variables were recorded qualitatively. Table 4 summarizes the probe and optical examination of quartz. The column for "low salinity inclusions" represents the presence and relative abundance of low salinity fluid inclusions in the chip. Figure 2 A shows a group of low salinity fluid inclusions from sample CMXB. Low salinity fluid inclusions are an important indicator of the quantity of K in the sample, and therefore should correlate to argon signal size. Figure 2 B shows a fluid inclusion from CMXB more

typical of Capitan high salinity fluid inclusions. Figure 2 C is another single high salinity fluid inclusion from sample W3G. A much higher abundance of low salinity inclusions were observed in samples from CMX and W3. Although it was not a quantitative determination, no low salinity inclusions were observed in MTE.

The relative amount of cloudy areas in the quartz was noted, because cloudy areas in feldspars, known as turbid feldspars, are thought to represent areas with increased diffusion rates (Parsons, 1988). The amount of cloudiness might therefore be related to argon loss in the sample. "Cloudy quartz areas" represent the relative amount of cloudy areas in the quartz. "Scope" represents the extent to which the cloudiness was present using transmitted light microscopy, 5 to 40 times magnification. The cloudy chip shown in Figure 3 A is a microphotograph of MTEE. "Optical" is the extent that the cloudiness was visible to the naked eye as seen in Figure 3 B and C. Figure 3 C shows a view of quite clear quartz from chip W3D. Figure 3 C shows an example of how the cloudy quartz chip in Figure 3 A, MTEE, appears in transmitted light. W3 had the least number of cloudy areas, and MTE had at least one cloudy region in each chip.

"Planes or random fluid inclusions" show whether the fluid inclusions were present in planes or random locations in the quartz, providing some indication of the primary or secondary nature of the fluid inclusions, examples of planar, and random fluid inclusions are shown in Figure 4 A and B respectively. Figure 4 C shows an intermediate group of fluid inclusions. Capitan fluid inclusions have been shown to be primarily (> 90% type 1 inclusions) from one generation of fluid. Campbell et al. (1995), show that the lower salinity type 3, and type 4 inclusions have lower temperatures of homogenization and are present in secondary planes

The "image" column of the table shows whether cations were present in element (X-ray) mapping on the electron microprobe. Examples of the microprobe images and maps are shown in Figure 5. "Analysis" shows the presence of cations in the quartz quantitative analysis. W3 showed the largest concentrations of lattice cations, however this was not seen in the argon analysis, which revealed that the bulk sample of W3 had the lowest amount of Cl, K, and Ca.

The presence of necked down fluid inclusions (Figure 6), which in some cases crossed fractures in the quartz, may represent rapid diffusion paths. The column labeled rapid diffusion paths indicates the extent to which these fluid inclusions were observed in the sample. An example of pitted quartz representing large quantities of small fluid inclusions in the quartz, visible on the surface of the quartz chip using microprobe imaging is shown in Figure 7.

Table 4 Summary of characterization of HDFIC chips

Sample	Low Salinity Inclusions[1]	Cloudy Quartz Areas		Planes or Random Inclusions[4]	High levels of Matrix Cations		Rapid Diffusion Paths[7]	Pitted Quartz Areas[8]	Notes
		Scope[2]	Optical[3]		Image[5]	Analysis[6]			
CMXA	0	3	1	P>R	3	0	3	0	
CMXB	4	2	1	P>R	0	0	3	0	
CMXC	0	1	1	R	3	0	3	0	
CMXD	3	0	3	P>R	0	0	0	0	Very thick section fluid inclusions not visible
CMXE	3	3	3	P>R	4	3	4	3	Necked Down inclusions intersecting cracks
MTEA	0	4	3	R	0	0	0	0	
MTEB	0	3	3	P>R	0	3	2	0	
MTEC	0	3	3	R	0	0	1	3	
MTED	0	3	4	P	0	0	0	0	High salinity abundant growth plane inclusions
MTEE	0	4	5	P	4	0	0	0	
W3A	3	0	0	P>R	3	5	0	0	
W3B	2	1	0	P>R	2	0	3	3	
W3C	2	0	1	P	3	2	0	0	
W3D	3	3	0	P>R	3	2	3	0	Large range of inclusion salinity
W3E	0	3	1	P>R	2	5	4	3	Similar growth bands to MTED and MTEE
W3F	1	0	0	P	4	2	0	0	
W3G	3	0	3	P	3	2	3	0	

1 The degree to which upon optical examination low salinity inclusion were present on a scale from 0-5 with 0 = none and 5 = all of the inclusions seen were low salinity.
2 The degree to which upon optical examination cloudy quartz was present same scale as in 1
3 The degree to which upon microscopic examination cloudy quartz was present scale as in 1
4 The degree to which the fluid inclusions were present in planes or randomly within the quartz. P=planes and R=randomly
5 The degree to which Cations were seen in the x-ray maps of the quartz scale as in 1
6 The degree to which Cations were present in quantitative analysis of the quartz scale as in 1
7 The degree to which necked down inclusions crossing fractures was observed with a microscope in the quartz. Scale as in 1
8 The degree to which pits were observed using SE imaging

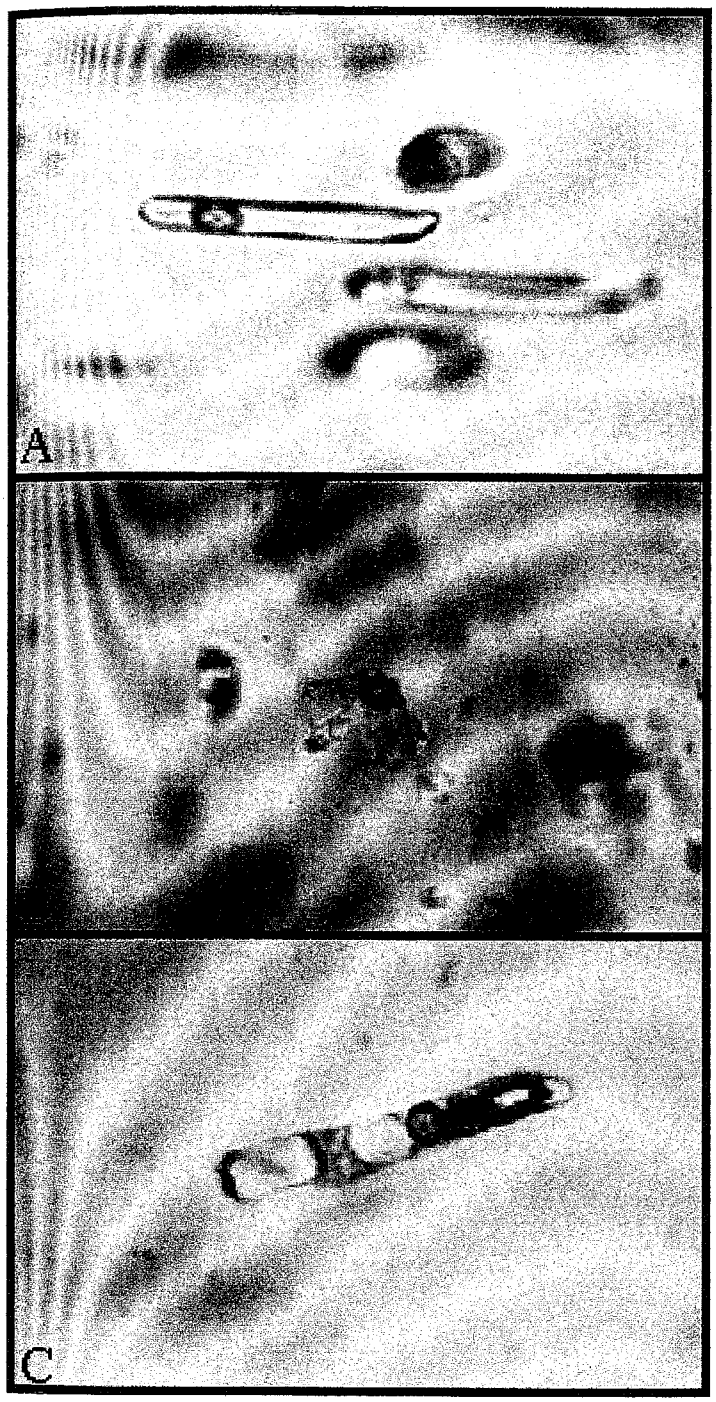

Figure 2 Photomicrographs of fluid inclusions in quartz to show the variation in salinity. All of the images are in transmitted light without cross-polars. A.) Low salinity fluid inclusions from sample CMXB, 40x magnification. B.) High salinity fluid inclusion from sample CMXB, 40x magnification. C.) High salinity fluid inclusion from sample W3G, 40x magnification.

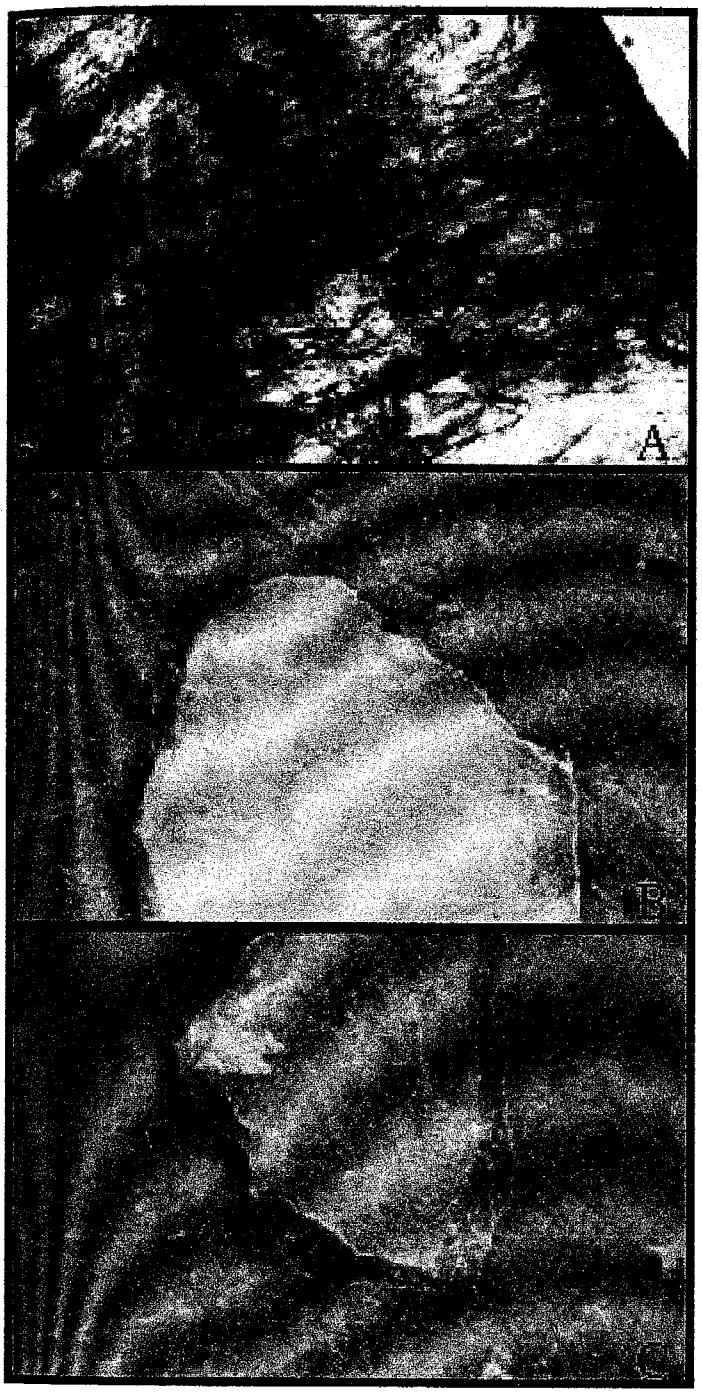

Figure 3 Photographs of Quartz to show Cloudiness A.) Photomicrograph of cloudy quartz sample MTEE, 5x magnification, in transmitted light without cross-polars. B.) Photograph of sample MTEE showing cloudy quartz. C.) Photograph of sample W3D showing clear quartz.

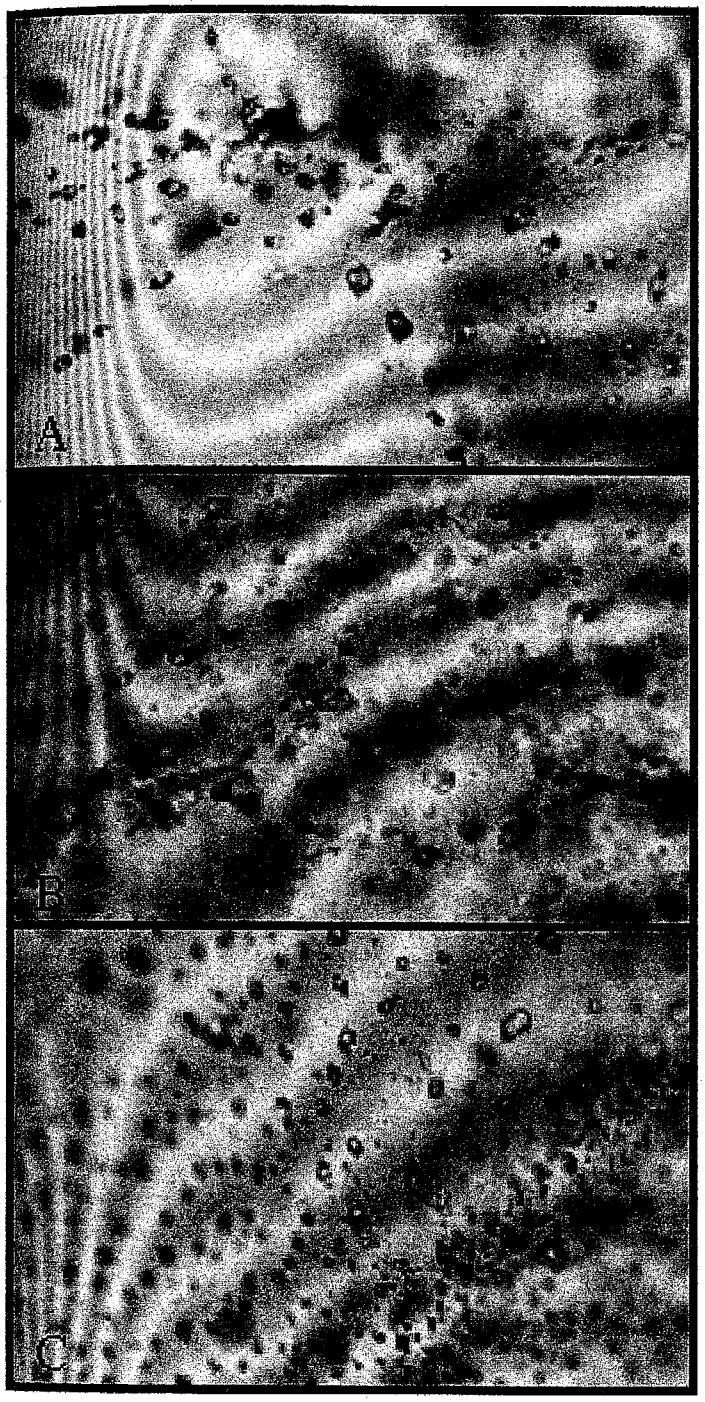

Figure 4 Photograph showing planes and random fluid inclusions. All of the images are in transmitted light without cross-polars. A.) Photomicrograph of sample W3F showing planes of fluid inclusions 10x magnification. B.) Photomicrograph of sample MTEE showing random fluid inclusion locations, 40x magnification. C.) Photomicrograph of sampleW3F showing planes and random fluid inclusions, 10x magnification.

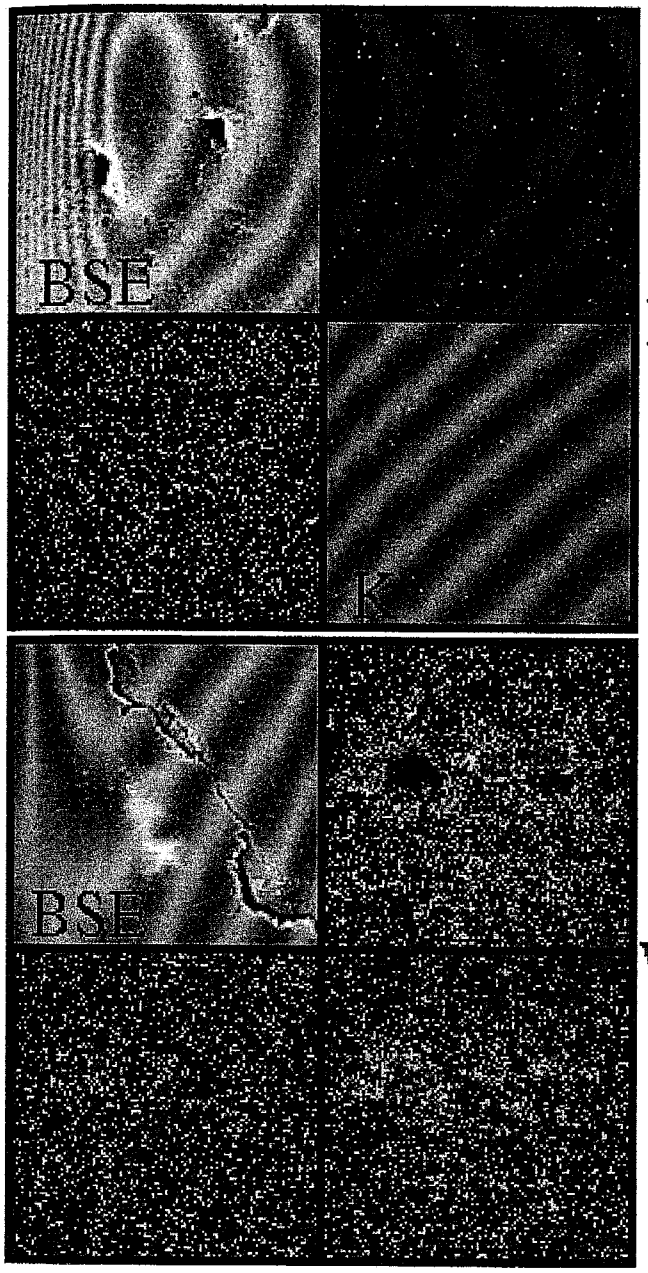

Figure 5 BSE and x-ray maps of cations on the surface of the quartz chips. Sample MTEC shows abundant fluid inclusion pits, but a remarkable absence of x-ray counts for Na, K, and Cl. All three elements show background levels. Sample W3F shows high concentrations of elements Na, K, and minor Cl even where there are no fluid inclusion pits. The bright area in the BSE image is probably a fluid inclusion, which has ruptured under the surface of the carbon coat, and is causing some localized charging.

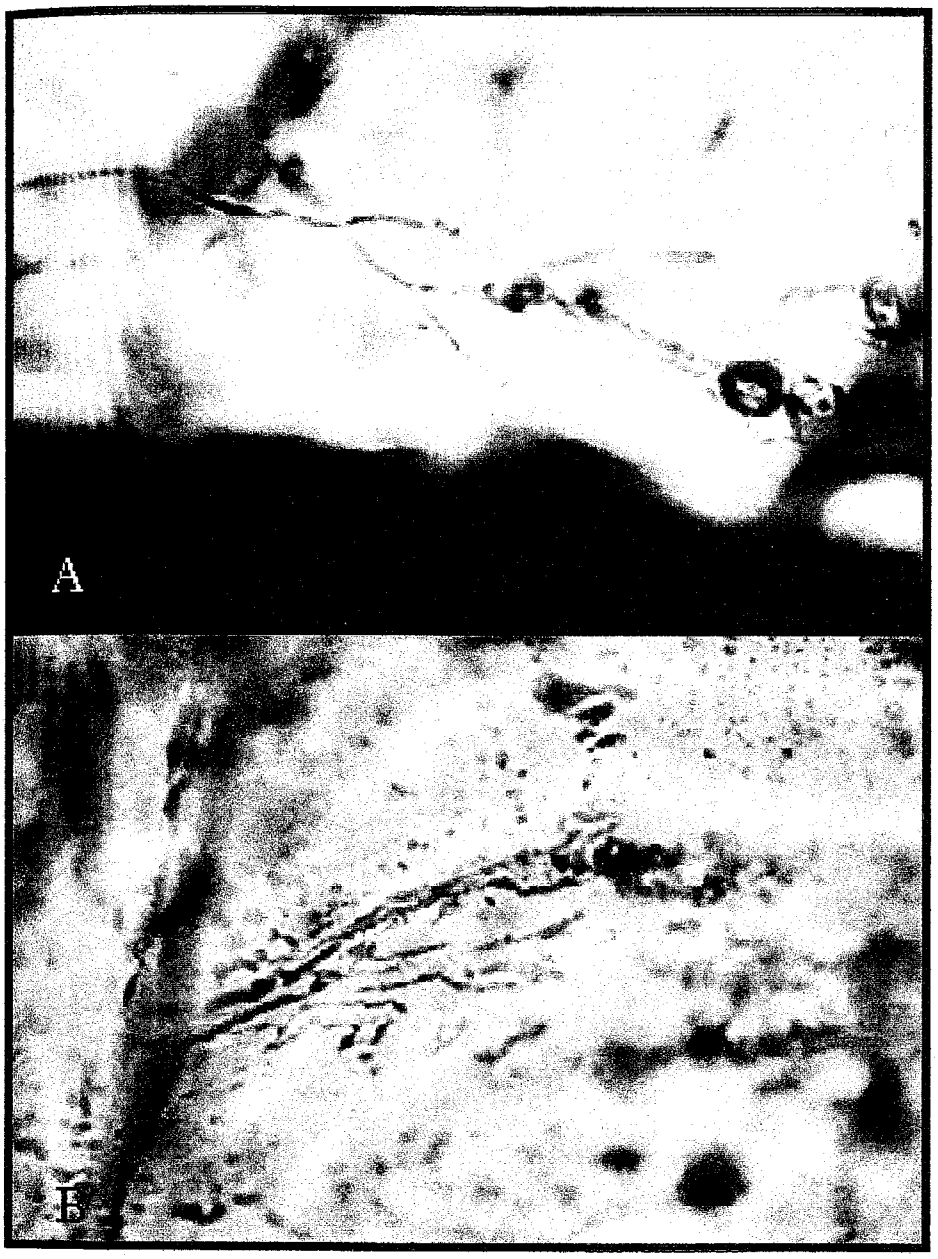

Figure 6 Photographs of necked-down fluid inclusions Both of the images are in transmitted light without cross-polars. A.) Photomicrograph of a single necked down fluid inclusion from sample W3E 20x magnification. B.) Photomicrograph of sample CMXE 20x magnification showing several necked down fluid inclusions intersecting a fracture in the quartz. This could be a pathway for rapid diffusion of Ar out of the fluid inclusion.

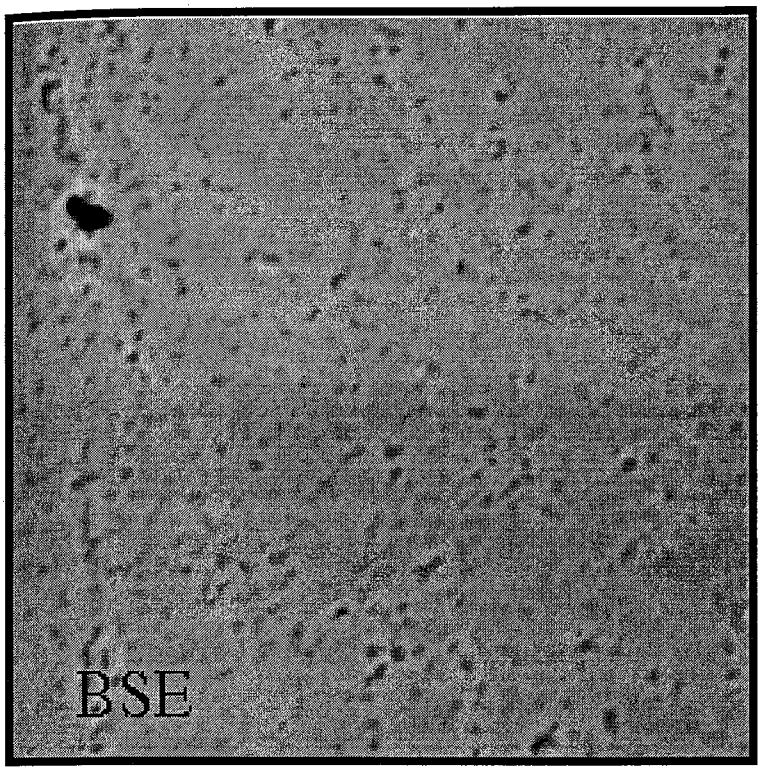

Figure 7 BSE image of sample W3B showing a strongly pitted surface. These pits probably represent a large population of very small fluid inclusions supporting the idea that there is a continuum of fluid inclusion size in the sample.

5.1.2. Electron Microprobe Results

5.1.2.1. Adularia

Electron microprobe imaging and quantitative analysis revealed that the adularia was composed of two intergrown phases, albite and orthoclase. Many previous authors have referred to this cryptoperthitic feldspar as adularia and to maintain continuity we will continue this nomenclature. The cryptoperthitic lamellae range in size from < 1 μm to ~50 μm. In addition, larger mm size areas composed of only one feldspar are present. The compositions of both endmembers varied widely. All of the endmember

The compositions of both endmembers varied widely. All of the endmember compositions are given in Table 5, and full data are in Appendix G. The orthoclase compositions range from $Ab_{38}Or_{61}An_1$to Ab_7Or_{93}. The albite compositions range from $Ab_{69}Or_{30}An_1$ to $Ab_{98}Or_1An_1$, but in one sample the An endmember was as high as 3%. The analysis are plotted on the Or – Ab axis of a ternary diagram in Figure 8. The large range in endmember compositions is typical of feldspars forming at 600-650° C (Klein, 1985). This temperature range matches the T_h values obtained from the fluid inclusions in quartz, helping to confirm the plutonic origin of the fluids, and temporal association of the feldspar and quartz.

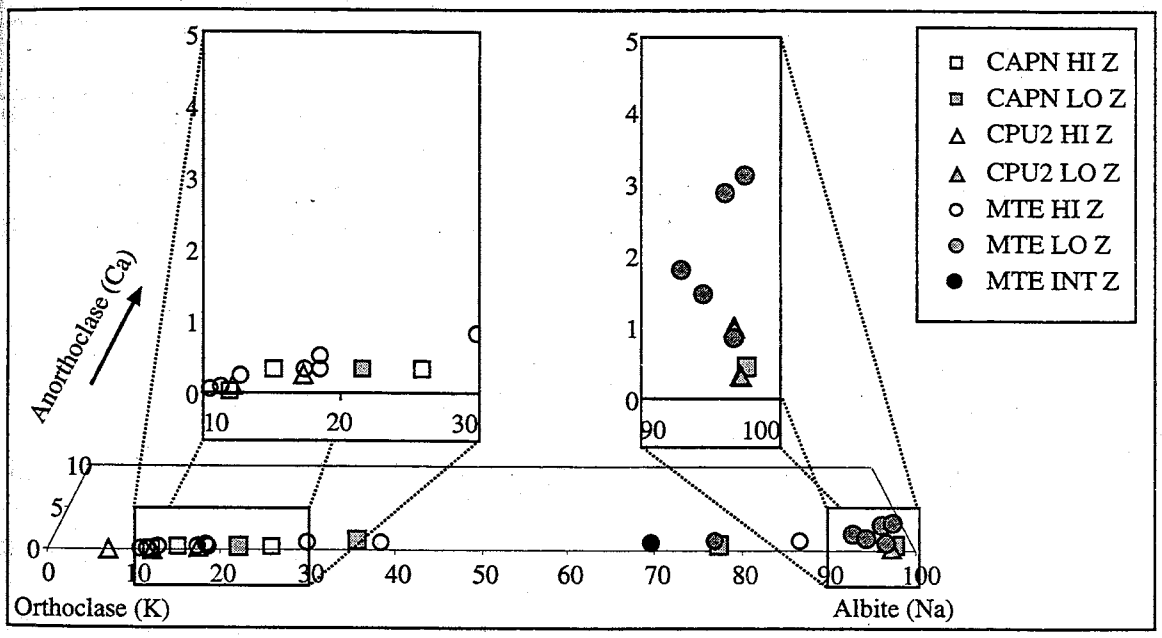

Figure 8. Or – Ab axis of ternary diagram showing results of electron microprobe analysis of Capitan adularia.

Table 5. Adularia quantitative analysis endmember compositions.

Sample	BSE	Ab[1]	Or[2]	An[3]	Sample	BSE	Ab[1]	Or[2]	An[3]
MTE	Hi Z	**38.02**	**61.15**	**0.82**	MTE	Lo Z	**96.01**	**0.91**	**3.08**
CAPN	Lo Z	35.55	64.08	0.38	CAPN	Lo Z	**98.12**	**1.45**	**0.43**
MTE	Hi Z	29.56	69.65	0.79	CAPN	Lo Z	97.46	2.02	0.52
CAPN	Hi Z	25.8	73.91	0.29	MTE	Lo Z	94.73	2.42	2.85
CAPN	Lo Z	21.99	77.79	0.23	CPU2	Lo Z	**97.1**	**2.61**	**0.29**
MTE	Hi Z	18.37	81.14	0.48	CPU2	Lo Z	96.18	2.83	0.99
MTE	Hi Z	18.44	81.24	0.32	MTE	Lo Z	96.25	2.92	0.83
MTE	Hi Z	17.4	82.31	0.29	MTE	Lo Z	93.86	4.72	1.42
CPU2	Hi Z	17.33	82.44	0.23	MTE	Lo Z	92.08	6.15	1.77
CAPN	Hi Z	15.15	84.53	0.32	MTE	Hi Z	86.43	12.46	1.11
MTE	Hi Z	12.85	86.93	0.22	CAPN	Lo Z	77.21	21.78	1.01
CPU2	Hi Z	12.19	87.72	0.09	MTE	Lo Z	76.57	22.35	1.08
CAPN	Hi Z	**12.2**	**87.8**	**0**	MTE	Int Z	**69.35**	**29.78**	**0.87**
MTE	Hi Z	11.54	88.39	0.07					
MTE	Hi Z	10.77	89.19	0.04					
CPU2	Hi Z	**6.94**	**93**	**0.06**					
	Min	6.94	61.15	0		Min	69.35	0.91	0.29
	Max	38.02	93	0.82		Max	98.12	29.78	3.08

9 Albite endmember composition in weight percent
10 Orthoclase endmember composition in weight percent
11 Anorthoclase endmember composition in weight percent

Note: Bold numbers represent the maximum and minimum endmember compositions

5.1.2.2. Quartz

Quantitative analysis of quartz from the electron microprobe (tables of complete data are found in Appendix H are shown as weight percent trace oxides versus sample name (Figure 9). Each point represents the average value for three individual point analysis of quartz. The analyses were performed to determine the budget of K and other elements in the quartz. Although the concentrations in the quartz are low the variation observed is real and not a result of analytical error. The theoretical detection limit for this analysis was at most 0.006 weight percent for each of the elements shown and the concentrations in many quartz samples were higher than this. However, on 20 replicate analysis of a pure quartz standard, background values for Na_2O, CaO and K_2O are 0.001,

0.004, 0.004 respectively (average and 1σ values are give in Table 6 full data are in Appendix I). Albite and anorthoclase were analyzed to determine the error on low concentrations Ca, Na, and K. The albite totals are high (average 104.866) due to Na loss associated with the small beam used to analyze the quartz. The CaO 1σ error was 0.009 weight percent the Na_2O 1σ error was slightly higher at 0.01 weight percent and K_2O 1σ error was 0003 weight percent. Therefore we feel that the values determined for Na_2O, CaO and K_2O are meaningful being above background and outside analytical error.

Table 6 Summary of standard values and error of quantitative quartz analysis.

	SiO_2	Al_2O_3	CaO	Na_2O	K_2O	Total
Quartz Average[1]	99.608	**0.001**	**0.004**	**0.001**	**0.004**	99.617
Quartz 1 σ	0.216	**0.001**	**0.004**	**0.001**	**0.003**	0.214
Anorthoclase Average[2]	43.877	36.339	18.792	**0.723**	**0.015**	99.746
Anorthoclase 1 σ	0.201	0.158	0.057	**0.010**	**0.004**	0.251
Albite Average[2]	73.651	22.024	**0.025**	9.153	**0.013**	104.866
Albite 1 σ	0.520	0.240	**0.009**	0.700	**0.003**	0.918

1 Number of analysis (n) = 20
2 Number of analysis (n) = 5

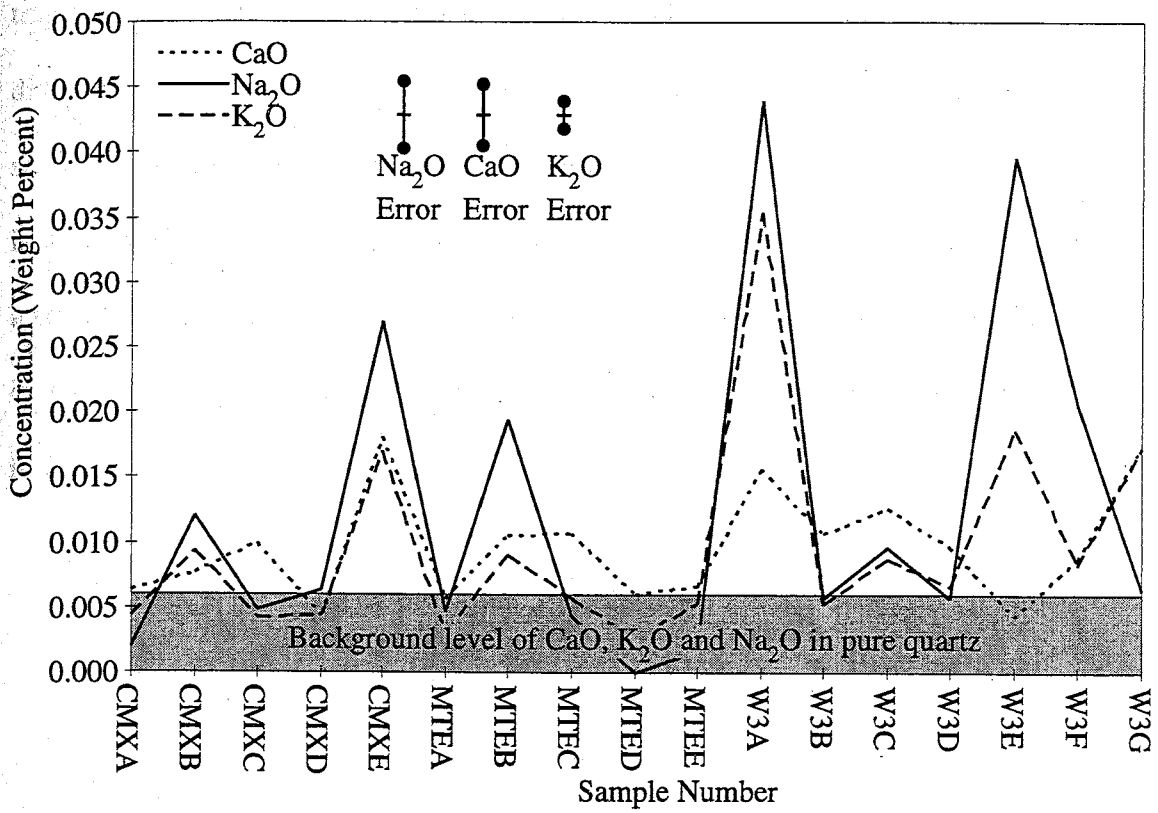

Figure 9 Values for weight percent oxides from quantitative quartz analysis from electron microprobe data. The average value for the three analyses was taken for each High density fluid inclusion chip (HDFIC.)

One of the primary assumptions on which this study was based was that the quartz would be a non-contributing substrate, and thus allow measurement of the fluid inclusions. This, however, was not the case. Many micron to sub-micron sized solid inclusions of K-bearing phases were found in the quartz using the imaging capability of the electron microprobe. In several instances it was difficult, due to the small size of the solids, to determine the mineral phase, but the presence of K and other elements were determined using electron microprobe X-ray element maps of the surfaces. Some of the phases identified were K and Na salts, anhydrite, and hematite. In addition, a phase containing only K and P was found. This phase may be glass inclusions that were

trapped as an immiscible phase. The majority of solid inclusions were less than 2 μm in diameter, although several salts were observed that are as large as 30 μm. These large salts may be related to the fluid inclusion salts reported by Campbell et al. (in review). It is unclear whether the smallest inclusions are actually solid inclusions or if they represent a small fluid inclusion within 5 μm of the surface, which would be detectable by BSE image or X-ray element maps. Quantitative analyses of the solid inclusions are presented in Campbell et al. (in review).

5.2. $^{40}Ar/^{39}Ar$ Step-Heating Analyses

5.2.1. Step Heating Results from Adularia

Six samples of vein adularia and one sample of adularia from the granite were analyzed to obtain the age of the veins and the pluton. The age spectra from these samples are shown in Figure 10. The total gas ages and plateau ages are given in Table 7. Complete data tables are given in Appendix J. The ages are given in millions of years along with the 2σ error, sample weight and J factor. All of the spectra, to varying degrees, show ages which increase with increasing temperatutre. Six of the seven adularia age spectra satisfy the plateau age criteria of Fleck et al. (1977). The plateau ages of these six age spectra agree closely, averaging 27.85 ± 0.55 Ma. The age spectrum from sampleW3ADL, which failed to meet plateau criteria, has a saddle shape, with old ages at both the low temperature and high temperature steps. The minimum age in the center of the spectra represents a maximum age for the vein. In general, large amounts of gas evolved from all the samples in the low temperature steps of the heating schedule. The ages are old in the first step or two, then decrease in age, and rise to the plateau age in all of the spectra, except W3ADL and MTEADL. The plateau typically begins at 800-900°C, and there is generally an increase in age during the last steps of the heating schedule. MTEADL had only one step beneath the 800° - 900° C beginning of the plateau temperatures. Presumably, the MTEADL spectra would show initial low ages if there were better resolution in the low temperature heating schedule. In addition, the Cl concentrations (weight normalized), as determined by argon analysis, are statistically identical to the concentration observed in the quartz. The high Cl concentration may be

due to fluid inclusions in the adularia. No fluid inclusions were directly observed, but are suspected to be present due to the milky color of the feldspar. However, the K_2O concentrations are significantly higher in the adularia, causing several orders of magnitude difference in the Cl/K ratios between the adularia and quartz.

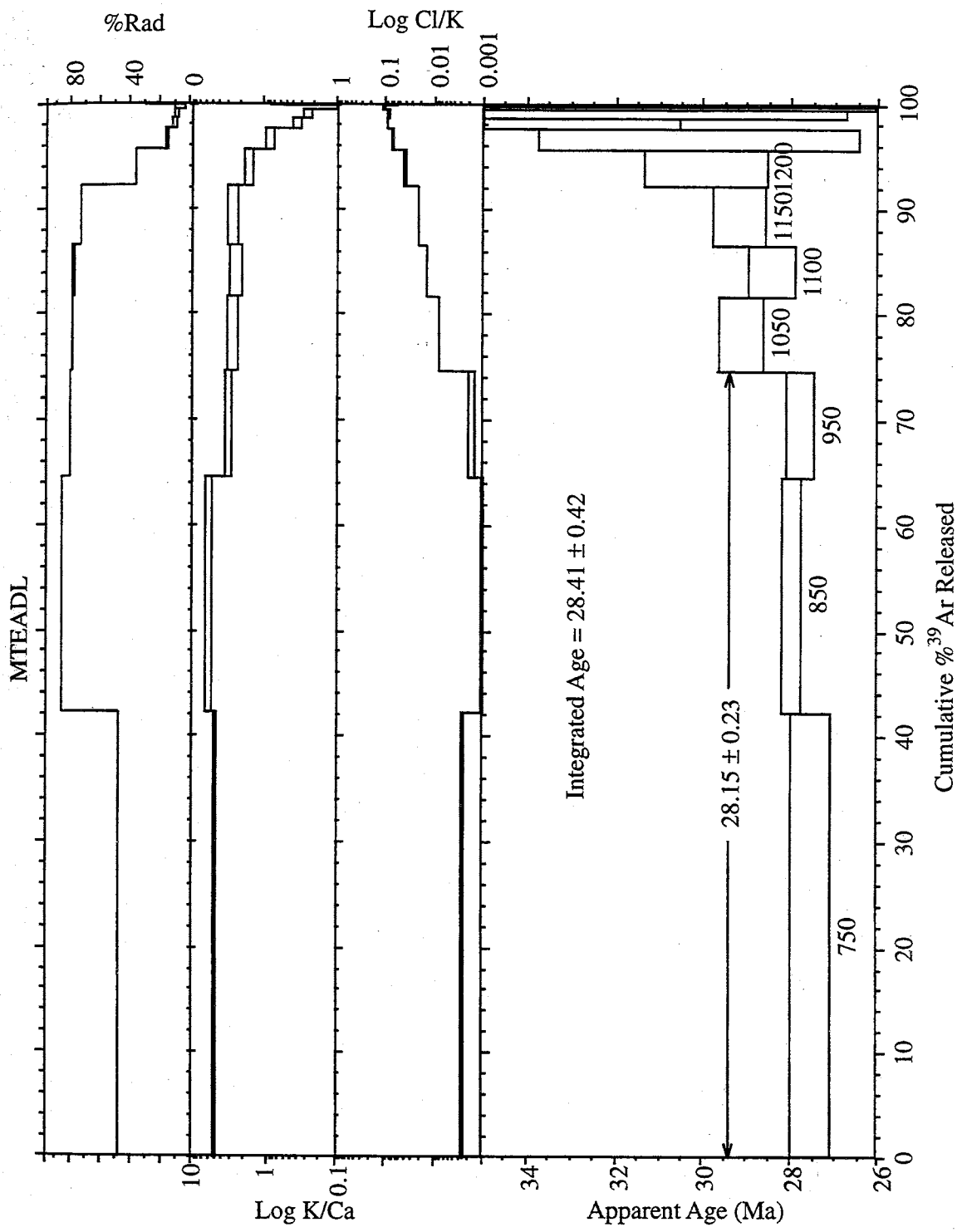
%Rad
80
40
0
Log Cl/K
1
0.1
0.01
0.001
MTEADL
Log K/Ca
10
1
0.1
Integrated Age = 28.41 ± 0.42
28.15 ± 0.23
750
850
950
1050
1100
1150
1200
Apparent Age (Ma)
34
32
30
28
26
Cumulative %39Ar Released
0
10
20
30
40
50
60
70
80
90
100

Figure 10 A

Figure 10 Age Spectra from Capitan Adularia A.) MTEADL B.) W3ADL C.) CPU2ADL D.) HHADL E.) ADADL F.) FNADL G.) CMX2ADL. All of the samples except ADADL are from veins located in the prospects as shown in Figure 1.

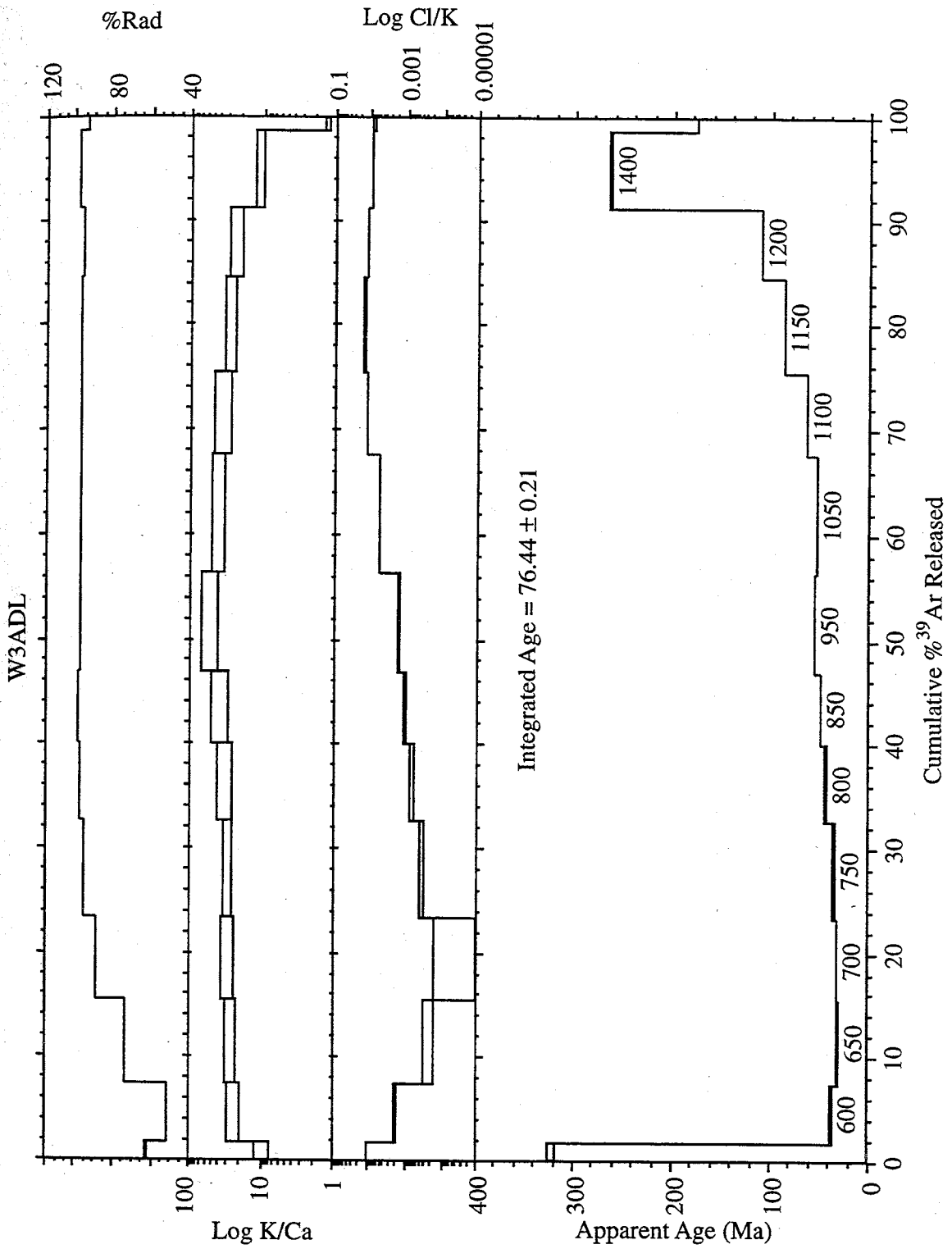
W3ADL
%Rad
120
80
40
Log Cl/K
0.1
0.001
0.00001
Integrated Age = 76.44 ± 0.21
1400
1200
1150
1100
1050
950
850
800
750
700
650
600
Cumulative %^{39}Ar Released
0
10
20
30
40
50
60
70
80
90
100
Log K/Ca
100
10
1
Apparent Age (Ma)
400
300
200
100
0

Figure 10 B

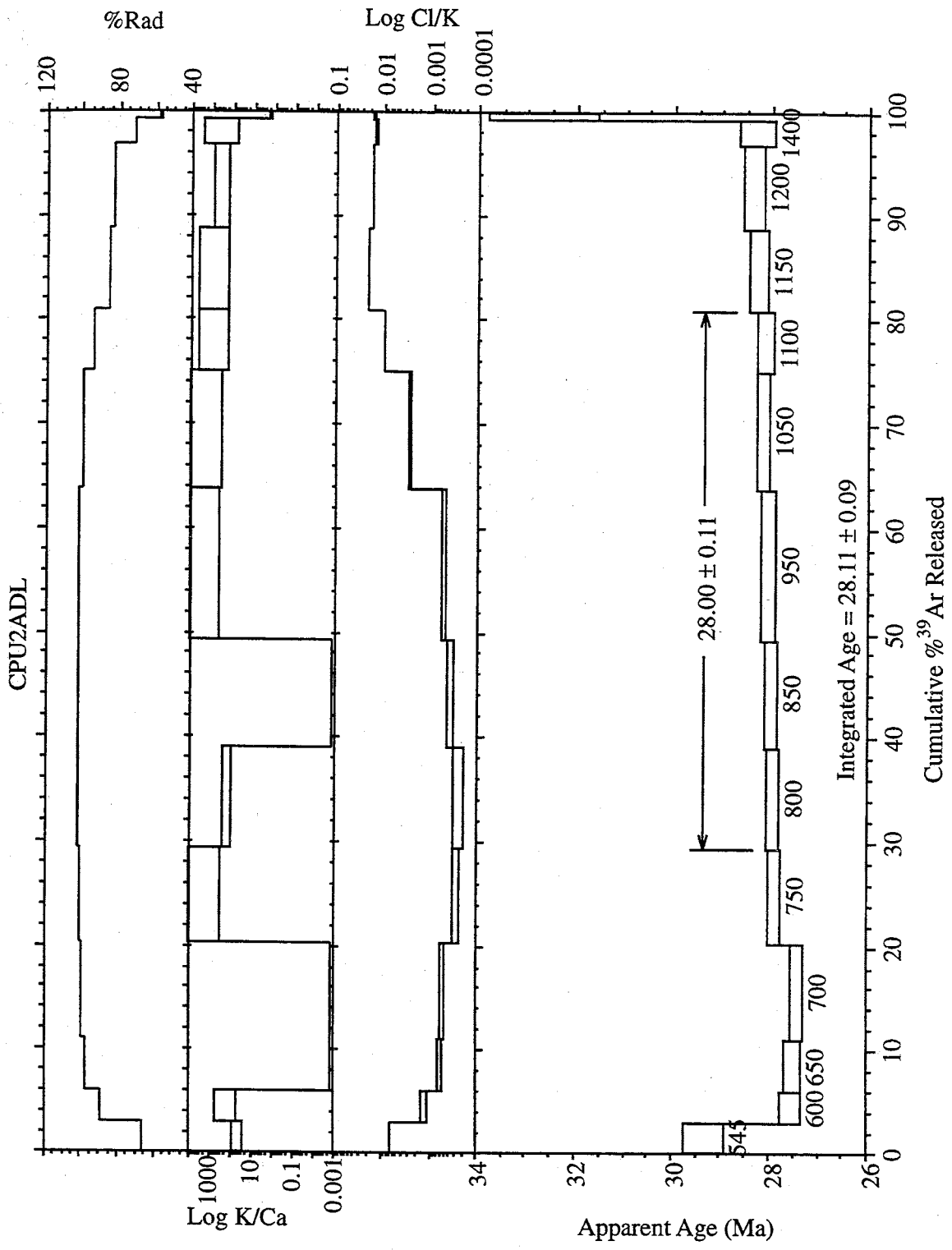
%Rad
Log Cl/K
120
80
40
0.1
0.01
0.001
0.0001
CPU2ADL
28.00 ± 0.11
Integrated Age = 28.11 ± 0.09
Cumulative %^{39}Ar Released
1400
1200
1150
1100
1050
950
850
800
750
700
650
600
545
1000
10
0.1
0.001
Log K/Ca
34
32
30
28
26
Apparent Age (Ma)
100
90
80
70
60
50
40
30
20
10
0

Figure 10 C

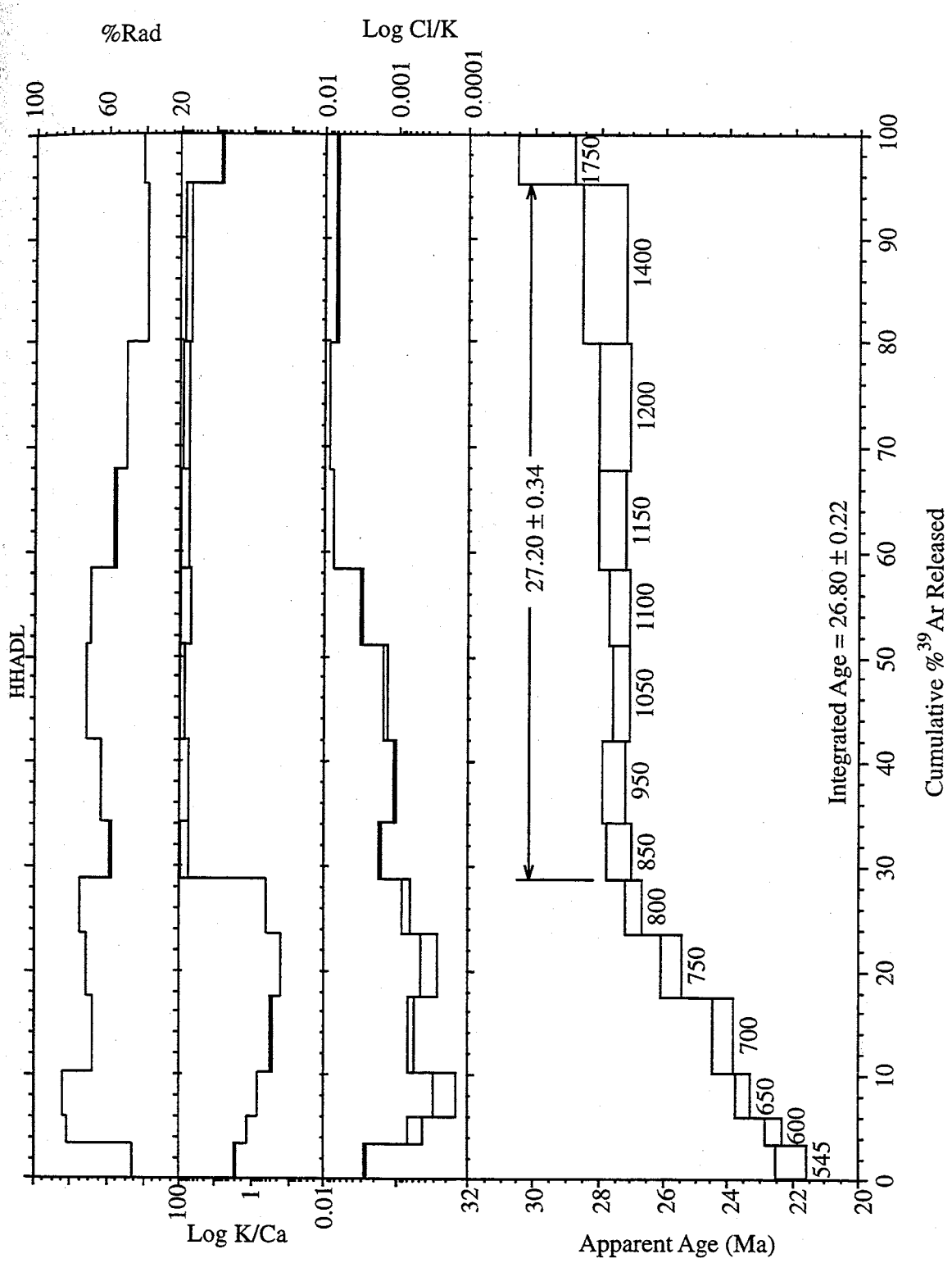
%Rad
100
60
20
Log Cl/K
0.01
0.001
0.0001
HHADL
Log K/Ca
100
1
0.01
27.20 ± 0.34
1750
1400
1200
1150
1100
1050
950
850
800
750
700
650
600
545
Integrated Age = 26.80 ± 0.22
Apparent Age (Ma)
32
30
28
26
24
22
20
0
10
20
30
40
50
60
70
80
90
100
Cumulative %^{39}Ar Released

Figure 10 D

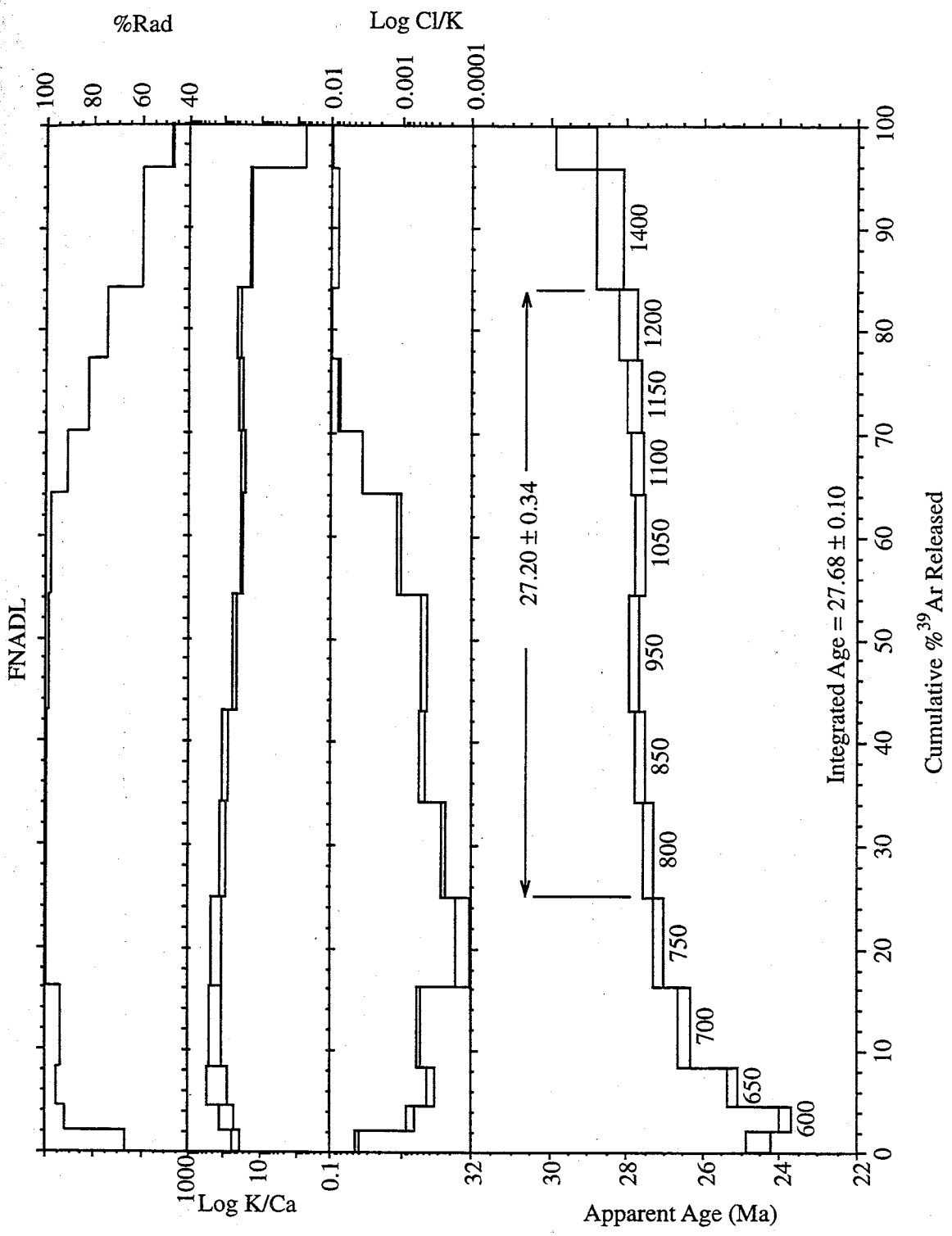
%Rad
Log Cl/K
100
80
60
40
0.01
0.001
0.0001
FNADL
1000
10
0.1
Log K/Ca
32
30
28
26
24
22
Apparent Age (Ma)
27.20 ± 0.34
1400
1200
1150
1100
1050
950
850
800
750
700
650
600
Integrated Age = 27.68 ± 0.10
0
10
20
30
40
50
60
70
80
90
100
Cumulative %^{39}Ar Released

Figure 10 E

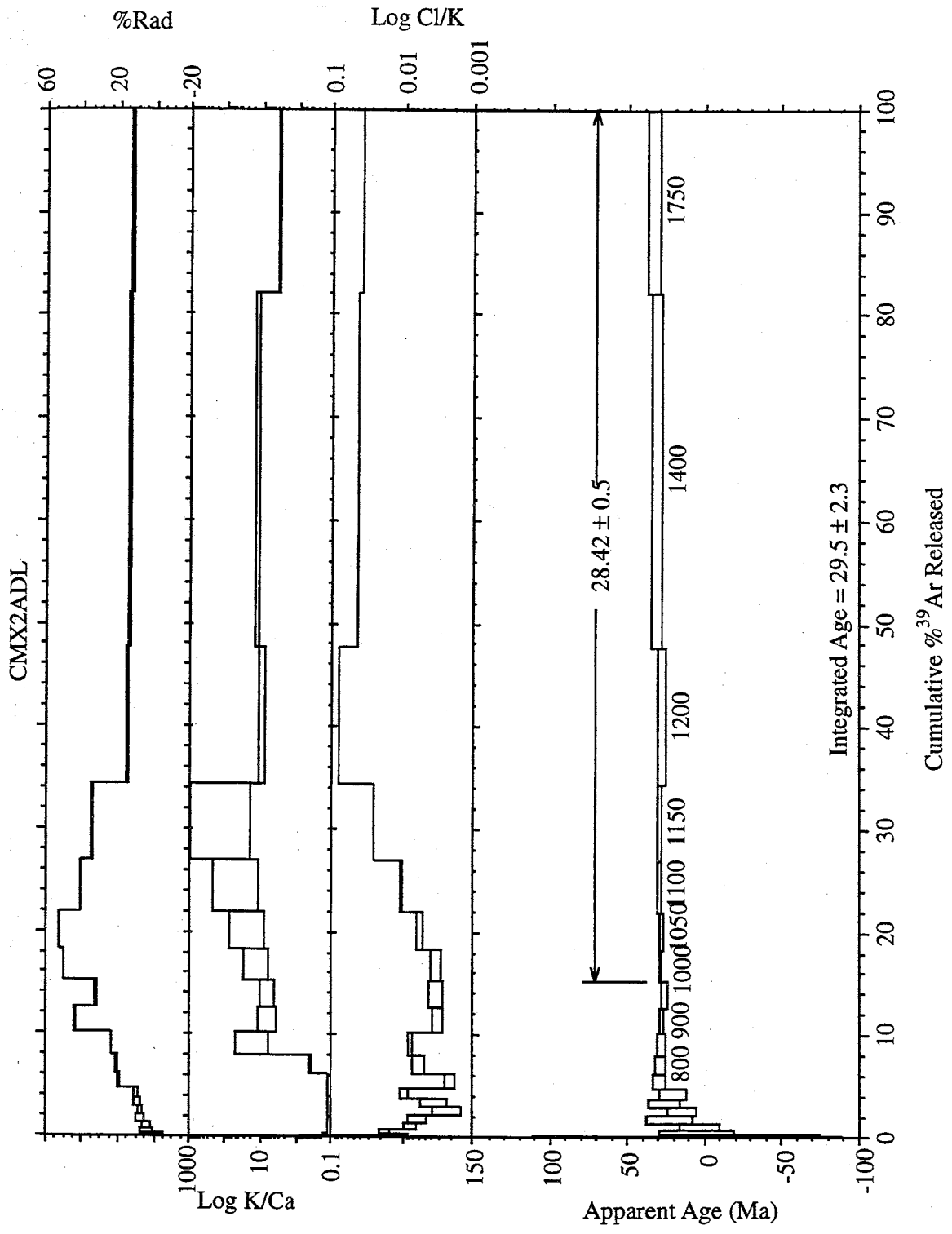
%Rad
Log Cl/K
60
20
-20
0.1
0.01
0.001
CMX2ADL
28.42 ± 0.5
1750
1400
1200
1150
1100
1050
1000
900
800
Integrated Age = 29.5 ± 2.3
Cumulative %^{39}Ar Released
100
90
80
70
60
50
40
30
20
10
0
1000
10
0.1
Log K/Ca
150
100
50
0
-50
-100
Apparent Age (Ma)

Figure 10 F

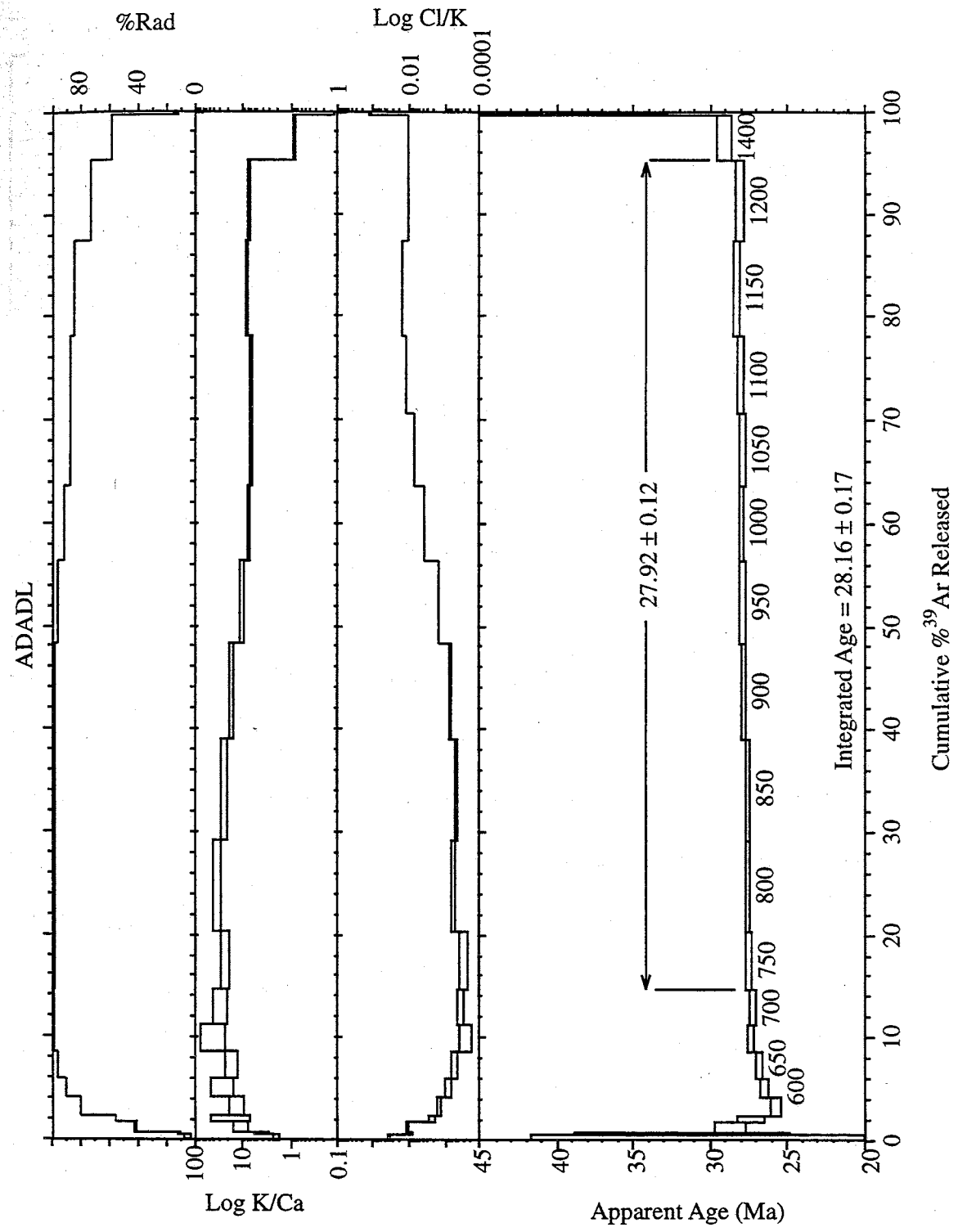
%Rad
Log Cl/K
ADADL
Log K/Ca
Apparent Age (Ma)
27.92 ± 0.12
Integrated Age = 28.16 ± 0.17
Cumulative %^{39}Ar Released

Figure 10 G

Table 7. Summary of Capitan adularia ages

Sample	Type	Weight mg	J	Integrated Age Ma	Error 2σ	Plateau Age Ma	Error 2σ
MTEADL	Vein	15.45	.003780	28.41	0.83	28.15	0.46
W3ADL	Vein	14.88	.003785	76.44	0.42	31.60	2.00
CPU2ADL	Vein	15.60	.003785	28.11	0.17	28.00	0.22
HHADL	Vein	11.04	.003795	26.86	0.44	25.80	1.10
FNADL	Vein	14.79	.003815	27.68	0.19	27.20	0.67
CMX2ADL	Vein	15.11	.003815	29.50	4.60	28.42	0.99
ADADL	Pluton	14.34	.003820	28.16	0.35	27.92	0.23

5.2.2. Step Heating Low Fluid Inclusion Density Grains Results

Step-heating analyses were originally performed on fluid inclusion-poor tips or quartz crystals. As discussed above, fluid inclusions in Capitan quartz more abundant close to the base of the crystals. Figure 11 shows the age spectra from quartz grains obtained from tips of the crystals. The amount of material analyzed was large, up to 200 mg, and the number of fluid inclusions contained within that material was highly variable. Spectra from five separate analyses of large grains are shown in Figure 11. Four behaviors are evident and are described below. Complete data tables are given in Appendix K. Table 8 gives a summary of the ages and Cl/K ratios.

The first behavior is seen only in sample CMX53 (Figure 11 A). The integrated age is low (23.5 ± 1.3) relative to the age (28.3 ± 0.1) of cogenetic adularia. The intermediate temperature steps for CMX53 are quite young averaging 1.0 ±0.7 Ma. The ages and radiogenic yields are variable with large errors in the lowest temperature steps. Also, an increase in age occurs in the high temperature steps at approximately 1400°. The Cl/K ratio is low (<7) throughout the spectra, but is especially low, (<1) in the intermediate steps. This Cl/K value provides an excellent indicator of the minerals being

analyzed in the $^{40}Ar/^{39}Ar$ measurement. Most k-bearing minerals do not have a Cl/K ratio as high as the quartz from Capitan. For instance sylvite has a Cl/K of 1, and most feldspars have negligible Cl driving the Cl/K ratio towards zero. This quartz sample has an unusually low Cl/K ratio, but also exhibits behavior anomalous relative to the other quartz crystals.

The second behavior is shown in sample CPU253 (Figure 11 B). The middle temperature range (800°-1200° C) yields an age (28.6 ± 1.1 Ma) that is statistically identical to the known age of the pluton. It has relatively high radiogenic yield (> 50%), and a very low Cl/K ratio of < 0.05.

Two samples, MTEE53 and HH53 grains (Figure 11 C and D) exhibit the third behavior, which was expected behavior from the quartz. The ages are old, relative to the known age of the pluton, and the grains have Cl/K ratios similar to the 6.5 ratio obtained from crush-leach analysis of quartz. The radiogenic yields are significantly lower than seen in CPU253 and higher than CMX53.

The fourth behavior is seen only in W353 (Figure 11 E). Almost no gas is released until the last 2 high temperature steps, which yield young (7.76 and 1.27 Ma) ages. The Cl/K and radiogenic yields are also very low (< 1 and 17.6 % respectively). Possible reasons for these four behaviors will be examined in detail later.

Table 8 Summary of Ages and Cl/K ratios from Low Fluid Inclusion Density Grains

		Integrated Age			800-1200° C			< 800° C			> 1200° C		
		Cl/K	Age	±1σ	Cl/K	Age	±1σ	Cl/K	Age	±1σ	Cl/K	Age	±1σ
Sample	Irradiatio		(Ma)	(Ma)		(Ma)	(Ma)		(Ma)	(Ma)		(Ma)	(Ma)
MTEE53	53-TB1	6.5	56.6	11.2	6.1	32.0	3.9	6.9	54.6	9.8	6.5	42.6	4.3
W353	53-TB1	0.2	3.8	0.3	7.4	27.8	13.2	-248.8	20.0	3.6	0.1	2.1	1.5
CMX53	53-TR2	0.9	23.5	1.3	0.3	1.0	0.7	4.9	63.0	44.7	0.9	3.9	5.4
CPU253	53-TR2	0.1	36.3	2.9	0.1	28.6	1.1	5.5	263.3	69.3	0.1	28.6	1.2
HH53	53-TR2	3.0	79.1	5.8	2.2	36.5	3.0	6.9	81.5	24.5	1.9	68.1	11.6

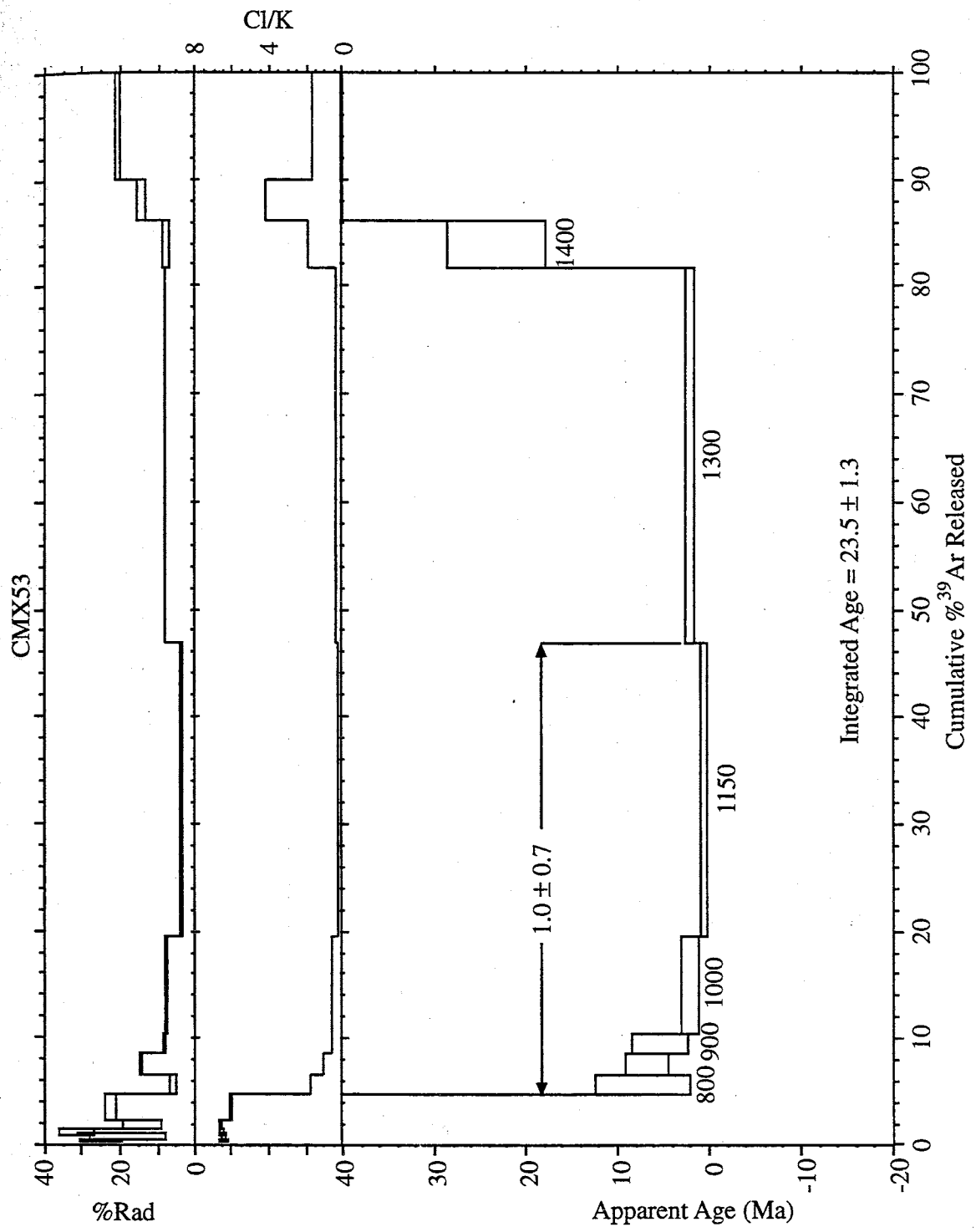
CMX53
Cl/K
8
4
0
%Rad
40
20
0
Apparent Age (Ma)
40
30
20
10
0
-10
-20
1400
1300
1150
1000
900
800
1.0 ± 0.7
Integrated Age = 23.5 ± 1.3
Cumulative %^{39}Ar Released
0
10
20
30
40
50
60
70
80
90
100

Figure 11 A

Figure 11 Age spectra from step-heating quartz grains A.) CMX2 shows a very young plateau age from a single large grain and bulk Cl/K of less than 1. B) CPU2 shows an plateau age from a single large grain approaching the known age of the pluton, but has a very low Cl/K ratio. C.) Single large grain age spectra from MTE showing a old high temperature age plateau, and Cl/K similar to crush-leach values. D.) Single large grain age spectra from HH showing another old plateau with a Cl/K similar to crush leach values

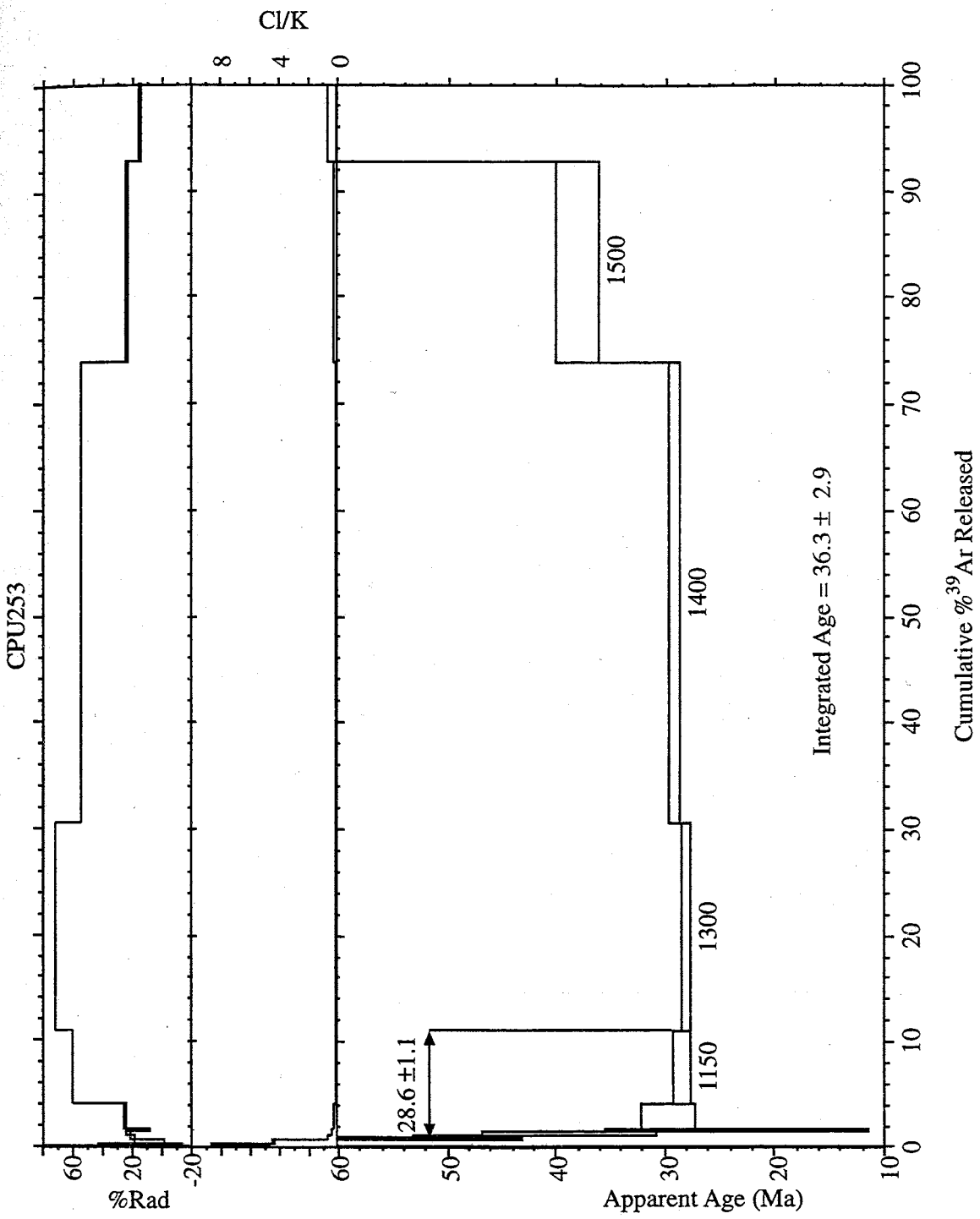
Cl/K
8
4
0
CPU253
100
90
80
70
60
50
40
30
20
10
0
1500
1400
1300
1150
Integrated Age = 36.3 ± 2.9
Cumulative %^{39}Ar Released
28.6 ±1.1
60
20
-20
%Rad
60
50
40
30
20
10
Apparent Age (Ma)

Figure 11 B

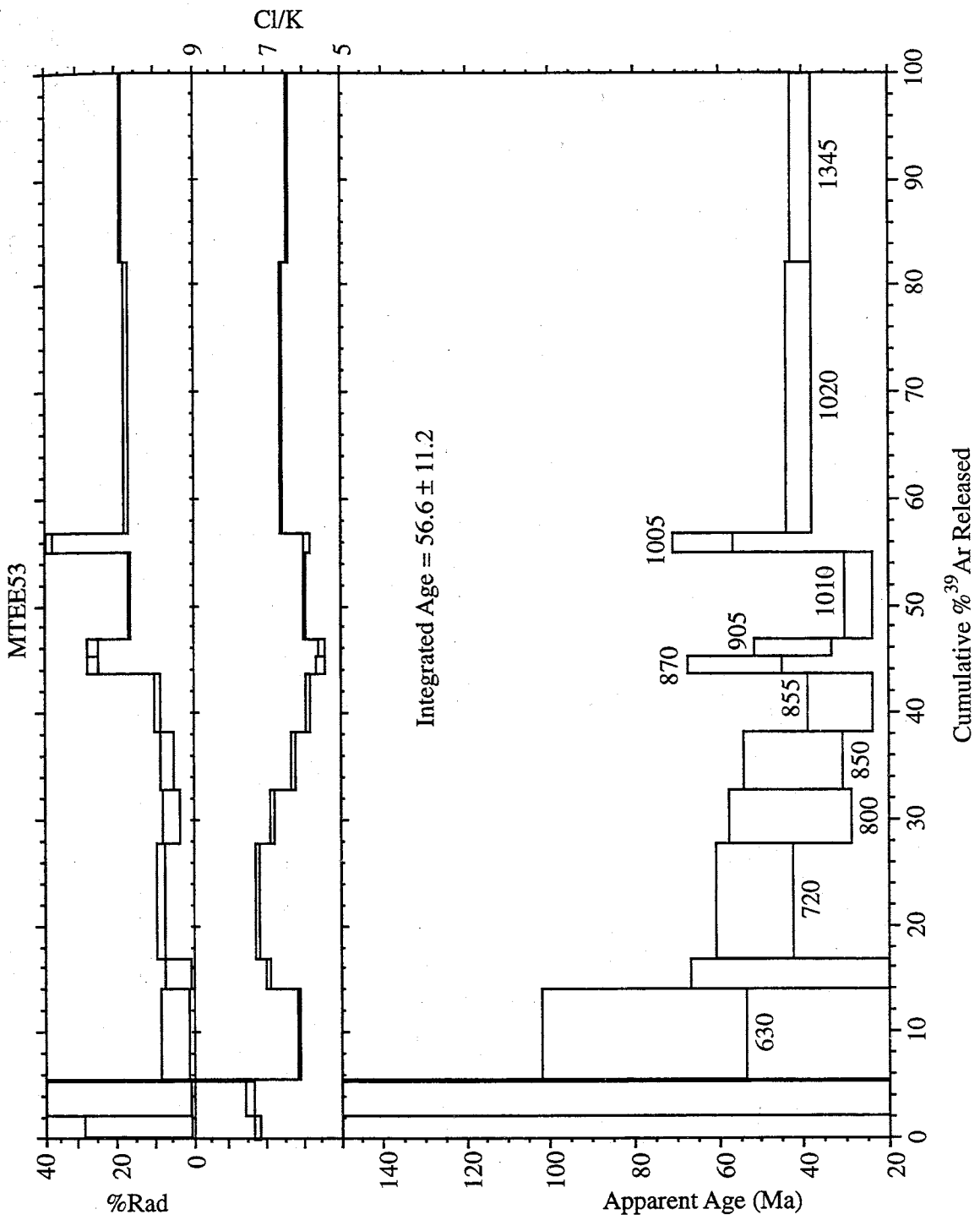
MTE53
Cl/K
9
7
5
%Rad
40
20
0
Integrated Age = 56.6 ± 11.2
Apparent Age (Ma)
140
120
100
80
60
40
20
Cumulative %^{39}Ar Released
0
10
20
30
40
50
60
70
80
90
100
630
720
800
850
855
870
905
1010
1005
1020
1345

Figure 11 C

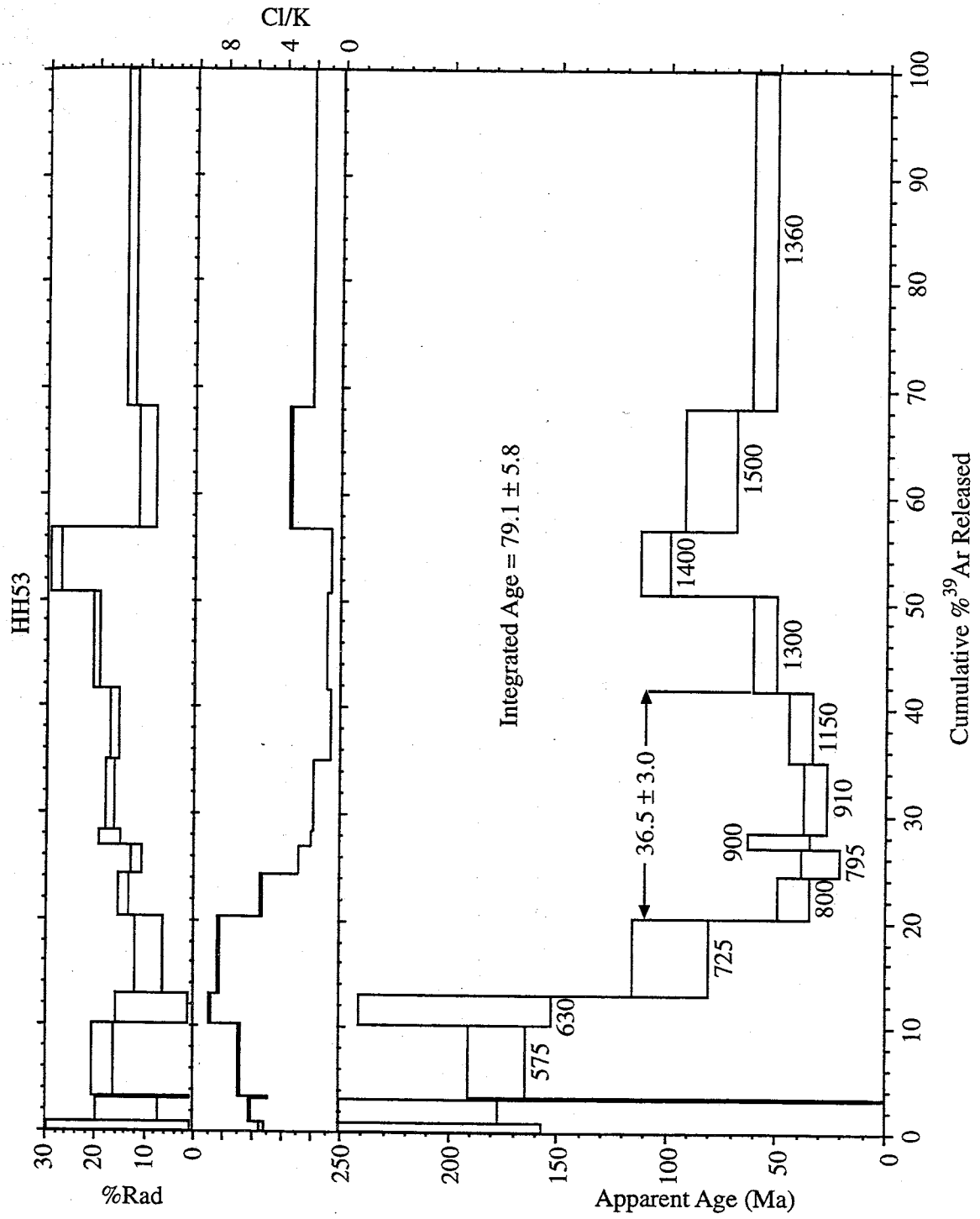
HH53
Cl/K
8
4
0
%Rad
30
20
10
0
Apparent Age (Ma)
250
200
150
100
50
0
Integrated Age = 79.1 ± 5.8
36.5 ± 3.0
575
630
725
800
795
900
910
1150
1300
1400
1500
1360
Cumulative %^{39}Ar Released
0
10
20
30
40
50
60
70
80
90
100

Figure 11 D

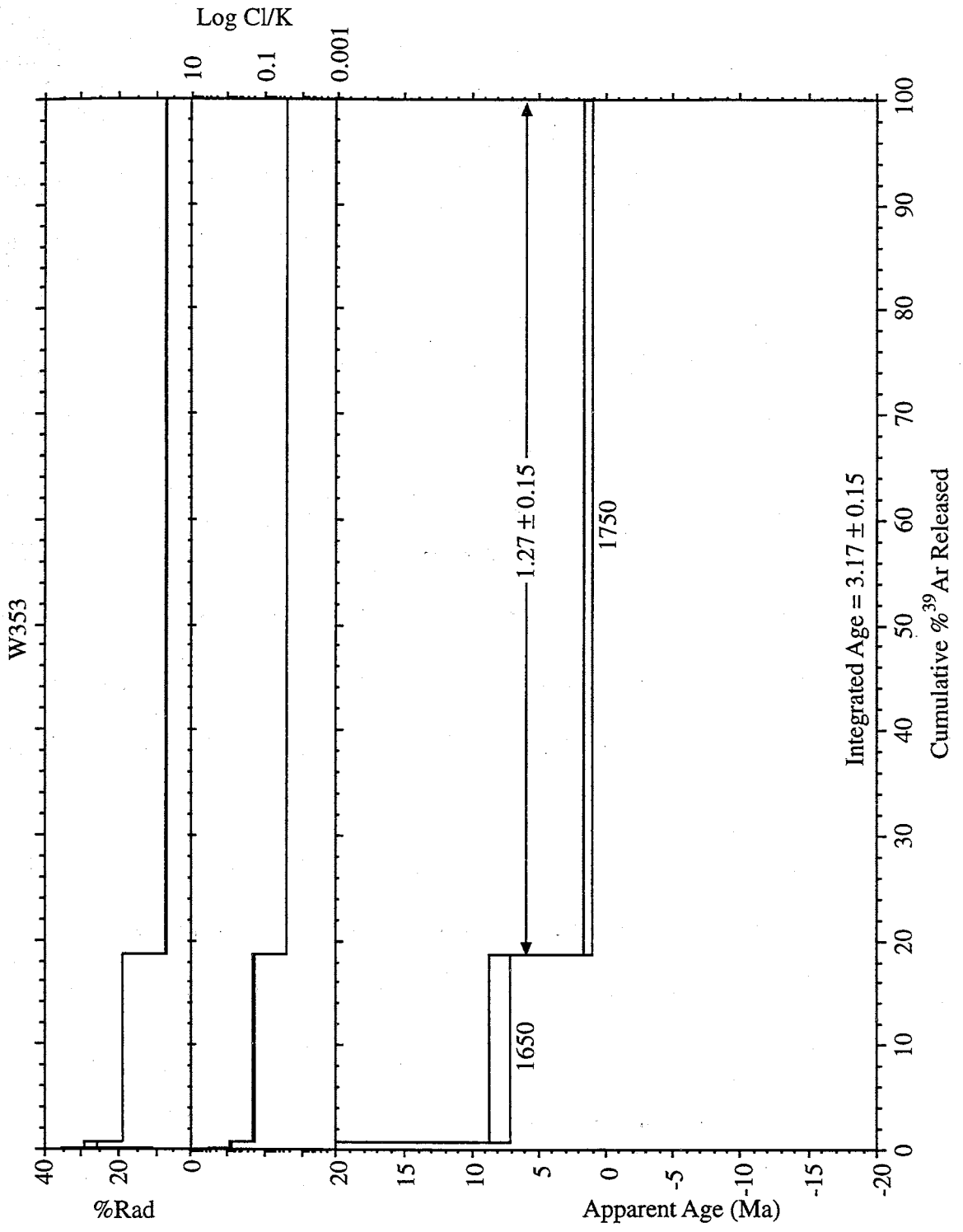
Log Cl/K
10
0.1
0.001
W353
1.27 ± 0.15
1750
1650
Integrated Age = 3.17 ± 0.15
Cumulative %^{39}Ar Released
%Rad
Apparent Age (Ma)

Figure 11 E

5.2.3. Results from Pre-irradiation Crushing

Samples from MTE and CPU2, each with two crushed size fractions, were used to determine the effect of crushing prior to irradiation. The samples were crushed to <53 μm (MTE<5353 and CPU<5353) and 53-63 μm (MTE>5353 and CPU>5353). The uncrushed splits of these samples were presented in the previous section, shown in Figure 11 B and C respectively. Each of the crushed samples weight approximately 200 mg, similar to the weight of the uncrushed large grains. The ages determined from the crushed samples (Figure 12) are significantly younger than the uncrushed samples (Figure 11 B and C). All four crushed separates yield ages under 10 Ma, for the temperature steps below 900° C. The young age steps do not quite overlap at 2σ error but contain a significant proportion of the ^{39}Ar. Above 900° C there is an increase in the age accompanied by an increase in Cl/K. The Cl/K is significantly lower than in the uncrushed large grain samples. The bulk Cl/K is less than 1 for all four samples. Both samples show a decrease in age from the uncrushed grain to the 53-63 μm the <53 μm. However, both splits from both samples have integrated ages that agree within error. The signal sizes normalized to weight are similar in all of the samples, however the radiogenic yield of all the samples from MTE and the crushed samples from CPU2 are relatively low compared to large grain analyses from CPU2 (Figure 11 B). Complete data tables are given in Appendix L.

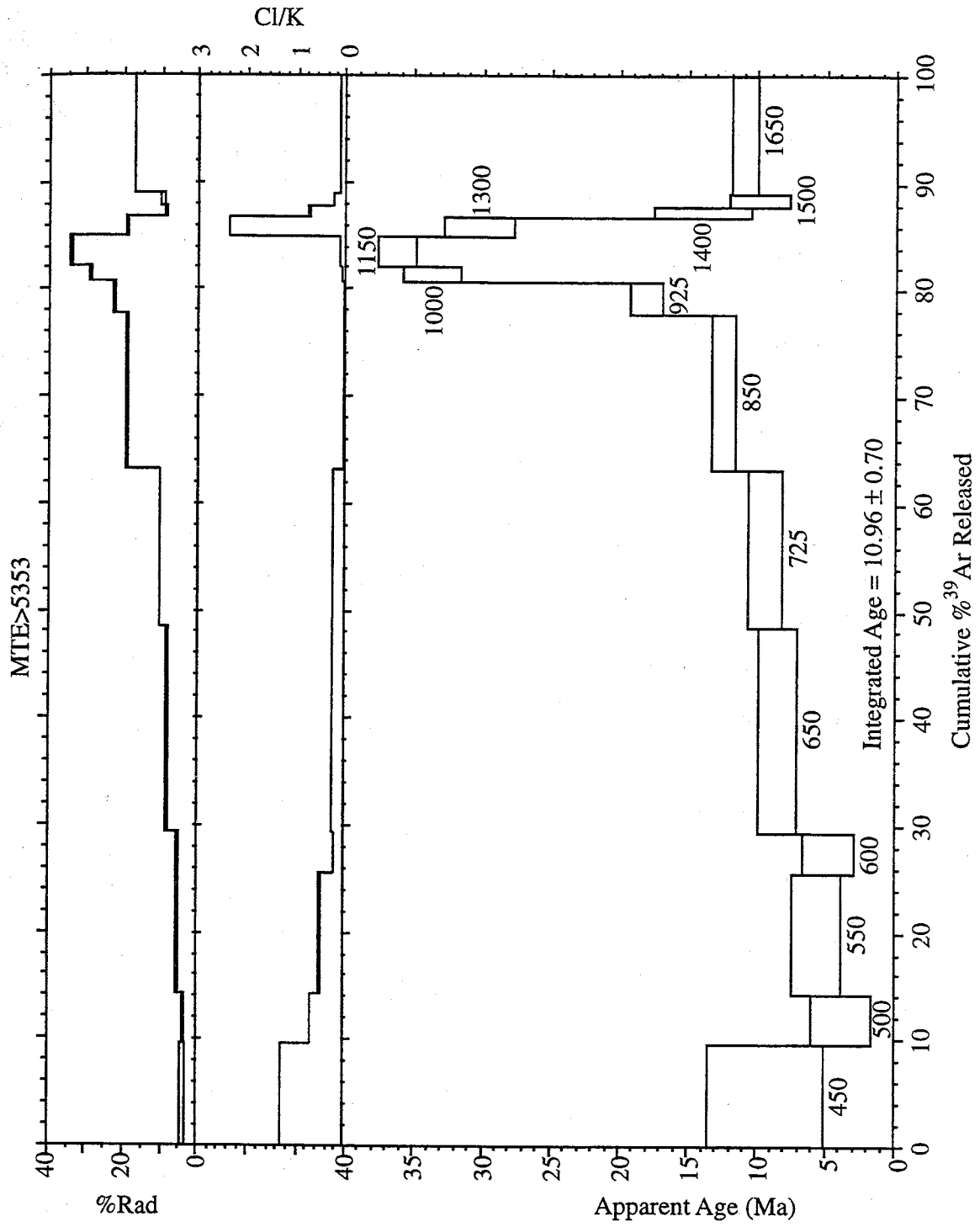
Cl/K
MTE>5353
%Rad
Apparent Age (Ma)
Integrated Age = 10.96 ± 0.70
Cumulative %^{39}Ar Released
450
500
550
600
650
725
850
925
1000
1150
1300
1400
1500
1650

Figure 12 A

Figure 12 Age spectra from quartz crushed prior to irradiation. A and B.) Two size fractions from MTE quartz are shown 63-53μm, <53μm, respectively. The age of the sample plateau is younger with increased crushing. C and D.) Similar age spectra from CPU2 Quartz showing similar behavior. In both samples the Cl/K ratio is low relative to the values obtained through crush leach analysis. Results from the uncrushed (14-20 mesh) samples of MTE and CPU are shown in Figure 11 B and C.

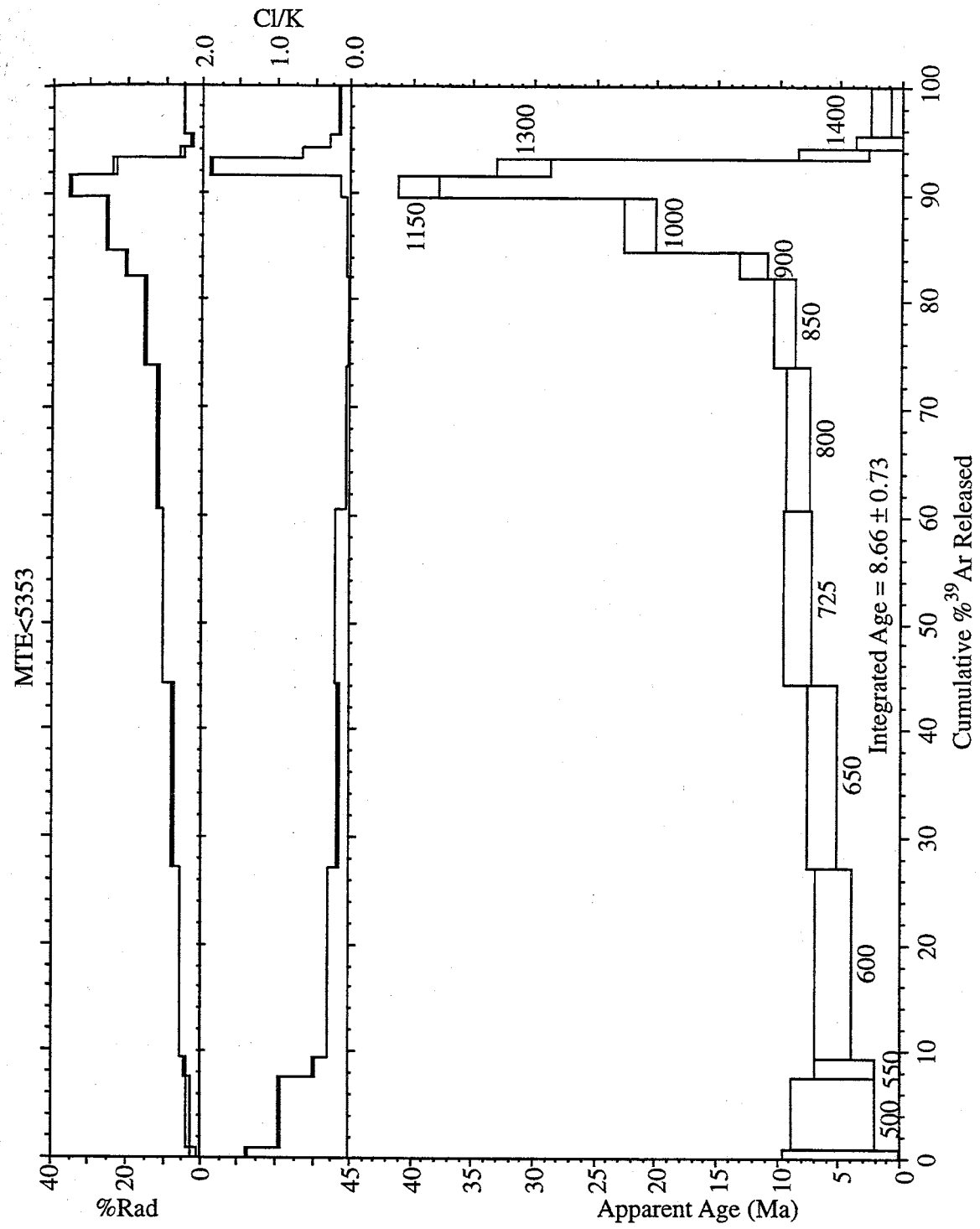
Cl/K
2.0
1.0
0.0
MTE<5353
1400
1300
1150
1000
900
850
800
725
650
600
550
500
Integrated Age = 8.66 ± 0.73
Cumulative %^{39}Ar Released
%Rad
Apparent Age (Ma)

Figure 12 B

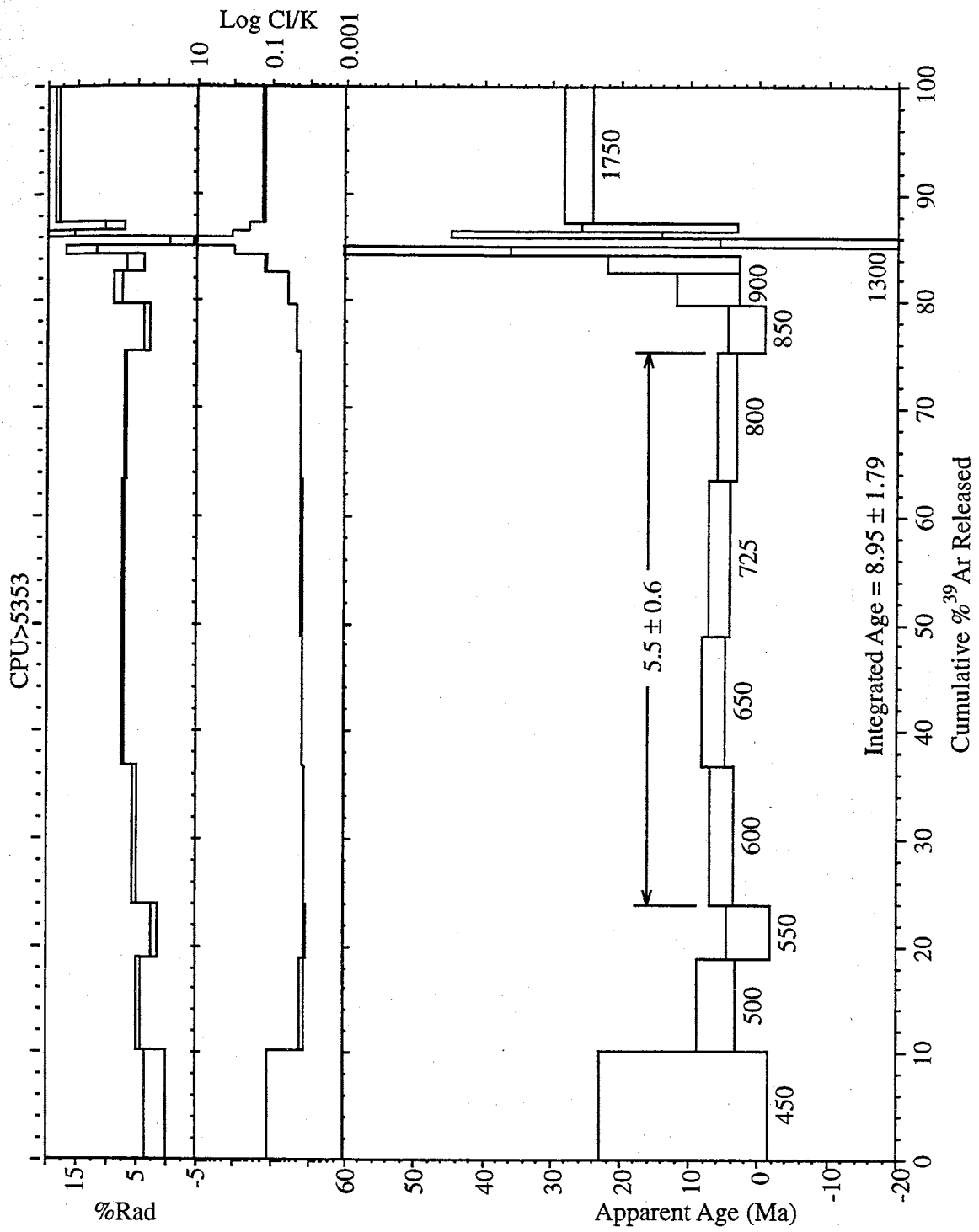
Log Cl/K
10
0.1
0.001
CPU>5353
%Rad
15
5
-5
60
50
40
30
20
10
0
-10
-20
Apparent Age (Ma)
1750
900
850
800
725
650
600
550
500
450
1300
5.5 ± 0.6
Integrated Age = 8.95 ± 1.79
Cumulative %^{39}Ar Released
0
10
20
30
40
50
60
70
80
90
100

Figure 12 C

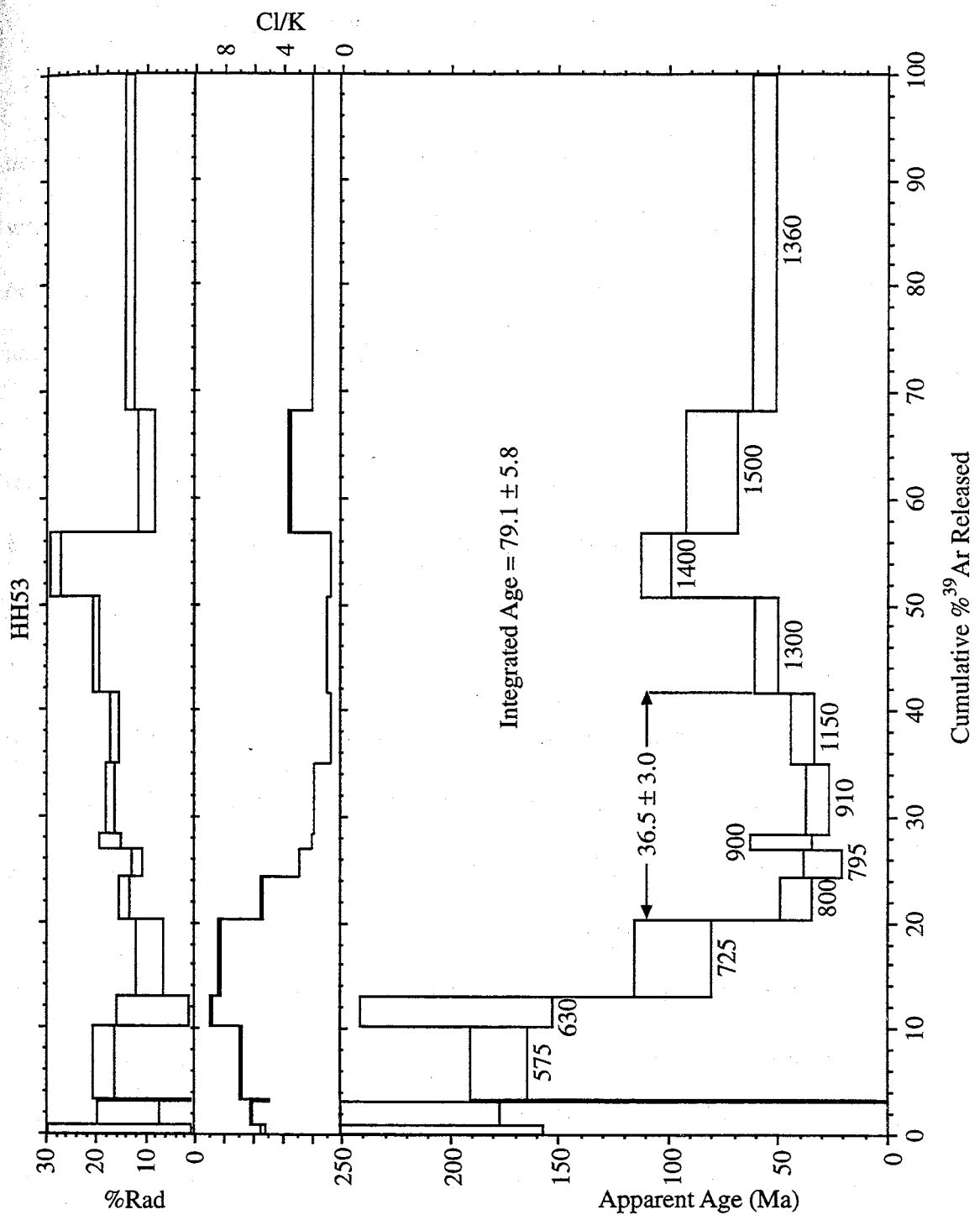
HH53
Cl/K
8
4
0
%Rad
30
20
10
0
Apparent Age (Ma)
250
200
150
100
50
0
Integrated Age = 79.1 ± 5.8
36.5 ± 3.0
575
630
725
800
795
900
910
1150
1300
1400
1500
1360
0
10
20
30
40
50
60
70
80
90
100
Cumulative % ^{39}Ar Released

Figure 12 D

5.2.4. Step Heating of High Fluid Inclusion Density Chips

To resolve the issues that arise during analysis of grains of low fluid inclusion density tips of the quartz, polished chips of quartz from closer to the base of the crystal which have a higher density of fluid inclusions were examined and analyzed. The higher density of inclusions was expected to raise the signal size and the electron microprobe and optical examination should have prevented contamination by adhered adularia.

Age spectra produced from step heating the high fluid inclusion density chips (HFIDC) are all similar. Complete data tables are given in Appendix F. The spectra from step heating the HFIDCs shown in Figure 13 have variable, but relatively high radiogenic yields, typically rising during the high temperature part of the spectra. K/Ca ratios (not show on these diagrams, but given in Appendix F) tend to decrease at high temperatures (above 900°C). The Cl/K ratios of the samples remain essentially constant at approximately 6.5 (equal to the value obtained by crush leach analysis, Section 3) throughout the heating schedule except for the 800 - 1200° C steps. For these steps, both the Cl/K and age decrease (Figure 13). Also, this heating interval is where the smallest amount of gas was released, despite raising the temperature several hundred degrees C°. Six of the eight ages agree within error at this temperature range, but are significantly older than the age of the Capitan pluton and veins (Table 9). The age spectra from sample MTEB (Figure 13 H) has a slightly different appearance, compared tot he other sampleswhich is a result of the abbreviated heating schedule used to maximize the signal size in this particularly small sample. Presumably, this spectrum would exhibit a similar pattern if it were step heated with similar resolution. However, more importantly, all samples from CMX and MTE (Figure 13 A, B, C, G, and H) yield well-defined high

temperature plateau segments. The plateau ages have low uncertainties and are much older that the age of the pluton. These ages are given in Table 9. Samples from W3 (Figure 13 D, E, and F) show erratic behavior in the high temperature steps of the age spectra, possibly due to low fluid inclusion density. The high temperature steps of samples from MTE and CMX meet the criteria for plateaus (3 or more steps that overlap within 2σ and represent 50% or more of the total ^{39}Ar released), containing up to five steps and up to 55% of the ^{39}Ar released in this portion of the spectra.

Another way of presenting the data is an age probability distribution diagram (Deino and Potts, 1991). The age probability distribution diagram is a type of "weighted" histogram (Figure 14). The ages obtained from analysis are weighted with respect to their errors and a curve representing the relative probability of each age occurring is shown in the bottom panel. The middle panel shows the apparent ages with their errors. The top panel shows the Cl/K ratio for each analysis. Wide peaks in the relative probability curve represent large uncertainties. Narrow peaks represent small uncertainties in the age. The height of the peaks represents the relative probability of the age's occurrence. Age probability distribution diagrams for the medium temperature (800°-1200°C) and the high temperature steps (1200° - 1800°C) steps of all of the HFIDCs are shown in Figure 14 A and B, respectively.

Table 9 Summary of middle and high temperature ages from HFIDCs

		Integrated Age			800-1200° C			< 800° C			> 1200° C		
		Cl/K	Age	±1s	Cl/K	Age	±1s	Cl/K	Age	±1s	Cl/K	Age	±1s
Sample	Irradiation		(Ma)	(Ma)		(Ma)	(Ma)		(Ma)	(Ma)		(Ma)	(Ma)
CMXA	91-TB1	6.2	159.0	10.2	5.8	43.4	5.0	6.5	150.9	46.3	6.1	81.7	4.1
CMXB	91-TB1	6.8	239.4	26.2	6.9	36.2	26.9	6.8	263.9	90.0	6.6	145.1	11.9
CMXC	91-TB1	6.7	253.1	14.3	5.9	61.2	15.3	7.0	195.9	70.5	6.5	166.9	5.1
CMXD	91-TB1	6.7	328.5	14.8	3.8	83.9	7.7	7.7	281.1	65.3	6.3	205.1	14.9
CMXE	91-TB1	5.7	432.7	22.4									
CMXEC	91-TB1	9.6	144.7	33.2	2.7	197.2	65.8	13.1	27.0	23.3	6.0	175.5	37.2
CMXET	91-TB1	6.7	359.3	25.1									
MTEB	91-TB1	7.6	71.7	22.3	6.2	55.0	18.2	8.5	105.1	10.8	7.1	66.0	3.2
MTEC1	91-TB1	2.2	46.4	3.6	1.4	37.2	10.3	7.6	172.7	0.0	3.9	51.3	0.0
MTEC2	91-TB1	7.5	56.6	17.0	6.1	43.0	10.7	8.6	57.9	6.7	7.1	47.4	2.1
MTED	91-TB1	6.9	57.0	15.0	6.1	34.1	11.5	7.9	74.3	10.9	6.5	43.1	2.3
MTEE	91-TB1	7.1	163.9	49.3									
MTEELC	91-TB1	7.4	79.8	13.6	6.6	50.7	17.9	9.2	107.0	15.4	6.9	85.4	2.3
MTEESC	91-TB1	7.4	96.8	26.4	4.0	113.9	29.3	9.4	27.5	31.6	6.6	87.0	6.1
MTEET	91-TB1	7.3	100.9	23.9									
W3A	91-TB1	7.6	213.1	5.6	7.0	48.1	9.6	7.8	214.8	150.9	7.3	125.2	15.1
W3CD	91-TB1	6.1	236.9	7.2	5.1	50.9	6.7	6.3	182.5	61.2	6.1	214.2	32.4
W3E	91-TB1	5.0	416.8	28.0	2.0	47.0	14.0	7.3	342.2	127.9	4.2	346.8	77.0
W3F	91-TB1	5.4	488.9	32.5									
W3FC	91-TB1	9.3	425.7	441.8	1.5	906.3	142.7	15.7	290.1	132.6	4.7	149.2	394.6
W3FT	91-TB1	6.2	475.6	118.2									
W3G	91-TB1	7.1	572.7	18.6	6.1	85.9	15.9	7.7	341.5	147.3	5.9	424.2	69.6

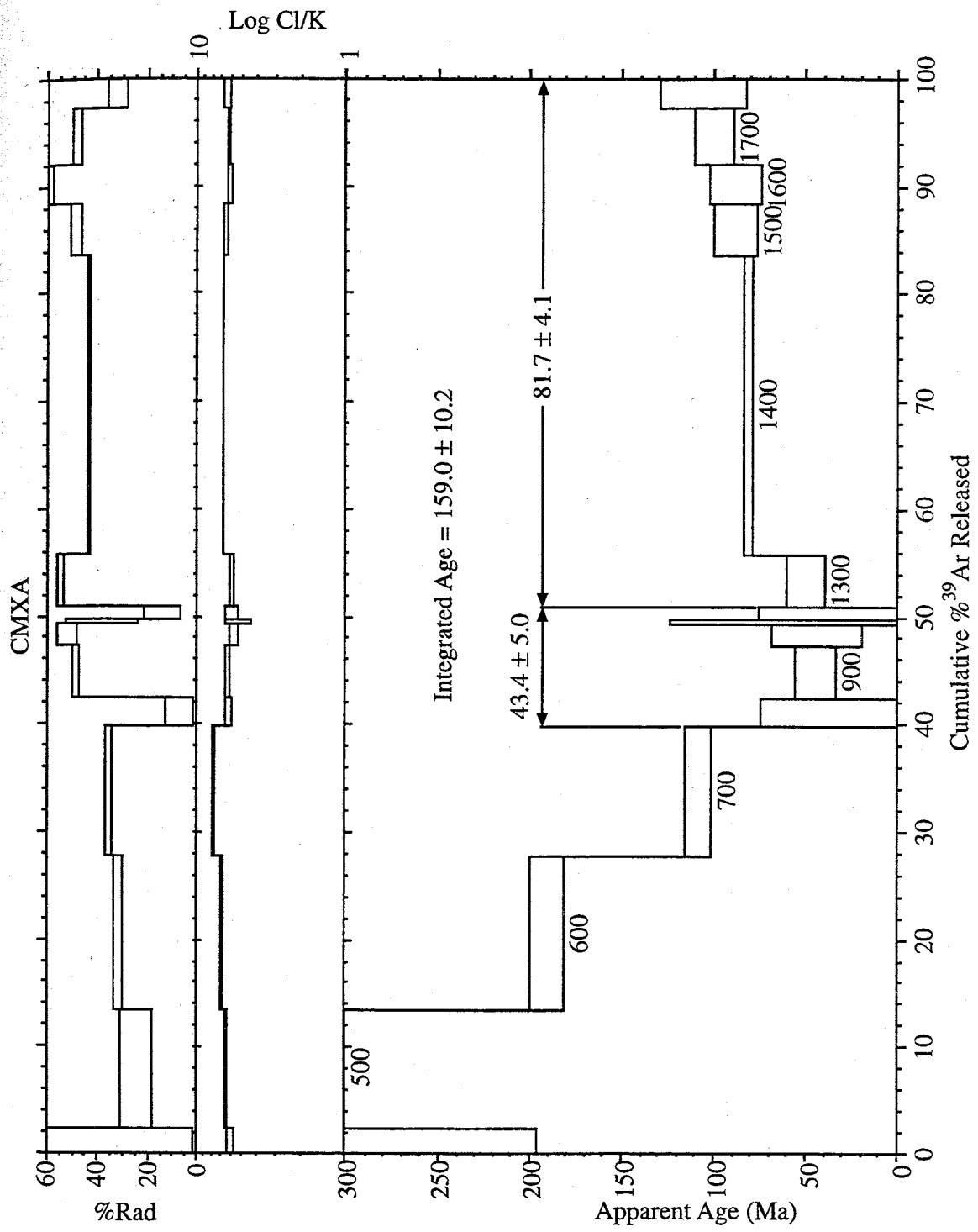
Log Cl/K
10
1
CMXA
%Rad
60
40
20
0
300
250
200
150
100
50
0
Apparent Age (Ma)
Integrated Age = 159.0 ± 10.2
81.7 ± 4.1
43.4 ± 5.0
500
600
700
900
1300
1400
1500
1600
1700
100
90
80
70
60
50
40
30
20
10
0
Cumulative %39Ar Released

Figure 13 A

Figure 13 Age spectra from step-heating of HFIDCs of quartz. A.) CMXA showing a saddle shaped spectra B.) CMXB showing a saddle shaped spectra C.) CMXD showing a saddle shaped spectra D.) W3A showing a saddle shaped spectra E.) W3E showing a saddle shaped spectra F.) W3G showing a saddle shaped spectra G.) MTED showing a plateau age of 43.1 ± 2.3 Ma H.) MTEB shows a plateau age of 66.0 ± 3.2 Ma.

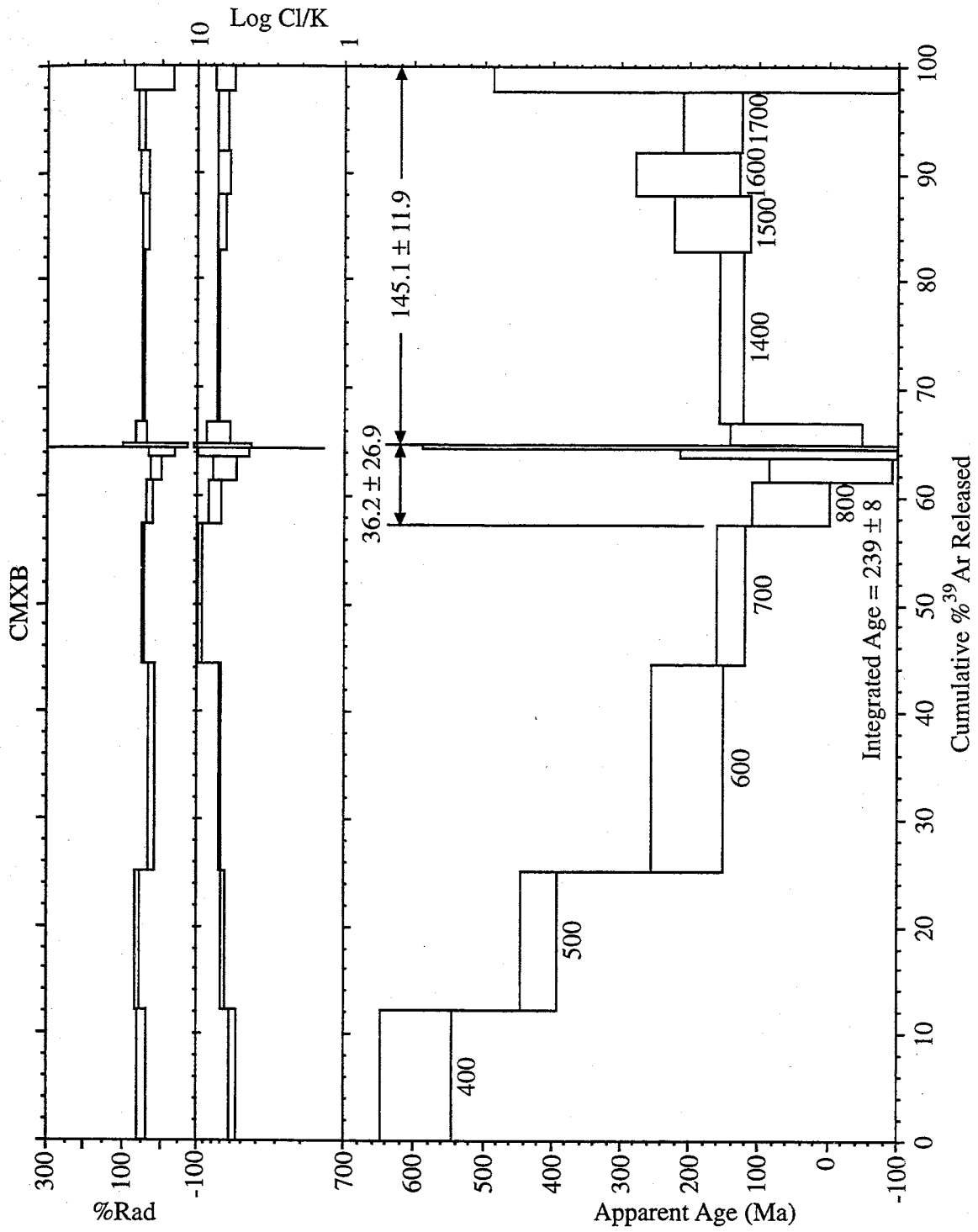
Log Cl/K
10
1
CMXB
145.1 ± 11.9
36.2 ± 26.9
Integrated Age = 239 ± 8
Cumulative %^{39}Ar Released
%Rad
Apparent Age (Ma)
300
100
-100
700
600
500
400
300
200
100
0
-100
100
90
80
70
60
50
40
30
20
10
0
400
500
600
700
800
1400
1500
1600
1700

Figure 13 B

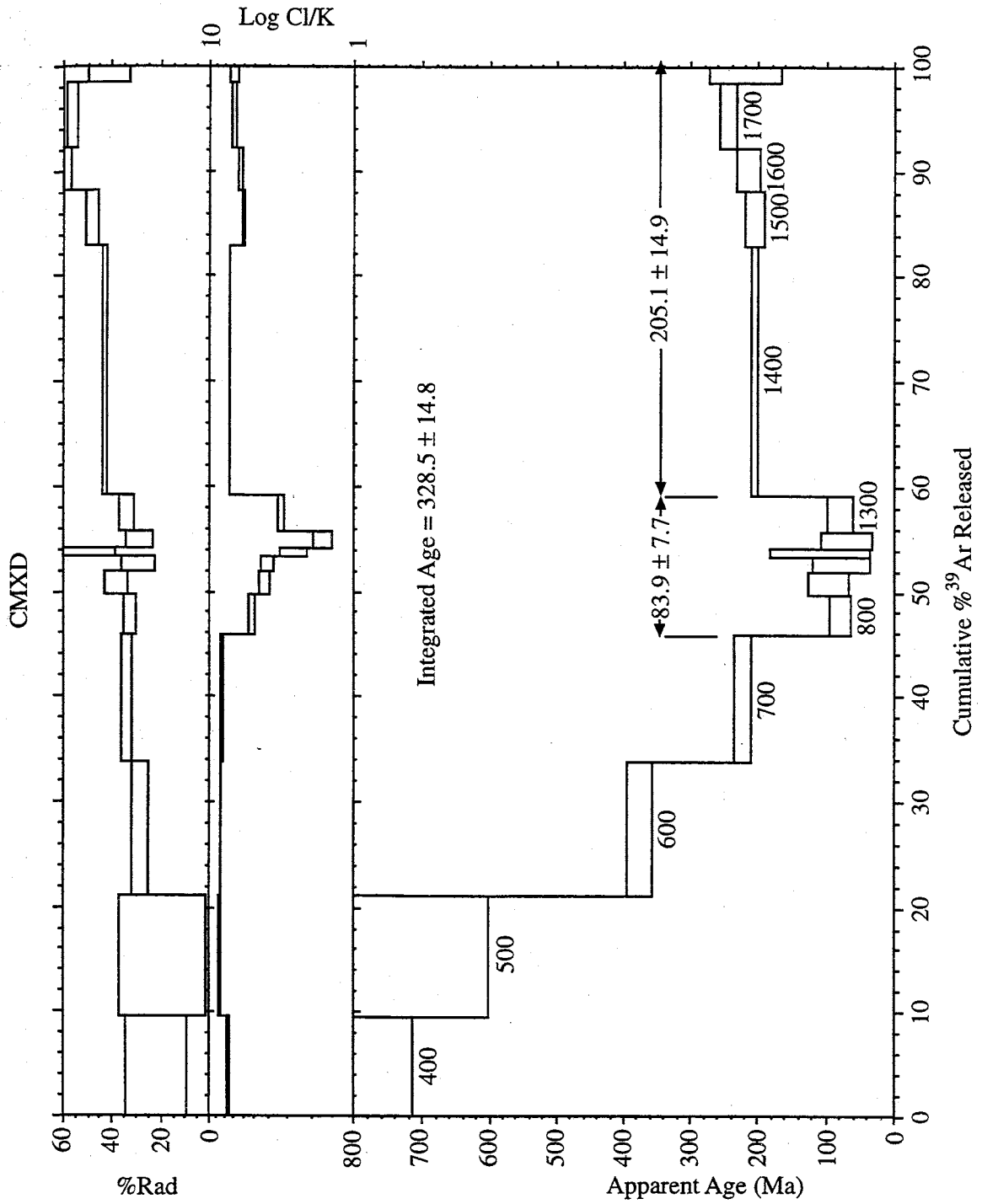
CMXD
Log Cl/K
10
1
Integrated Age = 328.5 ± 14.8
205.1 ± 14.9
83.9 ± 7.7
400
500
600
700
800
1300
1400
1500
1600
1700
%Rad
Apparent Age (Ma)
Cumulative %^{39}Ar Released

Figure 13 C

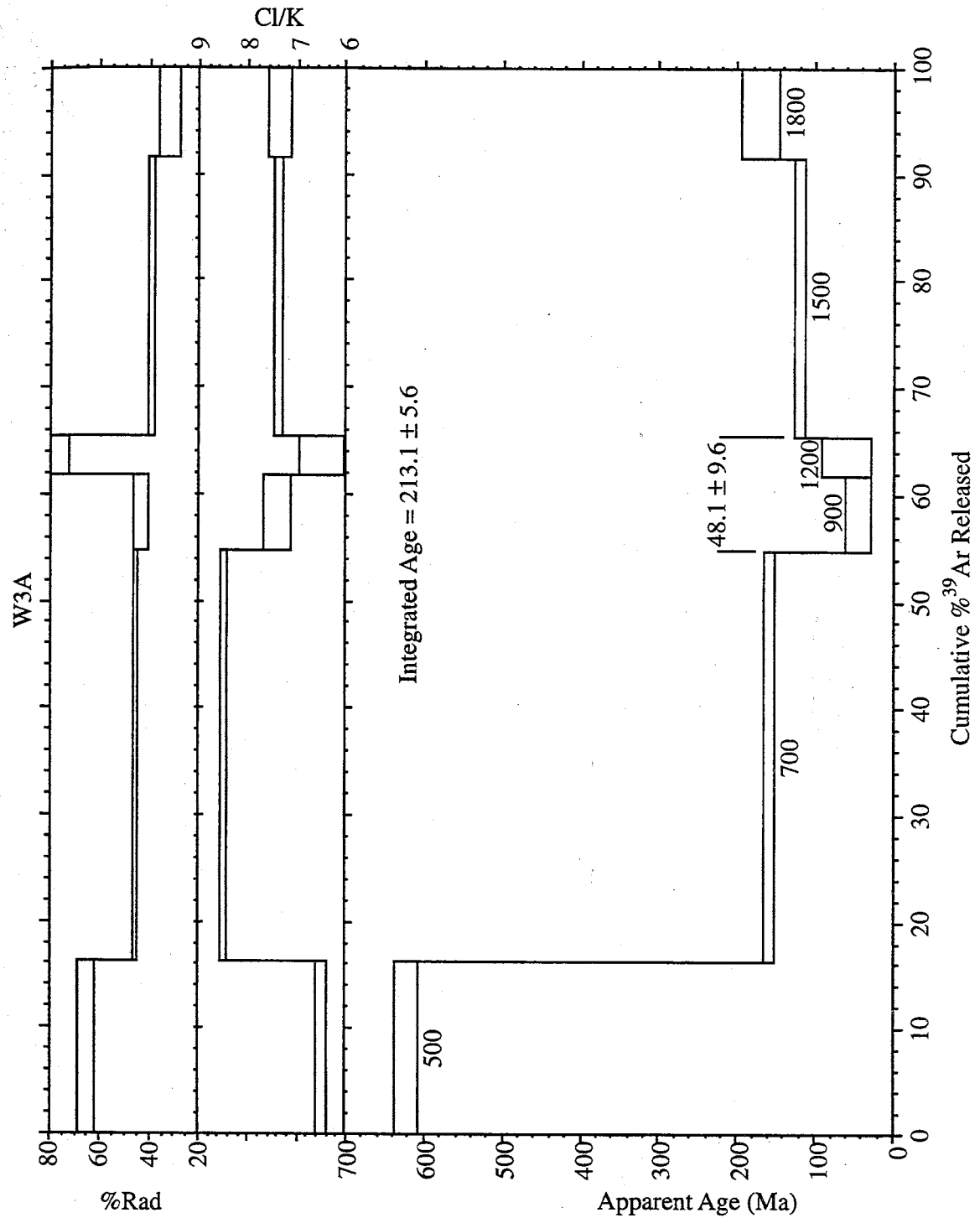
W3A
Cl/K
9
8
7
6
Integrated Age = 213.1 ± 5.6
48.1 ± 9.6
500
700
900
1200
1500
1800
%Rad
80
60
40
20
Apparent Age (Ma)
700
600
500
400
300
200
100
0
Cumulative %^{39}Ar Released
0
10
20
30
40
50
60
70
80
90
100

Figure 13 D

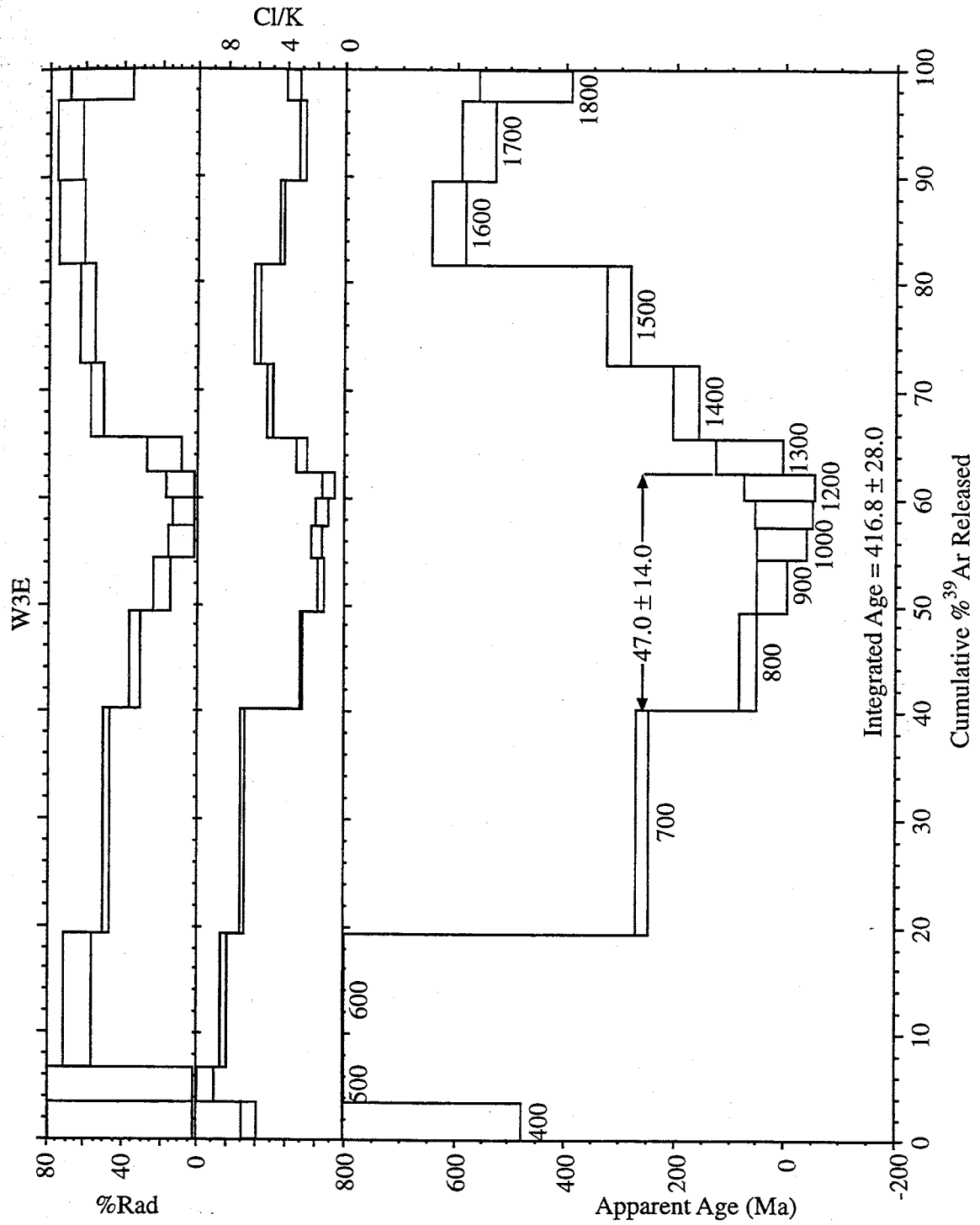
W3E
Cl/K
8
4
0
%Rad
80
40
0
800
600
400
200
0
-200
Apparent Age (Ma)
Integrated Age = 416.8 ± 28.0
47.0 ± 14.0
400
500
600
700
800
900
1000
1200
1300
1400
1500
1600
1700
1800
0
10
20
30
40
50
60
70
80
90
100
Cumulative % ^{39}Ar Released

Figure 13 E

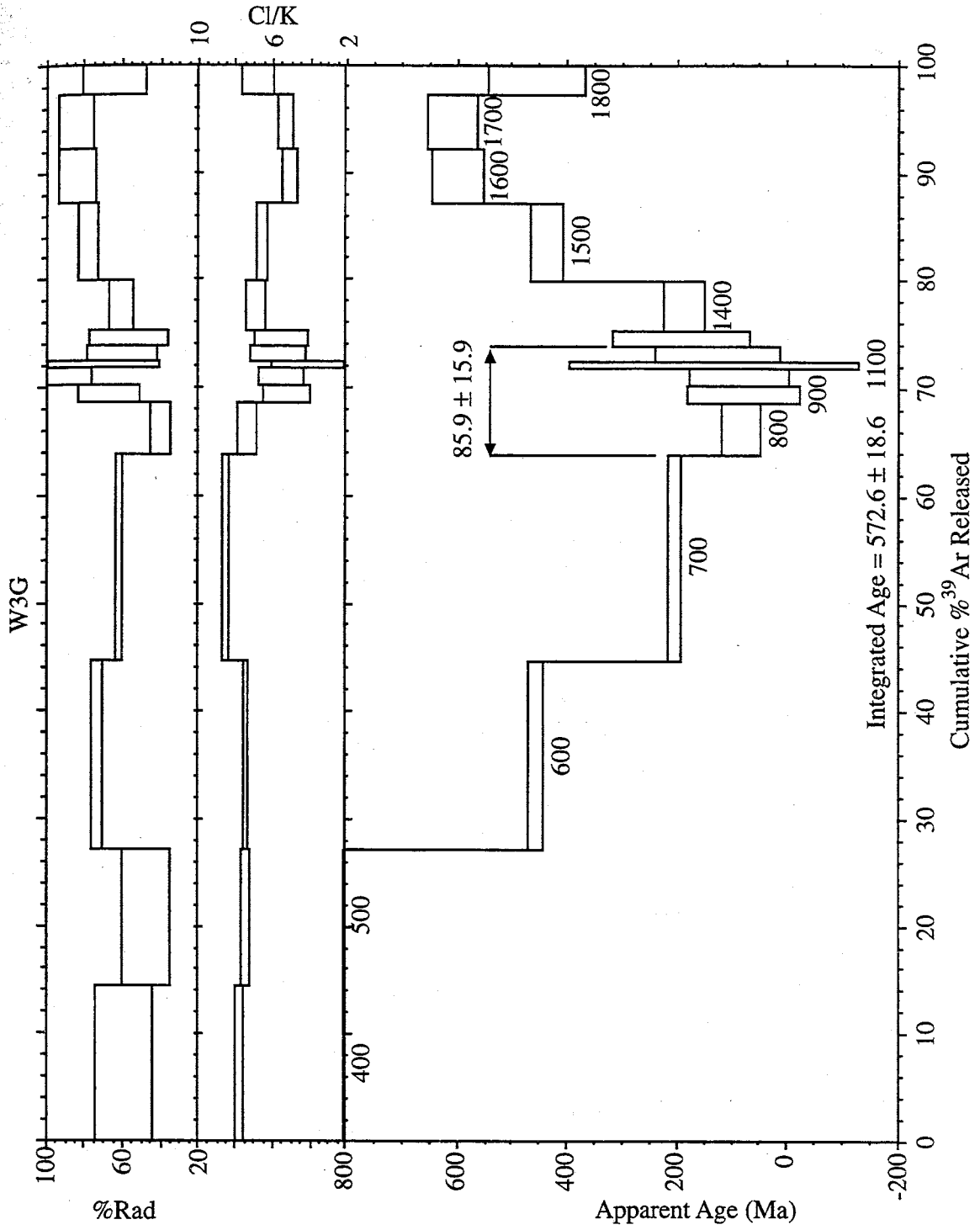
W3G
Cl/K
10
6
2
%Rad
100
60
20
Apparent Age (Ma)
800
600
400
200
0
-200
Cumulative %^{39}Ar Released
0
10
20
30
40
50
60
70
80
90
100
Integrated Age = 572.6 ± 18.6
85.9 ± 15.9
400
500
600
700
800
900
1100
1400
1500
1600
1700
1800

Figure 13 F

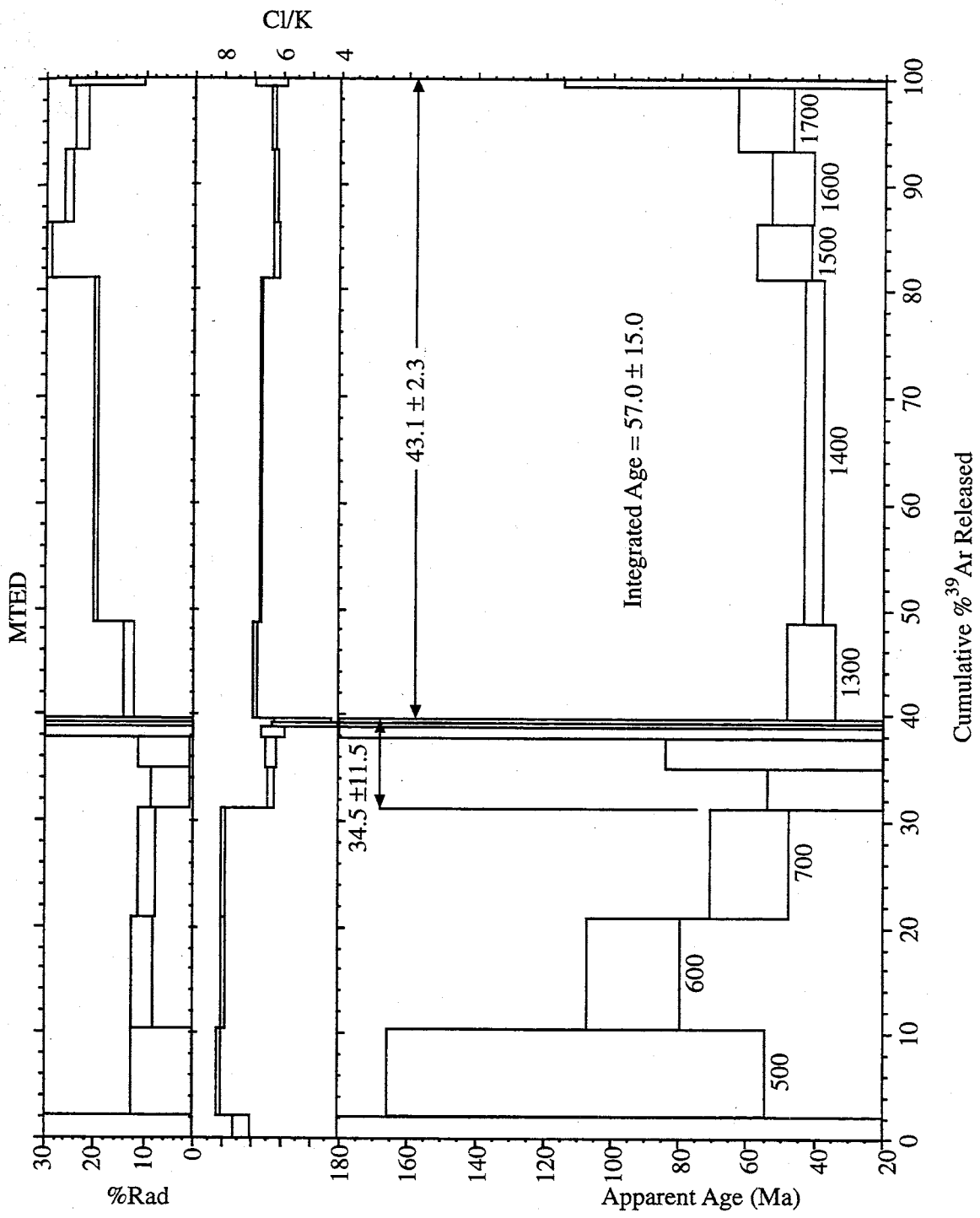
Cl/K
8
6
4
MTED
30
20
10
0
%Rad
180
160
140
120
100
80
60
40
20
Apparent Age (Ma)
43.1 ± 2.3
34.5 ±11.5
Integrated Age = 57.0 ± 15.0
1700
1600
1500
1400
1300
700
600
500
100
90
80
70
60
50
40
30
20
10
0
Cumulative %^{39}Ar Released

Figure 13 G

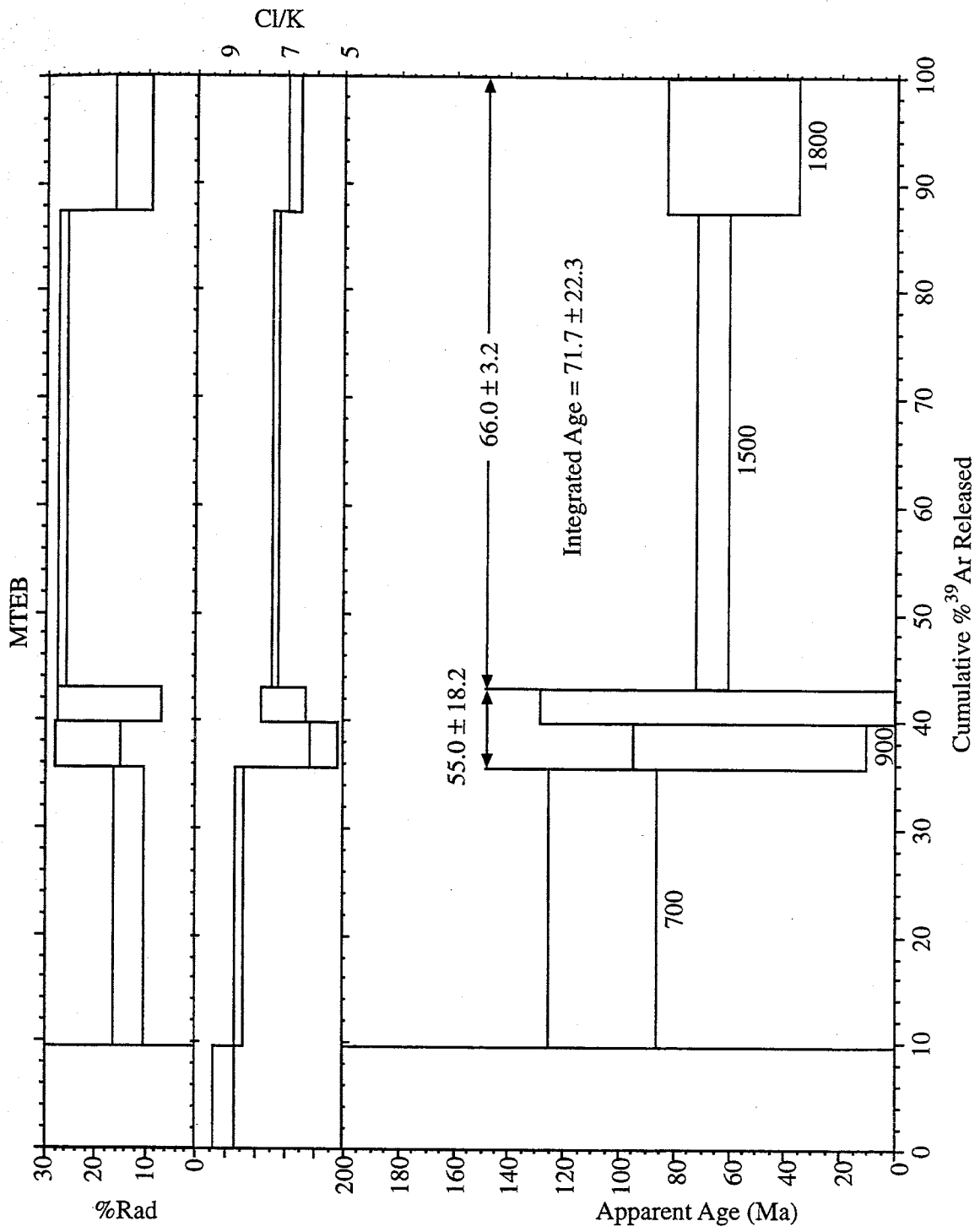
MTEB
%Rad
Cl/K
Apparent Age (Ma)
Cumulative %^{39}Ar Released
Integrated Age = 71.7 ± 22.3
66.0 ± 3.2
55.0 ± 18.2
700
900
1500
1800

Figure 13 H

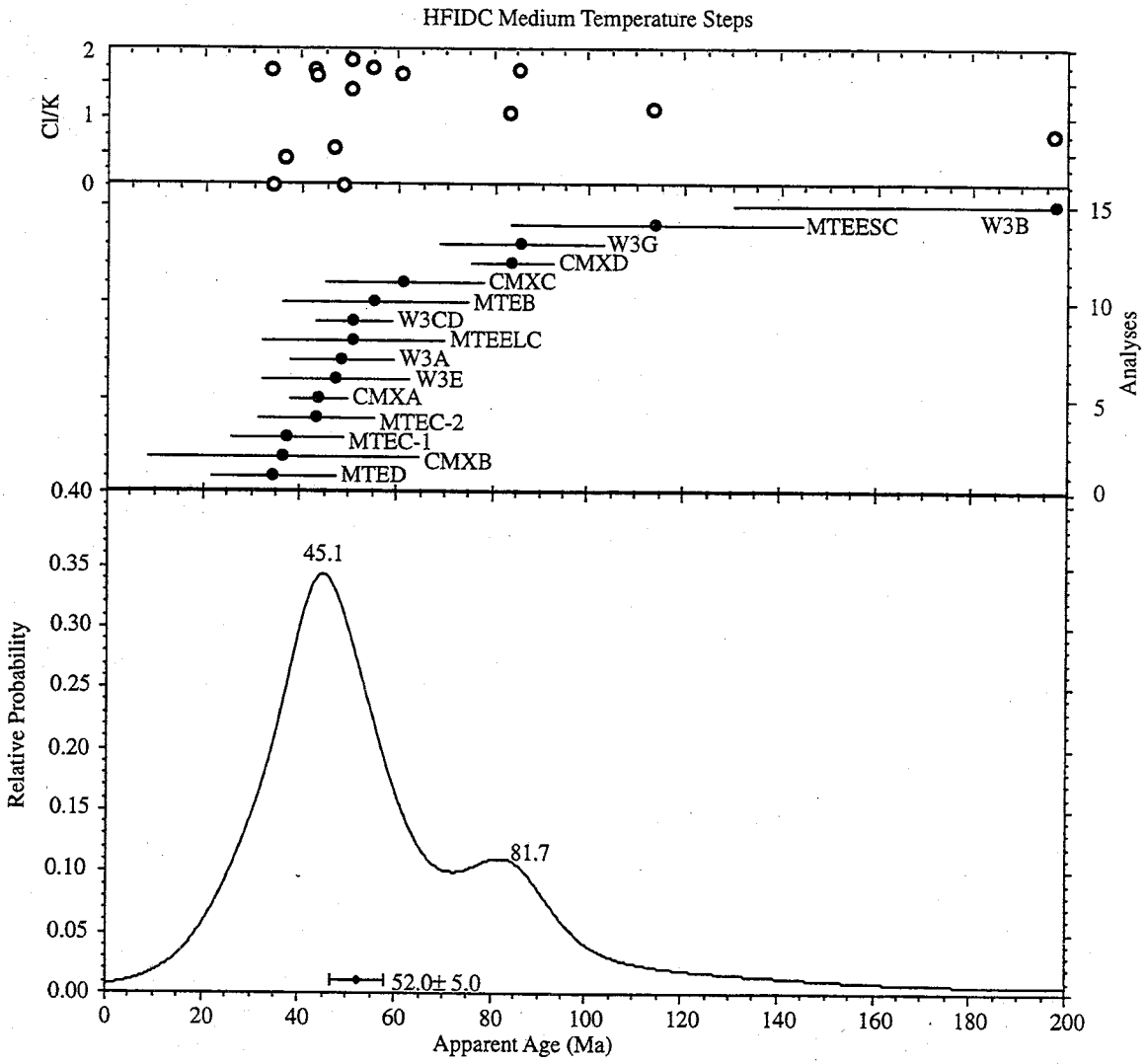
HFIDC Medium Temperature Steps
Cl/K
2
1
0
MTEESC
W3B
W3G
CMXD
CMXC
MTEB
W3CD
MTEELC
W3A
W3E
CMXA
MTEC-2
MTEC-1
CMXB
MTED
15
10
5
0
Analyses
0.40
0.35
0.30
0.25
0.20
0.15
0.10
0.05
0.00
Relative Probability
45.1
81.7
52.0± 5.0
0
20
40
60
80
100
120
140
160
180
200
Apparent Age (Ma)

Figure 14 A

Figure 14 Age probability distribution diagrams for medium and high temperature ages from HFIDCs A.) Medium temperature steps B.) High temperature steps Also shown are the sample numbers and Cl/K ratios.

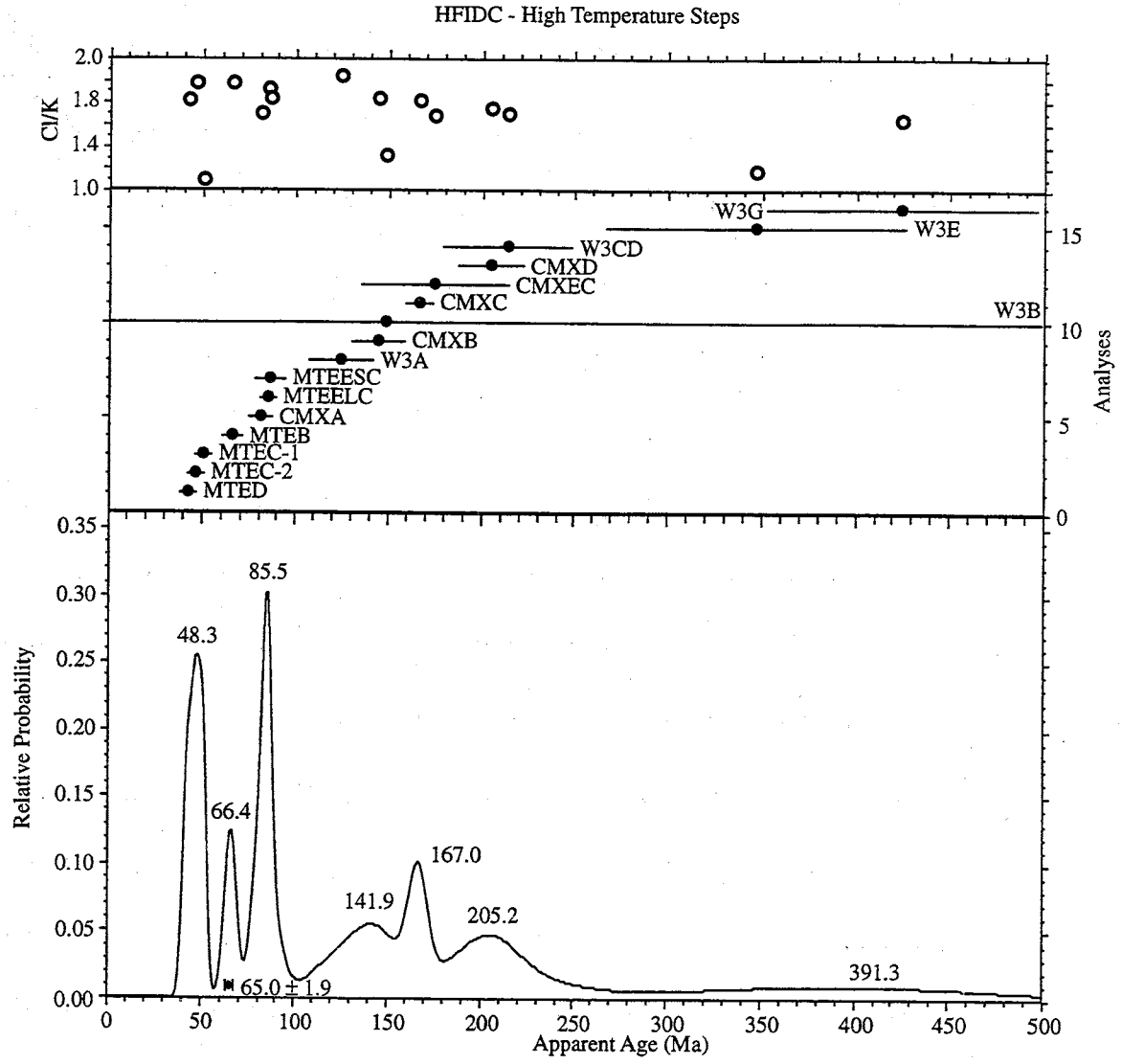
HFIDC - High Temperature Steps
Cl/K
2.0
1.8
1.4
1.0
W3G
W3E
W3CD
CMXD
CMXEC
CMXC
W3B
CMXB
W3A
MTEESC
MTEELC
CMXA
MTEB
MTEC-1
MTEC-2
MTED
15
10
5
0
Analyses
0.35
0.30
0.25
0.20
0.15
0.10
0.05
0.00
Relative Probability
85.5
48.3
66.4
167.0
141.9
205.2
391.3
65.0 ± 1.9
0
50
100
150
200
250
300
350
400
450
500
Apparent Age (Ma)

Figure 14 B

5.2.5. In Vacuo Crushing and Subsequent Step Heating of Crushed Material

Our initial expectations were that the majority of the $^{40}Ar_E$ was located in the fluid inclusions, and that by using *in vacuo* crushing, the $^{40}Ar_E$ would be released during the crushing steps. Subsequently, by step heating the crushed material the correct age could be obtained from the argon contained in the quartz lattice or daughter minerals within inclusions. Five samples were crushed in the *in vacuo* crusher, 2 samples from the low fluid inclusion density grains and 3 from the HFIDCs. Between 21 and 83% of the total ^{39}Ar (from crushing and step-heating of the crushed material) was released from the sample during the crushing steps. This represents an order of magnitude higher fraction of gas released from crushing than has been reported in prior crushing (Harrison et al., 1993; Turner and Wang, 1992). Two examples of the crushing experiments are shown in this section (complete data tables and age spectra are given in Appendix M). The age spectra in Figure 15 A and B (MTEET and CMXET respectively) show both the crushing steps and the subsequent heating steps on single age spectrum. Placing all of the normalized (by sensitivity and weight) data from both crushing and subsequent step-heating on one spectrum allows for direct comparison of the gas released during crushing and during subsequent step-heating. Table 10 shows the ages, Cl/K and $\%^{39}Ar$ released by crushing, for the two samples discussed above. The Cl/K for these samples remain fairly constant, and agree well with the values obtained by crush leach analysis.

The individual spectra derived from crushing and step-heating are shown in Figure 15 C-G. The Ar released upon crushing MTEE, (Figure 15 C) yields a fairly flat spectrum with an age of 180 Ma. Following crushing, the sample was removed from the

crusher and sieved to produce two size fractions, MTEESC and MTEELC. The smaller size fraction (< 168 μm, MTEESC), presumably had fewer intact fluid inclusions. The two splits were step heated and showed significantly lower plateau ages of 88 ± 6 and 84.5 ± 1.6 Ma for MTEESC (< 168μm) and MTEELC (> 168μm), respectively (Figure 15 D, E). These high temperature plateau ages agree within error. However, the effect of crushing is evident in the low temperature steps. MTEESC released 42.3% of the ^{39}Ar beneath 800° C, whereas MTEELC released only 22.8% of the ^{39}Ar in the same temperature range. Additionally, the total gas ages from the low temperature steps are 27.5 ± 31.6 and 107.0 ± 15.4 Ma for MTEESC and MTEELC, respectively.

CMXE (Figure 15 F) shows a similar behavior to MTEE, although it was crushed 25 times instead of 12 times (MTEE), and all of the crushed material was step-heated together (instead of two size splits). Because the sample was crushed twice as long, the remaining crushed material was finer than sample MTEE and presumeably, more fluid inclusions were broken. During the late crushing steps the age decreases and the age is young during the low temperature part of the step-heating spectrum. However, there is no clear plateau in the higher temperature steps of CMXEC as was observed in both the MTEELC and MTEESC age spectra.

Table 10 Summary of ages obtained by *in vacuo* crushing Capitan quartz

		Integrated Age			800-1200° C			< 800° C			> 1200° C		
		Cl/K	Age	±1σ	Cl/K	Age	±1σ	Cl/K	Age	±1σ	Cl/K	Age	±1σ
Sample	Irradiation		(Ma)	(Ma)		(Ma)	(Ma)		(Ma)	(Ma)		(Ma)	(Ma)
MTEC64	64-TR2	4.6	90.2	57.1									
MTEC64T	64-TR2	4.7	100.7	49.3									
MTEPC64	64-TR2	4.9	116.9	37.2	0.4	162.9	52.6	5.6	89.5	11.5	3.8	62.0	85.3
W3C64	64-TR2	3.5	296.2	207.8									
W3C64T	64-TR2	5.2	187.4	100.3									
W3PC64	64-TR2	6.3	121.6	35.4	0.9	405.6	44.6	7.2	112.8	36.3	4.3	155.8	24.6
CMXE	91-TB1	5.7	432.7	22.4									
CMXEC	91-TB1	9.6	144.7	33.2	2.7	197.2	65.8	13.1	27.0	23.3	6.0	175.5	37.2
CMXET	91-TB1	6.7	359.3	25.1									
MTEE	91-TB1	7.1	163.9	49.3									
MTEELC	91-TB1	7.4	79.8	13.6	6.6	50.7	17.9	9.2	107.0	15.4	6.9	85.4	2.3
MTEESC	91-TB1	7.4	96.8	26.4	4.0	113.9	29.3	9.4	27.5	31.6	6.6	87.0	6.1
W3F	91-TB1	5.4	488.9	32.5									
W3FC	91-TB1	9.3	425.7	441.8	1.5	906.3	142.7	15.7	290.1	132.6	4.7	149.2	394.6
W3FT	91-TB1	6.2	475.6	118.2									

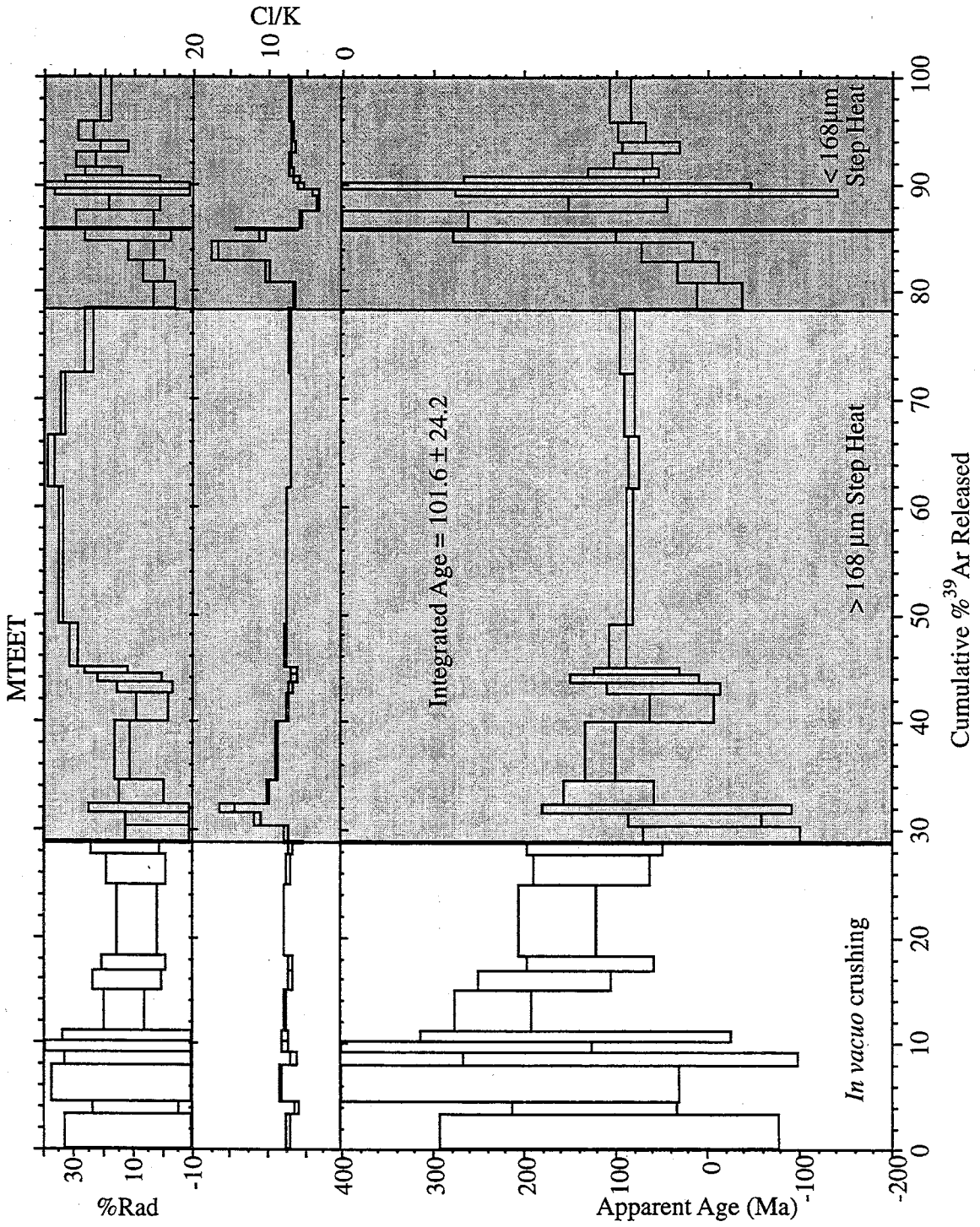
MTEET
%Rad
Cl/K
Apparent Age (Ma)
Integrated Age = 101.6 ± 24.2
< 168µm Step Heat
> 168 µm Step Heat
In vacuo crushing
Cumulative %39Ar Released

Figure 15 A

Figure 15 *In vacuo* crushing and post-crush step-heat age spectra of quartz. A.) Combined age spectra from the crushing and post-crush step-heating for sample MTEET. B.) Similar combined spectra from CMXET C.) A) The age spectra from *in vacuo* crushing (part of A) large single HFIDC, MTEE. After crushing the sample was split into a large > 168 μm split and a small < 168μm mesh split. post-crush step-heat of these two fractions are shown in D.) and E.) respectively. F.) shows the age spectra from *in vacuo* crushing (part of B) of a large single HFIDC, CMXE. G.) is the post-crush step-heat of the crushed material (also part of B).

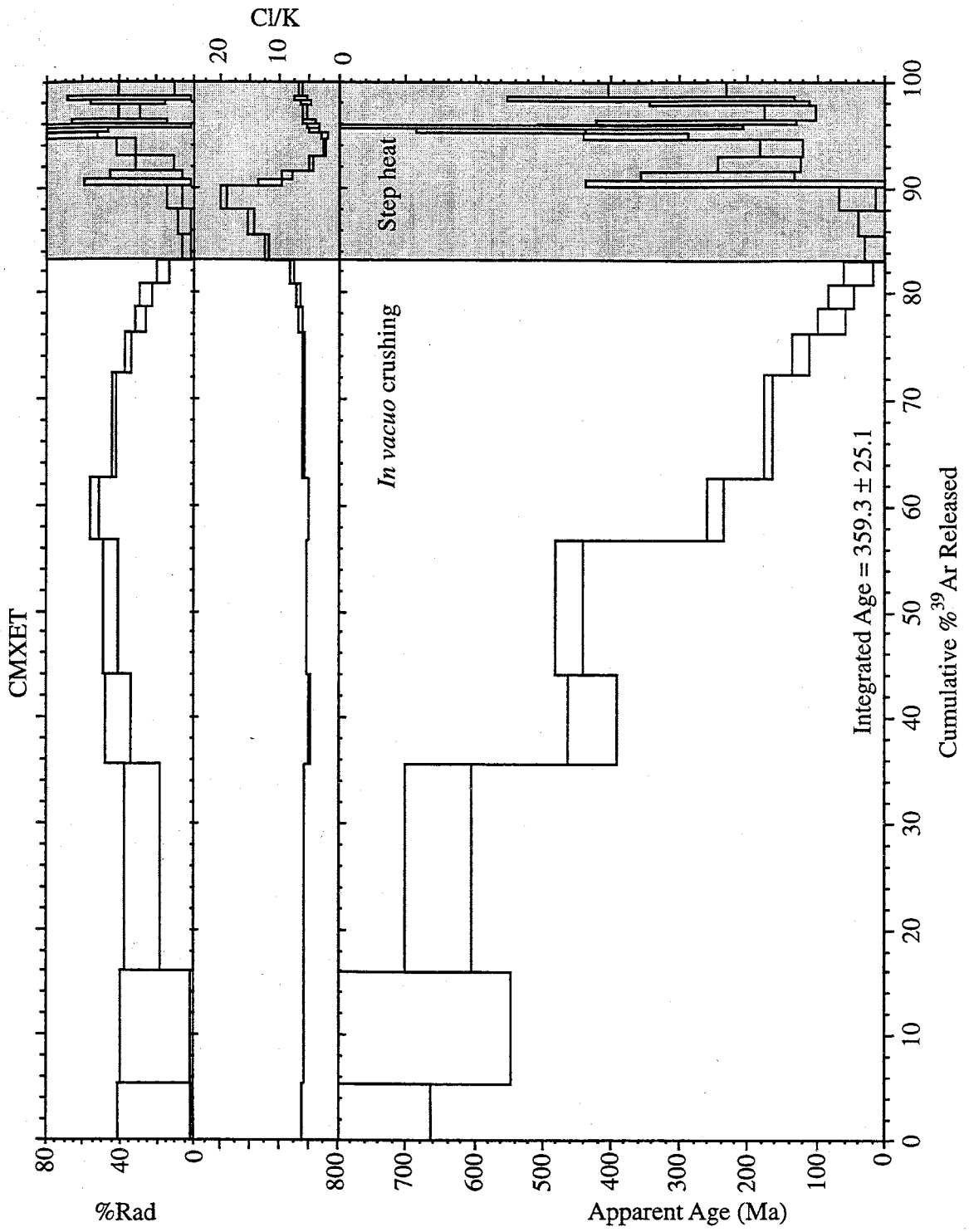
Cl/K
20
10
0
Step heat
In vacuo crushing
CMXET
Integrated Age = 359.3 ± 25.1
Cumulative %^{39}Ar Released
%Rad
Apparent Age (Ma)

Figure 15 B

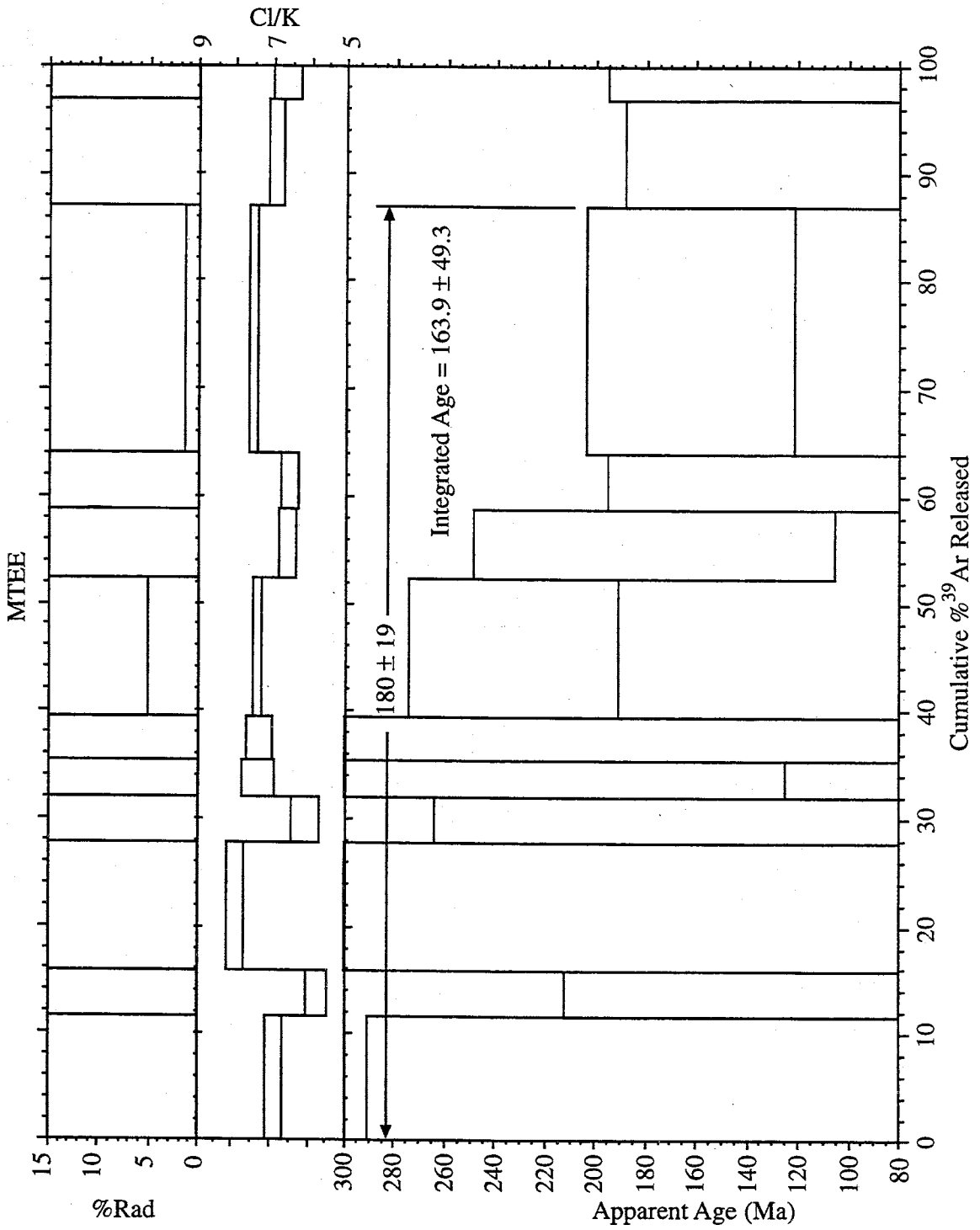
Cl/K
9
7
5
MTEE
Integrated Age = 163.9 ± 49.3
180 ± 19
Cumulative %^{39}Ar Released
100
90
80
70
60
50
40
30
20
10
0
15
10
5
0
%Rad
300
280
260
240
220
200
180
160
140
120
100
80
Apparent Age (Ma)

Figure 15 C

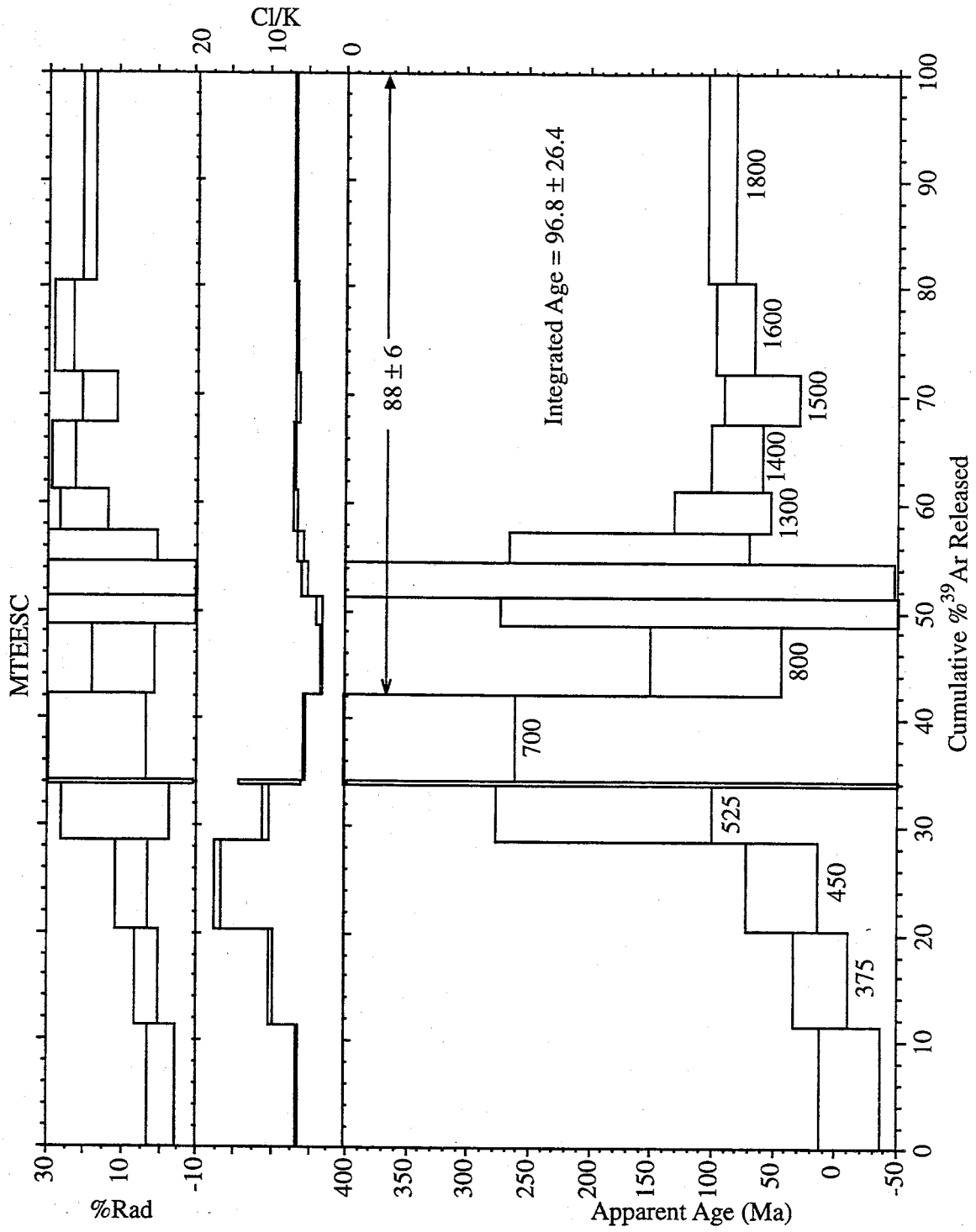
MTEESC
%Rad
Cl/K
Apparent Age (Ma)
Integrated Age = 96.8 ± 26.4
88 ± 6
Cumulative %^{39}Ar Released
1800
1600
1500
1400
1300
800
700
525
450
375

Figure 15 D

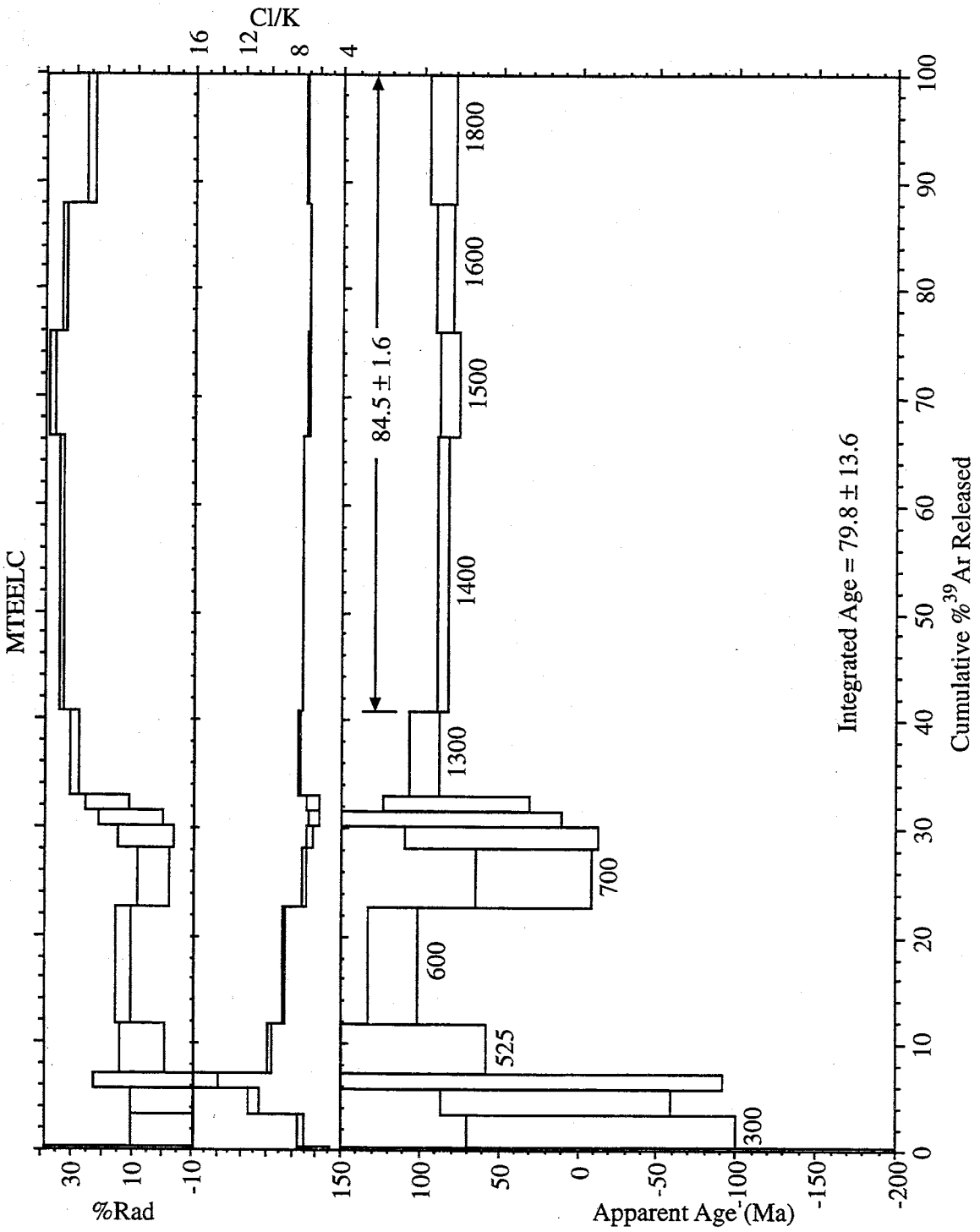
MTEELC
Cl/K
16
12
8
4
84.5 ± 1.6
1800
1600
1500
1400
1300
700
600
525
300
Integrated Age = 79.8 ± 13.6
Cumulative %^{39}Ar Released
100
90
80
70
60
50
40
30
20
10
0
-200
-150
-100
-50
0
50
100
150
Apparent Age (Ma)
30
10
-10
%Rad

Figure 15 E

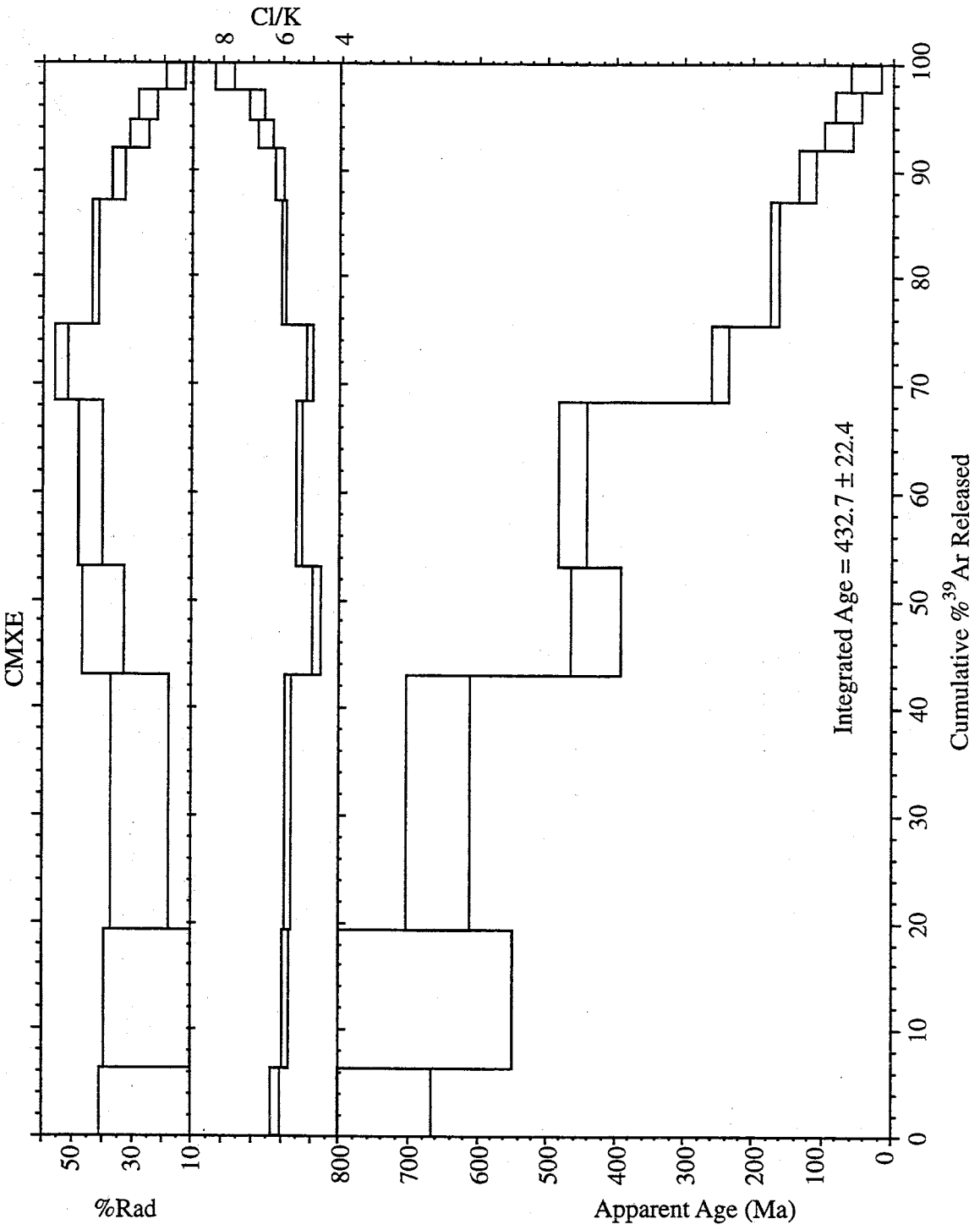
Cl/K
8
6
4
CMXE
50
30
10
%Rad
800
700
600
500
400
300
200
100
0
Apparent Age (Ma)
Integrated Age = 432.7 ± 22.4
0
10
20
30
40
50
60
70
80
90
100
Cumulative %39Ar Released

Figure 15 F

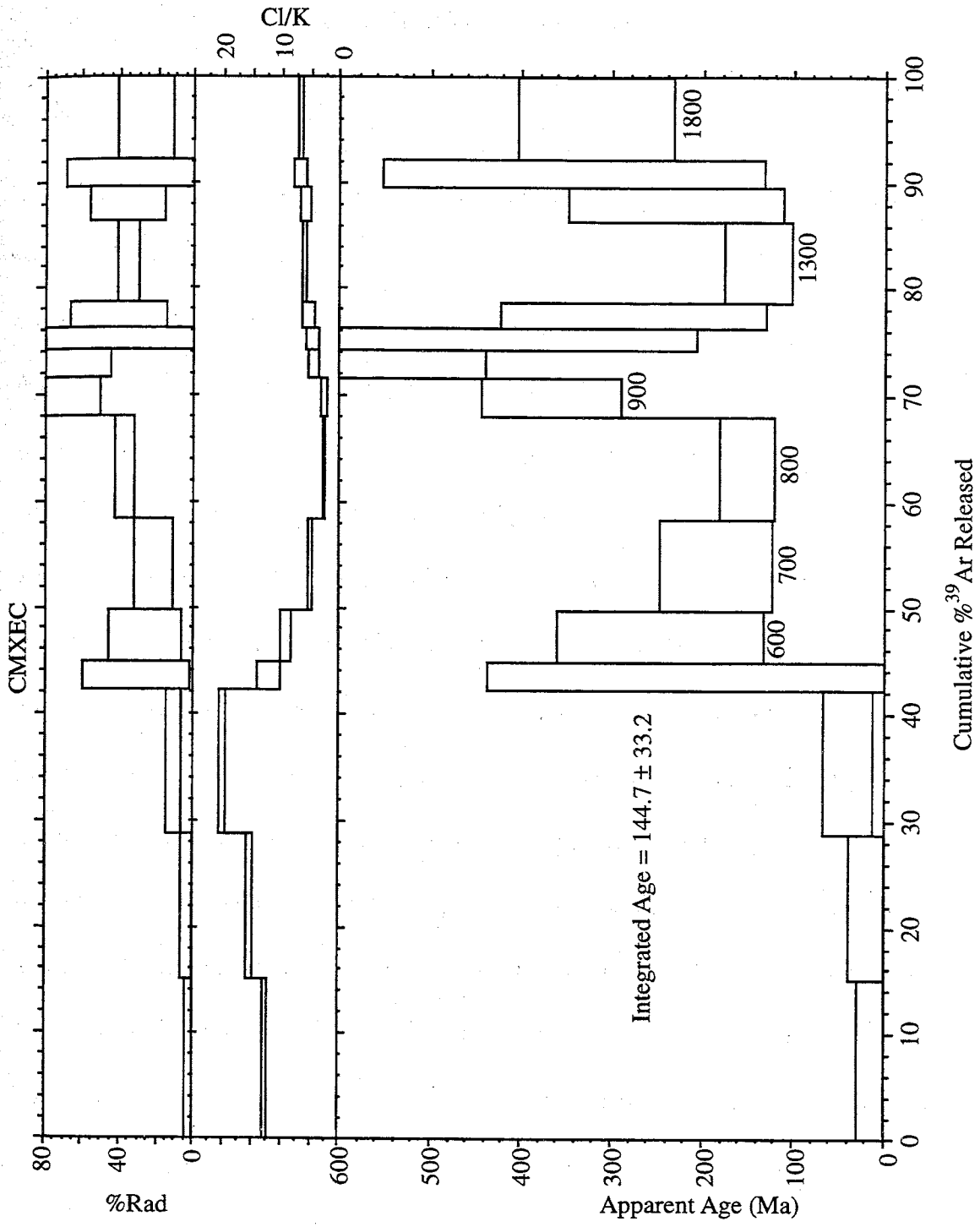
Cl/K
20
10
0
CMXEC
1800
1300
900
800
700
600
Integrated Age = 144.7 ± 33.2
Cumulative %^{39}Ar Released
100
90
80
70
60
50
40
30
20
10
0
80
40
0
%Rad
600
500
400
300
200
100
0
Apparent Age (Ma)

Figure 15 G

5.3. $^{40}Ar/^{39}Ar$ Laser and Furnace Total Fusion Analyses

5.3.1. Laser Fusions Analyses

Thirty-five small (~ 5 mg) quartz grains broken from a single large grain of MTE were analyzed by laser fusion (MTELF1-35) to investigate the homogeneity of the quartz. The quartz was difficult to fuse and therefore it probably did not totally degas. An age probability distribution diagram of the laser analyses is shown in Figure 16. Also shown in Figure 16 are the Cl/K ratios, which do not appear to have any correlation to the ages obtained. The ages range from –103.7 ± 106.1 Ma to 6.615 ± 115.7 Ga. Although there is a large variation in age the errors are large (shown are 1σ deviation) and come close to overlapping at 2σ deviation. The moles of ^{39}Ar shows a bell shaped curve, showing that the oldest and youngest ages are from samples with the smallest signal size. The negative ages and the several billion years old ages are probably a result of random error associated with signal size, and therefore are not representative of any geologic process. The individual samples were heterogeneous, but were not outside the range seen in the other samples in this study. The weight percent K_2O calculated from the argon signal ranged from 0.014 to 0.000058. The average value was 0.0028 with a 1σ deviation of 0.0026. The upper range of this agrees well with the values obtained from electron microprobe analysis. The Cl/K ratio obtained from argon analysis ranged from 1.91 to 29.99 with an average of 10.56 and a 1σ deviation of 6.55. These values within error agree with the values determined from crush leach analysis. Complete data tables are given in Appendix N. Statistically, the ages of these samples are not identical at the

2σ level, which could explain some of the variability in behavior that is seen in other argon analysis.

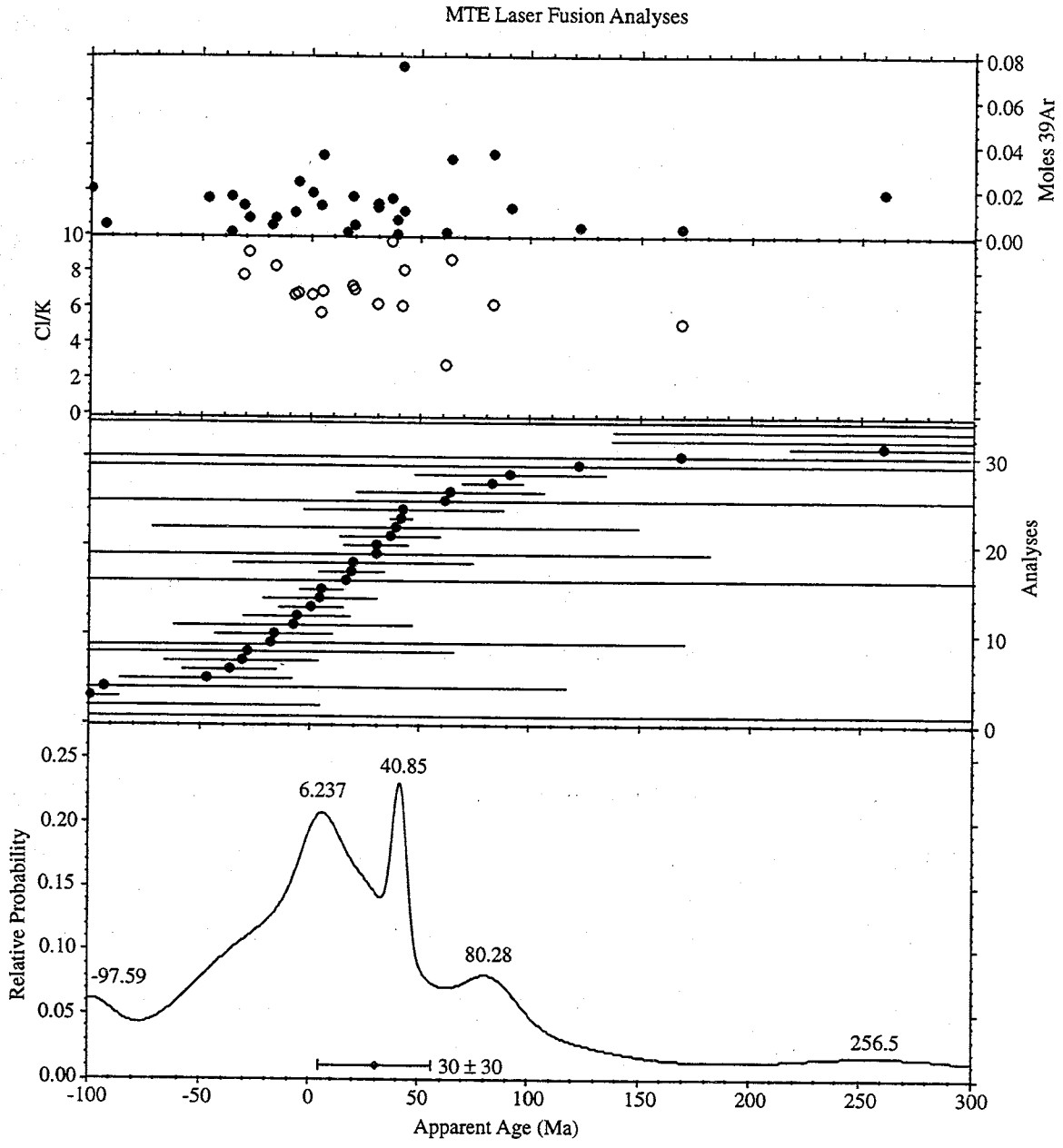

Figure 16 Age probability distribution diagram showing ages of laser fusions of MTE quartz.

5.3.2. Furnace Fusion Analyses

To better understand the behavior of the laser fusions results and to determine if the inability to completely fuse the samples with the laser was a problem, 20 splits of quartz grains were fused in the furnace in one 1750°C heating step. An age probability distribution diagram of this data is shown in Figure 17. The samples were from 3 prospects (W3, CMX2, and CPU2) and from two irradiations (NM-53 and NM-64). A variety of sample sizes from approximately 5 to 20 mg were used. Most ages obtained from these fusion analyses, with the exception of two, are statistically equal to or older than the age of the pluton. One sample, W3FF6, yielded a precise young total gas age of 8.7 ± 1.8 Ma (2σ). This sample also had the only Cl/K ratio of less than 1 (0.1). Another sample, W3FF1, yielded an imprecise age of 10 ± 19.9 Ma (Cl/K of 6.5), which overlaps the age of the pluton at 1σ. All of the other Cl/K ratios ranged from 1.1 – 9.7 which are typical of samples from Capitan. Perhaps coincidentally, 5 of the samples have total gas ages that agree with the age of the pluton within 1σ. A summary of the results is given in Table 11, and complete data are in Appendix N. Again there is no obvious correlation between the Cl/K ratio and age. Similar to the results of the laser fusion analyses several negative ages were obtained. These are from some of the smallest samples and may be related to small signal size.

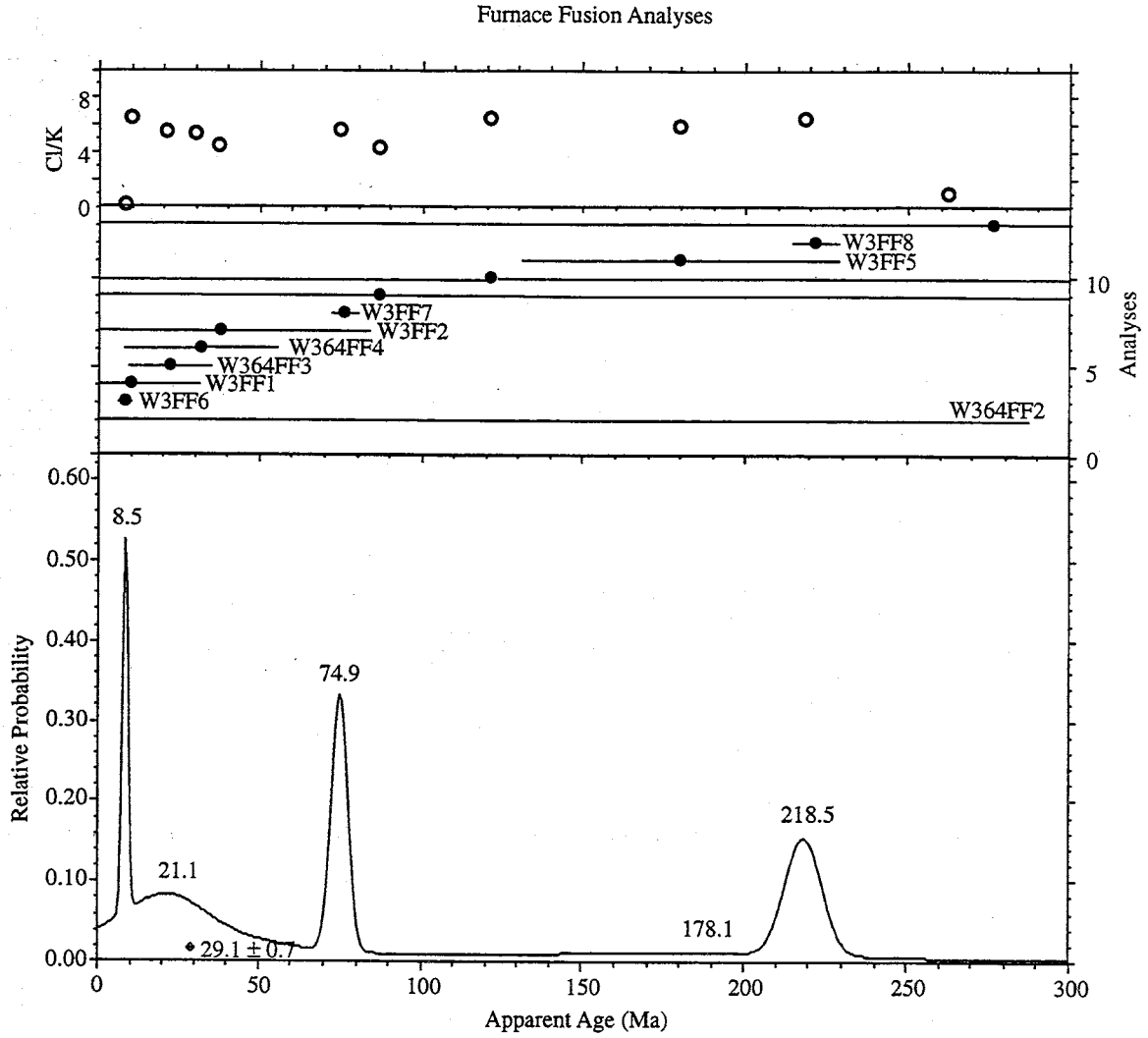

Figure 17 Age probability distribution diagram of quartz furnace fusion analyses.

Table 11 Summary of quartz furnace fusion data.

	Integrated Age			Concentration		
	Cl/K	Age	±1s	Weight %		
Sample		(Ma)	(Ma)	CaO	Cl-	K_20
W3FF1	6.5	10.0	19.9	B/D	0.0328734	0.0067404
W3FF2	4.4	37.8	44.4	B/D	0.0093151	0.0028075
W3FF3	4.5	86.8	285.1	0.056418	0.0018889	0.0005634
W3FF4	6.4	121.6	618.6	B/D	0.0037212	0.0007774
W3FF5	5.9	180.0	47.1	B/D	0.0251786	0.0056551
W3FF6	0.1	8.7	0.9	0.1098904	0.0241668	0.2519191
W3FF7	5.6	76.1	2.5	0.0410972	0.0866214	0.0204695
W3FF8	6.4	221.6	5.6	0.0578208	0.0881042	0.0182691
CPU2FF1	5.9	177.0	187.3	0.0184395	0.0140424	0.0031819
CMX2FF1	6.1	72.5	51.2	0.0879326	0.0166599	0.0036439
CMX2FF2	4.2	117.3	701.5	0.0332786	0.0015902	0.0005034
CMX2FF3	6.9	147.4	30.2	0.0561444	0.0435584	0.0083691
W3FF1	2.1	-236.0	10532.7	B/D	0.0004102	0.0002628
W3FF2	2.6	-200.1	574.0	B/D	0.0014389	0.0007478
W3FF3	5.5	-22.3	307.6	0.0098414	0.0921012	0.0223208
W3FF4	5.3	22.6	11.5	0.0111098	0.0187741	0.0047505
W3FF5	1.1	32.0	22.1	B/D	0.0002322	0.0002936
W3FF6	5.9	276.5	427.3	0.0011944	0.0128267	0.0029032
W3FF7	9.7	575.2	17.3	B/D	0.0024141	0.0003295
W3FF8	1.6	719.9	186.5	0.0005578	0.0004425	0.0003663

5.4. Argon Signals

5.4.1. Release Temperatures

During step-heating experiments the temperature of gas release was monitored, which may provide some information about where the gas is sited within the sample. ^{40}Ar has three major sources in these samples, the radiogenic component derived from decay of K ($^{40}Ar^*$), an atmospheric component ($^{40}Ar_{atm}$), and an additional component, called $^{40}Ar_E$. ^{39}Ar is primarily derived in the reactor from ^{39}K, and secondarily from Ca. For these particular samples ^{38}Ar is primarily derived in the reactor from ^{37}Cl, but there is also a small component present in atmosphere and some is reactor derived from K. ^{37}Ar is derived in the reactor from Ca. Finally, ^{36}Ar (generally the smallest signal) is almost entirely atmospheric, except for a minor contribution from reactor derived Ca interference.

Overall for Capitan quartz, two gas release peaks are observed, one at approximately 600°, and another at 1400° C. Figure 18 shows moles of gas released vs. temperature for the various argon isotopes. $^{39}Ar_K$ (Figure 18 D) has a less significant peak at 1400°C but has more gas released in the 1700° range, and $^{37}Ar_{Ca}$ also has a less significant peak at 1400° C.

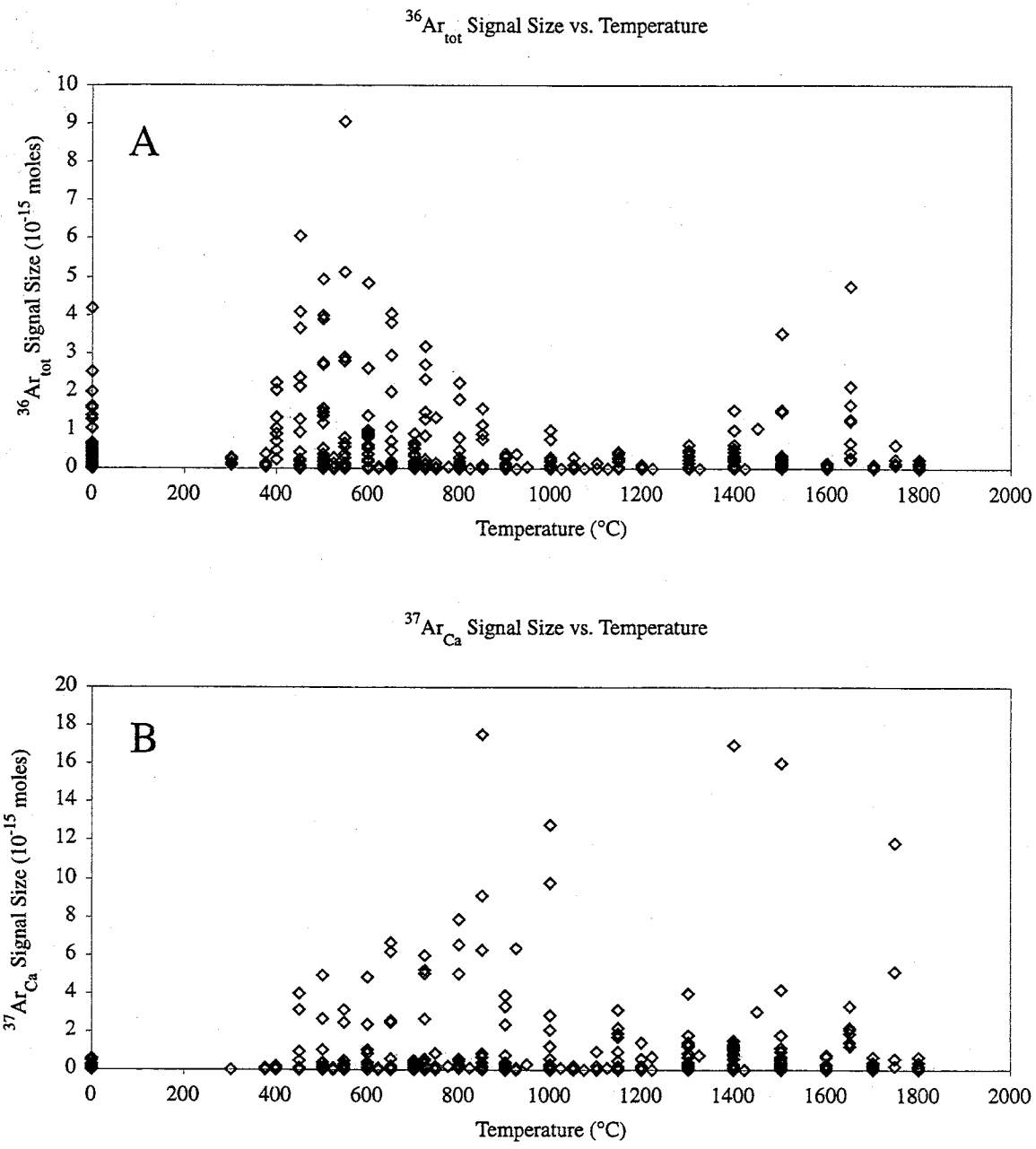
$^{36}Ar_{tot}$ Signal Size vs. Temperature
A
$^{36}Ar_{tot}$ Signal Size (10^{-15} moles)
Temperature (°C)
$^{37}Ar_{Ca}$ Signal Size vs. Temperature
B
$^{37}Ar_{Ca}$ Signal Size (10^{-15} moles)
Temperature (°C)

Figure 18 A, B

Figure 18 Signal size vs. temperature. A.) $^{36}Ar_{tot}$ signal size. Note the peaks at 500 and 1400 ° C. The lower temperature peak should represent fluid inclusion gas and the 1400° peak may be small fluid or solid inclusions or lattice gas. B.) $^{37}Ar_{Ca}$ signal size shows two peaks, one at approximately 500° and one at 1400°. C.) $^{38}Ar_{Cl}$ signal size, again shows two peaks although the low temperature peak occurs at a slightly higher temperature of 700° C. This could be a result of partial annealing of the decrepitation pathways. D.) $^{39}Ar_{K}$ signal size possibly shows 3 release peaks, with a slight increase at 1750-1800° C. The lower peaks correspond nicely to the ^{39}Ar and $^{38}Ar_{Cl}$ peaks E.) $^{40}Ar_{tot}$ signal size. Again the 500 and 1400° peaks are well correlated to ^{36}Ar peaks

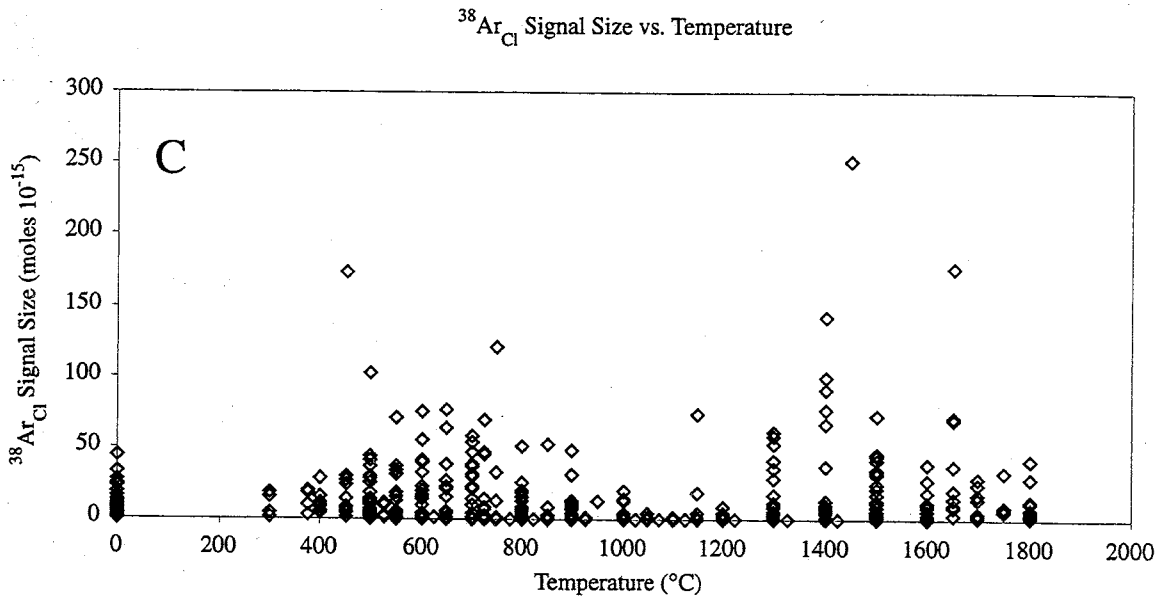
$^{38}Ar_{Cl}$ Signal Size vs. Temperature
C
$^{38}Ar_{Cl}$ Signal Size (moles 10^{-15})
300
250
200
150
100
50
0
0
200
400
600
800
1000
1200
1400
1600
1800
2000
Temperature (°C)

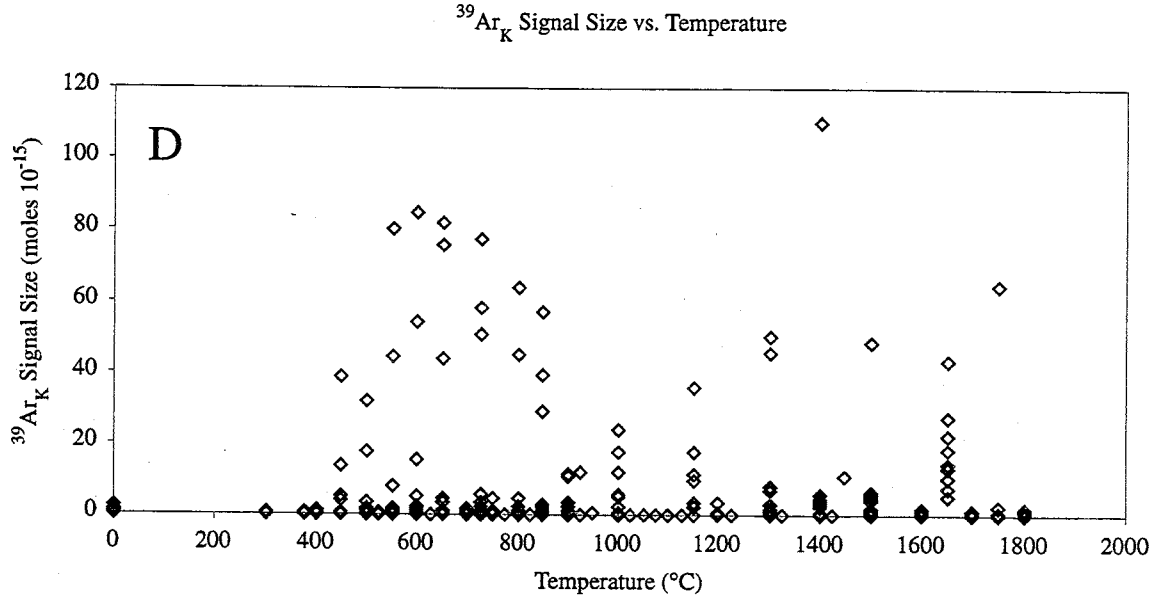
$^{39}Ar_{K}$ Signal Size vs. Temperature
D
$^{39}Ar_{K}$ Signal Size (moles 10^{-15})
120
100
80
60
40
20
0
0
200
400
600
800
1000
1200
1400
1600
1800
2000
Temperature (°C)

Figure 18 C, D

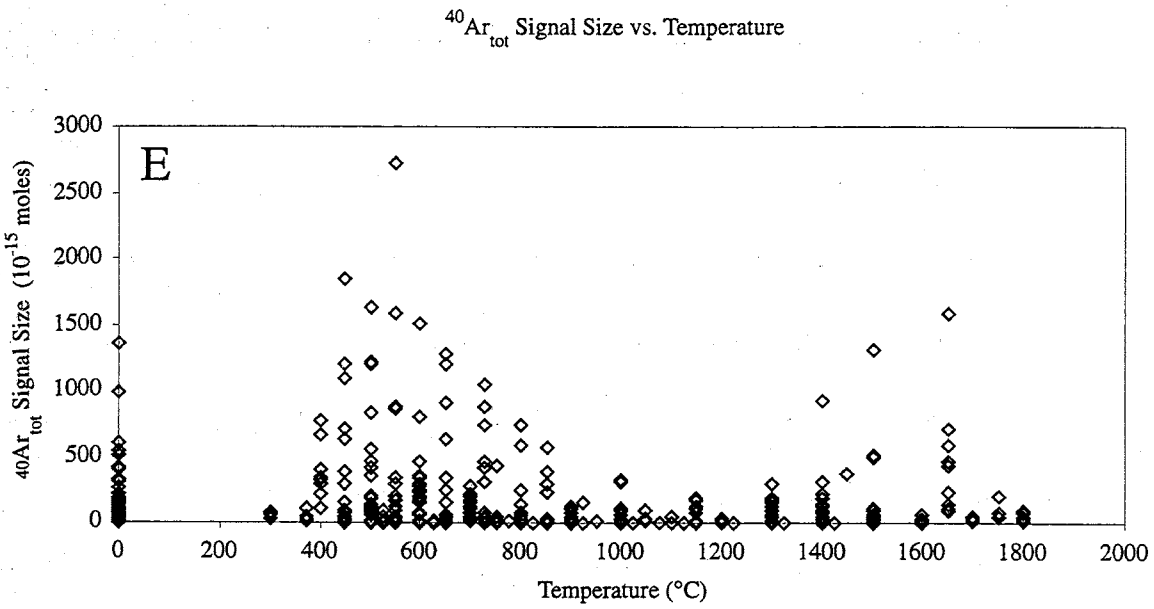
$^{40}Ar_{tot}$ Signal Size vs. Temperature
E
$^{40}Ar_{tot}$ Signal Size (10^{-15} moles)
3000
2500
2000
1500
1000
500
0
0
200
400
600
800
1000
1200
1400
1600
1800
2000
Temperature (°C)

Figure 18 E

In order to better understand the temperature release patterns, an acoustical method of determining the temperature at which the inclusions decrepitate (decrepitometry) was used (Roedder, 1984). A highly sensitive microphone records the fracturing of the quartz, which occurs as a result of decrepitation, with respect to temperature. A decrepigram is a plot of temperature versus the number of fluid inclusions decrepitated during each temperature interval. Decrepigrams for two samples were generated and are shown in Figure 19. MTE 1 is a sample from the first irradiation, in which grains were used instead of polished chips. MTE 2 is a sample composed of several polished chips very similar to chips MTE B - E used for the third irradiation group, to maximize the number of inclusions contained in the quartz. The steep peaks on the decrepigrams help confirm that the fluid inclusions are decrepitating in the 500 - 600° C range. Thus, decrepitation, and subsequent release of fluid inclusion gas, is largely responsible for the argon release peak in that temperature range. Sample MTE 2 had less material than MTE 1 but also had a much larger fluid inclusion population (represented by the area under the curve), confirming that using polished chips from crystal bases increased the concentration of fluid inclusions. The peak seen at 800°C has not been seen before and may be a result of noise in the room. It is widely believed that all inclusions of reasonable size decrepitate below that temperature.

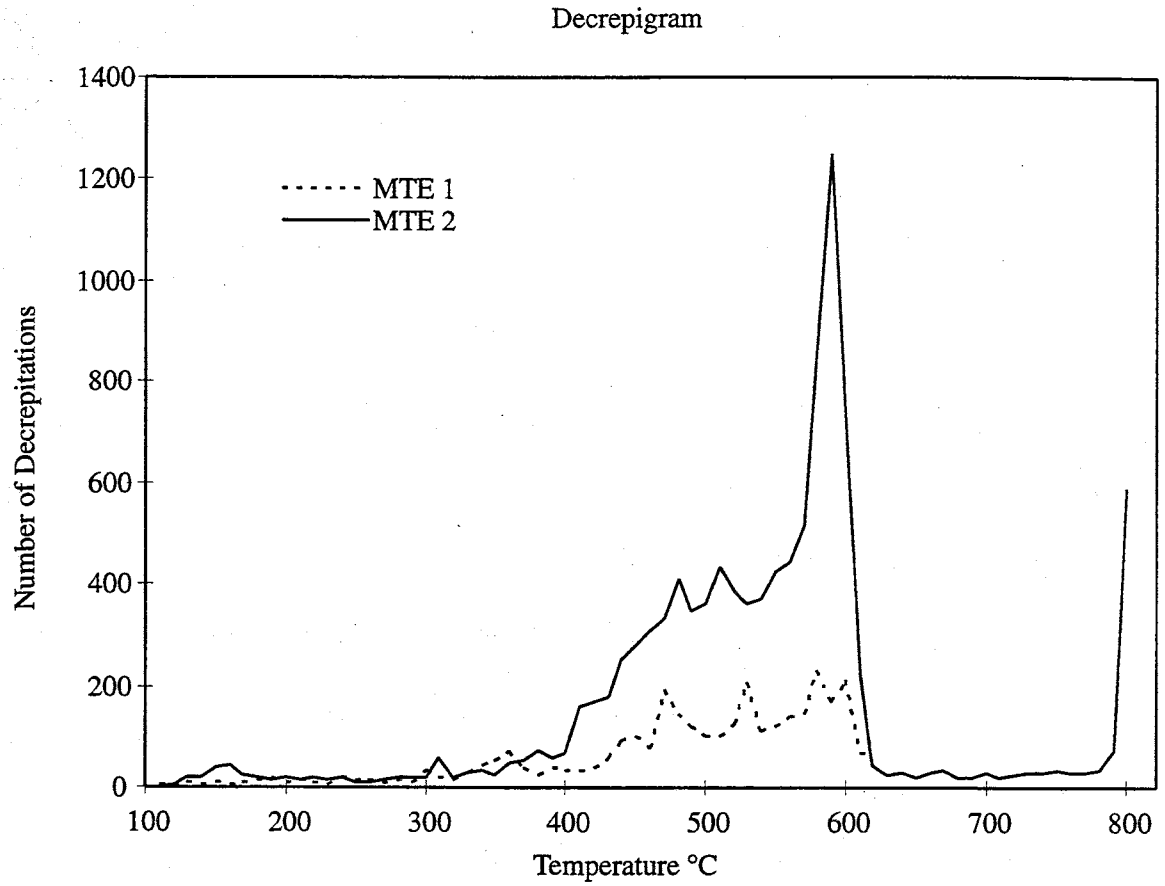

Figure 19 Decrepigrams for MTE quartz. An audible measure of the number of fluid inclusions decrepitating. Note the strong peaks at 550-600°C, this correlates well with the release diagrams shown in Figure 18.

5.4.2. Homogeneity

The chemical and physical homogeneity of the samples was examined to help establish the cause of the large variability in the argon spectra from quartz grains. The signals from the laser and furnace fusions of the small grains (Section 5.3) help to explain some of the variation seen in the larger samples. Figure 20 shows two age spectra from the same sample and serves as an example of how chemically variable bulk samples can be explained as a result of contamination. MTEC-1 is a small 6 mg fragment broken off

the main chip (HFIDC) during irradiation. It was run using an abbreviated 4 step-heating schedule to determine at what temperature most gas evolved. MTEC-2, the larger part of the chip, was run later. The difference in the two spectra is striking. The total amount of gas released, Cl/K ratio, and temperature of release imply that some form of high K contaminant was present in the MTEC-1 small chip.

The argon isotope signals from each chip were recalculated as weight percent oxides, to compare with the microprobe analysis. CaO was calculated using the ^{37}Ar signal and K_2O was calculated using ^{39}Ar signal. In addition Ar and Cl were calculated using ^{40}Ar and ^{38}Ar signals. Table 12 shows the calculated concentrations from analyses of these two samples. The Cl concentrations are statistically indistinguishable from each other and the other samples that were analyzed. However, the K_2O concentration of MTEC-1 is significantly larger than the concentration found in other samples. MTEC-2 is an order of magnitude larger than MTEC-1 in total sample weight, and yet, some isotopes (when normalized to account for the difference in weight) evolved only half as much gas. The weight normalized concentrations of CaO, Cl- and K2O from MTEC-2 are 24, 14, and 11% of the concentrations seen in MTEC-1. The molar ratios are discussed further in the next section. Complete data tables for sample MTEC can be found in Appendix O.

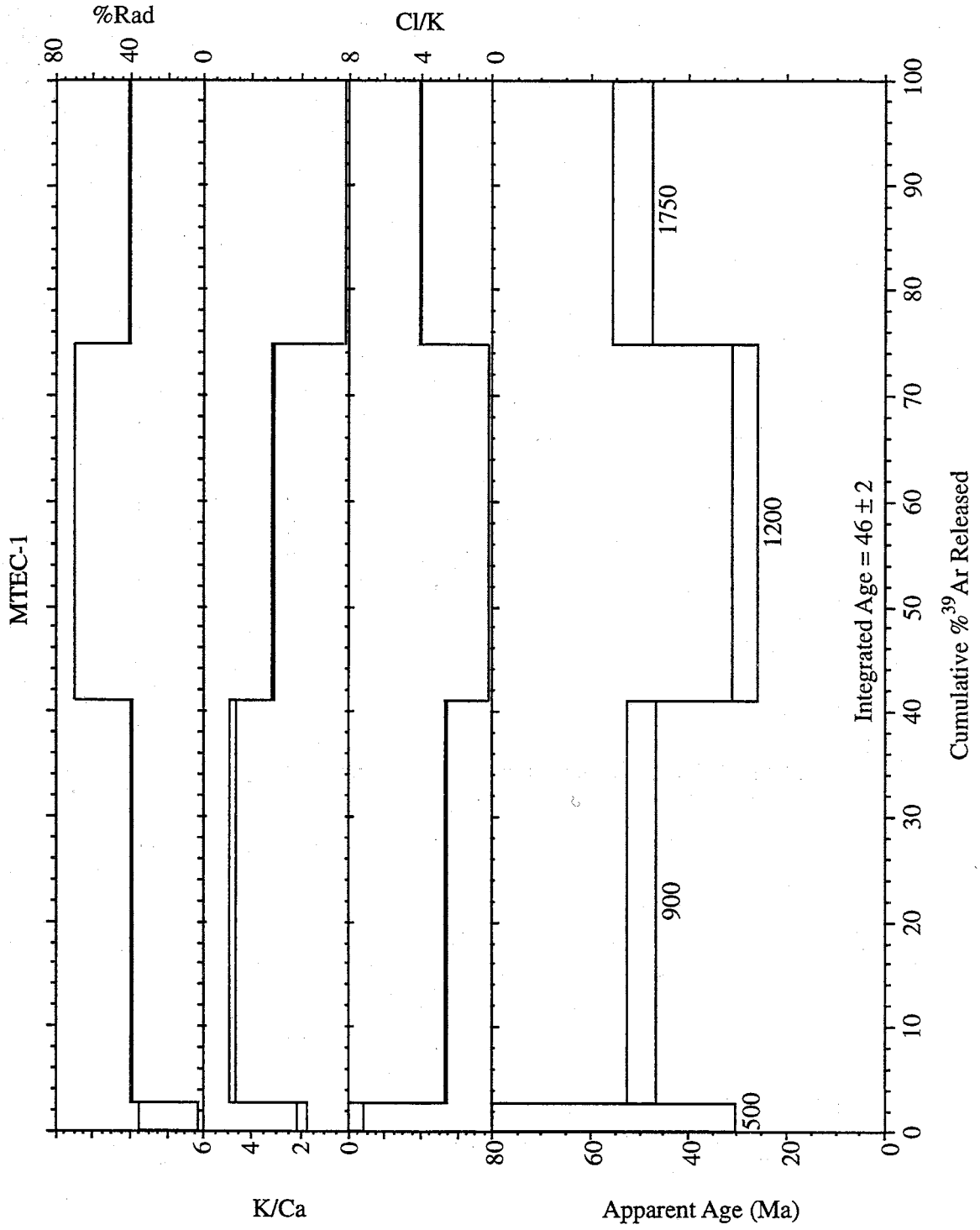
%Rad
Cl/K
MTEC-1
1750
1200
900
500
Integrated Age = 46 ± 2
Cumulative % ^{39}Ar Released
K/Ca
Apparent Age (Ma)

Figure 20 A

Figure 20 Age spectra from two fragments of a single chip of MTEC quartz, broken after irradiation. A.) MTEC-1, a 6 mg piece B.) MTEC-2, a 78 mg piece. The age spectra are shown to emphasis the variability and effect of contamination.

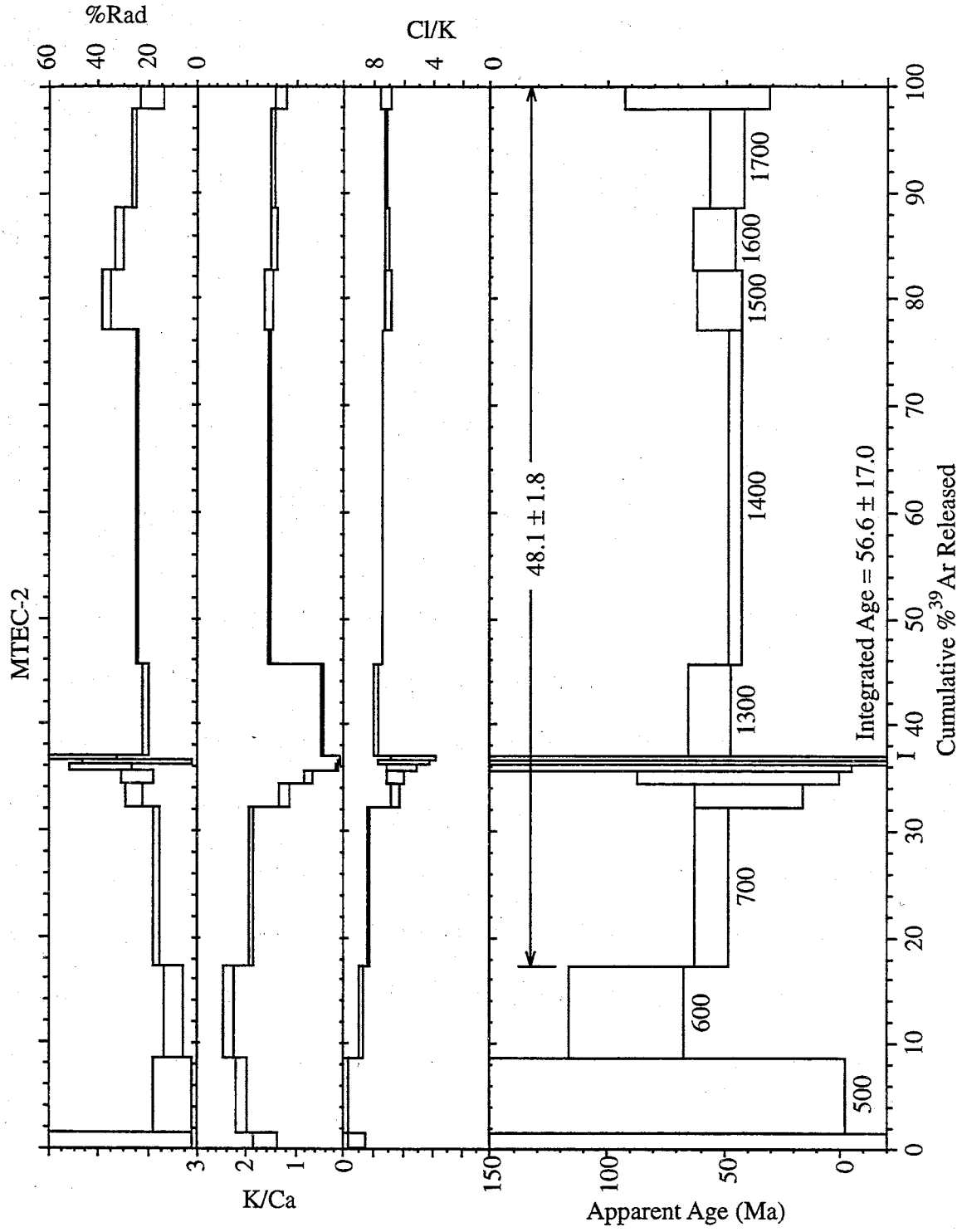
%Rad
Cl/K
MTEC-2
K/Ca
Apparent Age (Ma)
48.1 ± 1.8
Integrated Age = 56.6 ± 17.0
Cumulative %^{39}Ar Released
500
600
700
1300
1400
1500
1600
1700

Figure 20 B

Table 12 Comparison of gas release from sample MTEC-1 and MTEC-2

MTEC-1							
	Total moles	moles/mg					
$^{36}Ar_{tot}$	5.54E-16	8.66E-17		Moles	Moles/ 100g	Wt %	
$^{37}Ar_{Ca}$	1.28E-14	2.01E-15	Ca	5.82E-08	9.09E-04	5.10E-02	CaO
$^{38}Ar_{Cl}$	7.29E-14	1.14E-14	Cl	1.13E-06	1.77E-02	6.27E-01	Cl-
$^{39}Ar_{K}$	9.30E-15	1.45E-15	K	2.03E-07	3.16E-03	1.49E-01	K_2O
$^{40}Ar_{tot}$	2.28E-13	3.56E-14					
J	3.74E-03						
MTEC-2							
	Total moles	moles/mg					
$^{36}Ar_{tot}$	4.52E-15	5.76E-17		Moles	Moles/ 100g	Wt %	
$^{37}Ar_{Ca}$	8.06E-15	1.03E-16	Ca	1.72E-07	2.20E-04	1.23E-02	CaO
$^{38}Ar_{Cl}$	3.34E-13	4.26E-15	Cl	1.95E-06	2.49E-03	8.83E-02	Cl-
$^{39}Ar_{K}$	1.22E-14	1.56E-16	K	2.67E-07	3.40E-04	1.60E-02	K_2O
$^{40}Ar_{tot}$	1.44E-12	1.83E-14					
J	3.74E-03						

Another example of the heterogeneity of the sample is the surface expression of the fluid inclusion density as seen on the electron microprobe. Figure 21 shows a BSE and a topographic BSE image of W3 quartz. A topographic BSE image is a procedure in which half of the BS detectors are turned off allowing some shadowing in the image giving an image of surface topography. These images show the large physical variability in small area (~200μm). There is a striking difference in the abundance of fluid inclusion pits in the top right half of the image and the lower left portion. The image shows great variability in quantity of fluid inclusions. There is no apparent grain boundary at the interface between the high density fluid inclusion area and the adjoining low density fluid inclusion area.

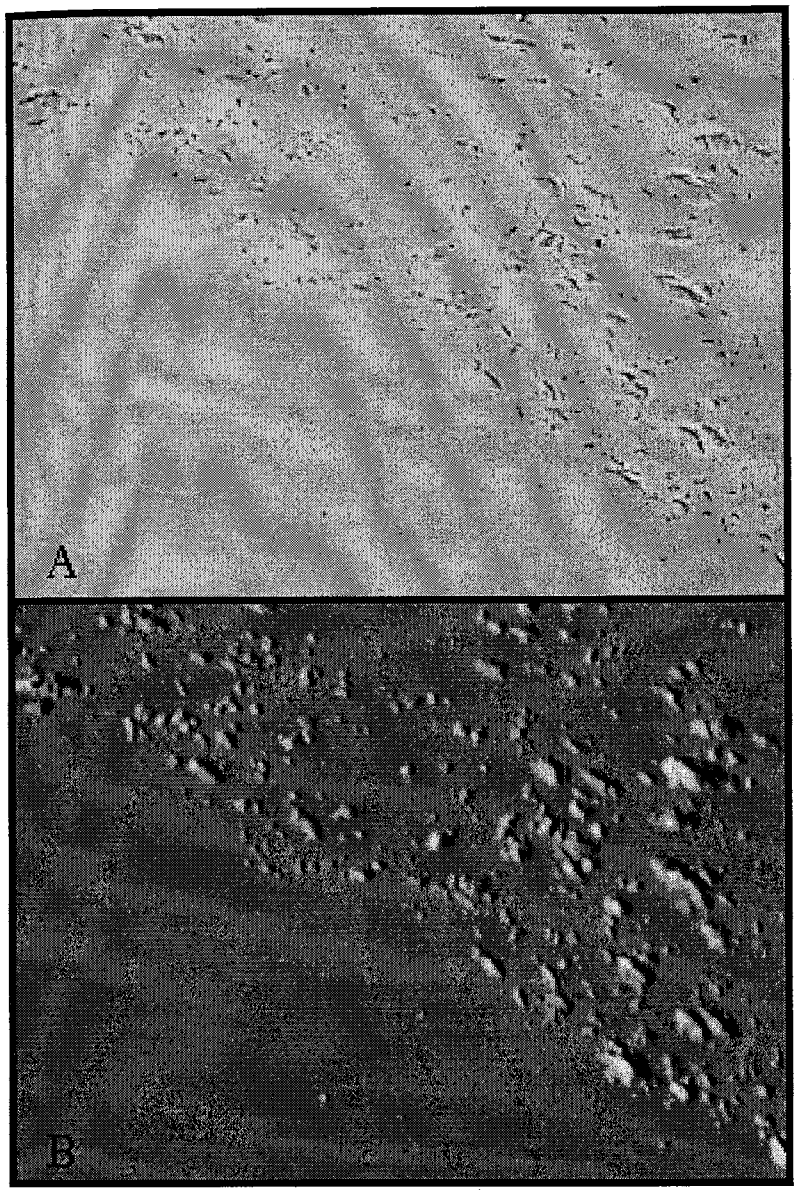

Figure 21 BSE and Topographic BSE image of W3 quartz. A.) BSE image showing the great variability in fluid inclusion density. There is no apparent grain boundary at the intersection of the high density area and the low density area. B.) shows more clearly that the variability seen in the BSE image is a result of pits on the surface.

5.5. Argon Correlation

Many different plots and methods were used to examine the data for systematic variation. The 3-D CAKE diagrams yielded consistent results, but had very poor regressions. Data from these fits are given in Appendix P. The figures are not shown due to the difficulty of representing 3-D space in two dimensions. Several two dimensional diagrams were also plotted. Most of the two-dimensional correlation diagrams do not exhibit well-defined correlation. Two diagrams that do show correlation are described in the following sections. These are standard isochron diagrams, and $^{38}Ar_{Cl}/^{40}Ar$ vs. $^{39}Ar_{K}/^{40}Ar$, showing the Cl/K ratio as the slope.

5.5.1. Isochron Diagrams

The applicability and use of isochrons in the $^{40}Ar/^{39}Ar$ dating method has long been recognized. $^{36}Ar/^{40}Ar$ is plotted against $^{39}Ar_{K}/^{40}Ar$. An atmospheric intercept value of 0.003384 (1/295.5) on the $^{36}Ar/^{40}Ar$ axis represents modern day atmosphere. Most of the intercept values for best fits to the Capitan data are significantly less than 0.0034 suggesting the presence of excess argon. The $^{39}Ar_{K}/^{40}Ar$ intercept is proportional to the age of the sample and is also dependant on the J valueirradiation parameter. For samples from irradiation NM-91a value of 0. 234 is equivalent to an age of 28.3 Ma, the age of the Capitan pluton (Campbell et al., 1994). Most of the age intercepts are significantly older than the age of the pluton. All of the isochrons from the HFIDC are shown in Appendix Q. Results from the individual sample isochrons are summarized in Table 13. The MSWDs for the isochron fits are listed in Table 13, and range from 1.2 to 105. The most important conclusion to draw from the isochrons is that the argon released from

these samples are not a simple two component mix, between radiogenic and atmospheric ^{40}Ar.

Table 13 Isochron data from HFIDCs.

Sample	Intercept[1] ($^{40}Ar/^{36}Ar$)	Error[2]	Age[3] (Ma)	Error[4]	MSWD[5]
W3FC	199.0	21.50	1000.35	65.78	3.110
CMXEC	250.5	14.70	390.15	24.78	7.192
MTEECL	296.8	2.20	84.72	1.93	3.771
MTEEC	303.3	5.70	124.46	20.73	1.889
MTEET	303.7	1.40	78.28	1.5	7.015
MTEC-2	304.5	2.50	42.87	1.94	1.152
MTED	304.9	1.60	38.13	1.48	3.889
MTEE CS	309.6	4.20	52.04	3.39	12.091
MTEB	311.8	4.50	58.7	4.42	2.105
CMXD	343.6	2.20	171.14	3.13	21.204
CMXD	352.3	2.20	150.27	2.8	34.757
MTEC-1	368.4	7.30	26.91	1.59	8.155
CMXA	373.4	2.70	54.14	1.73	13.511
CMXEC	375.5	2.80	145.27	3.49	104.186
CMXA	375.8	2.70	51.43	1.62	10.775
CMXE	389.4	2.90	83.03	1.8	60.529
CMXET	389.6	2.90	99.66	2.47	95.499
CMXB	404.3	6.70	69.55	3	32.745
W3F	426.0	7.80	446.55	6.04	87.290
W3FT	428.6	7.80	444.31	5.95	47.221
W3A	458.8	16.30	35.84	4.04	18.769
CMXEC	472.1	22.20	-163.11	11.56	25.619
CMXC	535.7	8.80	37.85	2.56	15.366
W3CD	563.2	6.40	-1.05	0.05	38.093
W3G	688.3	10.40	128.48	3.99	51.395
W3E	856.6	18.10	-238.54	13.96	25.344
W3FC	879.5	221.50	-1124.13	320.95	4.671
W3A	979.8	25.30	-334.77	20.14	76.182

1 $^{40}Ar/^{36}Ar$ intercept
2 2σ error (Ma) associated with $^{40}Ar/^{36}Ar$ intercept
3 Age (Ma) calculated from $^{39}Ar/^{40}Ar$ intercept
4 2σ error associated with age intercept
5 MSWD for best fit isochron.

Notes: The goodness of fit is considered poor for all the samples except MTEC-2 and the MTEEC. Not all steps are used for each of the isochron diagrams. Points that gave negative slopes for example were removed.

5.5.2. Cl/K Correlation Diagrams

$^{38}Ar_{Cl}/^{40}Ar$ vs. $^{39}Ar_{K}/^{40}Ar$ plot is a two dimensional diagram which represents correlation between Cl and K in the samples. This plot is the same as the bottom plane of the CAKE diagram from Turner and Bannon (1992) and Turner and Wang (1992). The graphs for the HFIDCs are shown in Figure 21. This is the second of the correlation diagrams that show consistent results for the Capitan samples. The Cl/K ratio generated from these plots is remarkably homogenous. The Cl/K variations seen in the age spectra suggested this correlation. The slope of the best fit line is proportional to the Cl/K ratio. The values given for each sample are very similar to the bulk Cl/K ratio. These values are identical to the values obtained by crush leach (Campbell et al., 1995). The trend seen is very consistent and is a good indicator of what mineral is being analyzed. Sylvite for instance should have a Cl/K of 1, and feldspar has a negligible Cl content, relative to the K content, driving this ratio towards zero. The variable abundance of these minerals may account for some of the scatter in the plot. A summary of the bulk Cl/K ratios for all samples can be found in Appendix A.

Table 14 Data from best fit lines of $^{38}Ar_{Cl}/^{40}Ar$ vs. $^{39}Ar_{K}/^{40}Ar$ diagrams

Sample	Equation	M	B	R^2
CMXD	y = 0.0505x + 0.0029	0.0505	0.0029	R2 = 0.4314
CMXE	y = 0.0021x + 0.0084	0.0021	0.0084	R2 = 0.0207
MTEC-1	y = -0.0674x + 0.085	-0.0674	0.0850	R2 = 0.0971
MTEESC	y = 0.0282x + 0.0024	0.0272	0.0024	R2 = 0.7037
W3CD	y = 0.0547x - 0.0004	0.0547	-0.0004	R2 = 0.7818
W3E	y = 0.1118x - 0.0005	0.1118	-0.0005	R2 = 0.5018
W3F	y = 0.0096x + 0.0023	0.0096	0.0023	R2 = 0.6311
W3FCR	y = 0.03x + 0.0031	0.0300	0.0031	R2 = 0.6973
CMX A	y = 0.0515x - 0.0023	0.0515	-0.0023	R2 = 0.9859
CMXB	y = 0.042x - 0.0006	0.0420	-0.0006	R2 = 0.9846
CMXC	y = 0.0424x + 0.0006	0.0424	0.0006	R2 = 0.8933
CMXCR	y = 0.0378x + 0.0016	0.0378	0.0016	R2 = 0.9673
MTEB	y = 0.0427x - 0.0006	0.0427	-0.0006	R2 = 0.9444
MTEC-2	y = 0.0458x - 0.002	0.0458	-0.0020	R2 = 0.9434
MTED	y = 0.0442x - 0.0003	0.0442	-0.0003	R2 = 0.9939
MTEECR	y = 0.0439x - 0.0002	0.0439	-0.0002	R2 = 0.9602
MTEELC	y = 0.0421x - 0.0011	0.0421	-0.0011	R2 = 0.968
W3A	y = 0.0419x - 0.002	0.0419	-0.0020	R2 = 0.9884
W3G	y = 0.0505x - 0.0007	0.0505	-0.0007	R2 = 0.9073

	All		R^2>0.85	
	M	B	M	B
Standard Deviation	0.0332	0.0195	0.0040	0.0012
Average	0.0370	0.0050	0.0441	-0.0007
Minimum	-0.0674	-0.0023	0.0378	-0.0023
Maximum	0.1118	0.0850	0.0515	0.0016

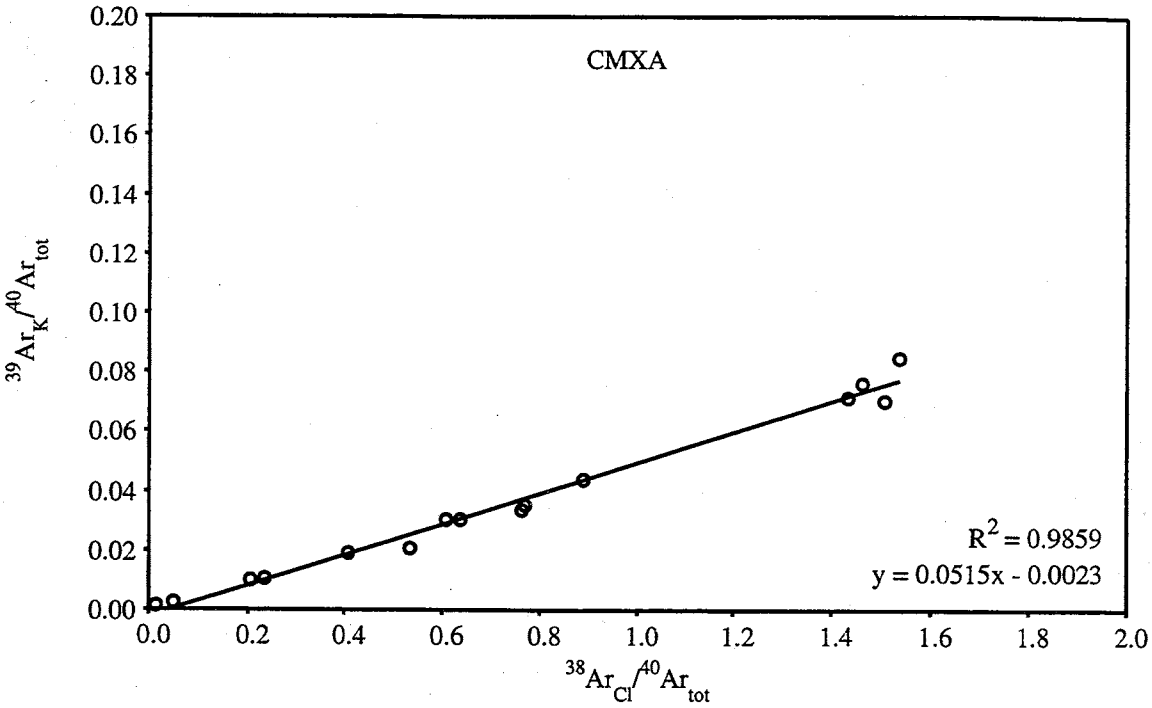
CMXA
$^{39}Ar_K/^{40}Ar_{tot}$
$^{38}Ar_{Cl}/^{40}Ar_{tot}$
$R^2 = 0.9859$
y = 0.0515x - 0.0023
0.00
0.02
0.04
0.06
0.08
0.10
0.12
0.14
0.16
0.18
0.20
0.0
0.2
0.4
0.6
0.8
1.0
1.2
1.4
1.6
1.8
2.0

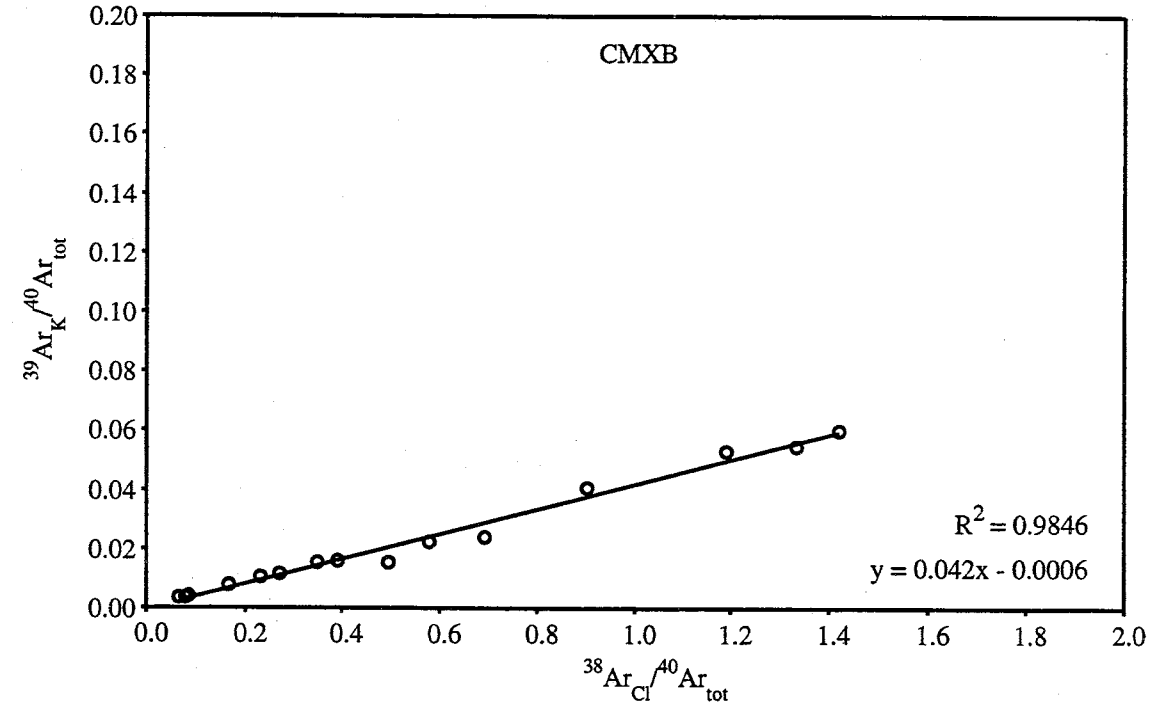
CMXB
$^{39}Ar_K/^{40}Ar_{tot}$
$^{38}Ar_{Cl}/^{40}Ar_{tot}$
$R^2 = 0.9846$
y = 0.042x - 0.0006
0.00
0.02
0.04
0.06
0.08
0.10
0.12
0.14
0.16
0.18
0.20
0.0
0.2
0.4
0.6
0.8
1.0
1.2
1.4
1.6
1.8
2.0

Figure 22 A, B

Figure 22 $^{38}Ar_{Cl}/^{40}Ar$ vs. $^{39}Ar_{K}/^{40}Ar$ correlation diagram. The slopes shown on the diagram represent the best fit line and are equal to the Cl/K ratio for the sample. R^2 values are shown along with the equation for the line in the lower right corner of the diagram.

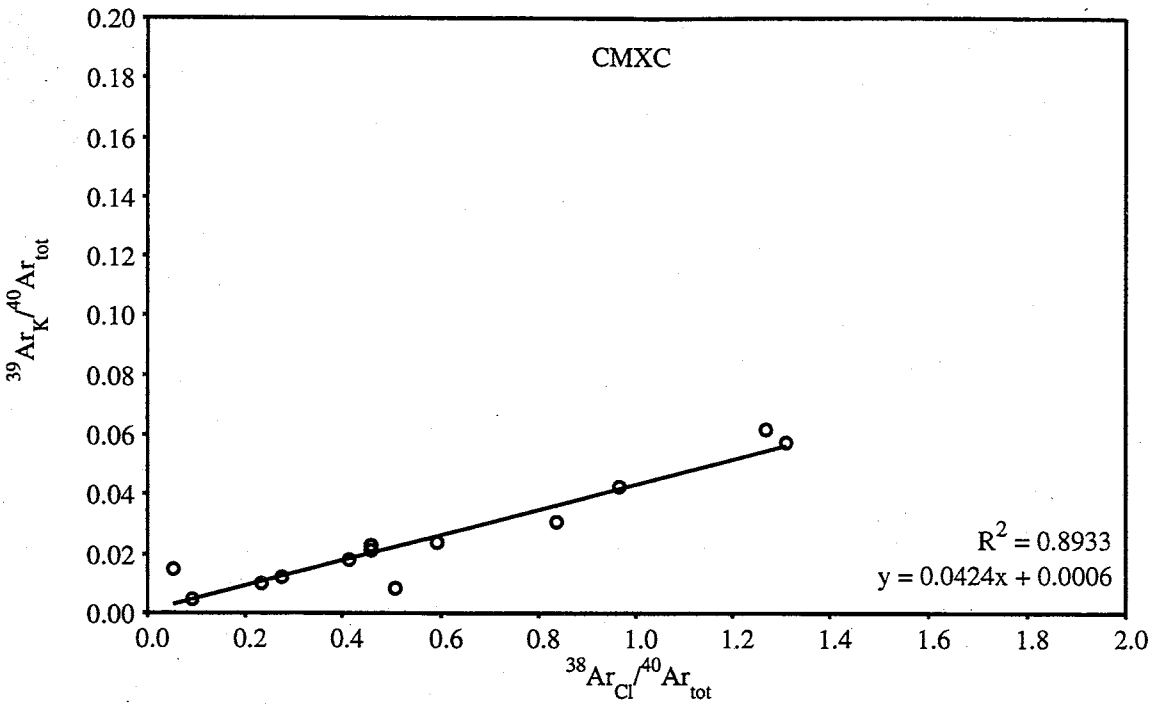
CMXC
$^{39}Ar_K/^{40}Ar_{tot}$
$^{38}Ar_{Cl}/^{40}Ar_{tot}$
$R^2 = 0.8933$
y = 0.0424x + 0.0006
0.00
0.02
0.04
0.06
0.08
0.10
0.12
0.14
0.16
0.18
0.20
0.0
0.2
0.4
0.6
0.8
1.0
1.2
1.4
1.6
1.8
2.0

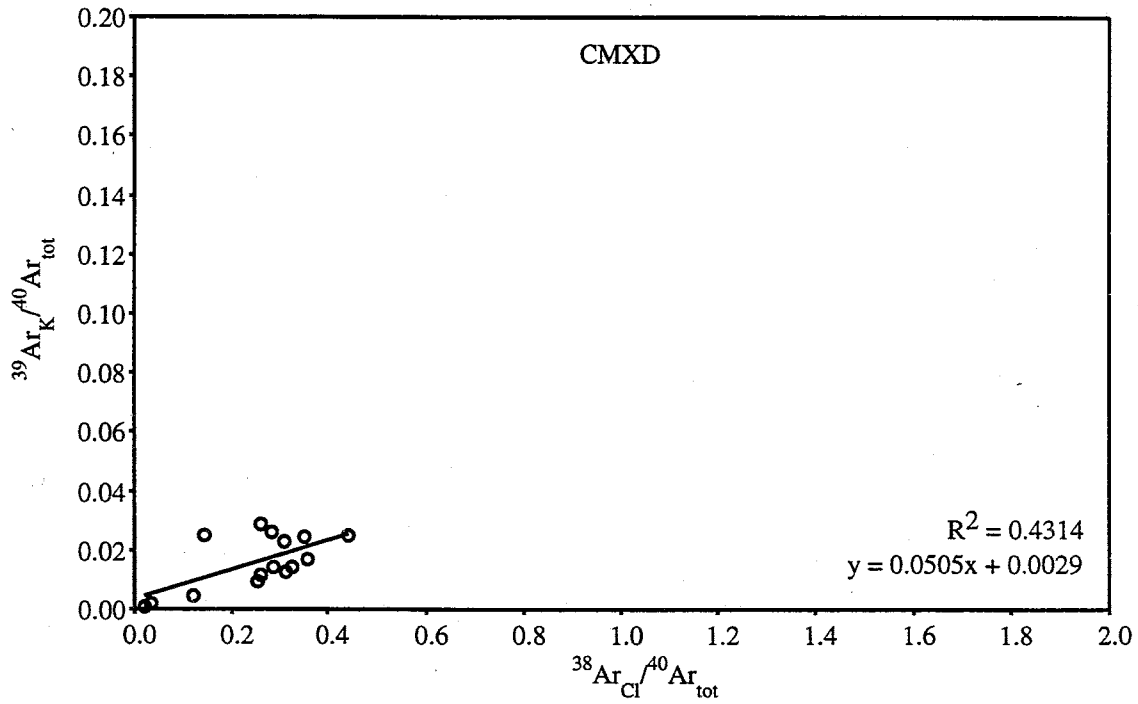
CMXD
$^{39}Ar_K/^{40}Ar_{tot}$
$^{38}Ar_{Cl}/^{40}Ar_{tot}$
$R^2 = 0.4314$
y = 0.0505x + 0.0029
0.00
0.02
0.04
0.06
0.08
0.10
0.12
0.14
0.16
0.18
0.20
0.0
0.2
0.4
0.6
0.8
1.0
1.2
1.4
1.6
1.8
2.0

Figure 22 C, D

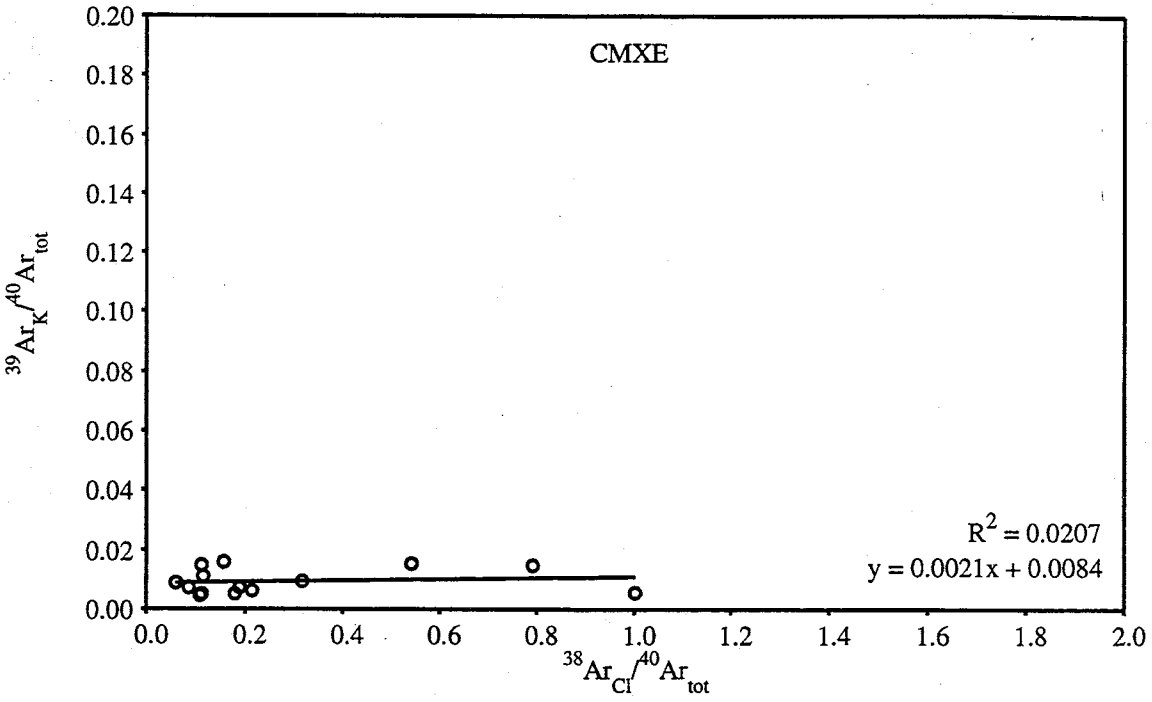
CMXE
$^{39}Ar_K/^{40}Ar_{tot}$
$^{38}Ar_{Cl}/^{40}Ar_{tot}$
$R^2 = 0.0207$
y = 0.0021x + 0.0084
0.00
0.02
0.04
0.06
0.08
0.10
0.12
0.14
0.16
0.18
0.20
0.0
0.2
0.4
0.6
0.8
1.0
1.2
1.4
1.6
1.8
2.0

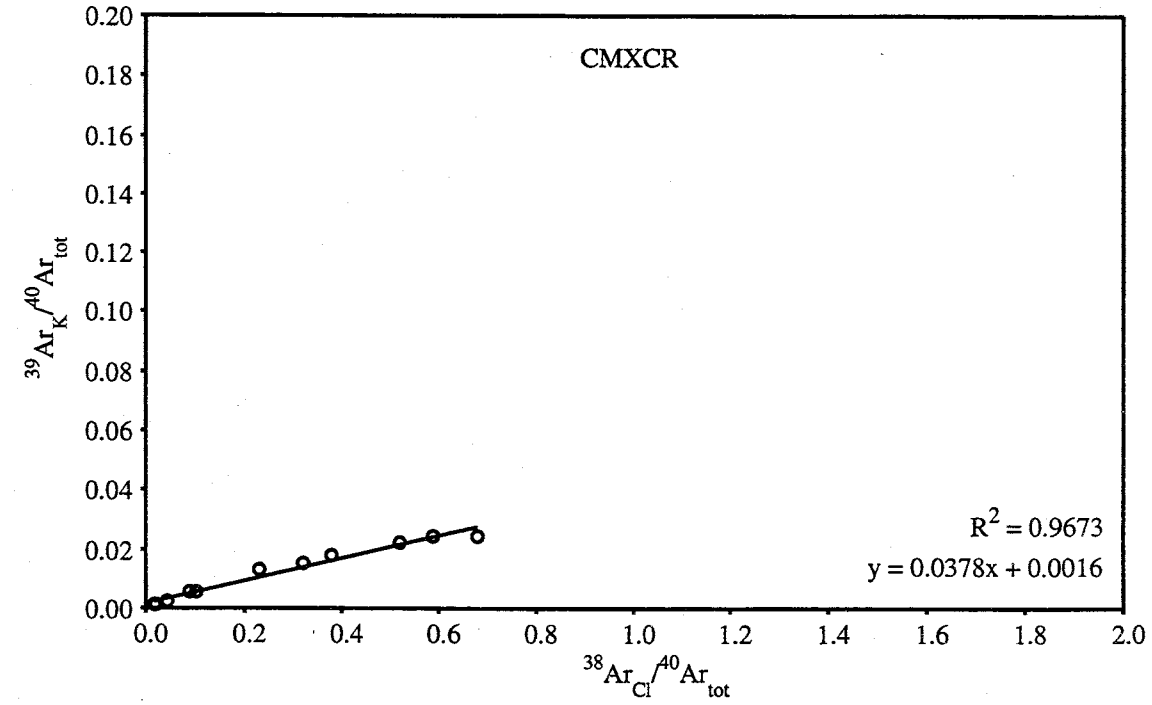
CMXCR
$^{39}Ar_K/^{40}Ar_{tot}$
$^{38}Ar_{Cl}/^{40}Ar_{tot}$
$R^2 = 0.9673$
y = 0.0378x + 0.0016
0.00
0.02
0.04
0.06
0.08
0.10
0.12
0.14
0.16
0.18
0.20
0.0
0.2
0.4
0.6
0.8
1.0
1.2
1.4
1.6
1.8
2.0

Figure 22 E, F

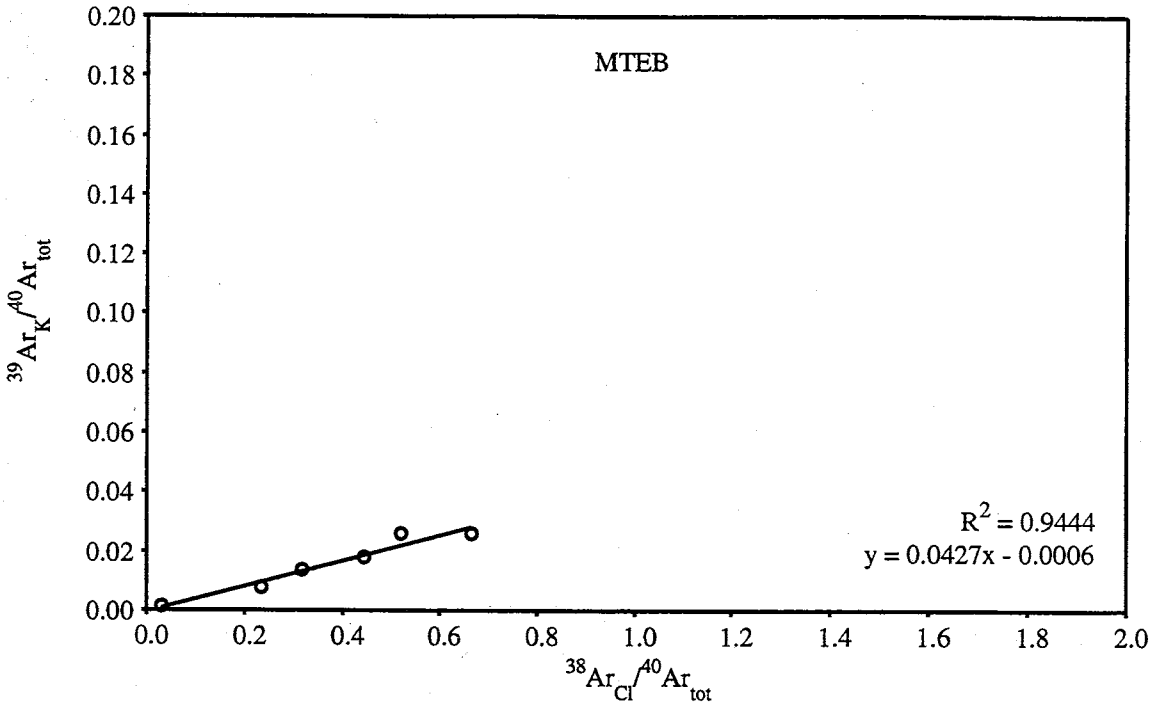
MTEB
$^{39}Ar_K/^{40}Ar_{tot}$
$^{38}Ar_{Cl}/^{40}Ar_{tot}$
$R^2 = 0.9444$
y = 0.0427x - 0.0006
0.00
0.02
0.04
0.06
0.08
0.10
0.12
0.14
0.16
0.18
0.20
0.0
0.2
0.4
0.6
0.8
1.0
1.2
1.4
1.6
1.8
2.0

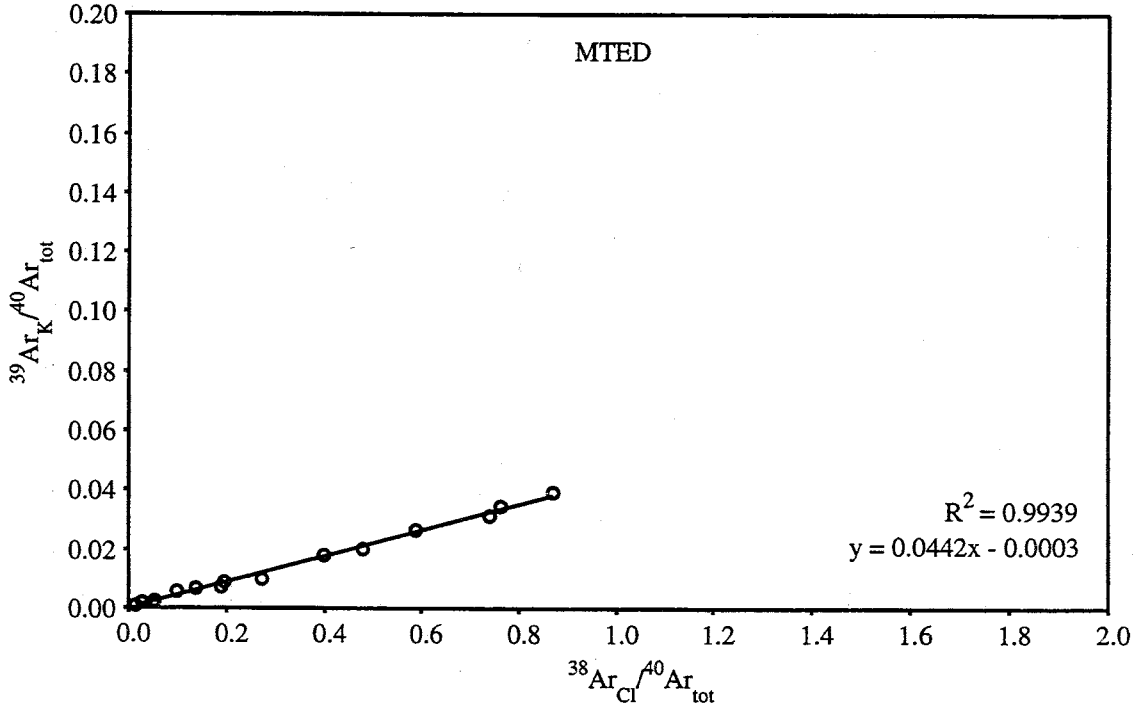
MTED
$^{39}Ar_K/^{40}Ar_{tot}$
$^{38}Ar_{Cl}/^{40}Ar_{tot}$
$R^2 = 0.9939$
y = 0.0442x - 0.0003
0.00
0.02
0.04
0.06
0.08
0.10
0.12
0.14
0.16
0.18
0.20
0.0
0.2
0.4
0.6
0.8
1.0
1.2
1.4
1.6
1.8
2.0

Figure 22 G, H

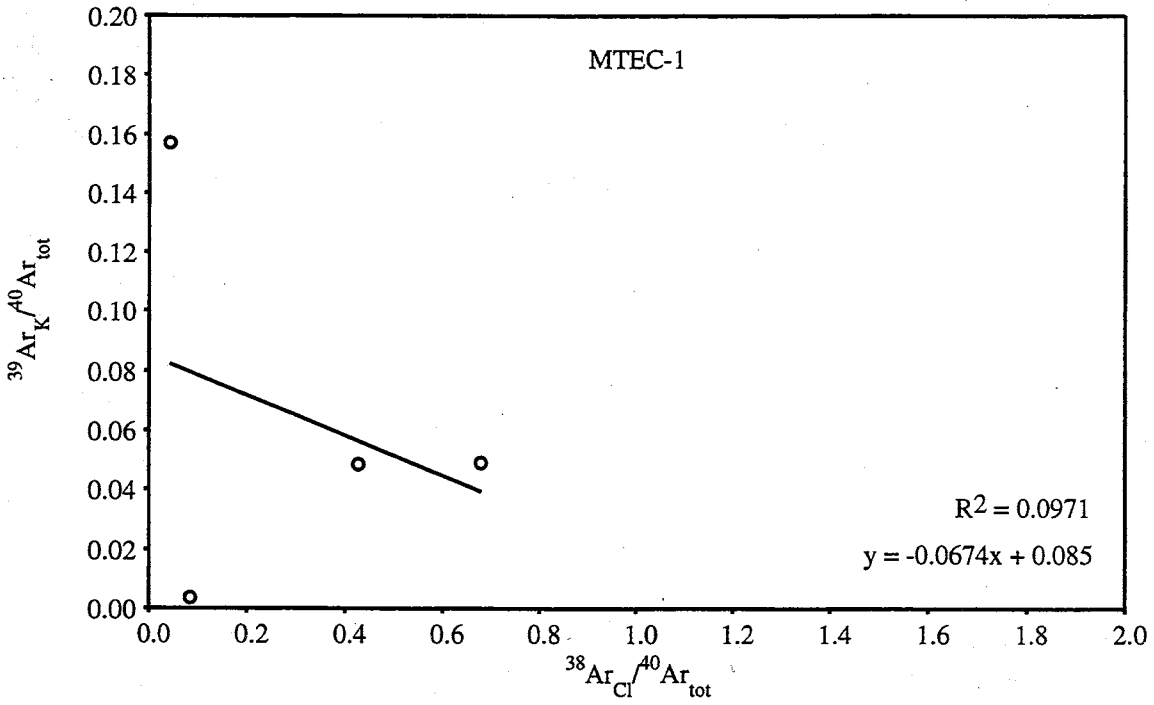
MTEC-1
$^{39}Ar_K/^{40}Ar_{tot}$
$^{38}Ar_{Cl}/^{40}Ar_{tot}$
$R^2 = 0.0971$
y = -0.0674x + 0.085
0.00
0.02
0.04
0.06
0.08
0.10
0.12
0.14
0.16
0.18
0.20
0.0
0.2
0.4
0.6
0.8
1.0
1.2
1.4
1.6
1.8
2.0

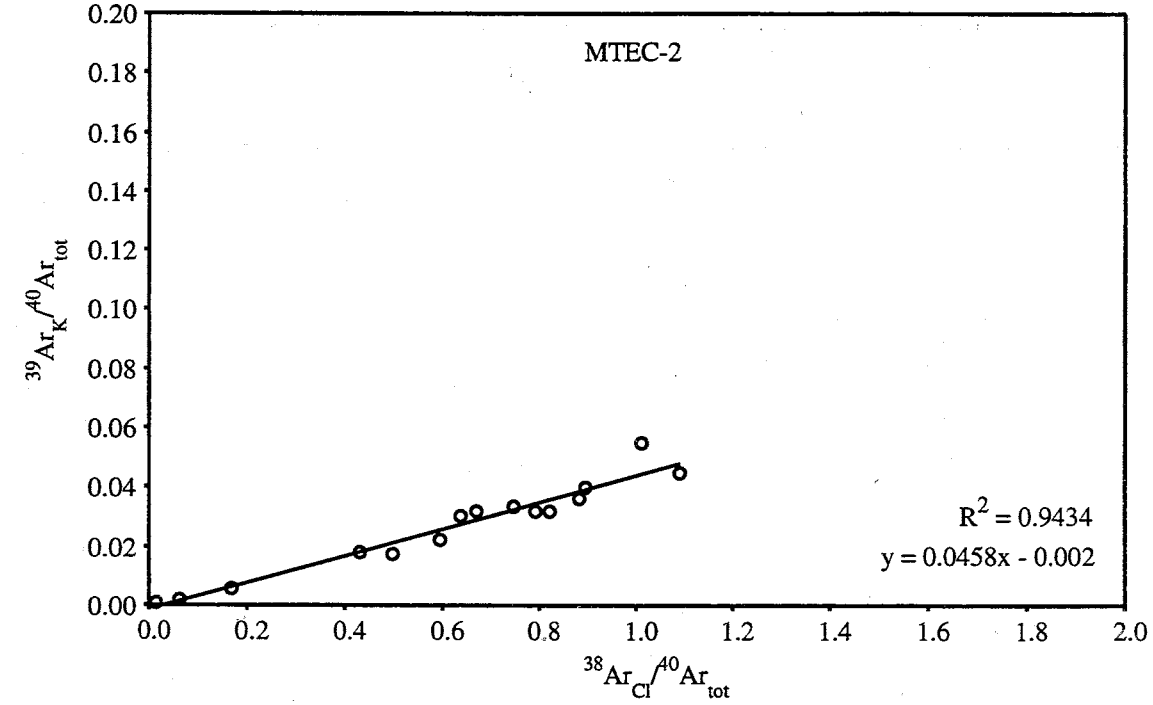
MTEC-2
$^{39}Ar_K/^{40}Ar_{tot}$
$^{38}Ar_{Cl}/^{40}Ar_{tot}$
$R^2 = 0.9434$
y = 0.0458x - 0.002
0.00
0.02
0.04
0.06
0.08
0.10
0.12
0.14
0.16
0.18
0.20
0.0
0.2
0.4
0.6
0.8
1.0
1.2
1.4
1.6
1.8
2.0

Figure 22 I, J

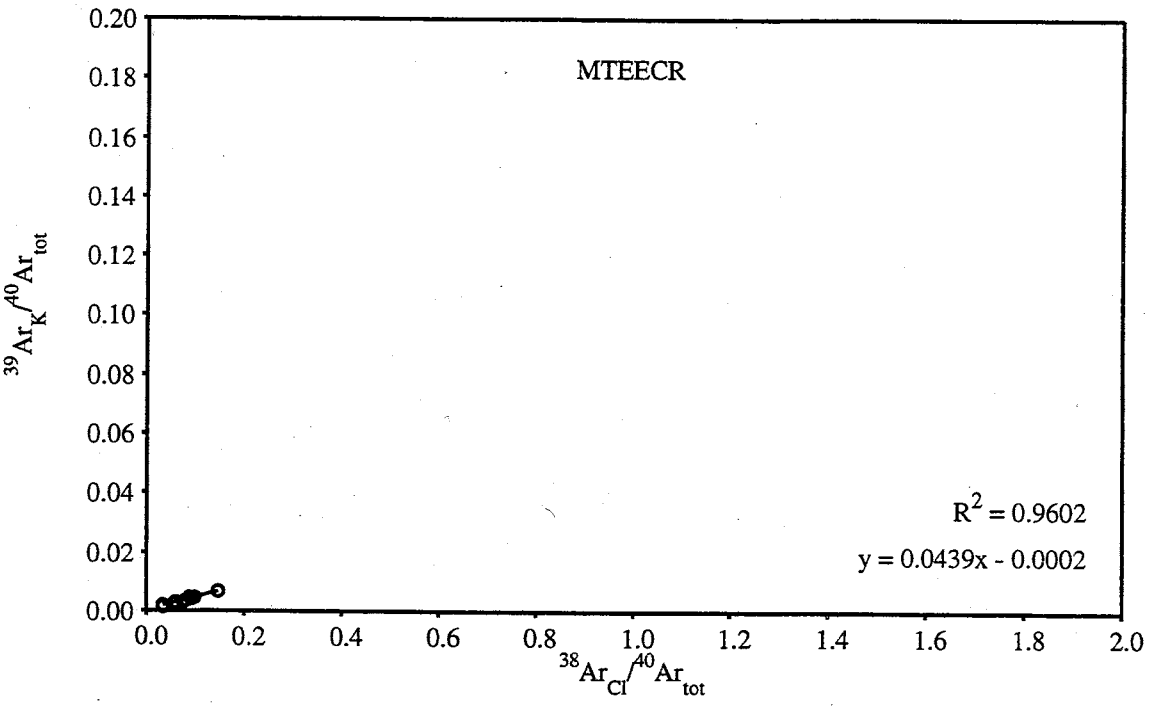
MTEECR
$^{39}Ar_K/^{40}Ar_{tot}$
$^{38}Ar_{Cl}/^{40}Ar_{tot}$
$R^2 = 0.9602$
y = 0.0439x - 0.0002
0.00
0.02
0.04
0.06
0.08
0.10
0.12
0.14
0.16
0.18
0.20
0.0
0.2
0.4
0.6
0.8
1.0
1.2
1.4
1.6
1.8
2.0

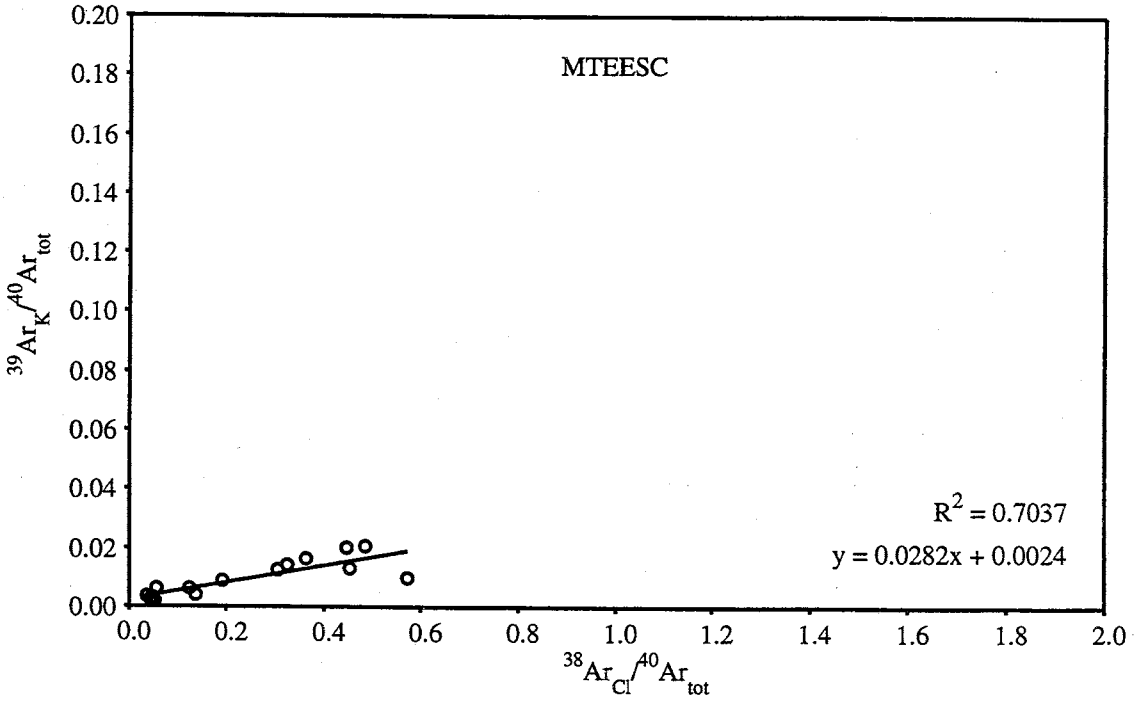
MTEESC
$^{39}Ar_K/^{40}Ar_{tot}$
$^{38}Ar_{Cl}/^{40}Ar_{tot}$
$R^2 = 0.7037$
y = 0.0282x + 0.0024
0.00
0.02
0.04
0.06
0.08
0.10
0.12
0.14
0.16
0.18
0.20
0.0
0.2
0.4
0.6
0.8
1.0
1.2
1.4
1.6
1.8
2.0

Figure 22 K, L

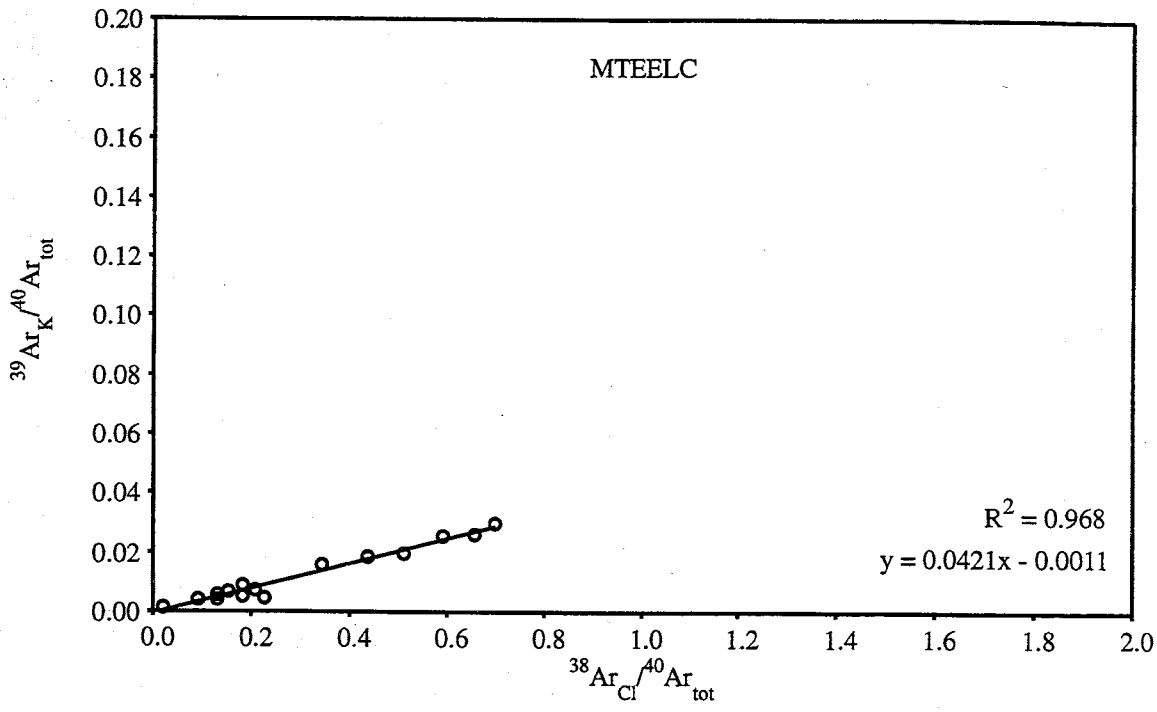
MTEELC
$R^2 = 0.968$
$y = 0.0421x - 0.0011$
$^{39}Ar_K/^{40}Ar_{tot}$
$^{38}Ar_{Cl}/^{40}Ar_{tot}$
0.00
0.02
0.04
0.06
0.08
0.10
0.12
0.14
0.16
0.18
0.20
0.0
0.2
0.4
0.6
0.8
1.0
1.2
1.4
1.6
1.8
2.0

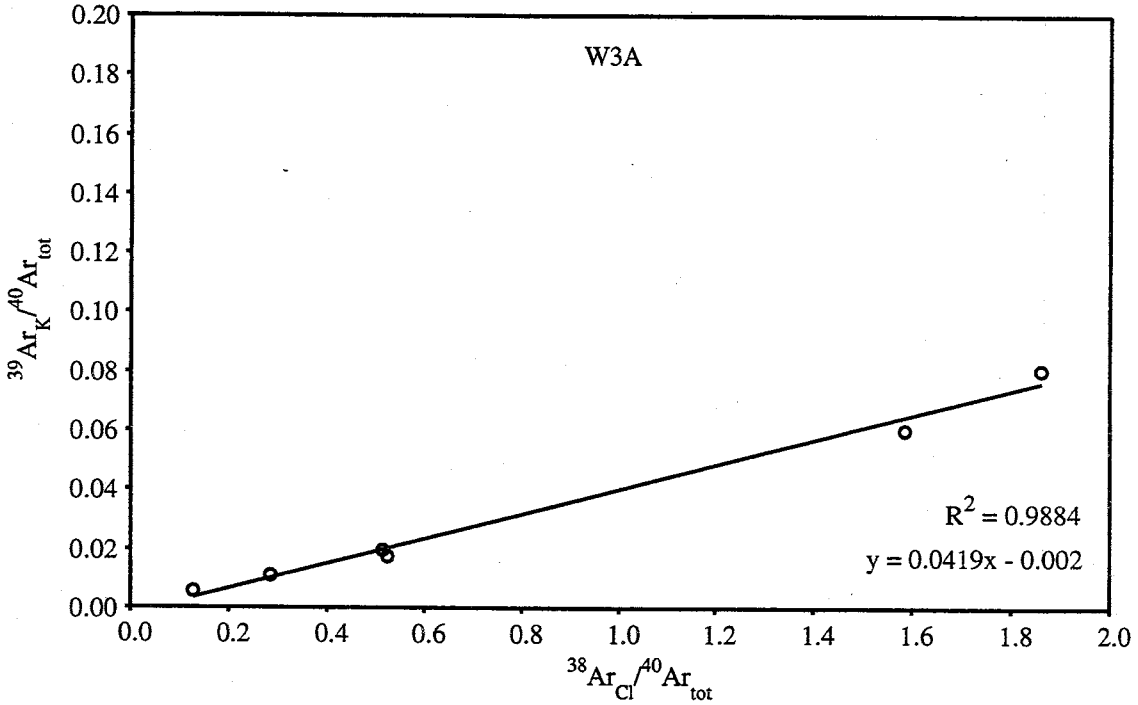
W3A
$R^2 = 0.9884$
$y = 0.0419x - 0.002$
$^{39}Ar_K/^{40}Ar_{tot}$
$^{38}Ar_{Cl}/^{40}Ar_{tot}$
0.00
0.02
0.04
0.06
0.08
0.10
0.12
0.14
0.16
0.18
0.20
0.0
0.2
0.4
0.6
0.8
1.0
1.2
1.4
1.6
1.8
2.0

Figure 22 M, N

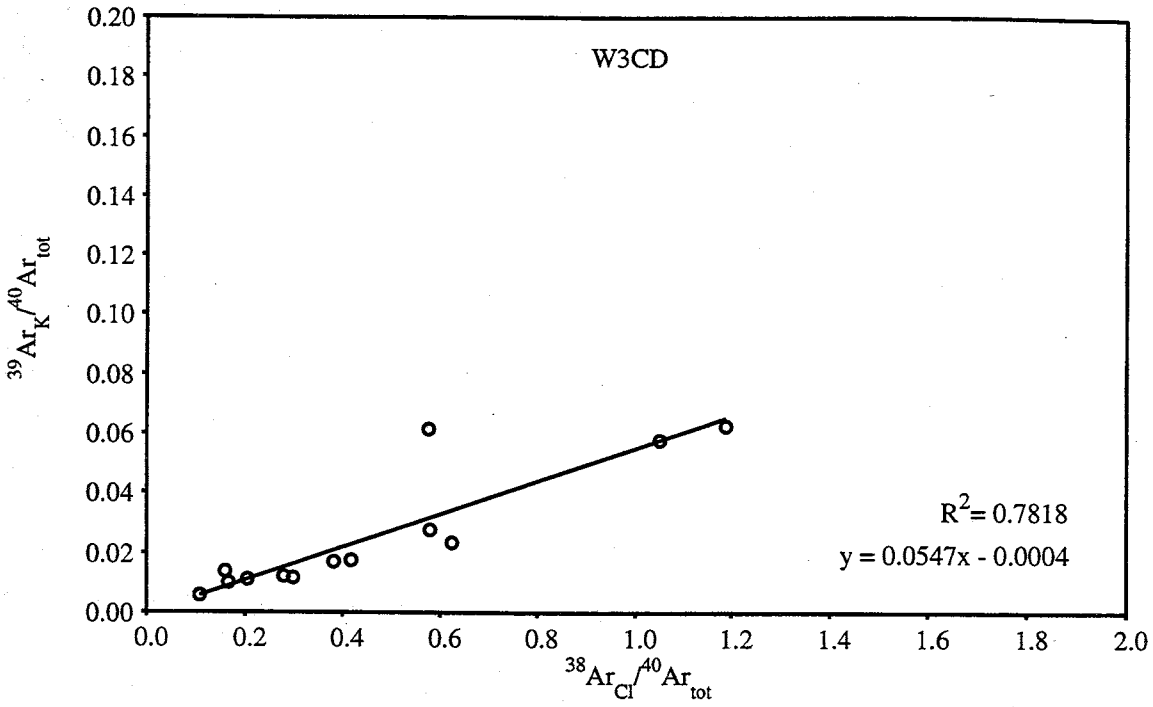
W3CD
$^{39}Ar_K/^{40}Ar_{tot}$
$^{38}Ar_{Cl}/^{40}Ar_{tot}$
$R^2 = 0.7818$
y = 0.0547x - 0.0004
0.00
0.02
0.04
0.06
0.08
0.10
0.12
0.14
0.16
0.18
0.20
0.0
0.2
0.4
0.6
0.8
1.0
1.2
1.4
1.6
1.8
2.0

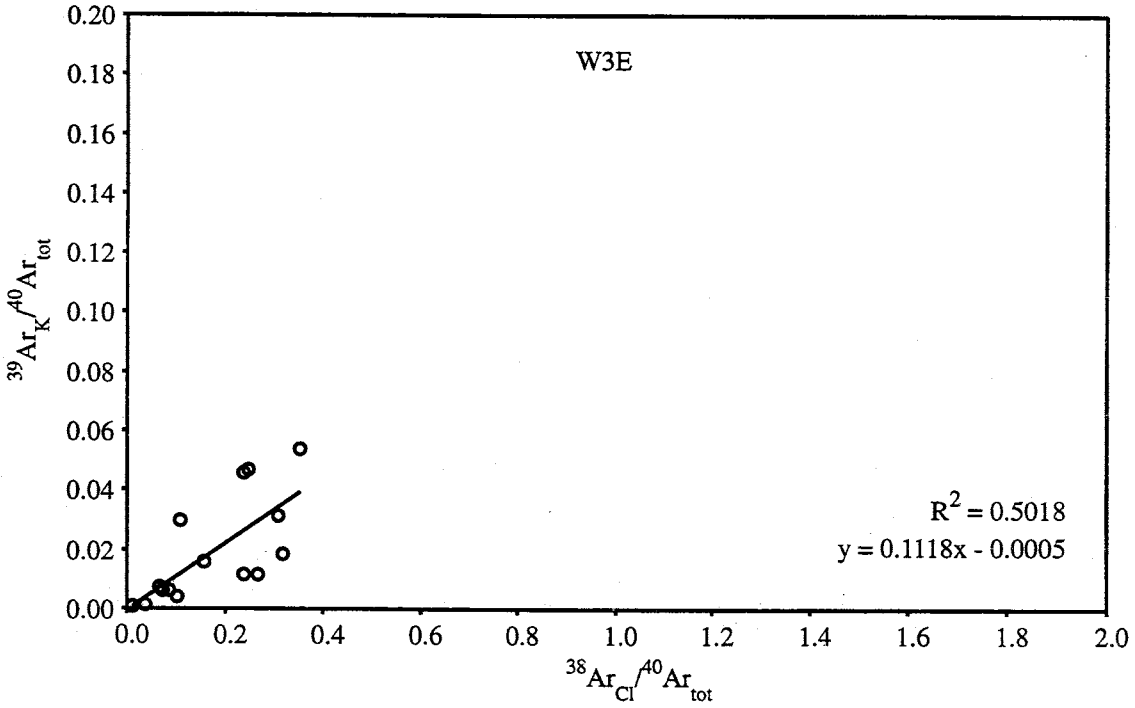
W3E
$^{39}Ar_K/^{40}Ar_{tot}$
$^{38}Ar_{Cl}/^{40}Ar_{tot}$
$R^2 = 0.5018$
y = 0.1118x - 0.0005
0.00
0.02
0.04
0.06
0.08
0.10
0.12
0.14
0.16
0.18
0.20
0.0
0.2
0.4
0.6
0.8
1.0
1.2
1.4
1.6
1.8
2.0

Figure 22 O, P

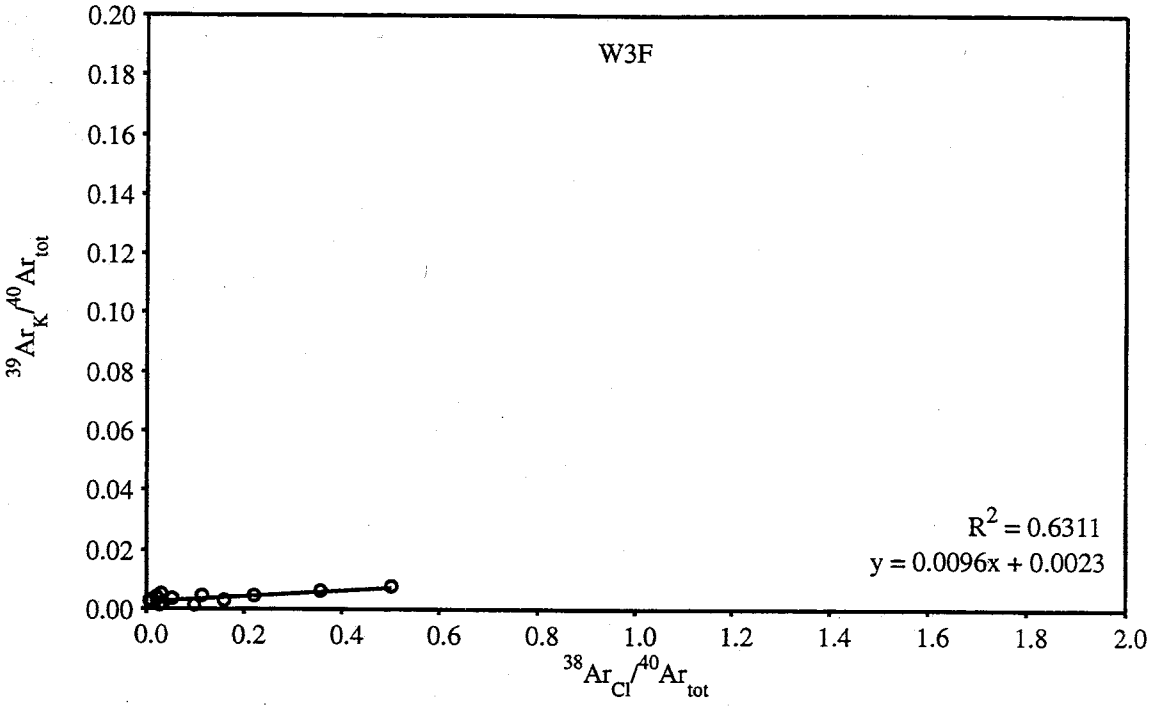
W3F
$^{39}Ar_K/^{40}Ar_{tot}$
$^{38}Ar_{Cl}/^{40}Ar_{tot}$
$R^2 = 0.6311$
y = 0.0096x + 0.0023
0.00
0.02
0.04
0.06
0.08
0.10
0.12
0.14
0.16
0.18
0.20
0.0
0.2
0.4
0.6
0.8
1.0
1.2
1.4
1.6
1.8
2.0

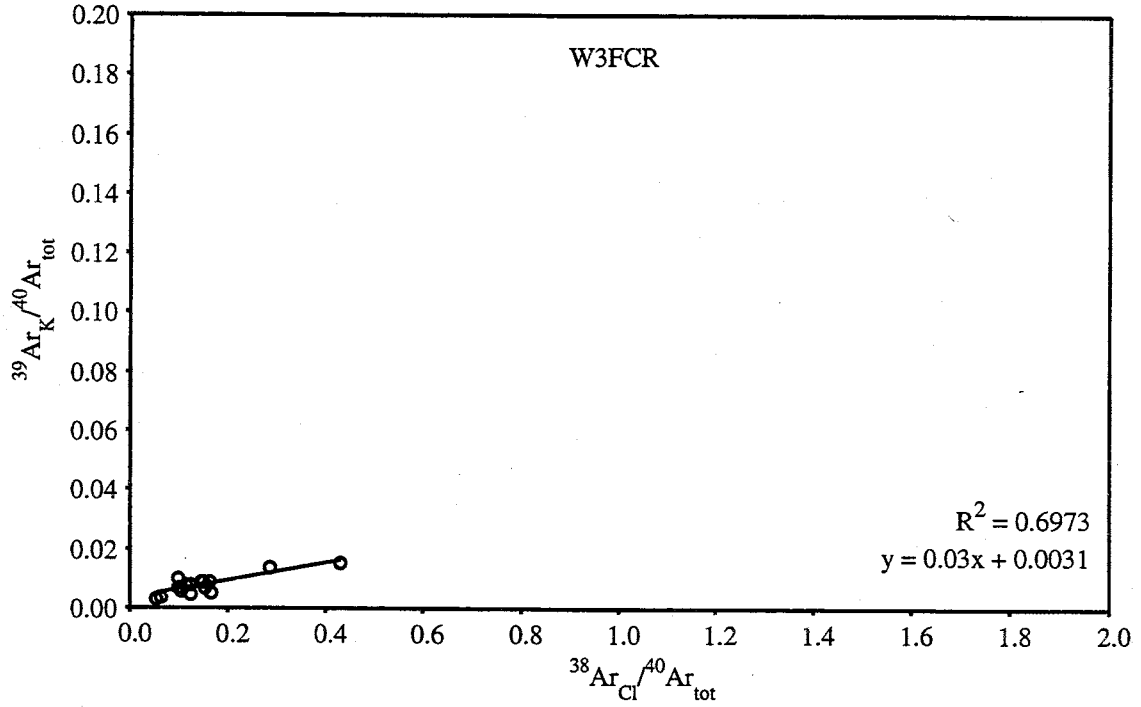
W3FCR
$^{39}Ar_K/^{40}Ar_{tot}$
$^{38}Ar_{Cl}/^{40}Ar_{tot}$
$R^2 = 0.6973$
y = 0.03x + 0.0031
0.00
0.02
0.04
0.06
0.08
0.10
0.12
0.14
0.16
0.18
0.20
0.0
0.2
0.4
0.6
0.8
1.0
1.2
1.4
1.6
1.8
2.0

Figure 22 Q, R

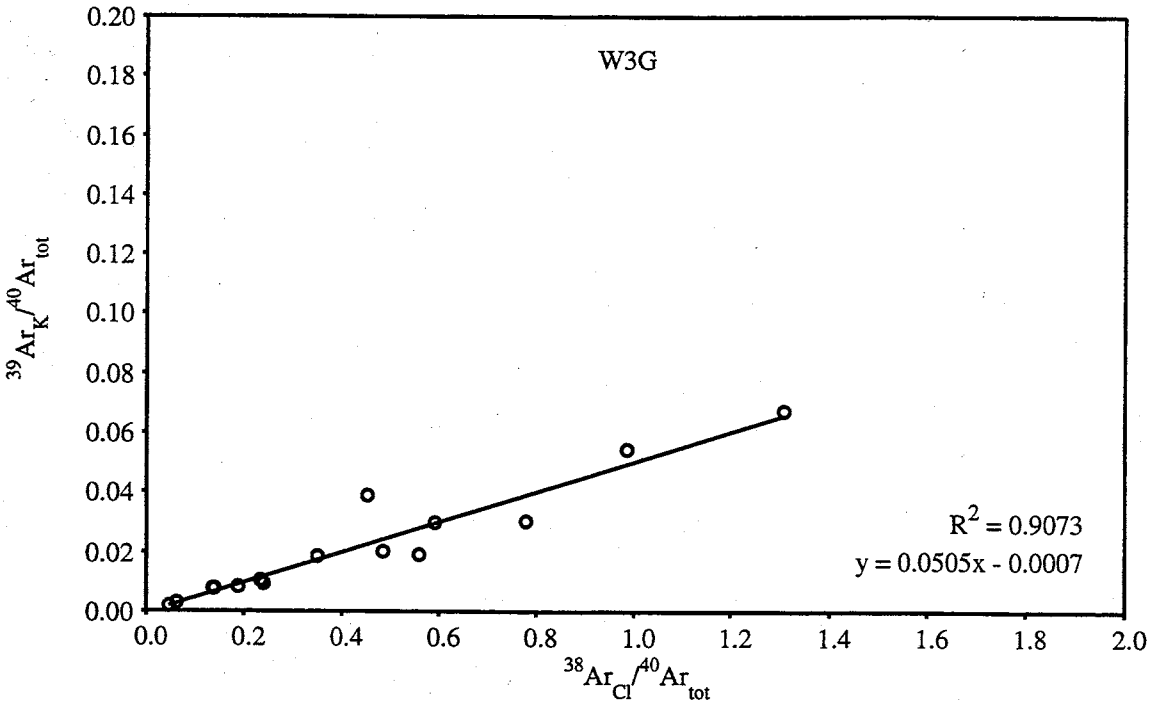
W3G
$^{39}Ar_K/^{40}Ar_{tot}$
$^{38}Ar_{Cl}/^{40}Ar_{tot}$
$R^2 = 0.9073$
y = 0.0505x - 0.0007
0.00
0.02
0.04
0.06
0.08
0.10
0.12
0.14
0.16
0.18
0.20
0.0
0.2
0.4
0.6
0.8
1.0
1.2
1.4
1.6
1.8
2.0

Figure 22 S

6. DISCUSSION

6.1. Adularia

Adularia from Capitan were analyzed to obtain an age of emplacement of the pluton, thus allowing direct comparison to ages obtained from cogenetic vein quartz. Six of the seven adularia samples gave a mean age of 27.85 ± 0.55 Ma. The seventh adularia was a vein sample from W3, which presumably contained excess argon. The minimum age, 31.60 ± 2.00 Ma, in this spectrum represents a maximum age for the pluton emplacement. The plateau age of 27.85 ± 0.55 Ma represents the age of emplacement. The single K-feldspar sample from the pluton had a plateau age of 27.92 ± 0.12 Ma. These ages obtained from the veins agree to the pluton sample within 1σ deviation, and support the assertion that the veins are of magmatic origin. These ages also agree well with the previously obtained age of 28.3 ± 0.1 Ma. Aside from the plateau segment, the spectra display young ages in the low temperature steps that could be related to argon loss (Figure 10). Several processes could result in the apparent argon loss, including: 1) post formation re-heating, 2) protracted cooling of the pluton, and 3) minor alteration to fine grained clay minerals.

Evidence to support a post-formation heating event has not been documented at Capitan. The temperatures of homogenization of the fluid inclusions, as well as the stable isotope data, suggest that the majority of the fluid inclusions (> 90%) are primary magmatic inclusions formed at high temperatures. However, in two of the sample locations (W3 and CMX), there are small populations of low salinity low temperature type 3 and type 4 fluid inclusions present in the quartz. These could have formed during a

hydrothermal event that post-dated pluton cooling. However, the stable isotope data have a magmatic signatures. One possible explanation is that the Capitan pluton was reheated by nearby emplacement of another igneous body. An argument in favor of this explanation is that the Capitan pluton lies on the Capitan linament, which has been a long-term source of igneous activity. Nevertheless, this explanation seems unlikely.

Thermal considerations rule out protracted cooling of the pluton. A pluton the size of Capitan should have crystallized within about 32 Ky. (Allen and McLemore, 1991) and cooled to ambient conditions with 1 M. y. (cf. Heizler et al. 1988). Additionally, apatite fission track thermochronologic data from the Capitan pluton indicate that the region cooled below 100°C by 26-28 Ma (Kelley and Chapin, 1995). If in fact the age gradients measured in the adularia are related to argon loss caused by diffusion out of the sample, the event causing the diffusive loss would have to be a low temperature (<100° C) and the adularia would have to have unusually low argon retentivities. Argon kinetic data obtained during the step-heating of the adularia (not shown) appear to indicate anomalously low activation energies and high diffusivities. These kinetic parameters will need to be confirmed by additional experiments, but if they are correct they allow for argon transport below 100°C. Based on this, it is plausible that apatite fission track ages could approximate the age of the pluton, with the small diffusion domains of the adularia recording very low temperature cooling. As was previously noted, Capitan adularia is actually cryptoperthitic feldspar containing albite and orthoclase lamellae. These lamellae range from micron to millimeters in size. These microstuctures may be responsible for the low closure temperatures of the adularia (cf. Fitzgerald and Harrison, 1993). Intergrowths and microstructures have been used to

explain complex argon kinetics in feldspars (Parsons et al., 1988; Fitzgerald and Harrison, 1993; Foland, 1994; Burgess et al., 1992) and could be the cause for the exceptionally low retentivity of the adularia from Capitan.

The third possibility for the age gradients in the adularia spectra is alteration and/or a younger clay contaminant. The samples were chosen to minimize the effect of alteration but, in two samples, HHADL and FNADL, some alteration was seen. It is possible that due to the small size of the sample some evidence of alteration was missed or not visible in other samples. Alteration to clay could cause argon loss, or the growth of a K-bearing alteration phase after emplacement might yield initially young ages in spectra.

6.2. Young Ages in Quartz

Several samples of fluid-inclusion-bearing quartz yielded ages much younger than the known age of the pluton (Appendix R). These ages are not geologically meaningful with respect to the age of the pluton, but could be the result of some other geologic process. These young apparent ages are difficult to understand in samples that are known to contain $^{40}Ar_E$. However, the young ages are associated with higher K_20 concentrations, which could be responsible for swamping the $^{40}Ar_E$ signal. To obtain young ages the sample must have lost ^{40}Ar, or alternatively, gained ^{39}Ar. ^{39}Ar is produced from ^{39}K in the reactor during irradiation, therefore, the addition of an K bearing contaminant after irradiation will not cause the age of the sample to appear young. Upon further examination, all of the young ages were from samples irradiated at the same time (irradiation number NM-53). The young ages were observed in samples crushed prior to

irradiation and in large uncrushed samples, and in samples packed for irradiation in either aluminum trays or in quartz tubes.

Three possible explanations exist for the young ages observed in samples crushed prior to irradiation, from irradiation NM-53, including: 1) loss of $^{40}Ar^*$ as a result of crushing prior to irradiation, 2) the addition of an external, young, K-rich contaminant prior to irradiation, and 3) a geological process. Young ages were observed in large grain size samples and smaller uncrushed grains. These young ages were anomalous; only 7 of 65 furnace analysis (10.8%) and 3 of 35 laser analysis (8.6%) were more than 2σ younger than the plateau age of the associated veins (28.3 ± 0.1 Ma). All of the young furnace-heated samples had Cl/K ratios less than 1, and all of the samples with old apparent ages have Cl/K ratios greater than 1. In contrast, the laser-heated samples with statistically young apparent age had Cl/K ratios that were statistically indistinguishable from the bulk Cl/K ratios ($\approx$6.5) obtained from crush leach analysis. A graph of the bulk K_2O and Cl^- concentrations, age and Cl/K ratio versus the sample name is shown in Figure 22. The young samples from irradiation NM-53 (shown on the left hand side of the graph) have Cl concentrations that are statistically indistinguishable from samples from other irradiations. The samples that give young ages have a K concentration that are significantly larger than the old samples. Many individual steps within the old, well-behaved, samples had low Cl/K ratios but the bulk ratio was always between 4.5 and 8. The lower Cl/K ratios could be indicative of contribution from the geologic cause of the young ages.

The first explanation suggested to account for young ages requires the sample to be crushed prior to irradiation. The siting of potassium and argon within the quartz

crystal, and their relative mobility are important factors to consider. If the sample is irradiated prior to crushing, $^{40}Ar^*$ remains sited with the K within the crystal. If the sample is crushed prior to irradiation, $^{40}Ar^*$ may be lost whereas K is not affected. The K is not as mobile as the Ar gas, and thus remain within the quartz crystal. As a result, crushing induced argon loss would make the sample appear younger than it is. However, this process would not change the Cl/K ratio of the sample, as is seen in the furnace-heated samples from NM-53, because no additional K is added to the sample. Cl loss could reduce the Cl/K ratio, but no significant decrease in Cl was observed in the young samples. Effects of crushing samples prior to irradiation has been previously investigated, because almost all samples are crushed during sample preparation, but was not found to be a problem. Harrison et al. (1993) state "that any adverse consequences arising from these effects [crushing] ... are exceedingly small."

The possibility of contamination by an external contaminant during irradiation or analysis is considered unlikely. The samples that yielded young ages, but were not crushed prior to irradiation cannot be explained by the above hypothesis. A young, K-rich contaminant could, theoretically, be the cause of the young ages in the samples. The low Cl/K ratio and high K concentration consistent with K being added to the sample. Precautions were taken to avoid contamination, such as the use of new sieves for sample preparation, and the complete cleaning of the crucible and replacement of the furnace liner prior to analysis. However, because the contaminant would have to be irradiated with the samples, it had to be mixed in with the samples prior to irradiation. In addition, because the young ages were exhibited in the gas that evolved at temperatures as high as 1750°C, the contaminant would have to be internal to the quartz lattice, or within a phase

which degassed at very high temperature. One could invoke an irradiated grain trapped above the furnace falling into the furnace at high temperatures, but this would not be likely to occur in more than one sample. As previously mentioned, young ages were observed in 7 of 65 samples analyzed in the furnace (both total fusion and step-heating). The young ages were observed in samples irradiated both in quartz tubes and Al trays. The tube surrounding the trays was broken following departure from New Mexico Tech. There was no evidence of wetting, which could be indicative of possible surface contamination during irradiation. Additionally, all of the samples with young ages were not in the tube that was broken, and therefore it is unlikely that the young ages are a result of contamination during irradiation. The possibility exists that the samples were contaminated in the laboratory during sample preparation or during analysis. This too is unlikely due to the high temperatures associated with the young ages, (for example the 1.0±0.7 Ma age plateau, from 800° - 1300°C, in sample CMX2, Figure 11 A and the 1.27 ± 0.15 Ma age 1750° C step, Figure 11E). The contaminant cannot merely be something adhered to the surface of the sample, which would degas at relatively low temperatures. The sample must have an internal source of these young ages that is not released until the quartz begins to soften at high temperatures.

The only plausible explanation for the high temperature release of the young ages is a geologic source. The argon loss profiles observed in the adularia may provide a possible explanation for the young ages. For the total fusion analyses, young ages were measured in samples from CMX and W3 (Figure 17). Small solid inclusions of the adularia contained sporadically within the quartz cannot be ruled out. Several phases of solid inclusions were observed in the quartz, but no solid inclusions were positively

identified as adularia. This however, does not exclude the possibility that the inclusions are present, but perhaps to small to be identified. Feldspar and quartz are remarkably similar in appearance in BSE imaging due to the similar mean atomic Z. Therefore, they would be difficult to observe in the samples. In addition to the possibility of adularia inclusions, low salinity inclusions were noted in these samples. The presence of these inclusions could be contributing to the young ages, however, the rapid cooling of the pluton, and the magmatic stable isotope signature suggest that these low salinity inclusions formed soon after emplacement of the pluton. They may have decreased the age, but can not be the sole cause of the $\approx$ 1 Ma ages.

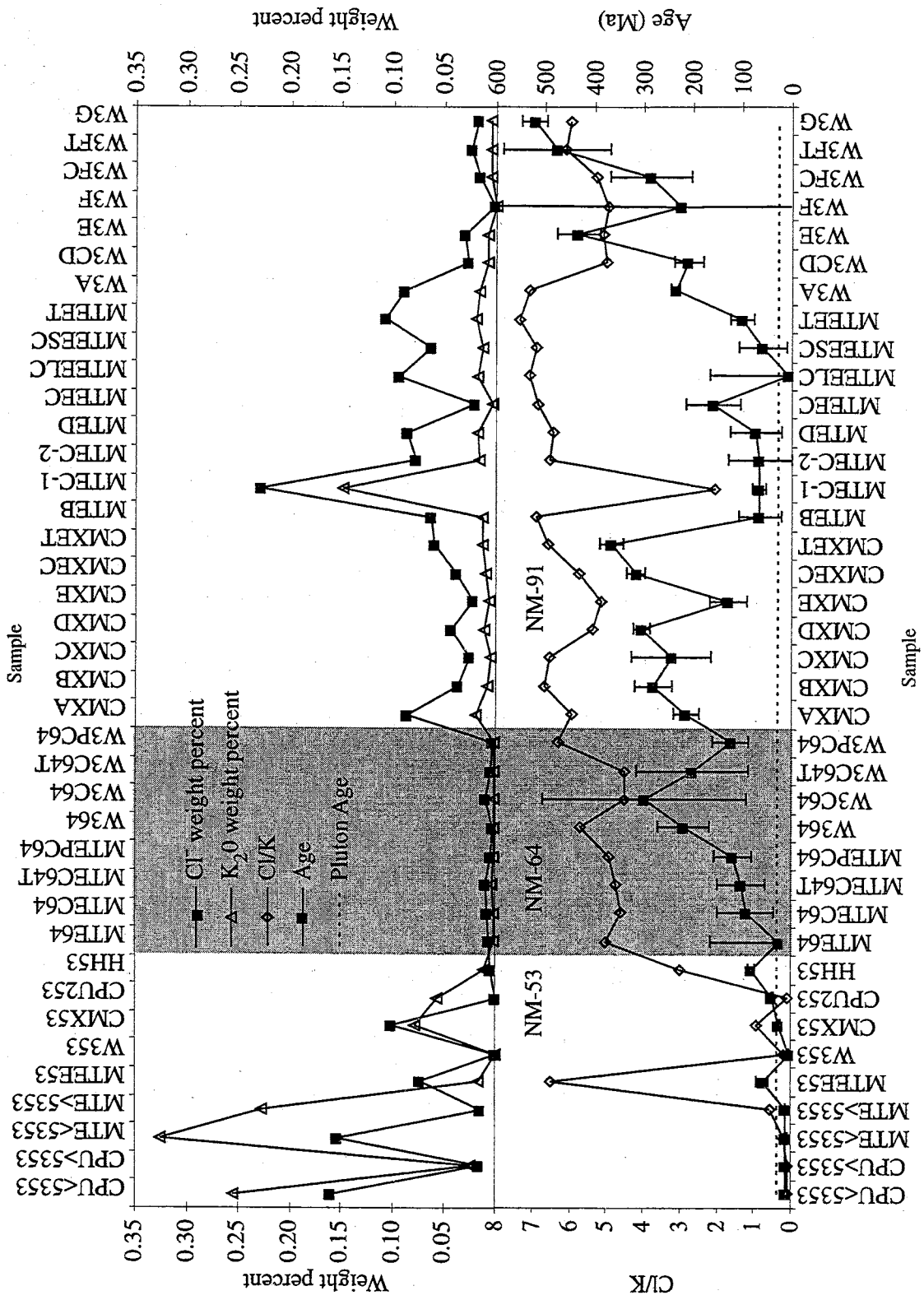

Figure 22 Summary of Cl/K, Age, Cl- and K_2O Concentrations from Capitan Quartz. All analysis except total fusion analyses are shown.

6.3. Old Ages

All of the samples from the second and third irradiations (NM-64 and NM-91) gave ages that were older or statistically equal to the known age of the pluton. Stable isotope data has shown that the veins, from which the samples were collected were primarily formed from magmatic fluids exsolved from the pluton (Campbell et al., 1995; Dunbar et al., 1996). These results, along with the crosscutting relationships, help confirm the maximum age for the vein quartz is 28.3 ± 0.1 Ma. The observed old ages are expected from samples containing excess argon, and the age spectra have shapes typical of samples containing excess argon (McDougall and Harrison, 1988). This age spectra shape is commonly referred to as a saddle-shaped spectrum. McDougall and Harrison (1988) summarize the literature, stating that the "central portions of the age spectra revealed geologically meaningful ages." If the age of Capitan vein quartz was unknown it might be reasonable to assign a maximum age of 45.07 ± 5.0 Ma to the pluton. This age is based on the minimum (saddle) age given by the spectra but is significantly older than the age of the pluton, and associated veins.

The behavior of $^{40}Ar_E$ within the samples is difficult to interpret. A number of authors have found excess argon associated with small fluid inclusions in feldspars. This association implies that the excess argon should be easily removed from the sample by removing the fluid (decrepitating the fluid inclusions). Biotite provides another well-studied example of ^{40}Ar behavior in minerals. Flat, geologically too old age spectra have been observed in biotite, and have been attributed to homogenization of the signal due to the mineral's instability in the furnace, causing delamination or dehydration (Pankhurst et al., 1973; Harrison et al., 1985; McDougall and Harrison, 1988). This explanation

however, does not appear applicable to a cleavage -free, anhydrous mineral such as quartz. The $^{40}Ar_E$ is clearly not removable by crushing the sample. This implies that some fluid inclusions remain even after intensive crushing, or that the ^{40}Ar is located within solid inclusions in the lattice, or directly in the lattice itself. A discussion of the temperature at which gas is released may help to understand the siting of $^{40}Ar_E$ within Capitan quartz

The low temperature peak in gas release, at approximately 600° C, is apparently due to the decrepitation and degassing of fluid inclusions in the quartz (Figure 18). It has been shown that most fluid inclusions > 5 μm will decrepitate at or below (Roedder, 1984) the 573° C $\alpha - \beta$ transition in quartz (Klein and Hurlbut, 1993). Capitan fluid inclusions have been reported to decrepitate around 600° C (Banks et al., 1994; Phillips, 1991; Ratajeski and Campbell, 1994). This was also confirmed by the decrepigram shown in Figure 19. These decrepitation studies strongly suggest that the 600° C peak in gas release is related to fluid inclusion decrepitation.

Kelly et al. (1986) analyzed similar samples, from a granite hosted tungsten deposit in England, which were primarily quartz, and saw similar gas release peaks at 600° and 1400°, but also observed a peak in the range 700 – 1000° C. Capitan quartz released a remarkably small portion of the gas during this temperature range. Kelly et al. (1986) found that this intermediate release peak was especially prominent in high Ca samples. They note that the quartz samples they analyzed contained solid inclusions of sericite (white mica), so it is possible that this release is solely a result of degassing of mica inclusions. The presence of these included micas, which yield essentially flat age spectra (McDougall and Harrison, 1988) and are higher in K concentration than quartz,

could also be a reason that Kelly et al.'s samples approach a geologically correct age. Some Capitan quartz samples also yield results that approach the true age of the Capitan pluton. Samples were selected to minimize the chance of included phases, in order to attempt to truly date the inclusion fluids. Because there are limited numbers of solid inclusions, and presumably no fluid inclusions degassing during this temperature range, only a small part of the total gas is released in the 700° - 1000° C temperature range.

The high temperature release at 1400° C may be partially attributed to sub-micron sized fluid inclusions which do not build up the pressure required to fracture the quartz (decrepitation) allowing release of gas. These inclusions may remain trapped until the quartz begins to soften allowing rapid movement of Ar out of the system. It is also possible that the fractures caused by decrepitation at lower temperatures partially anneal after decrepitation, causing a portion of the gas to be trapped until higher temperature. Several other causes of high temperature release are given by Kelly (1986) and are applicable to the Capitan quartz. They are 1) daughter minerals, 2) captive minerals, 3) argon dissolved in the quartz structure, or 4) small gas-rich fluid inclusions formed as a result of boiling. These trapped, small, gas-rich fluid inclusions may be too tiny to be observed by microscope, which could explain their apparent absence in Capitan quartz. However, some gas-rich inclusions were seen in samples from W3 (Campbell et al., 1995). All of the above reasons could be contributing to the high temperature release in Capitan quartz .

In summary, we are unable to resolve the $^{40}Ar_E$ components that are causing the age of this quartz to be substantially older than the age of the pluton. The argon geochronology community has long recognized the effects of $^{40}Ar_E$ in minerals such as

biotite, but as a whole has underestimated the problems in thermally stable minerals. Van den Bogaard and Schirnick (1995) use $^{40}Ar/^{39}Ar$ laser analysis of quartz phenocrysts to provide "conclusive evidence for the longevity of the Long Valley magma system". This conclusion is problematic due to the thermal characteristics of plutons. The Long Valley system, similar to the Capitan system, should have cooled in a relatively short period of time. Van den Bogaard states that the origin of the quartz crystals he analyzed may be xenocrystic but excludes the possibility of them containing a substantial amount of $^{40}Ar_E$ (stated $^{40}Ar/^{36}Ar$ intercept of 296 ± 2). If quartz is able to obtain $^{40}Ar_E$ from a magma chamber and incorporate it into its structure so that it is indistinguishable from $^{40}Ar^*$, it will provide systematically old ages. Long Valley quartz contained K-bearing melt inclusions, and also had well-behaved isochrons. Although Capitan quartz possibly had small inclusions of KP glass, the isochrons were not well behaved. These systematically old ages are seen in Capitan quartz and it is possible that the quartz from Long Valley has similar properties, and is resulting in ages that are systematically old, causing the appearance of a long lived intrusion. Therefore, quartz should be analyzed with caution until the systematics of ^{40}Ar incorporation are understood. Capitan quartz, if interpreted in the same way as Long Valley manner, would provide an age twice as old as the known age of the pluton, which is not geologically reasonable due to the evidence for rapid cooling previously discussed. Figure 14 B shows an ideogram for the high-temperature, old ages from Capitan quartz. It is important to note that the plateau ages from the high temperature steps are relatively precise, much more precise than the scatter of the data suggest is statistically reasonable. All evidence suggests that Capitan pluton cooled rapidly. Because excess argon is released when the sample begins to soften, the spectrum

is artificially flattened, similar to the effect seen in biotite (Pankhurst et al., 1973; Harrison et al., 1985; McDougall and Harrison, 1988). In the Capitan veins, the cogenetic vein adularia provide a constraint on the age of the quartz. In systems where there is little or no constraint on the age, it is necessary to be cautious when interpreting age data.

7. CONCLUSIONS

Quartz veins associated with the Capitan pluton provide some of the best studied fluid inclusions in the world. The composition of the fluid inclusions is known from a variety of methods. The inclusions provide an excellent material for the testing of new analytical methods because of their large, abundant nature. If fluid inclusions in quartz are dateable using the $^{40}Ar/^{39}Ar$ method, these inclusions might have provided a best case scenario. The only additional characteristic that would be beneficial would be an older age, providing larger radiogenic yields. However, older environments containing fluid inclusions are unlikely to be primarily from a single generation, and as is seen in the samples from the Capitan pluton, even a small contribution from a source other than the primary fluid inclusions can have an impact on the age.

Although our attempt to date fluid inclusions was not successful, several pertinent observations have resulted from this study. 1) Quartz is not a neutral substrate. We have documented two distinct phases of solid K-bearing inclusions (KCl and KP glass) in addition to the fluid inclusions, and other solid phases. The release profiles observed in Capitan quartz can not be understood by interpreting the quartz as a blank slate containing fluid inclusions which decrepitate by 573° C or that can be broken by crushing, thereby evolving the argon contained within the inclusions. 2) Quartz and/or the inclusions contain an abundance of $^{40}Ar_E$, which cannot be removed by crushing the sample and which produces essentially flat, relatively high-precision portions of age spectra with ages that are too old for the deposit. 3) Crushing of these samples released large amounts of argon from the samples (up to 83.9% of the total ^{39}Ar), but did not

remove all of the $^{40}Ar_E$. By crushing the sample using a mortar and pestle style *in vacuo* crusher gas is evolved from the lattice of FCS, implying that gas is also removed from the lattice of the quartz during crushing. 4) Young ages obtained from Capitan quartz are probably a result of a geologically meaningful included phase. This is probably young, sub-micron inclusions of feldspar that have experienced ^{40}Ar loss, or a result of some process occurring within a population of small fluid inclusions which remain intact at high temperatures.

BIBLIOGRAPHY

Allen M. S. (1988) The Capitan Pluton, New Mexico: An example of a zoned granitic magma chamber. *Geological Society of America Abstracts with Programs*, A313.

Allen M. S. and McLemore V. T. (1991) Geological, geochemical and isotopic characteristics of the Lincoln County porphyry belt, N.M.: Implications for regional tectonics and mineral deposits. *New Mexico Geological Society Fall Field Conference Guidebook*, **42**, 97-115.

Banks D. A., Yardley B. W. D., Campbell A. R., and Jarvis K. E. (1994) REE composition of an aqueous magmatic fluid: A fluid inclusion study from the Capitan Pluton, New Mexico, U.S.A. *Chemical Geology* **113**, 259-272.

Brannon J. C., Podosek F. A., and McLimans R. K. (1991) Alleghenian age of the Upper Mississippi Valley zinc-lead deposit determined by Rb-Sr dating of sphalerite. *Nature* **356**, 509-511.

Burgess R., Kelley S. P., Parsons I., Walder F. D. I., and Worden R. H. (1992) $^{40}Ar/^{39}Ar$ analysis of perthite microstructures and fluid inclusions in alkali feldspars from the Klokken syenite, South Greenland. *Earth and Planetary Science Letters:109*, 147-167.

Campbell A. R., Banks D. A., Phillips R. S., and Yardley B. W. D. (1995) Geochemistry of the Th-U-REE mineralizing Magmatic Fluids, Capitan Mountains, New Mexico. *Economic Geology* **90**, 1271-1287.

Campbell A. R., Heizler M. T., and Dunbar N. W. (1994) $^{40}Ar/^{39}Ar$ dating of fluid inclusions in quartz from the Capitan Pluton, New Mexico. *Pan-American Conference on Research on Fluid Inclusions* **5**, 11.

Campbell A. R., Lundberg S. A. W., and Dunbar N. W. (Submitted) Solid inclusions of Salt in Quartz. *Chemical Geology.*

Cebula G. T., Kunk M. J., Mehnert H. H., Naeser C. W., Obradovick J. D., and Sutter J. F. (1986) The Fish Canyon Tuff, a potential standard for the $^{40}Ar/^{39}Ar$ and fission track dating methods: Sixth International Conference on Geochronology, Cosmochronology, and Isotope Geology. *Terra Cognita* **6**, 139-140.

Chesley J. T., Halliday A. N., Kyser T. K., and Spry P. G. (1994) Direct Dating of Mississippi Valley-type mineralization: use of Sm-Nd in Fluorite. *Economic Geology* **89**, 1192-1199.

Chesley J. T., Halliday A. N., and Scrivener R. C. (1991) Samarium-Neodymium Direct Dating of Fluorite Mineralization. *Science* **91**, 949-951.

Deino A. and Potts R. (1990) Single-crystal 40Ar/39Ar dating of the Olorgesailie Formation, Southern Kenya Rift. *Journal of Geophysical Research* **95**, 8453-8470.

Dunbar N. W., Campbell A. R., and Candela P. A. (1996) Physical, chemical, and mineralogical evidence for magmatic fluid migration within the Capitan pluton, New Mexico. *GSA Bulletin* **108**(3), 318-333.

Fitzgerald J. D. and Harrison T. M. (1993) Argon diffusion domains in K-feldspar I: Microstructures in MH-10. *Contributions to Mineralogy and Petrology: 113*, 367-380.

Fleck, R. J., Sutter, J. F., and Elliot, D. H. (1977) Intermretation of dicordant 40Ar/39Ar age-spectra of Mesozoic tholeiites from Antarctica. *Geochimica et Cosmochimica Acta* **41**, 15-32.

Foland K. A. (1994) Argon diffusion in K-feldspar, In Feldspars and their reactions I. Parsons ed. *Kluwer Academic Pu.*, 415-447.

Gulson B. L. (1992) Cassiterite: Potential for direct dating of mineral deposits and a precise age for the Bushveld Complex granites. *Geology* **20**, 355-358.

Gulson B. L. and Porritt P. M. (1987) Base metal exploration of the Mount Read Volcanics, western Tasmania: Part II. Lead isotope signatures and genetic implications. *Economic Geology* **82**, 291-307.

Harrison T. M., Duncan I., and McDougall I. (1985) Diffusion of ^{40}Ar in biotite: Temperature, pressure and compositions effects. *Geochimica et Cosmochimica Acta* **49**, 2461-2468.

Harrison T. M., Heizler M. T., and Lovera O. M. (1993) In vacuo crushing experiments and K-feldspar thermochronometry. *Earth and Planetary Science Letters* **117**, 169-180.

Harrison T. M., Heizler M. T., Lovera O. M., Wenji C., and Grove M. (1994) A chlorine disinfectant for excess argon released from K-feldspar during step heating. *Earth and Planetary Science Letters* **123**, 95-104.

Heizler M. T. and Harrison T. M. (1988) Multiple trapped argon isotope components revealed by $^{40}Ar/^{39}Ar$ isochron analysis. *Geochimica et Cosmochimica Acta* **52**, 1295-1303.

Jones M. T., Reed B. L., Doe B. R., and Lanphere M. A. (1977) Age of tin mineralization and plumbotectonics, Belitung, Indonesia. *Economic Geology* **72**, 745-752.

Kelley S., Turner G., W. B. A., and Shepherd T. J. (1986) The source and significance of argon isotopes in fluid inclusions from areas of mineralization. *Earth and Planetarty Science Letters* **79**, 303-318.

Kelley, S.A., and Chapin, C.E. (1995) Apatite fission-track thermochronology of Southern Rocky Mountain-Rio Grande rift- western High Plains provinces, *New Mexico Geological Society Guidebook* **46**, 87-95.

Klein C. and Hurlbut C. J. (1993) *Manual of Mineralogy*. John Wiley and Sons.

McCandless T. E., Ruiz J., and Campbell A. R. (1993) Rhenium behavior in molybdenite in hypogene and near-surface environments: Implications for Re-Os geochronometry. *Geochimica et Cosmochemica Acta* **57**, 889-905.

McDougall I. and Harrison T. M. (1988) *Geochronology and Thermochronology by the $^{40}Ar/^{39}Ar$ method*. Oxford University Press.

Nakai S., Halliday A. N., Kesler S. E., Jones H. D., Kyle J. R., and Lane T. E. (1993) Rb-Sr dating of sphalerites from Mississippi Valley-type (MVT) ore deposits. *Geochimica et Cosmochimica Acta* **57**, 417-427.

Pankhurst R. J., Moorbath S., Rex D. C., and Turner G. (1973) Mineral Age Patterns in Ca. 3700 My old Rocks fom West Greenland. *Earth and Planetary Science Letters* **20**, 157-170.

Parsons I., Rex D. C., Guise P., and Halliday A. N. (1988) Argon-loss by alkali feldspars. *Geochimica et Cosmochimica Acta : 52*, 1097-1112.

Petke T. and Diamond L. W. (1996) Rb-Sr dating of sphalerite based on fluid inclusion-host mineral isochrons; a clarification of why it works. *Economic Geology* **91**(5), 951-956.

Phillips R. (1990) Geochemistry of hydrothermal Th-U-REE quartz/fluorite veins from the Capitan pluton. Masters, New Mexico Tech.

Phillips R. S., Michaeltree D. B., Campbell A. R., and Hanson T. (1991) Geochemistry of smoky quartz veins from the Sierra Blanca igneous complex, New Mexico. *Geological Society of America Abstract with Programs*, 56.

Qiu H. N. (1996) $^{40}Ar/^{39}Ar$ dating of the quartz samples from two mineral deposits in western Yunnan (SW China) by crushing in vacuum. *Chemical Geology* **127**, 211-222.

Rama S. N. and Hart S. R. (1965) Excess Radiogenic Argon in Fluid Inclusions. *Journal of Geophysical Research* **70**, 509-511.

Ratajeski K. and Campbell A. R. (1994) Distribution of fluid inclusions in igneous quartz of the Capitan pluton, New Mexico, U.S.A. *Geochimica et Cosmochimica Acta* **58**(3), 1161-1174.

Roedder E. (1984) *Fluid Inclusions*. (Reviews in Mineralogy, Vol. 12) Mineralogical Society of America. 644 pp.

Samson S. D., and Alexander, E.C., Jr. (1987) Calibration of the interlaboratory $^{40}Ar/^{39}Ar$ dating standard, MMhb-1. *Chemical Geology* **66**, 27-34.

Shepherd T. J. and Darbyshire D. P. F. (1981) Fluid inclusion Rb-Sr isochrons for dating mineral depsits. *Nature* **290**(5807), 578-579.

Turner G. (1988) Hydrothermal fluids and argon isotopes in quartz veins and cherts. *Geochimica et Cosmochimica Acta* **52**, 1443-1448.

Turner G. and Bannon M. P. (1988) $^{40}Ar/^{39}Ar$ Analysis of fluid inclusions in quartz and Fluorite associated with mineralisation. *Chemical Geology* **70**(1-2), 132.

Turner G. and Bannon M. P. (1992) Argon isotope geochemistry of inclusion fluids from granite-associated mineral veins in southwest and northeast England. *Geochimica et Cosmochimica Acta* **56**, 227-243.

Turner G. and Wang S. (1992) Excess argon, crustal fluids and apparent isochrons from crushing K-feldspar. *Earth and Planetary Science Letters* **110**, 193-211.

Turrin B. D., McKee E. H., Theodore T. G., and Conrad J. E. (1988) $^{40}Ar/^{39}Ar$ Studies of Fluid Inclusions in Vein Quartz from Battle Mountain, Nevada. .

Van den Bogaard P. and Schirnick (1995) $^{40}Ar/^{39}Ar$ laser prove ages of Bishop Tuff quartz phenocrysts substantiate long-lived silicic magma chamber at Long Valley, United States. *Geology* **23**, 759-762.

APPENDICES

APPENDIX A J values, sample size, and molar concentrations from $^{40}Ar/^{39}Ar$ analysis

Table A- 1 Summary J values, sample size, and molar concentrations

ID	Irradiation	Cl/K	J	Weight	CaO	Cl-	K_20
CPU<5353	53-TB1	0.091	0.00384	~200	3.04E-02	1.31E-02	1.93E-01
CPU>5353	53-TB1	0.128	0.00384	~50	8.81E-02	7.34E-03	7.62E-02
MTE<5353	53-TB1	0.227	0.00382	~200	5.08E-02	4.10E-02	2.40E-01
MTE>5353	53-TB1	0.255	0.00383	~200	4.29E-02	3.79E-02	1.98E-01
MTEE53	53-TB1	6.497	0.00391	179.6	1.37E-02	1.13E-01	2.31E-02
MTELF1	53-TB1	25.584	0.00384	5.8	3.97E-03	2.57E-02	1.34E-03
MTELF2	53-TB1	20.851	0.00384	5.1	B/D	6.13E-02	3.91E-03
MTELF3	53-TB1	11.461	0.00384	6.1	1.40E-03	5.59E-03	6.47E-04
MTELF4	53-TB1	12.583	0.00384	6.1	3.70E-03	2.56E-02	2.71E-03
MTELF5	53-TB1	10.137	0.00384	4.6	1.36E-02	2.80E-02	3.67E-03
MTELF6	53-TB1	7.770	0.00384	7.1	7.56E-02	1.09E-02	1.86E-03
MTELF7	53-TB1	8.976	0.00384	5.0	B/D	9.57E-03	1.42E-03
MTELF8	53-TB1	13.784	0.00384	5.4	B/D	8.04E-03	7.75E-04
MTELF9	53-TB1	8.214	0.00384	5.1	1.35E-04	8.87E-03	1.43E-03
MTELF10	53-TB1	6.617	0.00384	4.8	5.88E-05	1.00E-02	2.02E-03
MTELF11	53-TB1	6.715	0.00384	4.7	1.40E-03	2.55E-02	5.05E-03
MTELF12	53-TB1	6.578	0.00384	5.5	B/D	1.70E-02	3.43E-03
MTELF13	53-TB1	5.588	0.00384	4.4	7.67E-04	1.26E-02	2.99E-03
MTELF14	53-TB1	6.837	0.00384	5.6	6.65E-03	3.29E-02	6.40E-03
MTELF15	53-TB1	28.941	0.00384	4.6	B/D	3.37E-03	1.55E-04
MTELF16	53-TB1	7.144	0.00384	4.1	B/D	2.17E-02	4.04E-03
MTELF17	53-TB1	6.916	0.00384	4.4	8.93E-04	4.49E-03	8.62E-04
MTELF18	53-TB1	11.120	0.00384	4.8	B/D	2.14E-02	2.56E-03
MTELF19	53-TB1	6.069	0.00384	4.7	5.79E-04	1.31E-02	2.88E-03
MTELF20	53-TB1	9.621	0.00384	6.9	4.05E-03	1.70E-02	2.34E-03
MTELF21	53-TB1	9.965	0.00384	4.4	B/D	1.06E-02	1.41E-03
MTELF22	53-TB1	5.952	0.00384	5.5	7.97E-03	6.16E-02	1.38E-02
MTELF23	53-TB1	8.039	0.00384	5.1	5.30E-03	1.22E-02	2.02E-03
MTELF24	53-TB1	2.713	0.00384	5.2	B/D	3.17E-04	1.55E-04
MTELF25	53-TB1	8.596	0.00384	5.0	B/D	4.42E-02	6.83E-03
MTELF26	53-TB1	6.151	0.00384	4.7	6.88E-03	3.61E-02	7.80E-03
MTELF27	53-TB1	10.267	0.00384	5.3	B/D	1.76E-02	2.28E-03
MTELF28	53-TB1	13.116	0.00384	5.7	4.10E-03	4.87E-03	4.94E-04
MTELF29	53-TB1	4.969	0.00384	7.9	B/D	9.89E-04	2.64E-04
MTELF30	53-TB1	10.313	0.00384	5.9	1.50E-02	2.42E-02	3.12E-03
MTELF31	53-TB1	29.989	0.00384	5.2	3.20E-04	1.01E-02	4.50E-04
MTELF32	53-TB1	13.841	0.00384	4.0	3.21E-03	2.54E-03	2.44E-04
MTELF33	53-TB1	13.534	0.00384	5.9	B/D	5.82E-04	5.71E-05
MTELF34	53-TB1	8.595	0.00384	4.8	B/D	6.36E-03	9.84E-04
MTELF35	53-TB1	1.907	0.00384	6.2	B/D	9.02E-04	6.28E-04
W353	53-TB1	0.150	0.00384	178.2	9.05E-03	5.02E-03	4.44E-02

Table 1-A con.

ID	Irradiation	Cl/K	J	Weight	CaO	Cl-	K_20
CPU2FF1	53-TR2	5.863	0.00381	8.0	1.84E-02	1.40E-02	3.18E-03
CMX2FF1	53-TR2	6.074	0.00382	6.2	8.79E-02	1.67E-02	3.64E-03
CMX2FF2	53-TR2	4.197	0.00382	6.7	3.33E-02	1.59E-03	5.03E-04
CMX2FF3	53-TR2	6.914	0.00382	4.9	5.61E-02	4.36E-02	8.37E-03
CMX53	53-TR2	0.888	0.00380	183.4	1.66E-02	4.82E-02	7.22E-02
CPU253	53-TR2	0.138	0.00377	163.2	6.87E-03	1.68E-02	1.61E-01
HH53	53-TR2	3.023	0.00379	167.4	5.19E-03	4.52E-02	1.99E-02
W3ADL	53-TR2	0.005	0.00379	14.9	1.83E-01	1.39E-02	4.08E+00
W3FF1	53-TR2	6.479	0.00378	5.2	B/D	3.29E-02	6.74E-03
W3FF2	53-TR2	4.408	0.00378	5.8	B/D	9.32E-03	2.81E-03
W3FF3	53-TR2	4.454	0.00378	5.2	5.64E-02	1.89E-03	5.63E-04
W3FF4	53-TR2	6.359	0.00378	6.6	B/D	3.72E-03	7.77E-04
W3FF5	53-TR2	5.915	0.00378	6.0	B/D	2.52E-02	5.66E-03
W3FF6	53-TR2	0.127	0.00384	20.8	1.10E-01	2.42E-02	2.52E-01
W3FF7	53-TR2	5.622	0.00384	18.0	4.11E-02	8.66E-02	2.05E-02
W3FF8	53-TR2	6.407	0.00384	20.8	5.78E-02	8.81E-02	1.83E-02
CPU2ADL	53-TR2	0.004	0.00379	15.6	4.15E-03	1.36E-02	4.19E+00
HHADL	53-TR2	0.003	0.00379	11.0	1.72E-01	1.38E-02	5.27E+00
FNADL	53-TR2	0.003	0.00381	14.8	2.14E-01	2.04E-02	9.46E+00
ADADL	53-TR2	0.005	0.00382	14.3	4.00E-01	1.48E-02	4.25E+00
CMX2ADL	53-TR2	0.033	0.00382	15.1	4.55E-02	1.49E-02	6.02E-01
MTE64	64-TR2	4.956	0.00351	101.5	2.91E-03	1.16E-02	3.11E-03
MTEC64	64-TR2	4.600	0.00351	204.2	9.35E-04	5.72E-03	1.65E-03
MTEC64T	64-TR2	4.725	0.00351	204.2	1.53E-04	9.69E-04	2.73E-04
MTEPC6	64-TR2	4.893	0.00351	197.5	5.93E-04	3.96E-03	1.07E-03
W364	64-TR2	5.719	0.00350	97.0	1.14E-03	9.73E-03	2.26E-03
W364FF1	64-TR2	2.074	0.00351	7.8	B/D	4.10E-04	2.63E-04
W364FF2	64-TR2	2.556	0.00351	7.3	B/D	1.44E-03	7.48E-04
W364FF3	64-TR2	5.482	0.00351	4.9	9.84E-03	9.21E-02	2.23E-02
W364FF4	64-TR2	5.250	0.00351	14.0	1.11E-02	1.88E-02	4.75E-03
W364FF5	64-TR2	1.051	0.00351	15.1	B/D	2.32E-04	2.94E-04
W364FF6	64-TR2	5.869	0.00351	21.1	1.19E-03	1.28E-02	2.90E-03
W364FF7	64-TR2	9.734	0.00351	10.8	B/D	2.41E-03	3.29E-04
W364FF8	64-TR2	1.605	0.00351	14.5	5.58E-04	4.42E-04	3.66E-04
W3C64	64-TR2	3.500	0.00351	297.2	2.62E-04	1.08E-03	4.12E-04
W3C64T	64-TR2	5.248	0.00351	297.2	2.66E-05	4.32E-04	1.09E-04
W3PC64	64-TR2	6.320	0.00350	144.4	1.82E-04	4.89E-03	1.03E-03
CMXA	91-TB1	6.241	0.00375	62.3	8.90E-03	9.21E-02	1.96E-02
CMXB	91-TB1	6.777	0.00374	45.4	2.80E-03	3.76E-02	7.38E-03
CMXC	91-TB1	6.682	0.00372	73.1	1.96E-03	2.67E-02	5.31E-03
CMXD	91-TB1	6.733	0.00371	105.5	6.09E-03	5.59E-02	1.10E-02
CMXE	91-TB1	5.675	0.00368	104.0	4.59E-03	3.92E-02	9.17E-03
CMXEC	91-TB1	9.558	0.00368	104.0	1.46E-03	2.25E-02	3.13E-03
CMXET	91-TB1	6.664	0.00368	104.0	6.04E-04	6.17E-03	1.23E-03
MTEB	91-TB1	7.555	0.00373	31.5	1.00E-02	7.03E-02	1.24E-02
MTEC-1	91-TB1	2.170	0.00374	6.4	6.31E-02	2.43E-01	1.49E-01
MTEC-2	91-TB1	7.549	0.00374	78.4	1.31E-02	9.10E-02	1.60E-02
MTED	91-TB1	6.894	0.00375	104.0	1.92E-02	9.38E-02	1.81E-02

Table 1-A con.

ID	Irradiation	Cl/K	J	Weight	CaO	Cl-	K_20
MTEE	91-TB1	7.086	0.00375	137.5	3.37E-03	2.13E-02	3.99E-03
MTEELC	91-TB1	7.407	0.00375	80.3	1.14E-02	9.91E-02	1.78E-02
MTEESC	91-TB1	7.392	0.00375	50.1	3.65E-03	6.87E-02	1.23E-02
MTEET	91-TB1	7.338	0.00375	137.5	1.02E-03	1.09E-02	1.97E-03
W3A	91-TB1	7.575	0.00360	31.4	9.50E-03	9.71E-02	1.70E-02
W3CD	91-TB1	6.093	0.00362	112.5	2.61E-03	3.40E-02	7.41E-03
W3E	91-TB1	4.963	0.00367	56.7	3.95E-03	3.02E-02	8.09E-03
W3F	91-TB1	9.342	0.00369	93.2	5.59E-04	7.93E-03	1.13E-03
W3FC	91-TB1	5.362	0.00369	58.9	1.73E-03	1.72E-02	4.26E-03
W3FT	91-TB1	6.194	0.00369	58.9	2.28E-04	2.51E-03	5.39E-04
W3G	91-TB1	7.050	0.00372	95.2	1.81E-03	2.17E-02	4.08E-03

APPENDIX B Furnace temperature gradient data

Table A- 2 Temperature Gradient Results

Ceramic versus Ceramic Thermocouples - Sept. 23, 1998				
Temperature	300		450	
Time (sec)	Omega	Eurotherm	Omega	Eurotherm
0	64		300	372
30	76	62	290	549
60	72	59	318	466
90	73	141	334	450
120	97	270	344	444
150	128	308	353	446
180	157	310	362	451
210	188	293	375	452
240	207	301	384	449
270	220	299	392	450
300	228	300	397	450
330	234	300	401	450
360	238	300	405	450
390	243	300	407	450
420	246	300	409	450
450	249	300	412	450
480	251	300	414	450
510	253	300	415	450
540	255	300	416	450
570	257	300		
600	258	300		
630	259	300		
660	261	300		
Temperature	600		750	
	Omega	Eurotherm	Omega	Eurotherm
0	450	572	500	708
30	456	619	598	749
60	487	610	626	754
90	508	599	648	751
120	519	596	665	750
150	528	600	681	750
180	538	601	691	750
210	545	600	703	750
240	547	600	711	750
270	552	600	715	750
300	556	600	718	750
330	558	600	719	750
360	562	600	720	750
390	563	600	721	750
420	564	600	721	750
450	564	600		

Table A-2 con.

Temperature	1000		1250	
	Omega	Eurotherm	Omega	Eurotherm
0			1000	1186
30	798	1002	1036	1214
60	857	1002	1147	1247
90	906	1004	1198	1251
120	946	1002	1220	1251
150	958	1001	1227	1251
180	967	1001	1229	1251
210	974	1000	1231	1250
240	976	1000	1231	1250
270	978	1000	1232	1250
300	978	1000	1233	1250
330	978	1000		
Temperature	1500			
	Omega	Eurotherm		
0				
30	1324	1440		
60	1400	1472		
90	1455	1491		
120	1476	1497		
150	1481	1499		
180	1485	1500		
210	1487	1500		
240	1488	1500		
270	1491	1500		
300	1492	1500		

APPENDIX C Isothermal duplicate analysis data

Figure A- 1 Age Spectra from Isothermal Duplicate Analysis

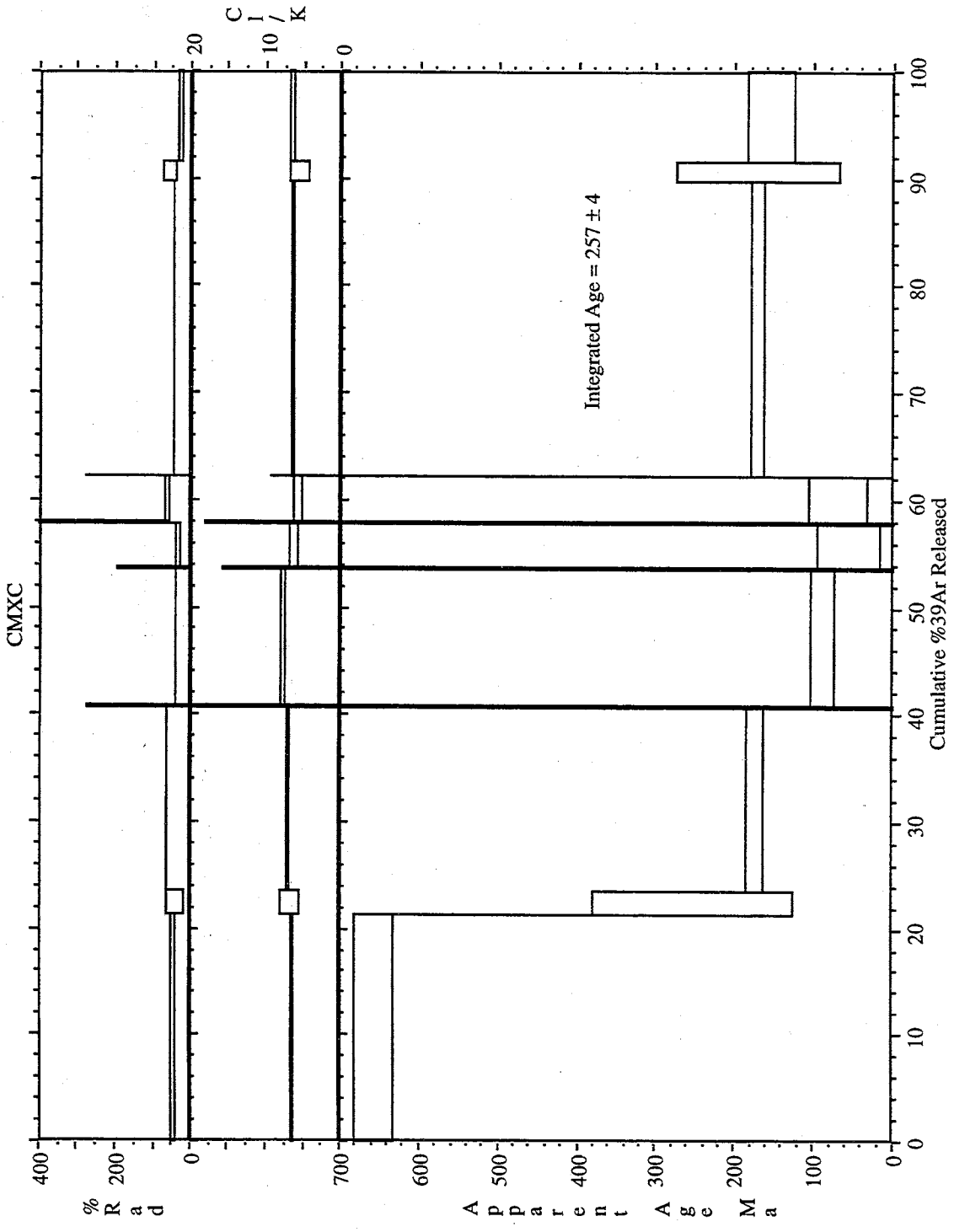

FigureA1 A

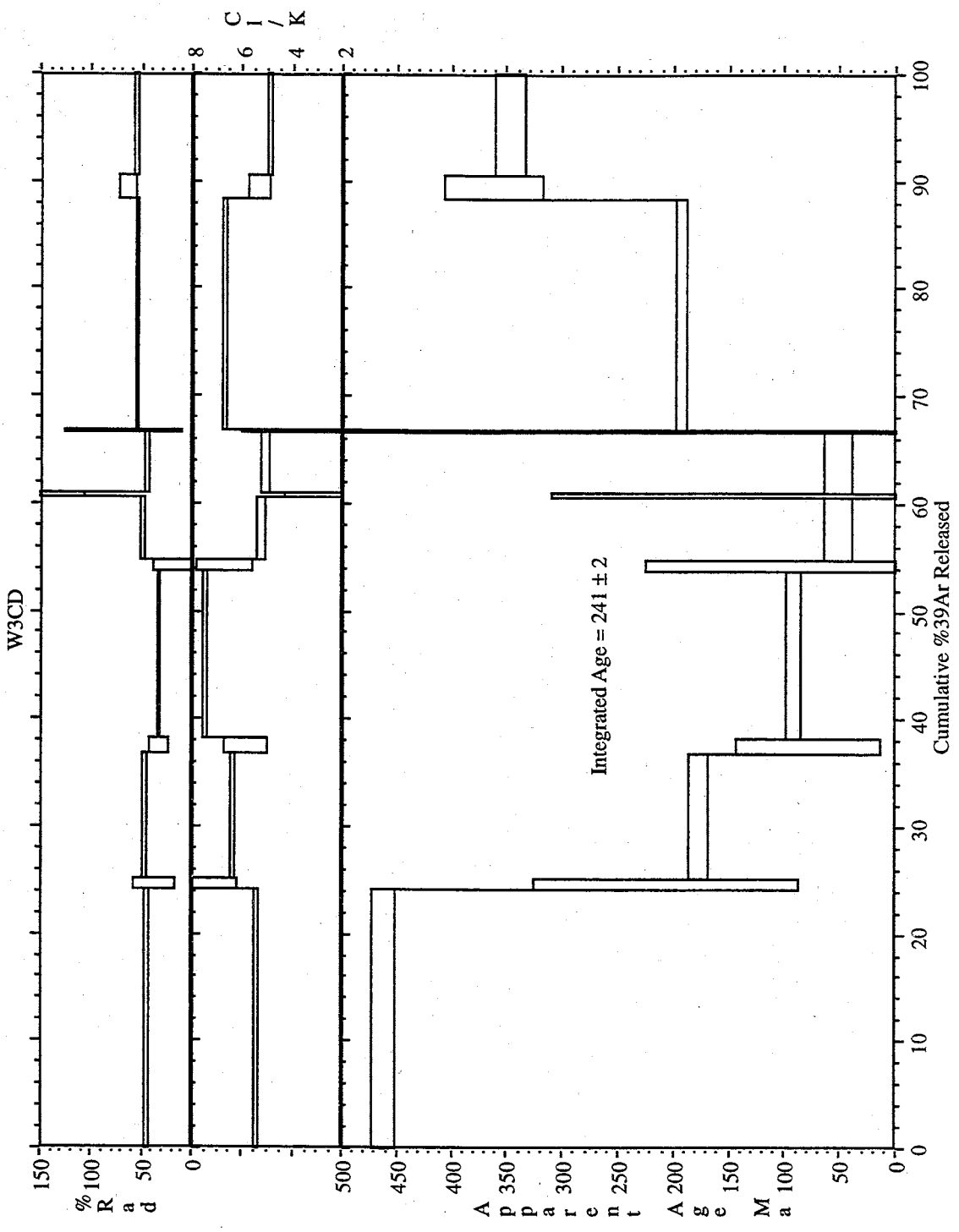
W3CD
Integrated Age = 241 ± 2
Cumulative %39Ar Released
% Rad
Apparent Age
Ca/K
0
10
20
30
40
50
60
70
80
90
100
0
50
100
150
200
250
300
350
400
450
500
2
4
6
8

FigureA1 B

Table A- 3 Data Table from Isothermal Duplicates

ID	Temp	$^{40}Ar/^{39}Ar$	$^{37}Ar/^{39}Ar$	$^{36}Ar/^{39}Ar$	$^{39}Ar_K$	K/Ca	Cl/K	$^{40}Ar^*$	^{39}Ar	Age	±1s
	(°C)			(x 10^{-3})	(x 10^{-15} mol)			(%)	(%)	(Ma)	(Ma)
W3CD tube:91, Quartz, 112.48, J=0.003621903±0.09%, D=1.00253±0.00119, NM-91, Lab#=9380-01											
A	550	180.600	0.090	343.709	1.904	5.6	5.4	43.8	24.2	454.07	5.38
B	550	90.276	0.051	195.036	0.074	10.0	7.5	36.1	25.2	201.47	59.49
C	650	60.096	0.099	108.225	0.925	5.2	6.4	46.8	36.9	174.85	4.53
D	650	36.385	0.118	82.878	0.098	4.3	5.9	32.6	38.2	75.99	32.20
E	750	43.285	0.157	98.599	1.223	3.2	7.5	32.7	53.7	90.08	3.22
F	750	86.229	0.222	238.650	0.080	2.3	6.7	18.2	54.7	99.78	59.66
G	900	16.109	0.364	27.875	0.454	1.4	5.3	48.9	60.5	50.74	6.32
H	900	16.353	0.471	-19.930	0.031	1.1	2.6	136.1	60.9	139.88	84.94
I	1200	17.442	0.521	32.789	0.447	0.98	5.1	44.5	66.6	50.06	6.45
J	1200	75.028	0.700	82.756	0.021	0.73	3.3	67.4	66.9	303.72	159.73
K	1500	57.789	0.284	91.700	1.681	1.8	6.7	53.1	88.2	190.17	2.80
L	1500	94.819	0.288	115.034	0.177	1.8	5.4	64.1	90.5	359.23	22.54
M	1800	105.714	0.283	162.165	0.748	1.8	4.9	54.7	100.0	342.92	6.80
total gas age			n=13		7.865	3.4				236.89	7.16
plateau			n=4	steps J-M	2.627	1.8			33.4	214.20	32.39
CMXC tube:91, Quartz, 73.14 mg, J=0.003723579±0.09%, D=1.00253±0.00119, NM-91, Lab#=9369-01											
A	550	247.325	0.150	444.423	0.807	3.4	6.5	46.9	21.4	647.69	11.93
B	550	103.690	0.016	217.233	0.076	32.9	6.7	38.1	23.4	247.40	63.63
C	650	42.202	0.108	51.945	0.650	4.7	6.9	63.6	40.7	171.83	4.92
D	650	122.450	0.480	260.122	0.008	1.1	17.3	37.2	40.9	282.98	670.84
E	750	32.977	0.204	67.197	0.472	2.5	7.7	39.8	53.4	85.99	7.08
F	750	47.493	0.411	41.543	0.008	1.2	6.1	74.2	53.7	222.39	358.16
G	900	23.518	0.521	52.634	0.156	0.98	6.3	33.9	57.8	52.83	19.68
H	900	17.485	0.600	-128.806	0.007	0.85	6.3	317.8	58.0	339.40	385.79
I	1200	16.215	0.458	20.170	0.156	1.1	5.7	63.3	62.1	67.68	18.37
J	1200	68.920	0.000	109.133	0.005	-	1.1	53.2	62.3	230.75	670.09
K	1500	56.467	0.351	102.322	1.038	1.5	6.5	46.5	89.8	168.16	4.11
L	1500	44.701	0.149	62.676	0.061	3.4	5.7	58.5	91.5	167.74	51.57
M	1800	84.413	0.263	207.015	0.322	1.9	6.5	27.5	100.0	149.72	15.28
total gas age			n=13		3.767	3.2				253.06	14.29
plateau			n=3	steps K-M	1.421	1.6			37.7	166.92	5.14

Isotopic ratios corrected for blank, radioactive decay, and mass discrimination, not corrected for interferring reactions.

Individual analyses show analytical error only; mean age errors also include error in J and irradiation parameters.

Analyses in italics are excluded excluded from mean age calculations.

Correction factors:

$(^{39}Ar/^{37}Ar)_{Ca}$ = 0.00065±0.00005

$(^{36}Ar/^{37}Ar)_{Ca}$ = 0.00026±0.00002

$(^{38}Ar/^{39}Ar)_K$ = 0.0119

$(^{40}Ar/^{39}Ar)_K$ = 0.0265±0.0024

APPENDIX D Sanidine *in vacuo* crushing data from $^{40}Ar/^{39}Ar$ analysis

Figure A- 2 Age Spectra from Crushing FC-1

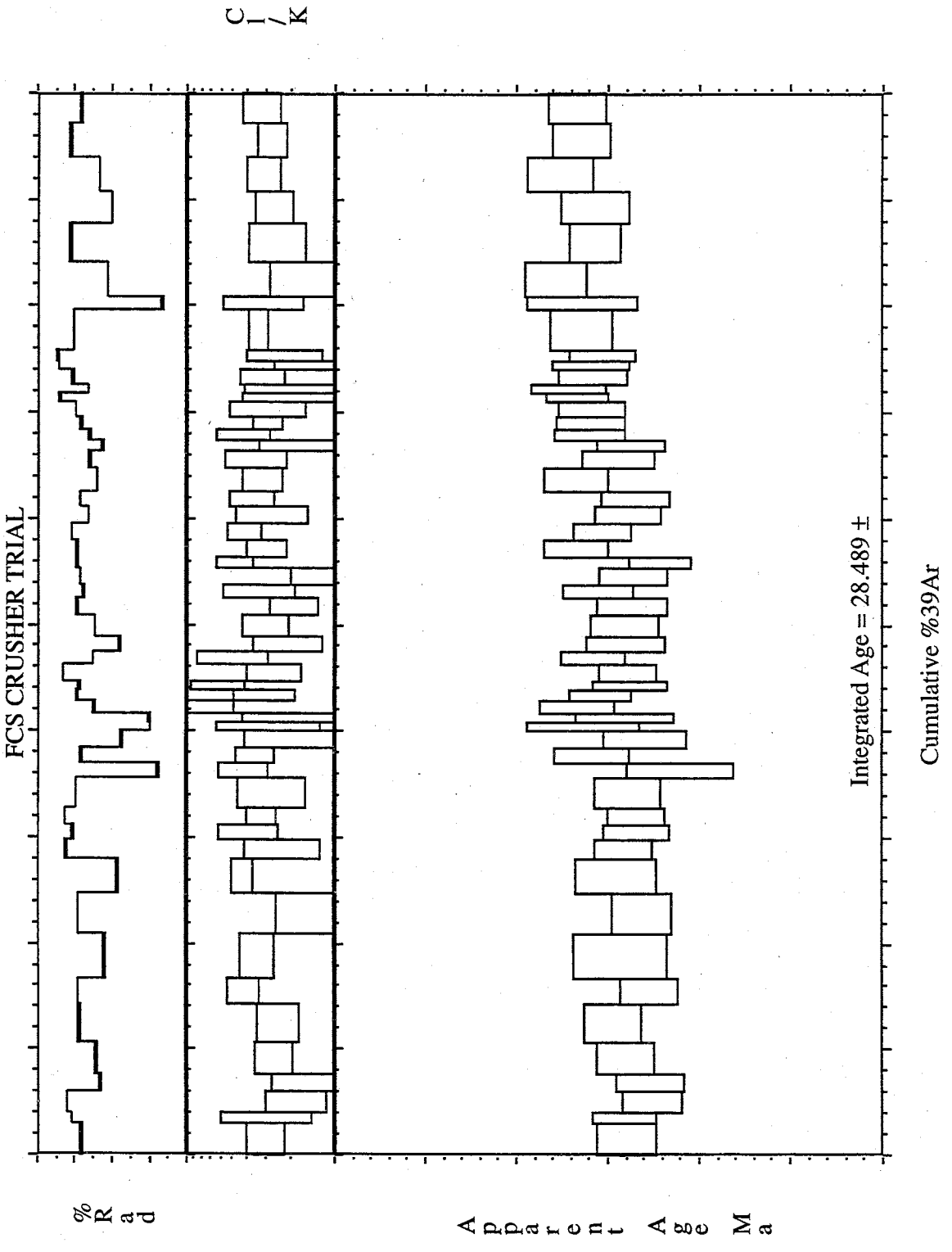

Figure A-2

Table A- 4 Data Table from Crushing FC-1

ID	Temp	$^{40}Ar/^{39}Ar$	$^{37}Ar/^{39}Ar$	$^{36}Ar/^{39}Ar$	$^{39}Ar_K$	K/Ca	Cl/K	$^{40}Ar^*$	^{39}Ar	Age	±1s
	(°C)			(x 10^{-3})	(x 10^{-16} mol)		(x 10^{-3})	(%)	(%)	(Ma)	(Ma)
fc-1, fc-1 sanidine 53.7 mg, J=0.00064991641162968±0.31%, D=1.0083±0.0017, nm-43, Lab#=4010-01											
A	0	26.07	0.0000	10.43	0.001	-	0.30	88.2	3.0	28.395	0.080
B	0	25.29	0.0000	7.735	0.000	-	0.29	91.0	4.0	28.406	0.088
C	0	24.88	0.0000	6.763	0.000	-	0.19	92.0	6.1	28.255	0.080
D	0	27.51	0.0000	15.63	0.000	-	0.15	83.2	7.6	28.269	0.095
E	0	27.32	0.0000	14.62	0.001	-	0.26	84.2	10.6	28.403	0.079
F	0	25.92	0.0222	9.721	0.001	23.0	0.24	88.9	14.4	28.471	0.081
G	0	25.70	0.0000	9.510	0.000	-	0.42	89.1	16.6	28.275	0.077
H	0	28.11	0.0000	17.24	0.001	-	0.34	81.9	21.0	28.43	0.13
I	0	25.72	0.0000	9.460	0.001	-	0.15	89.1	24.7	28.317	0.081
J	0	29.37	0.0000	21.41	0.001	-	0.42	78.5	27.9	28.46	0.11
K	0	24.92	0.0000	6.479	0.000	-	0.23	92.3	29.7	28.416	0.078
L	0	25.34	0.0000	8.112	0.000	-	0.38	90.5	31.2	28.340	0.090
M	0	24.75	0.0000	6.108	0.000	-	0.32	92.7	32.9	28.343	0.079
N	0	25.63	0.0000	8.924	0.001	-	0.27	89.7	35.6	28.393	0.091
O	0	33.65	0.0758	36.91	0.000	6.7	0.42	67.6	37.1	28.10	0.15
P	0	26.26	0.1246	10.56	0.000	4.1	0.35	88.1	38.4	28.58	0.10
Q	0	29.65	0.0707	22.81	0.000	7.2	0.20	77.3	40.1	28.30	0.11
R	0	33.27	0.1672	34.18	0.000	3.1	0.28	69.7	40.8	28.64	0.15
S	0	32.83	0.0000	33.27	0.000	-	0.13	70.1	41.7	28.41	0.13
S	0	27.38	0.0353	14.12	0.000	14.5	0.73	84.8	42.8	28.67	0.10
T	0	25.81	0.0000	9.133	0.000	-	0.30	89.5	43.9	28.542	0.087
U	0	25.82	0.1142	9.650	0.000	4.5	0.61	89.0	44.7	28.38	0.10
V	0	24.66	0.0711	5.676	0.000	7.2	0.26	93.2	46.2	28.389	0.080
W	0	27.21	0.1295	13.83	0.000	3.9	0.49	85.0	47.4	28.578	0.088
X	0	29.53	0.0384	22.14	0.000	13.3	0.21	77.9	48.9	28.40	0.11
Y	0	27.19	0.0928	14.20	0.000	5.5	0.30	84.6	50.8	28.403	0.093
Z	0	25.71	0.0598	9.279	0.000	8.5	0.19	89.4	52.4	28.368	0.097
AA	0	26.39	0.1525	11.14	0.000	3.3	0.32	87.6	53.8	28.551	0.098
AB	0	25.96	0.0000	10.13	0.000	-	0.092	88.5	55.3	28.364	0.093
AC	0	25.52	0.0901	9.096	0.000	5.7	0.47	89.5	56.4	28.215	0.085
AD	0	25.96	0.1183	9.323	0.000	4.3	0.29	89.4	57.9	28.673	0.089
AE	0	25.40	0.1930	7.855	0.000	2.6	0.41	90.9	59.5	28.529	0.080
AF	0	26.68	0.1725	12.55	0.000	3.0	0.27	86.2	61.1	28.393	0.091
AG	0	25.91	0.2228	10.06	0.000	2.3	0.36	88.6	62.6	28.351	0.093
AH	0	27.62	0.1581	14.94	0.000	3.2	0.31	84.1	64.9	28.673	0.086
AI	0	26.80	0.2945	12.85	0.000	1.7	0.35	85.9	66.3	28.445	0.098
AJ	0	27.81	0.1243	16.41	0.000	4.1	0.12	82.6	67.4	28.372	0.094
AK	0	26.91	0.2822	12.79	0.000	1.8	0.42	86.0	68.4	28.597	0.097
AL	0	26.25	0.0709	10.50	0.000	7.2	0.28	88.2	69.7	28.598	0.093
AM	0	25.84	0.0000	9.095	0.000	-	0.29	89.6	71.0	28.590	0.090
AN	0	24.67	0.0000	4.923	0.000	-	0.011	94.1	71.8	28.667	0.085
AO	0	26.96	0.0000	12.56	0.000	-	0.086	86.2	72.7	28.71	0.10
AP	0	25.56	0.0000	8.192	0.000	-	0.31	90.5	73.9	28.581	0.093
AQ	0	24.58	0.0000	4.816	0.000	-	0.035	94.2	74.9	28.60	0.11
AR	0	24.40	0.0000	4.382	0.000	-	0.22	94.7	75.9	28.531	0.090
AS	0	25.72	0.0000	8.540	0.001	-	0.33	90.2	79.7	28.646	0.086

Table A-4 con.

ID	Temp	$^{40}Ar/^{39}Ar$	$^{37}Ar/^{39}Ar$	$^{36}Ar/^{39}Ar$	$^{39}Ar_K$	K/Ca	Cl/K	$^{40}Ar^*$	^{39}Ar	Age	±1s
	(°C)			(x 10^{-3})	(x 10^{-16} mol)		(x 10^{-3})	(%)	(%)	(Ma)	(Ma)
AT	0	34.73	0.0000	39.06	0.000	-	0.30	66.8	80.9	28.64	0.15
AU	0	28.70	0.0000	18.26	0.001	-	0.15	81.2	84.1	28.783	0.086
AV	0	25.39	0.0000	7.651	0.001	-	0.25	91.1	87.8	28.569	0.069
AW	0	28.88	0.0000	19.43	0.001	-	0.26	80.1	90.8	28.570	0.095
AX	0	27.88	0.0000	15.52	0.001	-	0.31	83.5	94.0	28.761	0.089
AY	0	25.48	0.0000	7.718	0.001	-	0.27	91.0	97.1	28.650	0.078
AZ	0	26.33	0.0000	10.54	0.001	-	0.31	88.2	100.0	28.667	0.079
total gas age			n=53		0.022	3.4	0.3			28.489	0.087
plateau			n=53	steps A-AZ	0.022	3.4	0.3		100.0	28.485	0.091

Isotopic ratios corrected for blank, radioactive decay, and mass discrimination, not corrected for interferring reactions.

Individual analyses show analytical error only; mean age errors also include error in J and irradiation parameters.

Analyses in italics are excluded excluded from mean age calculations.

Correction factors:

$(^{39}Ar/^{37}Ar)_{Ca} = 0.00070 \pm 0.00005$

$(^{36}Ar/^{37}Ar)_{Ca} = 0.00026 \pm 0.00002$

$(^{38}Ar/^{39}Ar)_{K} = 0.0119$

APPENDIX E Molar signals from $^{40}Ar/^{39}Ar$ analysis

Table A- 5 Summary of Molar Signals Calculated from Argon Analysis

ID	$^{36}Ar_{tot}$	$^{37}Ar_{Ca}$	$^{38}Ar_{Cl}$	$^{39}Ar_{K}$	$^{40}Ar_{tot}$	$^{40}Ar^{*}$	$^{40}Ar_{K}$	$^{40}Ar_{P}$
CPU<5353	2.24E-14	4.58E-14	1.26E-13	3.85E-13	7.14E-12	5.10E-13	1.61E-12	-1.10E-12
CPU>5353	3.80E-15	3.47E-14	1.76E-14	3.82E-14	1.20E-12	8.05E-14	1.59E-13	-7.83E-14
MTE<5353	2.38E-14	6.35E-14	3.91E-13	4.78E-13	7.65E-12	6.03E-13	2.00E-12	-1.40E-12
MTE>5353	2.26E-14	5.35E-14	5.00E-13	3.94E-13	7.31E-12	6.19E-13	1.65E-12	-1.03E-12
MTEE53	2.30E-14	1.13E-14	9.91E-13	4.23E-14	5.95E-12	-8.59E-13	1.73E-13	-1.03E-12
MTELF1	8.91E-17	9.79E-17	7.09E-15	7.68E-17	2.52E-14	-1.12E-15	3.20E-16	-1.44E-15
MTELF2	B/D	B/D	1.49E-14	1.99E-16	9.29E-15	B/D	8.27E-16	B/D
MTELF3	4.72E-17	3.62E-17	1.62E-15	3.92E-17	1.34E-14	-5.11E-16	1.63E-16	-6.74E-16
MTELF4	1.22E-16	9.68E-17	7.50E-15	1.65E-16	3.50E-14	-1.11E-15	6.88E-16	-1.80E-15
MTELF5	5.59E-17	2.69E-16	6.19E-15	1.69E-16	1.56E-14	-8.72E-16	7.04E-16	-1.58E-15
MTELF6	7.81E-17	2.30E-15	3.70E-15	1.32E-16	2.25E-14	-5.76E-16	5.49E-16	-1.13E-15
MTELF7	B/D	B/D	2.30E-15	7.08E-17	2.12E-14	B/D	2.95E-16	B/D
MTELF8	B/D	B/D	2.08E-15	4.17E-17	1.47E-14	B/D	1.74E-16	B/D
MTELF9	8.09E-18	2.93E-18	2.15E-15	7.26E-17	2.22E-15	-1.73E-16	3.02E-16	-4.75E-16
MTELF10	7.30E-17	1.21E-18	2.31E-15	9.67E-17	2.15E-14	-1.06E-16	4.03E-16	-5.09E-16
MTELF11	1.40E-16	2.78E-17	5.69E-15	2.35E-16	4.11E-14	-2.08E-16	9.78E-16	-1.19E-15
MTELF12	B/D	B/D	4.48E-15	1.89E-16	1.01E-14	B/D	7.87E-16	B/D
MTELF13	5.19E-17	1.43E-17	2.63E-15	1.30E-16	1.54E-14	8.89E-17	5.42E-16	-4.53E-16
MTELF14	7.49E-17	1.59E-16	8.85E-15	3.58E-16	2.24E-14	2.61E-16	1.49E-15	-1.23E-15
MTELF15	B/D	B/D	7.44E-16	7.12E-18	1.01E-14	B/D	2.97E-17	B/D
MTELF16	B/D	B/D	4.29E-15	1.66E-16	7.73E-15	B/D	6.93E-16	B/D
MTELF17	7.97E-18	1.68E-17	9.47E-16	3.79E-17	2.46E-15	1.10E-16	1.58E-16	-4.85E-17
MTELF18	B/D	B/D	4.93E-15	1.23E-16	9.46E-14	B/D	5.12E-16	B/D
MTELF19	1.14E-17	1.15E-17	2.93E-15	1.34E-16	3.96E-15	5.99E-16	5.57E-16	4.20E-17
MTELF20	6.02E-17	1.20E-16	5.62E-15	1.62E-16	1.86E-14	8.73E-16	6.74E-16	1.99E-16
MTELF21	B/D	B/D	2.21E-15	6.13E-17	1.84E-14	B/D	2.56E-16	B/D
MTELF22	7.18E-17	1.88E-16	1.63E-14	7.59E-16	2.58E-14	4.58E-15	3.16E-15	1.42E-15
MTELF23	6.23E-17	1.16E-16	2.99E-15	1.03E-16	1.91E-14	6.37E-16	4.29E-16	2.08E-16
MTELF24	B/D	B/D	7.83E-17	7.99E-18	3.62E-15	B/D	3.33E-17	B/D
MTELF25	B/D	B/D	1.06E-14	3.42E-16	1.59E-13	B/D	1.43E-15	B/D
MTELF26	1.59E-16	1.38E-16	8.09E-15	3.64E-16	5.16E-14	4.48E-15	1.52E-15	2.96E-15
MTELF27	B/D	B/D	4.51E-15	1.22E-16	2.70E-14	B/D	5.07E-16	B/D
MTELF28	5.55E-17	1.01E-16	1.34E-15	2.83E-17	1.69E-14	5.20E-16	1.18E-16	4.02E-16
MTELF29	B/D	B/D	3.73E-16	2.08E-17	1.99E-14	B/D	8.67E-17	B/D
MTELF30	1.99E-16	3.76E-16	6.81E-15	1.83E-16	6.62E-14	7.38E-15	7.62E-16	6.62E-15
MTELF31	2.39E-17	7.14E-18	2.53E-15	2.34E-17	8.46E-15	1.41E-15	9.74E-17	1.31E-15
MTELF32	1.56E-17	5.51E-17	4.87E-16	9.75E-18	6.09E-15	1.47E-15	4.06E-17	1.43E-15
MTELF33	B/D	B/D	1.65E-16	3.37E-18	7.08E-15	B/D	1.40E-17	B/D
MTELF34	B/D	B/D	1.45E-15	4.67E-17	4.92E-14	B/D	1.95E-16	B/D
MTELF35	B/D	B/D	2.66E-16	3.87E-17	3.87E-13	B/D	1.61E-16	B/D
W353	9.77E-16	6.65E-15	4.29E-14	7.91E-14	3.31E-13	4.24E-14	3.30E-13	-2.87E-13
CPU2FF1	6.84E-16	6.27E-16	5.34E-15	2.52E-16	2.09E-13	6.82E-15	1.06E-15	5.76E-15
CMX2FF1	1.16E-16	2.31E-15	4.89E-15	2.23E-16	3.67E-14	2.38E-15	9.34E-16	1.44E-15
CMX2FF2	4.72E-17	9.51E-16	5.09E-16	3.36E-17	1.45E-14	5.78E-16	1.41E-16	4.38E-16
CMX2FF3	2.02E-16	1.17E-15	1.02E-14	4.08E-16	6.86E-14	9.07E-15	1.71E-15	7.36E-15
CMX53	8.78E-15	1.37E-14	4.20E-13	1.31E-13	3.07E-12	4.79E-13	5.51E-13	-7.20E-14
CPU253	1.96E-14	8.15E-15	1.27E-13	2.55E-13	7.20E-12	1.40E-12	1.08E-12	3.13E-13
CPU2ADL	8.56E-16	3.34E-15	1.00E-14	6.44E-13	2.95E-12	2.69E-12	2.72E-12	-2.96E-14

Table A-5 con.

ID	$^{36}Ar_{tot}$	$^{37}Ar_{Ca}$	$^{38}Ar_{Cl}$	$^{39}Ar_{K}$	$^{40}Ar_{tot}$	$^{40}Ar^{*}$	$^{40}Ar_{K}$	$^{40}Ar_{P}$
HH53	9.94E-15	4.22E-15	3.58E-13	3.28E-14	3.33E-12	3.92E-13	1.39E-13	2.54E-13
W3ADL	2.85E-15	1.67E-14	9.76E-15	5.99E-13	7.81E-12	6.97E-12	2.53E-12	4.44E-12
W3FF1	B/D	B/D	8.00E-15	3.42E-16	7.08E-15	B/D	1.45E-15	B/D
W3FF2	B/D	B/D	2.53E-15	1.59E-16	8.77E-15	B/D	6.73E-16	B/D
W3FF3	7.77E-18	1.24E-15	4.64E-16	2.89E-17	2.66E-15	3.65E-16	1.22E-16	2.43E-16
W3FF4	B/D	B/D	1.15E-15	5.02E-17	2.85E-14	B/D	2.12E-16	B/D
W3FF5	B/D	B/D	7.14E-15	3.34E-16	9.22E-14	B/D	1.41E-15	B/D
W3FF6	4.50E-15	9.80E-15	2.41E-14	5.25E-14	1.40E-12	6.64E-14	2.19E-13	-1.52E-13
W3FF7	6.65E-16	3.16E-15	7.46E-14	3.68E-15	2.38E-13	4.12E-14	1.53E-14	2.59E-14
W3FF8	1.82E-15	5.16E-15	8.80E-14	3.80E-15	6.66E-13	1.29E-13	1.58E-14	1.13E-13
HHADL	7.18E-15	3.39E-13	7.21E-15	5.75E-13	4.39E-12	2.27E-12	2.42E-12	-1.52E-13
FNADL	4.54E-15	9.54E-14	1.44E-14	1.39E-12	6.98E-12	5.63E-12	5.83E-12	-1.96E-13
ADADL	4.26E-15	2.30E-13	1.01E-14	6.06E-13	3.75E-12	2.49E-12	2.54E-12	-4.33E-14
CMX2ADL	1.08E-14	1.04E-13	1.07E-14	9.04E-14	3.59E-12	3.91E-13	3.79E-13	1.16E-14
MTE64	5.43E-15	1.53E-15	5.15E-14	2.88E-15	1.62E-12	1.21E-14	1.31E-14	-1.03E-15
MTEC64	5.61E-15	1.18E-15	5.14E-14	3.08E-15	1.70E-12	4.60E-14	1.41E-14	3.20E-14
MTEC64T	8.92E-16	2.37E-16	8.68E-15	5.09E-16	2.72E-13	8.49E-15	2.32E-15	6.17E-15
MTEPC6	3.20E-15	1.15E-15	3.43E-14	1.94E-15	9.82E-13	3.76E-14	8.84E-15	2.87E-14
W364	1.55E-15	1.47E-15	4.13E-14	2.00E-15	5.40E-13	8.04E-14	9.13E-15	7.13E-14
W364FF1	B/D	B/D	1.40E-16	1.87E-17	4.16E-14	B/D	8.54E-17	B/D
W364FF2	B/D	B/D	4.57E-16	4.96E-17	8.70E-15	B/D	2.26E-16	B/D
W364FF3	3.41E-16	1.89E-16	1.98E-14	1.00E-15	1.04E-13	3.59E-15	4.56E-15	-9.70E-16
W364FF4	2.93E-16	6.07E-16	1.15E-14	6.06E-16	8.95E-14	3.09E-15	2.76E-15	3.24E-16
W364FF5	B/D	B/D	1.54E-16	4.05E-17	1.03E-14	B/D	1.85E-16	B/D
W364FF6	1.41E-16	9.85E-17	1.18E-14	5.59E-16	1.01E-13	5.98E-14	2.55E-15	5.72E-14
W364FF7	B/D	B/D	1.14E-15	3.25E-17	3.79E-15	B/D	1.48E-16	B/D
W364FF8	8.90E-17	3.17E-17	2.81E-16	4.86E-17	4.69E-14	2.06E-14	2.21E-16	2.04E-14
W3C64	3.80E-15	3.32E-16	1.40E-14	1.12E-15	1.18E-12	5.80E-14	5.10E-15	5.29E-14
W3C64T	5.12E-16	2.97E-16	5.62E-15	2.97E-16	1.61E-13	9.59E-15	1.35E-15	8.23E-15
W3PC64	9.69E-16	1.93E-15	3.09E-14	1.35E-15	3.14E-13	2.77E-14	6.19E-15	2.15E-14
CMXA	3.52E-15	3.36E-15	2.69E-13	1.19E-14	1.35E-12	3.07E-13	5.09E-14	2.56E-13
CMXB	1.22E-15	8.49E-16	7.98E-14	3.26E-15	4.90E-13	1.28E-13	1.40E-14	1.14E-13
CMXC	6.30E-16	9.13E-16	9.09E-14	3.77E-15	3.47E-13	1.61E-13	1.62E-14	1.44E-13
CMXD	8.94E-15	3.10E-15	2.73E-13	1.12E-14	3.28E-12	6.34E-13	4.85E-14	5.86E-13
CMXE	9.47E-15	1.98E-15	1.87E-13	9.14E-15	3.49E-12	6.94E-13	3.97E-14	6.54E-13
CMXEC	8.09E-16	1.97E-15	9.66E-14	2.80E-15	3.05E-13	6.61E-14	1.22E-14	5.39E-14
CMXET	1.04E-15	4.18E-16	2.95E-14	1.23E-15	3.83E-13	7.68E-14	5.33E-15	7.15E-14
MTEB	1.87E-15	1.34E-15	1.03E-13	3.78E-15	5.94E-13	4.12E-14	1.62E-14	2.50E-14
MTEC-1	5.51E-16	1.28E-14	7.29E-14	9.30E-15	2.28E-13	6.49E-14	3.97E-14	2.52E-14
MTEC-2	4.52E-15	8.06E-15	3.34E-13	1.22E-14	1.44E-12	1.04E-13	5.23E-14	5.20E-14
MTED	8.49E-15	3.82E-14	4.57E-13	1.84E-14	2.67E-12	1.57E-13	7.84E-14	7.90E-14
MTEE	6.81E-15	1.95E-15	1.37E-13	5.36E-15	2.15E-12	1.36E-13	2.29E-14	1.14E-13
MTEELC	3.85E-15	5.05E-15	3.73E-13	1.39E-14	1.31E-12	1.69E-13	5.95E-14	1.09E-13
MTEESC	2.58E-15	2.35E-15	1.61E-13	6.04E-15	8.54E-13	9.08E-14	2.57E-14	6.50E-14
MTEET	1.36E-15	9.76E-16	7.01E-14	2.64E-15	4.43E-13	4.10E-14	1.13E-14	2.97E-14
W3A	6.34E-16	1.32E-15	1.37E-13	5.01E-15	3.70E-13	1.83E-13	2.23E-14	1.61E-13
W3CD	1.24E-15	1.66E-15	1.73E-13	7.86E-15	6.80E-13	3.13E-13	3.47E-14	2.78E-13
W3E	1.76E-15	1.01E-15	7.87E-14	4.39E-15	8.74E-13	3.54E-13	1.91E-14	3.35E-13
W3F	5.01E-16	3.10E-16	1.84E-14	5.47E-16	1.94E-13	4.54E-14	2.37E-15	4.30E-14
W3FC	7.91E-16	4.53E-16	4.67E-14	2.41E-15	4.46E-13	2.12E-13	1.05E-14	2.02E-13
W3FT	B/D	B/D	6.82E-15	3.05E-16	6.72E-14	B/D	1.32E-15	B/D

Table A-5 con.

ID	$^{36}Ar_{tot}$	$^{37}Ar_{Ca}$	$^{38}Ar_{Cl}$	$^{39}Ar_{K}$	$^{40}Ar_{tot}$	$^{40}Ar^{*}$	$^{40}Ar_{K}$	$^{40}Ar_{P}$
W3G	1.05E-15	8.76E-16	9.58E-14	3.76E-15	7.34E-13	4.23E-13	1.62E-14	4.07E-13

APPENDIX F HFIDC data from $^{40}Ar/^{39}Ar$ analysis

Table A- 6 Complete Data Table from HDFICs

ID	Temp	$^{40}Ar/^{39}Ar$	$^{37}Ar/^{39}Ar$	$^{36}Ar/^{39}Ar$	$^{39}Ar_K$	K/Ca	Cl/K	$^{40}Ar^*$	^{39}Ar	Age	±1s
	(°C)			(x 10^{-3})	(x 10^{-15} mol)			(%)	(%)	(Ma)	(Ma)
MTED tube:91, Quartz,104 mg, J=0.003750163±0.09%, D=1.00253±0.00119, NM-91, Lab#=9373-01											
A	400	1664.438	0.243	5597.398	0.397	2.1	7.2	0.6	2.2	69.03	246.19
B	500	550.558	0.178	1806.534	1.510	2.9	8.0	3.0	10.4	109.69	27.60
C	600	148.268	0.171	453.937	1.940	3.0	7.9	9.5	20.9	93.07	6.80
D	700	103.654	0.238	320.482	1.891	2.1	7.8	8.6	31.2	59.53	5.70
E	800	114.713	0.461	373.400	0.698	1.1	6.3	3.8	35.0	29.42	12.43
F	900	161.681	0.593	525.140	0.502	0.86	6.3	4.0	37.8	43.61	20.23
G	1000	415.699	0.959	1378.518	0.212	0.53	6.2	2.0	38.9	55.95	108.55
H	1100	631.884	2.803	2053.529	0.063	0.18	5.0	4.0	39.3	163.54	489.22
I	1200	189.339	2.853	586.097	0.077	0.18	5.2	8.6	39.7	107.49	125.81
J	1300	50.887	0.809	151.357	1.673	0.63	6.8	12.2	48.8	41.47	3.55
K	1400	32.206	2.863	89.207	5.934	0.18	6.6	18.8	81.1	40.48	1.34
L	1500	25.574	16.546	66.120	0.965	0.031	6.2	28.5	86.4	49.12	3.95
M	1600	28.951	0.623	74.032	1.240	0.82	6.1	24.5	93.1	47.40	3.15
N	1700	38.057	0.580	100.760	1.099	0.88	6.2	21.8	99.1	55.32	3.95
O	1800	57.001	0.595	160.355	0.165	0.86	6.3	16.9	100.0	64.06	25.12
total gas age			n=15		18.368	1.1				56.96	15.02
plateau			n=6	steps J-O	11.077	0.4			60.3	43.14	2.33
CMXD tube:91, Quartz, 105.5 mg, J=0.003705142±0.09%, D=1.00253±0.00119, NM-91, Lab#=9368-01											
A	400	700.365	0.176	1888.419	1.087	2.9	7.2	20.3	9.7	764.14	27.03
B	500	1255.640	0.168	3808.743	1.295	3.0	8.0	10.4	21.2	710.01	55.63
C	600	235.023	0.160	584.855	1.420	3.2	7.9	26.5	33.9	374.09	9.17
D	700	110.236	0.197	252.706	1.345	2.6	7.8	32.2	45.9	223.26	5.51
E	800	40.126	0.310	93.778	0.441	1.6	4.9	30.9	49.8	81.13	8.11
F	900	41.604	0.417	89.801	0.234	1.2	4.1	36.2	51.9	98.07	14.41
G	1000	44.177	0.611	108.301	0.165	0.83	3.8	27.6	53.3	79.76	21.26
H	1100	34.917	0.543	61.112	0.085	0.94	2.5	48.3	54.1	109.44	36.05
I	1200	40.390	0.303	99.876	0.185	1.7	1.6	26.9	55.7	71.27	18.59
J	1300	39.045	0.222	89.789	0.379	2.3	3.1	32.0	59.1	81.70	9.25
K	1400	79.617	0.420	158.998	2.679	1.2	6.9	41.0	83.0	206.01	2.74
L	1500	70.458	0.264	127.728	0.587	1.9	5.6	46.4	88.2	206.40	7.41
M	1600	59.089	0.235	84.036	0.446	2.2	5.9	58.0	92.2	215.56	8.26
N	1700	72.342	0.338	112.049	0.704	1.5	6.5	54.2	98.5	244.89	5.98
O	1800	88.884	0.342	181.978	0.172	1.5	6.5	39.5	100.0	220.68	26.07
total gas age			n=15		11.222	2.2				328.50	14.82
plateau			n=6	steps J-O	4.966	1.5			44.3	205.07	14.88
CMXA tube:91, Quartz, 62.27 mg, J=0.00375019±0.09%, D=1.00253±0.00119, NM-91, Lab#=9371-01											
A	400	1155.680	0.164	3602.446	0.286	3.1	5.6	7.9	2.4	530.48	167.62
B	500	421.854	0.114	1105.781	1.321	4.5	6.0	22.5	13.5	550.19	15.98
C	600	98.236	0.088	232.548	1.712	5.8	6.5	30.0	27.8	189.30	4.56
D	700	49.033	0.153	110.108	1.425	3.3	7.3	33.6	39.8	108.21	3.53

Table A-6 con.

ID	Temp	$^{40}Ar/^{39}Ar$	$^{37}Ar/^{39}Ar$	$^{36}Ar/^{39}Ar$	$^{39}Ar_K$	K/Ca	Cl/K	$^{40}Ar^*$	^{39}Ar	Age	±1s
	(°C)			(x 10^{-3})	(x 10^{-16} mol)			(%)	(%)	(Ma)	(Ma)
E	800	102.537	0.441	329.174	0.328	1.2	5.9	5.1	42.5	35.34	19.70
F	900	14.330	0.533	25.893	0.561	0.96	6.0	46.7	47.2	44.74	5.29
G	1000	13.249	0.582	22.415	0.237	0.88	5.4	50.1	49.2	44.42	12.16
H	1100	11.852	0.677	25.706	0.061	0.75	5.0	36.1	49.7	28.75	47.37
I	1200	33.269	0.516	98.912	0.139	0.99	5.6	12.2	50.9	27.23	24.16
J	1300	14.071	0.296	22.543	0.566	1.7	5.6	52.6	55.6	49.43	5.24
K	1400	29.828	0.388	59.233	3.333	1.3	6.3	41.3	83.6	81.56	1.29
L	1500	28.691	0.302	51.656	0.555	1.7	6.1	46.8	88.2	88.63	5.80
M	1600	23.121	0.264	33.172	0.432	1.9	5.7	57.6	91.9	87.91	6.93
N	1700	33.032	0.330	60.228	0.646	1.5	5.8	46.1	97.3	100.25	5.07
O	1800	52.695	0.449	123.786	0.324	1.1	6.0	30.6	100.0	105.95	11.66
total gas age			n=15		11.926	2.6				158.95	10.15
plateau			n=6	steps J-O	5.855	1.5			49.1	81.66	4.15
CMXB tube:91, Quartz, 45.44 mg, J=0.003737403±0.09%, D=1.00253±0.00119, NM-91, Lab#=9370-01											
A	400	286.392	0.102	616.491	0.399	5.0	5.4	36.4	12.2	593.40	25.94
B	500	137.680	0.079	231.481	0.420	6.5	6.4	50.3	25.1	415.30	13.38
C	600	294.332	0.125	887.894	0.633	4.1	6.6	10.9	44.5	203.48	25.58
D	700	65.715	0.197	149.416	0.422	2.6	9.0	32.8	57.4	139.77	10.00
E	800	45.235	0.423	125.295	0.129	1.2	7.3	18.2	61.4	54.58	27.85
F	900	24.779	0.659	84.789	0.072	0.77	6.2	-1.0	63.6	-1.70	43.78
G	1000	18.937	1.575	72.546	0.027	0.32	6.2	-12.7	64.4	-16.31	114.74
H	1100	16.765	2.994	-85.935	0.003	0.17	6.6	252.7	64.5	265.64	823.44
I	1200	42.772	3.392	142.091	0.012	0.15	8.2	2.4	64.8	6.87	288.33
J	1300	18.400	0.439	38.577	0.061	1.2	6.8	38.1	66.7	46.66	47.18
K	1400	63.344	0.392	141.565	0.521	1.3	6.9	34.0	82.7	139.56	8.14
L	1500	86.545	0.313	204.393	0.173	1.6	6.5	30.2	88.0	168.22	26.67
M	1600	96.693	0.384	219.304	0.127	1.3	6.2	33.0	91.9	203.20	37.63
N	1700	66.405	0.331	136.108	0.183	1.5	6.4	39.4	97.5	168.47	21.02
O	1800	262.820	0.273	799.882	0.081	1.9	6.3	10.1	100.0	170.09	155.76
total gas age			n=15		3.263	3.1				239.42	26.18
plateau			n=6	steps J-O	1.147	1.4			35.2	145.08	11.93
W3G tube:91, Quartz, 95.20 mg, J=0.003717819±0.09%, D=1.00253±0.00119, NM-91, Lab#=9376-01											
A	400	583.906	0.193	853.942	0.548	2.6	7.6	56.8	14.5	1449.1	22.07
B	500	406.576	0.165	752.200	0.476	3.1	7.3	45.3	27.2	941.54	24.34
C	600	107.586	0.131	104.690	0.659	3.9	7.3	71.2	44.7	452.30	7.05
D	700	53.880	0.204	74.002	0.718	2.5	8.4	59.4	63.8	202.83	5.01
E	800	33.355	0.309	70.436	0.185	1.6	7.2	37.6	68.7	82.22	17.21
F	900	18.491	1.090	22.322	0.057	0.47	5.1	64.6	70.2	78.49	50.14
G	1000	14.966	0.460	6.305	0.063	1.1	5.4	87.6	71.8	85.89	44.89
H	1100	25.962	0.846	17.895	0.022	0.60	3.3	79.8	72.4	133.91	129.40
I	1200	33.782	1.310	48.645	0.053	0.39	5.6	57.7	73.8	126.26	56.26
J	1300	55.168	0.422	84.715	0.053	1.2	5.4	54.6	75.2	191.66	62.48
K	1400	50.354	0.282	71.519	0.177	1.8	6.8	58.0	79.9	186.06	18.45
L	1500	97.215	0.220	81.780	0.274	2.3	6.4	75.1	87.2	433.46	14.02
M	1600	129.534	0.154	83.072	0.187	3.3	4.9	81.0	92.1	594.49	22.85

Table A-6 con.

ID	Temp	$^{40}Ar/^{39}Ar$	$^{37}Ar/^{39}Ar$	$^{36}Ar/^{39}Ar$	$^{39}Ar_K$	K/Ca	Cl/K	$^{40}Ar^*$	^{39}Ar	Age	±1s
	(°C)			(x 10^{-3})	(x 10^{-16} mol)			(%)	(%)	(Ma)	(Ma)
N	1700	131.591	0.181	82.929	0.192	2.8	5.1	81.4	97.3	604.60	22.03
O	1800	124.496	0.272	161.394	0.103	1.9	6.6	61.7	100.0	453.19	44.08
total gas age			n=15		3.764	2.7				572.69	18.59
plateau			n=6	steps J-O	0.986	2.4			26.2	424.23	69.56
W3E tube:91, Quartz, 56.74 mg, J=0.00367319±0.09%, D=1.00253±0.00119, NM-91, Lab#=9378-01											
A	400	1860.803	0.231	5501.530	0.161	2.2	6.2	12.6	3.7	1123.1	323.49
B	500	905.779	0.297	1374.228	0.136	1.7	9.5	55.2	6.8	1880.4	100.20
C	600	275.601	0.179	362.151	0.556	2.8	7.9	61.2	19.4	869.52	14.68
D	700	90.785	0.172	165.497	0.913	3.0	6.7	46.1	40.2	258.10	5.68
E	800	32.457	0.173	75.142	0.395	2.9	2.8	31.5	49.2	66.62	8.17
F	900	21.425	0.353	60.124	0.222	1.4	1.5	17.1	54.3	24.09	13.75
G	1000	18.752	0.391	59.010	0.137	1.3	1.8	7.0	57.4	8.72	22.20
H	1100	21.911	0.245	71.881	0.116	2.1	1.5	3.0	60.0	4.39	26.67
I	1200	33.890	0.185	108.357	0.105	2.8	1.0	5.5	62.4	12.27	31.65
J	1300	64.367	0.225	182.778	0.141	2.3	2.8	16.1	65.6	67.30	30.03
K	1400	55.073	0.361	90.629	0.296	1.4	4.9	51.4	72.4	178.41	11.66
L	1500	87.482	0.344	128.817	0.409	1.5	5.8	56.5	81.7	300.98	10.32
M	1600	168.979	0.194	200.961	0.345	2.6	4.1	64.8	89.5	610.33	16.05
N	1700	148.881	0.170	170.148	0.324	3.0	2.8	66.2	96.9	557.61	15.47
O	1800	162.931	0.164	275.553	0.135	3.1	3.4	50.0	100.0	472.44	41.80
total gas age			n=15		4.390	2.4				416.81	27.98
plateau			n=6	steps J-O	1.651	2.2			37.6	346.77	76.96
MTEB tube:91, Quartz, 31.50 mg, J=0.003728595±0.09%, D=1.00253±0.00119, NM-91, Lab#=9375-01											
A	500	965.853	0.304	3251.464	0.364	1.7	8.9	0.5	9.6	33.61	156.05
B	700	129.271	0.293	382.859	0.982	1.7	8.4	12.5	35.6	105.40	9.80
C	900	38.583	0.420	103.765	0.164	1.2	5.6	20.5	39.9	52.56	20.94
D	1200	56.720	0.463	160.610	0.123	1.1	7.0	16.3	43.1	61.31	33.26
E	1500	39.142	0.372	98.453	1.671	1.4	7.3	25.7	87.3	66.39	2.83
F	1800	75.240	0.403	224.363	0.480	1.3	6.6	11.9	100.0	59.20	11.96
total gas age			n=6		3.784	1.5				71.68	22.33
plateau			n=2	steps E-F	2.151	1.3			56.9	66.01	3.19
W3A tube:91, Quartz, 31.41 mg, J=0.003597799±0.09%, D=1.00253±0.00119, NM-91, Lab#=9381-01											
A	500	177.971	0.212	216.993	0.817	2.4	6.4	64.0	16.3	619.38	7.74
B	700	57.613	0.186	108.549	1.926	2.7	8.4	44.3	54.7	158.52	2.88
C	900	16.726	0.416	32.938	0.358	1.2	7.3	41.8	61.9	44.88	8.20
D	1200	12.462	0.511	10.271	0.176	1.00	6.4	75.7	65.4	60.27	15.81
E	1500	51.271	0.328	108.544	1.315	1.6	7.3	37.4	91.6	120.50	3.95
F	1800	92.025	0.276	217.986	0.420	1.8	7.3	30.0	100.0	170.86	12.29
total gas age			n=6		5.012	2.1				213.10	5.57
plateau			n=2	steps E-F	1.735	1.6			34.6	125.21	15.13
Isotopic ratios corrected for blank, radioactive decay, and mass discrimination, not corrected for interferring reactions.											

Table A-6 con.

Individual analyses show analytical error only; mean age errors also include error in J and irradiation parameters.									
Analyses in italics are excluded excluded from mean age calculations.									
Correction factors:									
$(^{39}Ar/^{37}Ar)_{Ca} = 0.00065 \pm 0.00005$									
$(^{36}Ar/^{37}Ar)_{Ca} = 0.00026 \pm 0.00002$									
$(^{38}Ar/^{39}Ar)_{K} = 0.0119$									
$(^{40}Ar/^{39}Ar)_{K} = 0.0265 \pm 0.0024$									

APPENDIX G Adularia electron microprobe data

Table A- 7 Electron microprobe analysis of Capitan adularia

Sample	Description	SiO_2	Al_2O_3	CaO	Na_2O	K_2O	Total
MTE	loz	68.87	19.71	0.18	11.29	0.52	100.56
MTE	hiz	68.40	19.48	0.15	3.96	9.68	101.67
MTE	hiz	63.60	18.13	0.01	1.31	15.23	98.28
MTE	hiz	63.98	18.84	0.01	1.22	15.41	99.46
MTE	loz	70.59	20.94	0.40	11.35	1.15	104.44
MTE	loz	71.61	21.56	0.59	10.83	0.42	105.01
MTE	hiz	66.51	19.05	0.10	1.99	13.38	101.04
MTE	loz	68.06	20.35	0.66	11.44	0.17	100.67
CPU2	loz	72.56	20.61	0.05	10.09	0.41	103.72
CPU2	hiz	65.09	18.50	0.02	1.36	14.89	99.86
CPU2	hiz	66.97	19.14	0.01	0.75	15.38	102.26
CPU2	loz	71.87	20.77	0.16	8.57	0.38	101.75
CPU2	hiz	57.82	16.17	0.04	1.57	11.38	86.98
CAPN	hiz	64.96	18.67	0.00	1.35	14.81	99.79
CAPN	loz	71.74	20.52	0.11	10.99	0.35	103.71
CAPN	loz	69.66	20.03	0.19	7.94	3.41	101.22
CAPN	loz	64.06	18.41	0.08	3.94	10.81	97.30
CAPN	loz	71.55	20.75	0.09	11.04	0.25	103.68
CAPN	hiz	59.22	17.03	0.06	2.71	11.80	90.81
CAPN	loz	70.81	20.11	0.03	1.62	8.72	101.29
CAPN	hiz	65.62	18.98	0.07	1.72	14.58	100.97
MTE	hiz	64.96	18.44	0.16	3.26	11.68	98.51
MTE	hiz	66.70	18.81	0.04	1.42	14.64	101.61
MTE	loz	71.46	20.46	0.28	10.15	0.78	103.12
MTE	loz	66.95	19.15	0.23	9.11	4.04	99.49
MTE	hiz	65.16	18.58	0.06	2.02	13.51	99.33
MTE	hiz	65.22	18.52	0.06	1.92	13.83	99.55
MTE	hiz	70.65	20.27	0.22	9.55	2.09	102.79
MTE	intz	66.77	18.87	0.18	7.99	5.22	99.03

APPENDIX H Quartz electron microprobe data

Table A- 8 Summary of electron microprobe data

Sample	SiO_2	Al_2O_3	CaO	Na_2O	K_2O	Total
CMXA1	100.21	0.01	0.01	0.00	0.00	100.22
CMXA2	99.98	0.01	0.01	0.01	0.01	100.00
CMXA3	100.31	0.01	0.01	0.00	0.01	100.33
CMXB1	99.81	0.01	0.00	0.01	0.01	99.83
CMXB2	99.22	0.01	0.02	0.03	0.02	99.30
CMXB3	100.19	0.01	0.00	0.00	0.01	100.21
CMXC1	99.21	0.01	0.01	0.01	0.01	99.24
CMXC2	99.44	0.00	0.01	0.00	0.00	99.45
CMXC3	99.34	0.01	0.01	0.00	0.01	99.37
CMXD1	99.96	0.01	0.01	0.01	0.00	99.99
CMXD2	100.22	0.01	0.00	0.00	0.00	100.23
CMXD3	98.66	0.01	0.01	0.01	0.01	98.70
CMXE1	97.49	0.02	0.01	0.00	0.01	97.53
CMXE2	99.39	0.02	0.01	0.01	0.01	99.44
CMXE3	98.02	0.01	0.03	0.06	0.04	98.15
MTEA1	100.01	0.01	0.02	0.00	0.01	100.06
MTEA2	100.46	0.02	0.00	0.00	0.00	100.48
MTEA3	100.13	0.01	0.01	0.00	0.00	100.15
MTEB1	100.47	0.01	0.01	0.01	0.01	100.51
MTEB2	100.37	0.02	0.01	0.01	0.01	100.40
MTEB3	100.44	0.01	0.01	0.03	0.01	100.52
MTEC1	100.72	0.01	0.02	0.01	0.01	100.77
MTEC2	100.91	0.01	0.01	0.00	0.00	100.94
MTEC3	100.85	0.01	0.01	0.00	0.00	100.88
MTED1	100.80	0.02	0.01	0.00	0.00	100.82
MTED2	101.01	0.02	0.00	0.00	0.00	101.03
MTED3	100.58	0.02	0.01	0.00	0.00	100.61
MTEE1	99.24	0.00	0.01	0.00	0.01	99.26
MTEE2	99.76	0.01	0.01	0.00	0.01	99.80
MTEE3	100.18	0.02	0.01	0.00	0.00	100.20
W3A1	98.27	0.45	0.03	0.11	0.07	98.93
W3A2	99.63	0.24	0.02	0.02	0.02	99.93
W3A3	100.74	0.27	0.00	0.00	0.01	101.03
W3B1	99.72	0.02	0.01	0.00	0.01	99.75
W3B2	100.26	0.01	0.01	0.00	0.00	100.30
W3B3	99.83	0.01	0.01	0.01	0.01	99.86
W3C1	98.69	0.02	0.02	0.02	0.01	98.75
W3C2	99.95	0.02	0.01	0.01	0.01	100.00
W3C3	99.83	0.02	0.01	0.00	0.01	99.86
W3D1	100.44	0.02	0.02	0.01	0.00	100.49
W3D2	100.27	0.03	0.00	0.01	0.01	100.31
W3D3	100.46	0.02	0.01	0.00	0.01	100.51
W3E1	100.23	0.33	0.01	0.06	0.03	100.66
W3E2	100.15	0.40	0.00	0.02	0.02	100.59
W3E3	99.45	0.23	0.01	0.03	0.01	99.72
W3F1	99.76	0.00	0.03	0.03	0.02	99.83
W3F2	100.42	0.02	0.00	0.00	0.00	100.44
W3F3	98.29	0.00	0.00	0.04	0.01	98.34

Table A-8 con.

Sample	SiO_2	Al_2O_3	CaO	Na_2O	K_2O	Total
W3G1	99.98	0.01	0.01	0.00	0.01	100.02
W3G2	100.41	0.01	0.02	0.01	0.02	100.46
W3G3	100.19	0.00	0.02	0.00	0.02	100.24

APPENDIX I Error analysis from electron microprobe data

Table A- 9 Standards and errors for electron microprobe analysis

Sample	SiO_2	Al_2O_3	CaO	Na_2O	K_2O	Total
qtz-1	99.382	0.000	0.011	0.000	0.001	99.394
qtz-2	99.666	0.000	0.000	0.000	0.005	99.671
qtz-3	99.722	0.000	0.007	0.002	0.005	99.736
qtz-4	99.646	0.000	0.001	0.003	0.008	99.658
qtz-5	99.601	0.001	0.000	0.000	0.010	99.612
qtz-6	99.454	0.001	0.006	0.000	0.003	99.464
qtz-7	99.165	0.001	0.004	0.000	0.009	99.179
qtz-8	100.022	0.000	0.006	0.001	0.001	100.030
qtz-9	99.666	0.000	0.001	0.000	0.000	99.667
qtz-10	99.661	0.000	0.003	0.000	0.000	99.664
qtz-11	99.364	0.001	0.000	0.000	0.004	99.369
qtz-12	99.822	0.002	0.003	0.000	0.004	99.831
qtz-13	99.942	0.000	0.003	0.000	0.000	99.945
qtz-14	99.447	0.000	0.001	0.000	0.003	99.451
qtz-15	99.560	0.001	0.007	0.002	0.004	99.574
qtz-16	99.642	0.002	0.003	0.000	0.002	99.649
qtz-17	99.876	0.003	0.004	0.000	0.003	99.886
qtz-18	99.652	0.000	0.008	0.004	0.000	99.664
qtz-19	99.569	0.000	0.000	0.000	0.003	99.572
qtz-20	99.296	0.005	0.012	0.000	0.005	99.318
Quartz Average	**99.608**	**0.001**	**0.004**	**0.001**	**0.004**	**99.617**
Quartz 1 σ	**0.216**	**0.001**	**0.004**	**0.001**	**0.003**	**0.214**
an-1	43.902	36.239	18.769	0.724	0.018	99.652
an-2	44.147	36.442	18.739	0.714	0.020	100.062
an-3	44.190	36.419	18.683	0.722	0.013	100.027
an-4	43.888	36.138	18.783	0.739	0.011	99.559
an-5	43.797	36.104	18.816	0.732	0.015	99.464
an-6	43.755	36.465	18.846	0.729	0.010	99.805
an-7	43.891	36.151	18.828	0.719	0.023	99.612
an-8	43.660	36.364	18.742	0.723	0.016	99.505
an-9	44.033	36.550	18.888	0.724	0.014	100.209
an-10	43.505	36.518	18.824	0.700	0.013	99.560
Anorthoclase	**43.877**	**36.339**	**18.792**	**0.723**	**0.015**	**99.746**
Anorthoclase 1 σ	**0.201**	**0.158**	**0.057**	**0.010**	**0.004**	**0.251**
al-1	73.565	22.108	0.037	9.829	0.018	105.557
al-2	74.306	21.987	0.040	8.735	0.013	105.081
al-3	73.653	22.416	0.028	9.327	0.016	105.440
al-4	74.135	21.736	0.023	9.744	0.008	105.646
al-5	72.691	22.006	0.030	9.487	0.009	104.223
al-6	74.198	22.396	0.017	9.376	0.012	105.999
al-7	72.792	21.590	0.021	8.925	0.016	103.344
al-8	73.657	22.000	0.019	9.803	0.014	105.493
al-9	73.600	22.006	0.023	8.945	0.008	104.582
al-10	73.912	21.991	0.011	7.363	0.016	103.293
Albite Average	**73.651**	**22.024**	**0.025**	**9.153**	**0.013**	**104.866**
Albite 1 σ	**0.520**	**0.240**	**0.009**	**0.700**	**0.003**	**0.918**

APPENDIX J Adularia data from $^{40}Ar/^{39}Ar$ analysis

Table A- 10 Complete Adularia Data Table

ID	Temp	$^{40}Ar/^{39}Ar$	$^{37}Ar/^{39}Ar$	$^{36}Ar/^{39}Ar$	$^{39}Ar_K$	K/Ca	Cl/K	$^{40}Ar^*$	^{39}Ar	Age	±2s
	(°C)			(x 10^{-3})	(x 10^{-15} mol)		(x 10^{-3})	(%)	(%)	(Ma)	(Ma)
MTE , Adularia, 15.45 mg , J=0.003780452±0.10%, NM-53, Lab#=6866-01											
A	750	8.53	0.12	15.02	13.25	4.40	2.55	47.70	42.34	27.56	0.46
B	850	4.81	0.09	2.20	6.96	5.42	0.98	86.10	64.59	28.01	0.22
C	950	5.14	0.17	3.44	3.13	3.03	1.75	80.00	74.60	27.79	0.31
D	1050	5.47	0.20	3.88	2.21	2.60	7.83	78.80	81.66	29.15	0.50
E	1100	5.40	0.22	4.00	1.53	2.35	14.41	77.90	86.54	28.45	0.51
F	1150	5.95	0.20	5.51	1.73	2.53	21.86	72.40	92.08	29.17	0.59
G	1200	12.26	0.32	26.51	1.08	1.58	41.08	36.10	95.52	29.94	1.41
H	1230	29.30	0.63	84.16	0.62	0.81	71.64	15.20	97.52	30.12	3.64
I	1260	55.35	1.43	168.47	0.32	0.36	94.62	10.20	98.53	38.17	7.63
J	1300	67.11	2.04	209.44	0.26	0.25	89.66	8.00	99.37	36.19	9.44
K	1350	86.12	11.32	275.60	0.10	0.05	108.11	6.40	99.70	37.56	19.61
L	1400	62.15	1.42	194.24	0.04	0.36	65.95	7.80	99.83	32.71	24.40
M	1500	283.24	30.40	763.39	0.00	0.02	-59.46	21.20	99.84	375.87	675.64
N	1750	44.42	16.66	109.24	0.05	0.03	2.59	30.10	100.00	90.11	17.18
total gas age			n=14		31.29	3.89				28.41	0.83
plateau			n=14	steps A-N	31.29	3.89			100.00	28.15	0.46
W3-3, Adularia, 14.88 mg , J=0.003785944±0.10%, NM-53, Lab#=6865-01											
A	550	86.36	0.06	117.23	3.80	8.26	9.58	59.90	1.81	322.47	3.51
B	600	11.19	0.02	19.17	11.97	20.42	1.51	49.10	7.52	37.16	0.61
C	650	6.27	0.02	5.77	16.70	23.09	0.20	72.40	15.50	30.72	0.26
D	700	5.32	0.02	2.15	16.64	25.10	0.02	87.60	23.44	31.55	0.19
E	750	5.47	0.02	0.81	19.16	24.98	0.30	95.20	32.59	35.23	0.17
F	800	6.65	0.02	0.54	15.61	28.13	0.58	97.20	40.04	43.65	0.21
G	850	7.51	0.02	0.45	14.52	32.06	0.91	97.90	46.97	49.55	0.22
H	950	8.48	0.01	0.59	19.65	44.72	1.33	97.60	56.35	55.70	0.26
I	1050	8.06	0.01	0.61	23.42	35.32	4.92	97.40	67.53	52.87	0.25
J	1100	9.73	0.02	0.83	16.56	30.84	10.20	97.20	75.43	63.46	0.28
K	1150	13.63	0.02	1.39	18.83	24.34	13.03	96.80	84.42	87.91	0.42
L	1200	17.51	0.03	2.25	14.17	19.98	10.62	96.10	91.19	111.35	0.49
M	1400	42.58	0.05	2.78	15.36	10.14	8.39	98.00	98.52	264.64	1.14
N	1750	29.13	0.42	6.54	3.10	1.20	7.82	93.40	100.00	176.91	1.01
total gas age			n=14		209.48	26.64				76.44	0.42
plateau			n=14	steps A-N	209.48	26.64			100.00	48.01	13.82
CPU2, Adularia, 15.60 mg , J=0.003785469±0.10%, NM-53, Lab#=6867-01											
A	550	6.94	0.02	8.72	7.01	28.73	5.60	62.50	3.11	29.39	0.41
B	600	4.73	0.01	2.13	6.65	96.18	1.16	86.10	6.06	27.62	0.22
C	650	4.35	0.00	0.86	11.27	-	0.53	93.50	11.07	27.58	0.17
D	700	4.24	0.00	0.54	20.97	-	0.48	95.60	20.37	27.50	0.13
E	750	4.24	0.00	0.31	20.24	2690.34	0.25	97.20	29.36	27.94	0.13
F	800	4.22	0.01	0.23	21.88	100.50	0.23	97.80	39.07	27.99	0.13

Table A-10 con.

ID	Temp	$^{40}Ar/^{39}Ar$	$^{37}Ar/^{39}Ar$	$^{36}Ar/^{39}Ar$	$^{39}Ar_K$	K/Ca	Cl/K	$^{40}Ar^*$	^{39}Ar	Age	±2s
	(°C)			(x 10^{-3})	(x 10^{-15} mol)		(x 10^{-3})	(%)	(%)	(Ma)	(Ma)
G	850	4.20	0.00	0.13	23.20	-	0.33	98.40	49.36	28.03	0.13
H	950	4.23	0.00	0.18	32.50	1895.05	0.48	98.10	63.78	28.10	0.14
I	1050	4.35	0.00	0.53	25.45	2811.06	2.49	95.80	75.08	28.21	0.14
J	1100	4.63	0.00	1.51	13.15	466.79	8.41	89.80	80.92	28.16	0.16
K	1150	5.09	0.00	3.00	17.83	515.16	18.43	82.00	88.83	28.32	0.19
L	1200	5.21	0.00	3.36	17.89	218.49	15.12	80.50	96.77	28.42	0.21
M	1400	6.15	0.00	6.54	5.50	257.86	13.51	68.10	99.21	28.36	0.37
N	1750	8.89	0.45	13.73	1.78	1.15	14.87	54.40	100.00	32.73	1.11
total gas age			n=14		225.32	1202.37				28.11	0.17
plateau			n=14	steps A-N	225.32	1202.37			100.00	28.00	0.22
HH, Adularia, 11.04 mg , J=0.003794634±0.10%, NM-53, Lab#=6868-01											
A	550	7.52	0.25	14.39	7.02	2.01	2.40	43.30	3.49	22.16	0.49
B	600	4.29	0.52	3.26	5.30	0.99	0.49	77.80	6.13	22.72	0.27
C	650	4.33	0.95	3.04	8.38	0.54	0.20	80.30	10.30	23.64	0.20
D	700	5.50	2.31	7.10	14.39	0.22	0.59	64.60	17.46	24.23	0.31
E	750	5.56	4.32	7.03	12.03	0.12	0.33	68.20	23.44	25.85	0.32
F	800	5.58	1.74	5.82	10.63	0.29	0.67	71.10	28.73	26.98	0.26
G	850	7.36	0.01	11.15	10.80	64.21	1.53	54.90	34.10	27.46	0.39
H	950	6.78	0.01	9.10	15.99	57.41	0.97	60.00	42.06	27.62	0.34
I	1050	5.95	0.01	6.41	18.19	76.30	1.31	67.70	51.11	27.39	0.27
J	1100	6.18	0.01	7.16	14.46	48.12	2.86	65.30	58.30	27.45	0.29
K	1150	7.75	0.01	12.33	19.17	51.66	6.67	52.60	67.84	27.69	0.41
L	1200	8.83	0.01	16.05	24.16	48.45	7.67	46.00	79.86	27.60	0.46
M	1400	11.81	0.01	25.96	30.93	44.72	6.14	34.80	95.25	27.93	0.69
N	1750	11.73	0.10	24.83	9.54	5.11	6.01	37.30	100.00	29.72	0.87
total gas age			n=14		200.99	36.42				26.86	0.44
plateau			n=14	steps A-N	200.99	36.42			100.00	25.77	1.15
FN, Adularia, 14.79 mg , J=0.003814656±0.10%, NM-53, Lab#=6869-01											
A	550	5.65	0.02	6.77	11.00	31.62	3.68	64.10	2.26	24.76	0.32
B	600	3.95	0.01	1.35	11.25	56.33	0.67	89.20	4.58	24.06	0.17
C	650	4.03	0.00	0.94	18.52	106.30	0.35	92.50	8.38	25.46	0.13
D	700	4.30	0.00	1.23	38.49	125.37	0.53	90.90	16.30	26.71	0.14
E	750	4.14	0.00	0.37	42.08	117.03	0.12	96.70	24.96	27.36	0.13
F	800	4.17	0.01	0.34	45.32	78.09	0.23	96.90	34.28	27.64	0.13
G	850	4.24	0.01	0.45	43.04	65.87	0.47	96.30	43.13	27.86	0.13
H	950	4.28	0.01	0.53	54.09	38.72	0.44	95.80	54.25	28.02	0.12
I	1050	4.32	0.02	0.72	48.18	22.67	1.01	94.50	64.16	27.87	0.14
J	1100	4.64	0.02	1.78	29.87	23.14	3.28	88.10	70.31	27.96	0.16
K	1150	5.19	0.02	3.59	33.73	25.72	6.96	79.00	77.24	28.02	0.20
L	1200	5.77	0.02	5.47	33.63	30.16	8.62	71.50	84.16	28.18	0.23
M	1400	7.33	0.04	10.51	56.21	13.46	7.22	57.30	95.72	28.67	0.34
N	1750	9.65	1.26	18.27	20.80	0.41	8.84	44.80	100.00	29.54	0.53
total gas age			n=14		486.18	52.65				27.68	0.19
plateau			n=14	steps A-N	486.18	52.65			100.00	27.20	0.67

Table A-10 con.

ID	Temp	$^{40}Ar/^{39}Ar$	$^{37}Ar/^{39}Ar$	$^{36}Ar/^{39}Ar$	$^{39}Ar_K$	K/Ca	Cl/K	$^{40}Ar^*$	^{39}Ar	Age	±2s
	(°C)			(x 10^{-3})	(x 10^{-15} mol)		(x 10^{-3})	(%)	(%)	(Ma)	(Ma)
AD, AD Adularia 14.34 mg, J=0.003820148±0.10%, NM-53, Lab#=6870-01											
A	500	165.57	0.30	546.79	1.20	1.72	31.25	2.40	0.57	27.28	14.67
B	500	61.44	0.16	191.91	0.66	3.24	6.96	7.70	0.88	32.18	6.98
C	550	11.17	0.06	23.36	1.87	8.74	9.88	38.00	1.76	29.01	1.05
D	550	7.87	0.03	12.87	1.34	14.82	1.92	51.40	2.39	27.65	0.84
E	600	5.00	0.05	3.97	3.71	11.06	1.28	76.10	4.14	26.01	0.33
F	600	4.60	0.02	2.22	3.99	21.57	0.71	85.20	6.03	26.82	0.27
G	650	4.34	0.04	1.17	5.37	13.52	0.45	91.50	8.57	27.14	0.21
H	650	4.28	0.02	0.74	5.74	32.81	0.22	94.30	11.27	27.64	0.20
I	700	4.26	0.02	0.73	7.19	23.98	0.32	94.30	14.67	27.51	0.18
J	750	4.23	0.03	0.48	12.00	18.53	0.25	96.10	20.33	27.81	0.15
K	800	4.27	0.02	0.56	18.64	28.47	0.49	95.50	29.13	27.86	0.15
L	850	4.28	0.03	0.62	21.15	19.73	0.39	95.10	39.11	27.84	0.14
M	900	4.31	0.04	0.59	19.57	13.82	0.58	95.40	48.35	28.14	0.14
N	950	4.48	0.06	1.15	17.07	8.61	1.21	91.90	56.40	28.19	0.16
O	1000	4.78	0.08	2.11	15.36	6.07	2.98	86.50	63.65	28.26	0.17
P	1050	5.01	0.09	2.91	14.68	5.43	5.94	82.40	70.59	28.23	0.19
Q	1100	4.98	0.10	2.77	15.77	5.21	9.67	83.20	78.03	28.35	0.19
R	1150	5.25	0.08	3.56	19.59	6.51	12.81	79.60	87.28	28.58	0.21
S	1200	6.02	0.08	6.27	16.81	6.02	8.36	68.90	95.21	28.39	0.26
T	1400	7.84	0.74	12.09	9.27	0.69	8.67	54.80	99.58	29.42	0.47
U	1750	54.81	70.32	184.60	0.88	0.01	105.53	10.30	100.00	40.41	7.29
total gas age			n=21		211.85	12.64				28.16	0.35
plateau			n=21	steps A-U	211.85	12.64			100.00	27.92	0.23
CMX2, CMX2 Adularia 15.11 mg, J=0.003815131±0.10%, NM-53, Lab#=6871-01											
A	500	1589.18	1.68	5321.72	0.04	0.30	66.33	1.10	0.12	111.65	598.87
B	500	1178.97	4.41	4033.15	0.02	0.12	29.44	-1.10	0.20	-88.51	649.61
C	550	194.92	4.55	675.43	0.07	0.11	11.34	-2.20	0.42	-30.30	43.77
D	550	146.06	7.20	493.50	0.14	0.07	16.16	0.50	0.86	5.21	24.38
E	600	71.06	9.05	241.39	0.20	0.06	7.32	0.60	1.50	2.75	12.68
F	600	87.61	11.72	288.44	0.20	0.04	6.03	3.70	2.14	22.43	14.58
G	650	56.36	17.29	187.90	0.26	0.03	2.36	3.80	2.97	14.83	9.16
H	650	66.17	23.92	217.17	0.27	0.02	3.76	5.70	3.81	26.43	10.20
I	700	48.14	27.50	160.04	0.31	0.02	9.23	6.10	4.79	20.49	8.23
J	750	26.14	18.00	78.72	0.43	0.03	2.10	16.20	6.16	29.25	3.72
K	800	24.77	1.63	69.72	0.60	0.31	5.52	17.20	8.07	29.16	3.45
L	850	20.73	0.04	55.99	0.69	12.67	7.16	20.10	10.26	28.40	2.62
M	900	10.27	0.10	20.78	0.72	5.08	3.01	40.00	12.53	28.05	1.61
N	950	13.45	0.10	32.52	0.84	4.89	3.18	28.40	15.17	26.09	2.03
O	1000	8.94	0.05	16.07	0.97	10.41	3.16	46.70	18.23	28.49	1.15
P	1050	8.47	0.03	14.65	1.17	18.20	5.27	48.60	21.94	28.10	1.08
Q	1100	11.46	0.01	24.38	1.59	38.39	9.62	36.90	26.97	28.86	1.42
R	1150	13.99	0.01	32.69	2.35	100.90	23.36	30.80	34.41	29.40	1.21
S	1200	35.73	0.07	107.00	4.20	6.94	71.73	11.40	47.68	27.91	2.79
T	1400	44.54	0.05	135.25	10.88	10.01	39.14	10.20	82.07	31.02	3.38
U	1750	51.49	0.21	157.73	5.67	2.48	35.68	9.50	100.00	33.20	4.11

Table A-10 con.

ID	Temp	$^{40}Ar/^{39}Ar$	$^{37}Ar/^{39}Ar$	$^{36}Ar/^{39}Ar$	$^{39}Ar_K$	K/Ca	Cl/K	$^{40}Ar^*$	^{39}Ar	Age	±2s
	(°C)			(x 10^{-3})	(x 10^{-15} mol)		(x 10^{-3})	(%)	(%)	(Ma)	(Ma)
total gas age			n=21		31.63	15.77				29.51	4.62
plateau			n=18	steps D-U	31.50	15.84			99.58	28.42	0.99

Isotopic ratios corrected for blank, radioactive decay, and mass discrimination, not corrected for interferring reactions.

Individual analyses show analytical error only; mean age errors also include error in J and irradiation parameters.

Correction factors:

$(^{39}Ar/^{37}Ar)_{Ca} = 0.00070 \pm 0.00005$

$(^{36}Ar/^{37}Ar)_{Ca} = 0.00026 \pm 0.00002$

$(^{38}Ar/^{39}Ar)_K = 0.0119$

$(^{40}Ar/^{39}Ar)_K = 0.0270 \pm 0.0020$

Appendix K Large grains data from $^{40}Ar/^{39}Ar$ analysis

Table A- 11 Complete Data Table from Large Grains

ID	Temp	$^{40}Ar/^{39}Ar$	$^{37}Ar/^{39}Ar$	$^{36}Ar/^{39}Ar$	$^{39}Ar_K$	K/Ca	Cl/K	$^{40}Ar^*$	^{39}Ar	Age	±1s
	(°C)			(x 10^{-3})	(x 10^{-16} mol)			(%)	(%)	(Ma)	(Ma)
MTEE53 Tube 3:4.7 cm, quartz 179.58 mg Single Large Grain, J=0.003910401±0.10%, D=1.0082±0.0018, NM-53, Lab#=6910-01											
A	500		0.341	3998.53	9.78	1.5	7.25	4.4	2.3	348.52	70.63
B	550	2110.744	0.252	7043.95	12.87	2.0	7.46	1.4	5.4	195.41	143.01
C	600	1769.814	0.224	5905.87	1.57	2.3	8.72	1.4	5.7	165.86	377.02
D	650	257.455	0.165	833.08	35.01	3.1	6.11	4.4	14.0	77.78	12.08
E	700	219.160	0.171	724.11	12.59	3.0	6.95	2.4	17.0	36.12	15.43
F	750	94.012	0.187	293.00	45.97	2.7	7.25	7.9	27.9	51.59	4.51
G	800	122.456	0.256	393.28	20.48	2.0	6.84	5.1	32.7	43.48	7.14
H	850	100.641	0.288	319.86	23.52	1.8	6.26	6.1	38.3	42.66	5.71
I	900	51.129	0.341	157.76	22.75	1.5	5.86	8.8	43.7	31.54	3.78
J	950	31.197	0.504	78.10	6.42	1.0	5.51	26.1	45.2	56.49	5.52
K	1000	23.665	0.414	59.37	6.83	1.2	5.51	25.9	46.8	42.73	4.54
L	1150	23.914	0.282	67.76	34.11	1.8	5.96	16.2	54.9	27.20	1.62
M	1300	24.670	0.366	52.29	8.29	1.4	5.89	37.4	56.8	63.92	3.58
N	1450	34.467	0.285	96.63	106.46	1.8	6.55	17.1	82.0	41.21	1.49
O	1650	31.114	0.276	85.54	76.00	1.8	6.41	18.7	100.0	40.67	1.36
total gas age			n=15		422.64	2.0	6.50			56.63	11.19
plateau			n=3	steps M-O	190.75	1.8	6.47		45.1	42.60	4.35
CPU253 -Vein Quartz 53:A1&A3, Large vein quartz, a1-54.1 mg, a3-107.1 mg, J=0.003771135±0.10%, D=1.0082±0.0018, NM-53, Lab#=6845-01											
A	450	6987.749	0.373	23036.92	1.02	1.4	3.81	2.6	0.0	936.23	2281.15
B	500	4846.634	0.757	15978.95	1.70	0.67	5.93	2.6	0.1	696.53	941.06
C	550	2586.504	0.235	8903.64	0.45	2.2	5.21	-1.7	0.1	-331.7	2106.59
D	600	923.048	0.678	2743.46	4.98	0.75	8.29	12.2	0.3	637.69	67.26
E	650	441.440	0.611	1351.16	3.46	0.83	5.07	9.6	0.5	266.49	43.84
F	725	478.976	0.567	1525.19	9.61	0.90	4.25	5.9	0.8	183.01	30.75
G	800	47.702	0.128	134.69	9.11	4.0	0.52	16.5	1.2	52.86	4.97
H	850	29.121	0.084	79.11	10.89	6.1	0.30	19.7	1.6	38.52	3.96
I	900	49.959	0.088	157.26	7.28	5.8	0.24	6.9	1.9	23.44	5.92
J	1000	19.844	0.054	52.25	58.14	9.4	0.13	22.1	4.2	29.57	1.23
K	1150	7.414	0.025	10.79	174.95	20.5	0.02	56.6	11.0	28.35	0.37
L	1300	6.011	0.013	6.24	500.15	38.3	0.02	68.9	30.6	27.97	0.16
M	1400	8.391	0.014	13.74	1104.00	36.5	0.02	51.3	73.8	29.06	0.21
N	1500	26.968	0.037	72.19	485.85	13.9	0.18	20.8	92.9	37.77	0.98
O	1650	86.941	0.102	258.77	182.46	5.0	0.55	12.0	100.0	69.78	3.37
total gas age			n=15		2554.04	28.0	0.14			36.31	2.87
plateau			n=4	steps L-O	2272.45	29.6	0.10		89.0	28.56	1.16
HH53 Vein Quartz 53:B1&B3, Large vein quartz, a1-28.51 mg, B3-138.9 mg, J=0.003786123±0.10%, D=1.0082±0.0018, NM-53, Lab#=6848-01											
A	450	900.510	0.178	2869.81	3.30	2.9	5.14	5.8	1.0	326.93	84.79
B	500	264.524	0.107	782.30	6.96	4.8	5.93	12.6	3.1	214.46	19.17

Table A-11 con.

ID	Temp	$^{40}Ar/^{39}Ar$	$^{37}Ar/^{39}Ar$	$^{36}Ar/^{39}Ar$	$^{39}Ar_K$	K/Ca	Cl/K	$^{40}Ar^*$	^{39}Ar	Age	±1s
	(°C)			(x 10^{-3})	(x 10^{-16} mol)			(%)	(%)	(Ma)	(Ma)
C	550	98.868	0.008	331.38	0.75	64.6	5.22	0.9	3.4	6.26	49.32
D	600	155.847	0.110	435.38	22.98	4.6	6.69	17.4	10.4	176.68	6.64
E	650	396.455	0.145	1239.05	8.62	3.5	8.64	7.6	13.0	195.95	22.04
F	725	176.413	0.138	547.12	23.75	3.7	8.09	8.3	20.2	97.87	8.74
G	800	46.417	0.161	136.07	13.65	3.2	5.25	13.3	24.4	41.82	3.65
H	850	40.459	0.234	121.91	8.35	2.2	2.73	10.9	26.9	29.99	4.25
I	900	44.569	0.196	126.16	4.63	2.6	1.89	16.3	28.3	49.04	6.91
J	1000	29.450	0.117	83.48	21.57	4.4	1.73	16.2	34.9	32.26	2.57
K	1150	37.326	0.065	106.63	22.32	7.9	0.59	15.5	41.7	39.16	2.77
L	1300	43.760	0.065	119.86	29.44	7.8	0.81	19.0	50.7	55.94	2.57
M	1400	58.345	0.090	143.49	20.10	5.7	0.61	27.3	56.8	105.62	3.57
N	1500	134.186	0.181	413.45	37.22	2.8	3.36	8.9	68.2	80.17	5.79
O	1650	68.380	0.137	202.78	104.44	3.7	1.86	12.3	100.0	56.76	2.77
total gas age			n=15		328.08	4.6	3.02			79.09	5.75
plateau			n=4	steps L-O	191.21	4.4	1.86		58.3	68.06	11.59
CMX2 Vein Quartz 53:C1&C3, Large vein quartz, a1-34.7 mg, C3-148.7 mg, J=0.003797862±0.10%, D=1.0082±0.0018, NM-53, Lab#=6851-01											
A	450	521.990	0.161	1446.92	3.03	3.2	5.06	18.1	0.2	552.86	46.41
B	500	376.969	0.148	898.37	2.80	3.5	6.28	29.6	0.4	636.98	34.26
C	550	426.554	0.130	1199.91	6.79	3.9	6.31	16.9	1.0	435.94	26.31
D	600	271.296	0.129	641.25	8.40	4.0	6.43	30.1	1.6	488.04	12.20
E	650	247.740	0.127	727.01	9.97	4.0	6.44	13.3	2.4	212.38	15.57
F	725	95.909	0.142	255.47	32.64	3.6	5.88	21.3	4.9	134.65	4.29
G	800	22.403	0.129	72.17	22.38	3.9	1.64	4.7	6.6	7.25	2.54
H	850	7.294	0.122	21.31	28.41	4.2	0.87	13.4	8.7	6.70	1.19
I	900	10.714	0.109	33.58	23.10	4.7	0.48	7.2	10.5	5.30	1.48
J	1000	4.765	0.102	14.99	117.26	5.0	0.47	6.7	19.5	2.17	0.47
K	1150	3.225	0.088	10.57	360.16	5.8	0.15	2.5	47.0	0.56	0.20
L	1300	4.263	0.088	13.35	453.29	5.8	0.21	7.0	81.6	2.04	0.26
M	1400	52.710	0.171	166.85	59.24	3.0	1.73	6.4	86.1	23.09	2.68
N	1500	99.565	0.231	292.61	50.32	2.2	4.00	13.1	90.0	87.55	4.24
O	1650	35.173	0.110	95.87	131.12	4.6	1.49	19.4	100.0	46.17	1.44
total gas age			n=15		1308.92	5.2	0.89			23.47	1.33
plateau			n=4	steps L-O	693.97	5.1	0.86		53.0	3.92	5.41
W3-3 64 E3, Quartz, 97.00 mg, J=0.00350216±0.09%, D=1.0045±0.0012, NM-64, Lab#=7678-01											
A	450	446.711	0.497	878.31	2.19	1.0	7.01	41.9	11.0	909.72	31.92
B	500	598.214	0.329	1381.53	0.32	1.6	7.43	31.8	12.6	920.26	238.84
C	550	608.730	0.223	1945.32	1.41	2.3	5.56	5.6	19.6	202.32	111.68
D	600	118.258	0.339	240.87	0.70	1.5	7.11	39.8	23.1	275.41	41.57
E	650	50.279	0.051	98.79	2.25	10.1	6.04	41.9	34.4	128.42	11.67
F	725	122.246	0.332	392.26	3.92	1.5	5.05	5.2	54.0	39.60	12.95
G	800	-16.051	0.692	-75.81	1.59	0.74	5.03	-39.7	61.9	39.87	12.25
H	850	39.816	0.500	169.89	0.20	1.0	2.17	-26.1	62.9	-66.79	80.71
I	900	-2.976	0.000	-48.52	0.30	-	3.28	-380.9	64.4	70.24	53.37
J	1000	3.348	0.054	36.83	0.69	9.4	4.11	-225.7	67.9	-48.39	27.46
K	1150	2.854	0.626	49.08	0.41	0.81	3.55	-407.4	69.9	-75.02	43.97

Table A-11 con.

ID	Temp	$^{40}Ar/^{39}Ar$	$^{37}Ar/^{39}Ar$	$^{36}Ar/^{39}Ar$	$^{39}Ar_K$	K/Ca	Cl/K	$^{40}Ar^*$	^{39}Ar	Age	±1s
	(°C)			(x 10^{-3})	(x 10^{-16} mol)			(%)	(%)	(Ma)	(Ma)
L	1300	41.244	0.300	99.78	0.64	1.7	4.91	28.5	73.1	72.81	29.76
M	1400	2184.714	2.919	7238.41	0.86	0.17	4.44	2.1	77.4	269.75	499.70
N	1500	177.537	0.832	464.44	1.80	0.61	6.02	22.7	86.4	238.49	21.97
O	1750	180.125	2.167	530.22	2.71	0.24	6.98	13.1	100.0	143.38	17.47
total gas age			n=15		19.99	2.4	5.72			215.69	51.73
plateau			n=4	steps L-O	6.01	0.5	6.11		30.1	161.57	36.06
MTE64 J3, Quartz, 101.45 mg, J=0.00350669±0.09%, D=1.0045±0.0012, NM-64, Lab#=7690-01											
A	450	5744.042	0.389	19487.92	2.09	1.3	5.07	-0.3	7.3	-95.05	1554.24
B	500	168.930	0.194	466.44	0.98	2.6	4.88	18.4	10.7	186.69	37.83
C	550	164.817	0.242	510.03	3.14	2.1	4.82	8.6	21.6	87.05	16.80
D	600	436.696	0.503	1416.06	1.29	1.0	5.54	4.2	26.1	112.03	79.90
E	650	127.650	0.370	407.09	3.02	1.4	5.85	5.8	36.6	45.97	14.22
F	725	171.570	0.411	555.11	2.03	1.2	4.52	4.4	43.6	47.11	26.20
G	800	53.897	0.305	152.26	2.93	1.7	4.61	16.5	53.8	55.48	9.22
H	850	159.330	1.344	578.57	0.49	0.38	2.86	-7.3	55.5	-74.72	88.35
I	900	11.902	2.111	99.53	0.47	0.24	2.95	-145.9	57.1	-113.55	46.86
J	1000	62.350	0.940	241.02	0.99	0.54	4.04	-14.2	60.6	-56.74	28.28
K	1150	49.422	0.912	219.53	0.81	0.56	3.41	-31.2	63.4	-100.24	29.56
L	1300	70.409	1.070	341.98	0.71	0.48	4.13	-43.4	65.9	-204.86	41.64
M	1400	210.978	0.566	723.32	2.34	0.90	5.62	-1.3	74.0	-17.46	26.26
N	1500	163.294	0.998	536.84	3.14	0.51	5.36	2.9	84.9	29.57	18.36
O	1750	171.040	0.348	549.25	4.35	1.5	5.09	5.1	100.0	54.46	15.51
total gas age			n=15		28.80	1.3	4.96			24.88	135.58
plateau			n=4	steps L-O	10.54	1.0	5.22		36.6	18.65	37.88
W353:Tube3, one large Quartz broken to six pieces, 178.18 mg, J=0.003841047±0.10%, D=1.0082±0.0018, NM-53, Lab#=6898-01											
A	450	-12.252	0.000	-39.27	-2.74	-	-1.68	5.5	-0.3	-4.68	9.61
B	500	5.698	0.005	11.30	-3.58	99.2	-0.66	40.9	-0.8	16.09	5.21
C	550	68.409	0.000	218.10	-0.70	-	5.04	5.7	-0.9	27.05	38.49
D	600	-93.760	0.322	-378.00	0.33	1.6	15.79	-19.1	-0.8	120.23	110.76
E	650	9.474	0.080	24.72	-1.99	6.4	10.32	22.7	-1.1	14.83	8.16
F	725	9.375	0.192	18.76	1.84	2.7	12.40	40.8	-0.9	26.29	8.94
G	800	9.085	0.112	19.38	6.58	4.6	8.50	36.8	0.0	22.99	2.71
H	850	14.162	0.239	-10.95	0.75	2.1	5.49	122.8	0.1	116.66	19.64
I	925	23.770	0.112	-57.22	0.40	4.5	4.37	171.1	0.1	261.82	33.10
J	1000	44.173	0.104	88.13	0.64	4.9	3.86	41.0	0.2	121.34	26.25
K	1150	64.199	0.424	143.75	0.48	1.2	2.31	33.8	0.3	144.65	39.60
L	1300	99.521	0.244	273.09	0.91	2.1	2.51	18.9	0.4	125.90	29.97
M	1400	74.292	0.394	178.13	1.40	1.3	0.86	29.2	0.5	144.19	16.09
N	1500	38.104	0.234	95.01	4.13	2.2	0.67	26.3	1.1	68.15	5.56
O	1650	6.367	0.089	17.68	140.67	5.8	0.16	17.6	18.8	7.76	0.40
P	1750	3.136	0.079	9.92	642.08	6.5	0.02	5.8	100.0	1.27	0.15
total gas age			n=16		791.19	5.8	0.15			3.78	0.34
plateau			n=5	steps L-P	789.18	6.3	0.05		99.7	2.14	1.53

Isotopic ratios corrected for blank, radioactive decay, and mass discrimination, not corrected for interferring reactions.

Table A-11 con.

Individual analyses show analytical error only; mean age errors also include error in J and irradiation parameters.							
Analyses in italics are excluded excluded from mean age calculations.							
Correction factors:							
$(^{39}Ar/^{37}Ar)_{Ca} = 0.00065 \pm 0.00005$							
$(^{36}Ar/^{37}Ar)_{Ca} = 0.00026 \pm 0.00002$							
$(^{38}Ar/^{39}Ar)_{K} = 0.0119$							
$(^{40}Ar/^{39}Ar)_{K} = 0.0250 \pm 0.0050$							

APPENDIX L Pre-irradiation crushed grains data from $^{40}Ar/^{39}Ar$ analysis

Table A- 12 Complete Data Table from Pre-Irradiation Crushed Grains

ID	Temp	$^{40}Ar/^{39}Ar$	$^{37}Ar/^{39}Ar$	$^{36}Ar/^{39}Ar$	$^{39}Ar_K$	K/Ca	Cl/K	$^{40}Ar^*$	^{39}Ar	Age	±1s
	(°C)			(x 10^{-3})	(x 10^{-16} mol)			(%)	(%)	(Ma)	(Ma)
MTE< 5353 MICRON ~200 mg, J=0.003816974±0.10%, D=1.0082±0.0018, NM-53, Lab#=6894-01											
A	450	74.207	0.102	250.16	51.14	5.0	1.32	0.4	1.1	1.82	3.84
B	500	37.960	0.084	125.68	317.38	6.1	0.90	2.1	7.7	5.50	1.71
C	550	21.347	0.062	69.95	81.84	8.2	0.44	3.1	9.4	4.50	1.20
D	600	17.763	0.057	57.31	847.36	8.9	0.25	4.5	27.2	5.54	0.73
E	650	14.673	0.075	46.36	818.27	6.8	0.13	6.5	44.3	6.54	0.61
F	725	13.489	0.078	41.41	772.03	6.6	0.16	9.1	60.5	8.46	0.59
G	800	11.587	0.124	35.01	639.69	4.1	0.02	10.6	73.9	8.42	0.50
H	850	9.944	0.232	28.90	393.13	2.2	0.01	14.0	82.1	9.57	0.41
I	900	9.243	0.337	25.29	116.02	1.5	0.02	19.1	84.5	12.14	0.59
J	1000	12.774	0.541	32.72	236.99	0.94	0.02	24.4	89.5	21.36	0.62
K	1150	17.068	0.323	38.23	95.54	1.6	0.11	33.8	91.5	39.30	0.85
L	1300	20.234	0.228	53.19	79.40	2.2	1.83	22.3	93.2	30.77	1.12
M	1400	18.063	0.285	58.32	45.75	1.8	0.63	4.6	94.1	5.67	1.41
N	1500	11.051	0.154	36.53	60.32	3.3	0.26	2.2	95.4	1.65	1.07
O	1650	6.297	0.087	20.36	220.75	5.9	0.13	4.1	100.0	1.79	0.41
Table A-6 con.											
	Temp	$^{40}Ar/^{39}Ar$	$^{37}Ar/^{39}Ar$	$^{36}Ar/^{39}Ar$	$^{39}Ar_K$	K/Ca	Cl/K	$^{40}Ar^*$	^{39}Ar	Age	±1s
	(°C)			(x 10^{-3})	(x 10^{-16} mol)			(%)	(%)	(Ma)	(Ma)
total gas age			n=15		4775.62	5.6	0.23			8.66	0.73
plateau			n=4	steps L-O	406.22	4.3	0.54		8.5	4.82	4.94
CPU< 5353:T1:3.2, MICRON ~200 mg, J=0.003839985±0.10%, D=1.0082±0.0018, NM-53, Lab#=6886-01											
A	450	78.548	0.070	262.37	139.07	7.3	0.13	1.3	3.6	6.89	3.49
B	500	26.237	0.089	99.58	4.03	5.7	0.12	-12.2	3.7	-22.37	7.81
C	550	19.791	0.040	64.12	801.24	12.9	0.02	4.1	24.5	5.67	0.83
D	600	14.859	0.043	47.82	540.72	11.8	0.01	4.7	38.5	4.88	0.68
E	650	14.393	0.056	45.19	436.94	9.1	0.01	7.1	49.9	7.04	0.63
F	725	14.689	0.098	45.26	508.61	5.2	0.02	8.8	63.1	8.95	0.65
G	800	13.079	0.145	40.32	449.33	3.5	0.02	8.8	74.7	7.95	0.55
H	850	10.044	0.219	30.88	287.97	2.3	0.02	9.1	82.2	6.29	0.51
I	900	9.688	0.309	29.35	108.69	1.7	0.03	10.5	85.0	7.01	0.62
J	1000	18.728	0.557	56.70	175.80	0.92	0.05	10.6	89.6	13.74	0.89
K	1150	39.827	0.661	107.58	25.49	0.77	0.50	20.2	90.2	55.03	2.47
L	1300	33.948	0.312	94.99	27.33	1.6	6.16	17.3	91.0	40.26	2.60
M	1400	27.612	0.190	79.71	30.82	2.7	0.84	14.7	91.8	27.82	1.93
N	1500	25.137	0.116	73.40	45.63	4.4	0.33	13.6	92.9	23.60	1.36
O	1650	21.296	0.080	60.27	272.07	6.4	0.20	16.3	100.0	23.84	0.88
total gas age			n=15		3853.75	7.5	0.09			9.12	0.85
plateau			n=4	steps L-O	375.86	5.5	0.70		9.8	25.33	2.50
MTE>5353:tube 1-c, 53-63 MICRON ~200mg, J=0.003828852±0.10%, D=1.0082±0.0018, NM-53, Lab#=6891-01											
A	450	47.991	0.082	157.71	384.41	6.2	1.25	2.9		9.31	2.07

Table A-12 con.

ID	Temp	$^{40}Ar/^{39}Ar$	$^{37}Ar/^{39}Ar$	$^{36}Ar/^{39}Ar$	$^{39}Ar_K$	K/Ca	Cl/K	$^{40}Ar^*$	^{39}Ar	Age	±1s
	(°C)			(x 10^{-3})	(x 10^{-16} mol)			(%)	(%)	(Ma)	(Ma)
B	500	23.670	0.060	78.12	177.26	8.5	0.64	2.4	5.0	3.89	1.08
C	550	19.468	0.056	63.03	442.16	9.1	0.45	4.2	17.4	5.66	0.91
D	600	16.495	0.053	53.38	153.86	9.6	0.18	4.2	21.8	4.83	0.93
E	650	17.002	0.088	53.28	753.77	5.8	0.23	7.3	43.0	8.54	0.70
F	725	15.115	0.090	46.45	579.27	5.7	0.22	9.0	59.2	9.42	0.64
H	850	10.062	0.308	27.90	567.77	1.7	0.01	18.0	75.2	12.49	0.42
I	925	12.314	0.526	32.81	120.68	0.97	0.02	21.4	78.6	18.09	0.59
J	1000	17.507	0.393	42.68	53.46	1.3	0.05	28.0	80.1	33.52	1.03
K	1150	15.987	0.186	36.19	115.55	2.7	0.10	33.0	83.4	36.12	0.73
L	1300	24.466	0.174	67.86	70.21	2.9	2.32	18.0	85.3	30.14	1.25
M	1400	26.429	0.238	82.53	33.89	2.1	0.71	7.7	86.3	13.99	1.74
N	1500	16.776	0.129	51.83	54.81	4.0	0.21	8.6	87.8	9.94	1.11
O	1650	9.973	0.076	28.26	432.31	6.7	0.09	16.0	100.0	11.02	0.45
total gas age			n=13		3555.00	5.5	0.25			10.96	0.70
plateau			n=4	steps L-O	591.22	5.8	0.40		16.6	12.85	3.28
CPU>5353, ~50.00 mg, 53-63 MICRON ~50mg, J=0.003844057±0.10%, D=1.0045±0.0012, NM-53, Lab#=6883-01											
A	450	160.476	1.004	537.96	39.37	0.51	0.10	1.0	10.3	10.79	6.05
B	500	21.656	1.493	70.62	32.75	0.34	0.01	4.0	18.9	6.06	1.36
C	550	17.035	0.163	56.87	18.96	3.1	0.01	1.3	23.9	1.49	1.54
D	600	16.143	0.213	52.06	49.06	2.4	0.01	4.6	36.7	5.18	0.88
E	650	13.962	0.560	44.16	46.20	0.91	0.01	6.7	48.8	6.43	0.84
F	725	12.806	0.476	40.52	55.55	1.1	0.01	6.6	63.4	5.82	0.77
G	800	10.561	1.115	33.68	45.13	0.46	0.01	6.3	75.2	4.62	0.76
H	850	9.751	0.000	32.03	17.29	-	0.02	2.7	79.7	1.80	1.32
I	900	14.426	2.089	45.63	11.18	0.24	0.03	7.5	82.7	7.45	2.23
J	1000	38.464	4.556	125.21	6.32	0.11	0.12	4.6	84.3	12.39	4.78
K	1150	57.064	6.937	168.61	2.69	0.074	0.84	13.6	85.0	53.19	8.72
L	1300	45.957	0.000	160.78	3.11	-	9.07	-3.4	85.9	-10.99	8.33
M	1400	24.886	3.511	70.70	2.23	0.15	0.92	17.0	86.4	29.22	7.61
N	1500	26.126	12.420	84.54	3.39	0.041	0.34	7.9	87.3	14.44	5.56
O	1650	21.733	0.449	60.75	48.36	1.1	0.14	17.4	100.0	26.10	1.02
total gas age			n=15		381.59	1.0	0.13			8.95	1.79
plateau			n=4	steps L-O	57.08	1.0	0.67		15.0	25.27	2.93

Isotopic ratios corrected for blank, radioactive decay, and mass discrimination, not corrected for interferring reactions.

Individual analyses show analytical error only; mean age errors also include error in J and irradiation parameters.

Analyses in italics are excluded excluded from mean age calculations.

Correction factors:
$(^{39}Ar/^{37}Ar)_{Ca}$ = 0.00065±0.00005
$(^{36}Ar/^{37}Ar)_{Ca}$ = 0.00026±0.00002
$(^{38}Ar/^{39}Ar)_K$ = 0.0119
$(^{40}Ar/^{39}Ar)_K$ = 0.0250±0.0050

APPENDIX M Crushing data from $^{40}Ar/^{39}Ar$ analysis

Table A-13 Complete Data Tables from Crushing

ID	Temp (°C)	$^{40}Ar/^{39}Ar$	$^{37}Ar/^{39}Ar$	$^{36}Ar/^{39}Ar$ (x 10^{-3})	$^{39}Ar_K$ (x 10^{-15} mol)	K/Ca	Cl/K	$^{40}Ar^*$ (%)	^{39}Ar (%)	Age (Ma)	±1s (Ma)
MTEET, 137.54 mg, J=0.003751717±0.09%, D=1.00253±0.00119, NM-91, Lab#=9372-01											
A	0	679.691	0.389	2245.407	0.622	1.3	6.9	2.4	2.5	106.3	92.0
B	0	230.187	0.349	716.111	0.235	1.5	5.7	8.1	3.4	121.6	45.1
C	0	789.192	0.366	2554.493	0.635	1.4	7.9	4.4	5.9	218.7	94.7
D	0	350.536	0.336	1143.342	0.223	1.5	6.1	3.6	6.8	83.9	90.3
E	0	348.378	0.303	1031.227	0.184	1.7	7.3	12.5	7.5	273.6	74.4
F	0	446.266	0.365	1436.237	0.215	1.4	7.3	4.9	8.3	142.2	84.4
G	0	310.381	0.369	926.109	0.695	1.4	7.3	11.8	11.1	232.9	20.9
H	0	255.125	0.348	770.232	0.338	1.5	6.5	10.8	12.4	177.3	35.8
I	0	234.218	0.293	726.947	0.286	1.7	6.5	8.3	13.5	126.8	34.0
J	0	329.297	0.381	1029.249	1.222	1.3	7.5	7.6	18.4	162.7	20.5
K	0	248.282	0.360	774.947	0.533	1.4	6.9	7.8	20.5	126.1	31.2
L	0	161.080	0.390	482.070	0.173	1.3	6.6	11.6	21.2	121.9	36.8
M	300	972.683	0.084	3374.208	0.066	6.1	6.2	-2.5	21.4	-173.3	887.7
N	375	275.347	0.055	939.116	0.402	9.3	7.2	-0.8	23.0	-14.8	42.6
O	450	213.094	0.067	714.117	0.350	7.7	11.0	1.0	24.4	13.8	36.2
P	525	235.391	0.125	774.212	0.196	4.1	15.0	2.8	25.2	44.1	67.6
Q	600	262.935	0.201	834.429	0.638	2.5	9.6	6.2	27.7	107.4	24.6
R	700	145.055	0.313	430.644	1.528	1.6	8.5	12.3	33.7	116.6	8.0
S	800	188.645	0.622	624.439	0.748	0.8	6.9	2.2	36.7	27.8	18.0
S	900	151.869	0.830	489.594	0.290	0.6	6.5	4.8	37.8	48.3	30.7
T	1050	119.960	0.705	365.422	0.197	0.7	6.1	10.0	38.6	79.5	34.9
U	1200	65.195	0.718	181.518	0.190	0.7	6.2	17.8	39.3	76.8	23.0
V	1300	51.748	0.363	124.963	1.093	1.4	7.4	28.6	43.6	97.7	4.7
W	1400	39.127	0.350	88.772	3.549	1.5	7.1	33.0	57.6	85.3	1.8
X	1500	34.060	0.336	73.912	1.369	1.5	6.6	35.9	63.0	80.9	3.0
Y	1600	39.920	0.379	91.873	1.632	1.3	6.6	32.0	69.5	84.5	2.8
Z	1800	55.536	0.397	143.589	1.694	1.3	6.8	23.6	76.2	86.6	3.9
AA	300	113.938	0.035	391.637	0.690	14.6	6.1	-1.6	78.9	-12.3	12.1
AB	375	77.719	0.051	257.202	0.539	9.9	9.8	2.2	81.0	11.4	11.1
AC	450	105.317	0.084	334.204	0.496	6.1	16.8	6.2	83.0	43.7	14.3
AD	525	276.781	0.121	837.438	0.311	4.2	10.5	10.6	84.2	188.2	43.8
AE	600	628.721	0.350	1925.784	0.028	1.5	9.8	9.5	84.3	364.4	925.5
AF	700	358.628	0.604	1031.329	0.489	0.8	5.3	15.0	86.3	332.3	35.8
AG	800	173.987	1.156	539.071	0.381	0.4	2.9	8.5	87.8	97.3	26.8
AH	900	305.755	1.480	1000.873	0.157	0.3	3.3	3.3	88.4	67.1	103.1
AI	1050	436.289	1.060	1383.756	0.199	0.5	5.3	6.3	89.2	176.9	111.4
AJ	1200	165.848	0.495	473.372	0.167	1.0	5.8	15.7	89.8	167.8	49.1
AK	1300	72.454	0.412	198.162	0.240	1.2	6.5	19.2	90.8	91.7	19.5
AL	1400	49.734	0.401	126.885	0.369	1.3	6.7	24.6	92.2	81.0	10.6
AM	1500	61.295	0.389	176.240	0.283	1.3	6.2	15.0	93.3	61.4	15.3
AN	1600	51.022	0.368	130.245	0.514	1.4	6.3	24.6	95.4	82.9	7.9
AO	1800	79.895	0.339	221.999	1.174	1.5	6.8	17.9	100.0	94.3	5.8
total gas age			n=42		25.340	2.3				101.6	24.2
plateau			n=42	steps A-AO	25.340	2.3			100.0	85.2	3.3

Table A-13 con.

ID	Temp (°C)	$^{40}Ar/^{39}Ar$	$^{37}Ar/^{39}Ar$	$^{36}Ar/^{39}Ar$ (x 10^{-3})	$^{39}Ar_K$ (x 10^{-16} mol)	K/Ca	Cl/K	$^{40}Ar^*$ (%)	^{39}Ar (%)	Age (Ma)	±1s (Ma)
CMXET, 103.95 mg, J=0.003682091±0.09%, D=1.00253±0.00119, NM-91, Lab#=9367-01											
A	0	917.935	0.202	2655.199	0.594	2.5	6.1	14.5	5.0	720.6	52.0
B	0	1150.685	0.208	3526.936	1.180	2.4	5.8	9.4	14.9	606.3	63.6
C	0	455.714	0.242	1156.661	2.153	2.1	5.7	25.0	32.9	632.0	22.8
D	0	187.397	0.240	395.234	0.924	2.1	4.8	37.7	40.6	416.9	18.1
E	0	185.862	0.221	366.916	1.397	2.3	5.4	41.7	52.3	452.6	10.4
F	0	76.794	0.196	126.612	0.638	2.6	5.0	51.3	57.7	244.2	6.5
G	0	65.732	0.179	133.085	1.079	2.8	5.9	40.2	66.7	167.3	3.6
H	0	56.975	0.201	129.343	0.431	2.5	6.0	32.9	70.3	120.4	6.5
I	0	45.016	0.200	112.759	0.252	2.5	6.5	26.0	72.4	76.0	10.1
J	0	41.586	0.203	108.361	0.252	2.5	6.8	23.0	74.6	62.4	9.6
K	0	41.572	0.229	121.748	0.237	2.2	7.9	13.4	76.5	36.7	10.6
L	300	80.965	0.063	275.821	0.425	8.1	12.2	-0.7	80.1	-3.7	13.5
M	375	67.150	0.130	222.711	0.378	3.9	14.8	2.0	83.3	8.8	13.2
N	450	70.244	0.362	219.697	0.382	1.4	19.6	7.6	86.5	35.0	13.3
O	525	194.916	0.979	568.191	0.073	0.5	11.6	13.9	87.1	171.5	126.3
P	600	165.706	1.507	433.597	0.133	0.3	8.7	22.7	88.2	234.5	56.6
Q	700	147.247	1.758	405.612	0.244	0.3	4.7	18.7	90.2	174.2	30.8
R	800	68.049	1.868	152.443	0.267	0.3	2.2	34.0	92.5	147.6	15.1
S	900	94.109	1.996	115.267	0.101	0.3	2.3	63.9	93.3	361.5	38.4
T	1050	140.835	1.548	145.021	0.073	0.3	4.2	69.6	93.9	556.7	61.9
U	1200	248.362	1.332	549.627	0.057	0.4	4.3	34.6	94.4	496.8	151.9
V	1300	115.616	0.350	243.432	0.071	1.5	5.0	37.8	95.0	269.1	73.1
W	1400	65.365	0.248	149.517	0.214	2.1	5.8	32.4	96.8	135.5	18.7
X	1500	109.929	0.199	251.479	0.087	2.6	5.5	32.4	97.5	222.3	58.8
Y	1600	198.816	0.240	487.858	0.077	2.1	6.3	27.5	98.2	330.8	105.2
Z	1800	217.242	0.251	566.416	0.218	2.0	6.6	23.0	100.0	304.1	43.0
total gas age			n=26		11.938	2.4				365.1	24.9
plateau			n=26	steps A-Z	11.938	2.4			100.0	166.2	22.9
W3FT, 58.86 mg, J=0.003690117±0.09%, D=1.00253±0.00119, NM-91, Lab#=9377-01											
A	0	335.734	0.250	388.894	0.098	2.0	6.0	65.8	3.3	1075.3	51.1
B	0	101.679	0.415	447.846	0.007	1.2	2.8	-30.1	3.6	-216.6	737.0
C	0	360.076	0.204	791.058	0.461	2.5	5.3	35.1	19.1	690.3	20.8
D	0	114.700	0.223	113.061	0.375	2.3	4.7	70.9	31.8	473.3	8.2
E	0	130.735	0.235	163.722	0.137	2.2	4.6	63.0	36.5	478.7	23.6
F	0	150.722	0.143	455.836	0.021	3.6	4.2	10.6	37.2	103.5	246.5
G	0	184.030	0.206	126.153	0.267	2.5	5.5	79.7	46.2	780.8	13.0
H	0	116.316	0.179	124.339	0.271	2.9	4.8	68.4	55.4	464.5	11.2
I	0	74.522	0.179	171.944	0.069	2.9	5.9	31.8	57.7	151.3	40.8
J	0	66.721	0.130	197.531	0.105	3.9	8.0	12.5	61.2	54.7	28.0
K	0	129.985	0.180	217.619	0.164	2.8	4.2	50.5	66.8	391.5	20.8
L	0	151.994	0.183	260.507	0.105	2.8	4.5	49.3	70.3	440.8	35.5
M	0	117.815	0.121	262.796	0.130	4.2	5.4	34.1	74.7	249.2	28.3
N	0	149.955	0.070	433.410	0.087	7.3	6.5	14.6	77.6	140.0	57.3
O	0	220.647	0.109	711.011	0.067	4.7	7.6	4.8	79.9	68.7	112.6
P	0	129.818	0.000	387.133	0.006	-	4.2	11.9	80.1	99.7	762.9
Q	0	205.754	0.124	693.993	0.041	4.1	9.6	0.3	81.5	4.4	178.1
R	300	754.785	0.058	2639.141	0.048	8.8	20.8	-3.3	83.1	-175.4	936.4

Table A-13 con.

ID	Temp	$^{40}Ar/^{39}Ar$	$^{37}Ar/^{39}Ar$	$^{36}Ar/^{39}Ar$	$^{39}Ar_K$	K/Ca	Cl/K	$^{40}Ar^*$	^{39}Ar	Age	±1s
	(°C)			(x 10^{-3})	(x 10^{-16} mol)			(%)	(%)	(Ma)	(Ma)
S	375	347.103	0.282	1205.122	0.057	1.8	15.6	-2.6	85.0	-61.0	345.0
T	450	132.017	0.130	402.340	0.060	3.9	18.4	9.9	87.1	85.2	115.8
U	525	169.574	0.652	415.119	0.031	0.8	16.9	27.7	88.1	288.3	226.4
V	600	248.608	0.747	527.829	0.034	0.7	15.4	37.3	89.3	530.8	247.5
W	700	229.838	0.888	421.027	0.051	0.6	7.4	45.9	91.0	593.3	142.8
X	800	215.510	1.202	266.302	0.053	0.4	1.9	63.5	92.8	738.1	114.8
Y	900	427.252	2.125	403.949	0.028	0.2	1.1	72.1	93.7	1371.0	276.6
Z	1050	320.336	0.836	329.901	0.043	0.6	2.2	69.6	95.2	1083.3	162.7
AA	1200	386.635	0.099	709.834	0.049	5.2	0.9	45.7	96.8	906.4	207.7
AB	1300	251.976	0.255	763.985	0.024	2.0	1.6	10.4	97.6	166.6	480.2
AC	1400	312.310	0.466	1028.874	0.016	1.1	4.9	2.7	98.2	54.4	995.4
AD	1500	561.209	0.259	1744.997	0.009	2.0	5.6	8.1	98.5	280.4	2713.6
AE	1600	586.996	0.486	1924.728	0.013	1.0	5.3	3.1	98.9	117.6	2238.7
AF	1800	777.300	0.208	2545.097	0.032	2.5	6.5	3.2	100.0	160.5	1145.0
total gas age			n=32		2.959	2.8				477.2	108.2
plateau			n=32	steps A-AF	2.959	2.8			100.0	502.0	32.0
MTEEC, 137.54 mg, J=0.003751717±0.09%, D=1.00253±0.00119, NM-91, Lab#=9372-01											
A	0	679.691	0.389	2245.407	0.622	1.3	6.9	2.4	11.6	106.3	92.0
B	0	230.187	0.349	716.111	0.235	1.5	5.7	8.1	16.0	121.6	45.1
C	0	789.192	0.366	2554.493	0.635	1.4	7.9	4.4	27.8	218.7	94.7
D	0	350.536	0.336	1143.342	0.223	1.5	6.1	3.6	32.0	83.9	90.3
E	0	348.378	0.303	1031.227	0.184	1.7	7.3	12.5	35.4	273.6	74.4
F	0	446.266	0.365	1436.237	0.215	1.4	7.3	4.9	39.4	142.2	84.4
G	0	310.381	0.369	926.109	0.695	1.4	7.3	11.8	52.4	232.9	20.9
H	0	255.125	0.348	770.232	0.338	1.5	6.5	10.8	58.7	177.3	35.8
I	0	234.218	0.293	726.947	0.286	1.7	6.5	8.3	64.0	126.8	34.0
J	0	329.297	0.381	1029.249	1.222	1.3	7.5	7.6	86.8	162.7	20.5
K	0	248.282	0.360	774.947	0.533	1.4	6.9	7.8	96.8	126.1	31.2
L	0	161.080	0.390	482.070	0.173	1.3	6.6	11.6	100.0	121.9	36.8
total gas age			n=12		5.361	1.4				163.9	49.3
plateau			n=12	steps A-L	5.361	1.4			100.0	169.2	17.3
CMXE tube:91, Crush Quartz, 103.95 mg, J=0.003682091±0.09%, D=1.00253±0.00119, NM-91,											
A	0	917.935	0.202	2655.199	0.594	2.5	6.1	14.5	6.5	720.6	52.0
B	0	1150.685	0.208	3526.936	1.180	2.4	5.8	9.4	19.4	606.3	63.6
C	0	455.714	0.242	1156.661	2.153	2.1	5.7	25.0	43.0	632.0	22.8
D	0	187.397	0.240	395.234	0.924	2.1	4.8	37.7	53.1	416.9	18.1
E	0	185.862	0.221	366.916	1.397	2.3	5.4	41.7	68.4	452.6	10.4
F	0	76.794	0.196	126.612	0.638	2.6	5.0	51.3	75.4	244.2	6.5
G	0	65.732	0.179	133.085	1.079	2.8	5.9	40.2	87.2	167.3	3.6
H	0	56.975	0.201	129.343	0.431	2.5	6.0	32.9	91.9	120.4	6.5
I	0	45.016	0.200	112.759	0.252	2.5	6.5	26.0	94.6	76.0	10.1
J	0	41.586	0.203	108.361	0.252	2.5	6.8	23.0	97.4	62.4	9.6
K	0	41.572	0.229	121.748	0.237	2.2	7.9	13.4	100.0	36.7	10.6
total gas age			n=11		9.138	2.4				432.7	22.4
plateau			n=11	steps A-K	9.138	2.4			100.0	180.0	34.7
W3F tube:91, Crush Quartz, 58.86 mg, J=0.003690117±0.09%, D=1.00253±0.00119, NM-91, Lab#=9377-											
A	0	335.734	0.250	388.894	0.098	2.0	6.0	65.8	4.1	1075.3	51.1

Table A-13 con.

ID	Temp	$^{40}Ar/^{39}Ar$	$^{37}Ar/^{39}Ar$	$^{36}Ar/^{39}Ar$	$^{39}Ar_K$	K/Ca	Cl/K	$^{40}Ar^*$	^{39}Ar	Age	±1s
	(°C)			(x 10^{-3})	(x 10^{-16} mol)			(%)	(%)	(Ma)	(Ma)
B	0	101.679	0.415	447.846	0.007	1.2	2.8	-30.1	4.4	-216.6	737.0
C	0	360.076	0.204	791.058	0.461	2.5	5.3	35.1	23.5	690.3	20.8
D	0	114.700	0.223	113.061	0.375	2.3	4.7	70.9	39.0	473.3	8.2
E	0	130.735	0.235	163.722	0.137	2.2	4.6	63.0	44.7	478.7	23.6
F	0	150.722	0.143	455.836	0.021	3.6	4.2	10.6	45.6	103.5	246.5
G	0	184.030	0.206	126.153	0.267	2.5	5.5	79.7	56.7	780.8	13.0
H	0	116.316	0.179	124.339	0.271	2.9	4.8	68.4	67.9	464.5	11.2
I	0	74.522	0.179	171.944	0.069	2.9	5.9	31.8	70.8	151.3	40.8
J	0	66.721	0.130	197.531	0.105	3.9	8.0	12.5	75.1	54.7	28.0
K	0	129.985	0.180	217.619	0.164	2.8	4.2	50.5	81.9	391.5	20.8
L	0	151.994	0.183	260.507	0.105	2.8	4.5	49.3	86.2	440.8	35.5
M	0	117.815	0.121	262.796	0.130	4.2	5.4	34.1	91.6	249.2	28.3
N	0	149.955	0.070	433.410	0.087	7.3	6.5	14.6	95.2	140.0	57.3
O	0	220.647	0.109	711.011	0.067	4.7	7.6	4.8	98.0	68.7	112.6
P	0	129.818	0.000	387.133	0.006	-	4.2	11.9	98.3	99.7	762.9
Q	0	205.754	0.124	693.993	0.041	4.1	9.6	0.3	100.0	4.4	178.1
total gas age			n=17		2.412	2.9				488.9	32.5
plateau			n=17	steps A-Q	2.412	2.9			100.0	501.4	43.6
MTEEC tube:91, Large Crushed Quartz 80.26 mg, J=0.003751717±0.09%, D=1.00253±0.00119, NM-91,											
A	300	972.683	0.084	3374.208	0.066	6.1	6.2	-2.5	0.5	-173.3	887.7
B	375	275.347	0.055	939.116	0.402	9.3	7.2	-0.8	3.4	-14.8	42.6
C	450	213.094	0.067	714.117	0.350	7.7	11.0	1.0	5.9	13.8	36.2
D	525	235.391	0.125	774.212	0.196	4.1	15.0	2.8	7.3	44.1	67.6
E	600	262.935	0.201	834.429	0.638	2.5	9.6	6.2	11.9	107.4	24.6
F	700	145.055	0.313	430.644	1.528	1.6	8.5	12.3	22.8	116.6	8.0
G	800	188.645	0.622	624.439	0.748	0.82	6.9	2.2	28.2	27.8	18.0
H	900	151.869	0.830	489.594	0.290	0.62	6.5	4.8	30.3	48.3	30.7
I	1050	119.960	0.705	365.422	0.197	0.72	6.1	10.0	31.7	79.5	34.9
J	1200	65.195	0.718	181.518	0.190	0.71	6.2	17.8	33.0	76.8	23.0
K	1300	51.748	0.363	124.963	1.093	1.4	7.4	28.6	40.9	97.7	4.7
L	1400	39.127	0.350	88.772	3.549	1.5	7.1	33.0	66.3	85.3	1.8
M	1500	34.060	0.336	73.912	1.369	1.5	6.6	35.9	76.1	80.9	3.0
N	1600	39.920	0.379	91.873	1.632	1.3	6.6	32.0	87.8	84.5	2.8
O	1800	55.536	0.397	143.589	1.694	1.3	6.8	23.6	100.0	86.6	3.9
total gas age			n=15		13.942	1.9				79.8	13.6
plateau			n=5	steps K-O	9.337	1.4			67.0	85.4	2.3
MTEE tube:91, Small Crushed Quartz 50.07 mg, J=0.003751717±0.09%, D=1.00253±0.00119, NM-91,											
A	300	113.938	0.035	391.637	0.690	14.6	6.1	-1.6	11.4	-12.3	12.1
B	375	77.719	0.051	257.202	0.539	9.9	9.8	2.2	20.3	11.4	11.1
C	450	105.317	0.084	334.204	0.496	6.1	16.8	6.2	28.6	43.7	14.3
D	525	276.781	0.121	837.438	0.311	4.2	10.5	10.6	33.7	188.2	43.8
E	600	628.721	0.350	1925.784	0.028	1.5	9.8	9.5	34.2	364.4	925.5
F	700	358.628	0.604	1031.329	0.489	0.84	5.3	15.0	42.3	332.3	35.8
G	800	173.987	1.156	539.071	0.381	0.44	2.9	8.5	48.6	97.3	26.8
H	900	305.755	1.480	1000.873	0.157	0.34	3.3	3.3	51.2	67.1	103.1
I	1050	436.289	1.060	1383.756	0.199	0.48	5.3	6.3	54.5	176.9	111.4
J	1200	165.848	0.495	473.372	0.167	1.0	5.8	15.7	57.3	167.8	49.1
K	1300	72.454	0.412	198.162	0.240	1.2	6.5	19.2	61.2	91.7	19.5

Table A-13 con.

ID	Temp	$^{40}Ar/^{39}Ar$	$^{37}Ar/^{39}Ar$	$^{36}Ar/^{39}Ar$	$^{39}Ar_K$	K/Ca	Cl/K	$^{40}Ar^*$	^{39}Ar	Age	±1s
	(°C)			(x 10^{-3})	(x 10^{-16} mol)			(%)	(%)	(Ma)	(Ma)
L	1400	49.734	0.401	126.885	0.369	1.3	6.7	24.6	67.4	81.0	10.6
M	1500	61.295	0.389	176.240	0.283	1.3	6.2	15.0	72.1	61.4	15.3
N	1600	51.022	0.368	130.245	0.514	1.4	6.3	24.6	80.6	82.9	7.9
O	1800	79.895	0.339	221.999	1.174	1.5	6.8	17.9	100.0	94.3	5.8
total gas age			n=15		6.037	4.0				96.8	26.4
plateau			n=5	steps K-O	2.579	1.4			42.7	87.0	6.1
CMXE tube:91, Crushed Quartz 50.46 mg, J=0.003682091±0.09%, D=1.00253±0.00119, NM-91,											
A	300	80.965	0.063	275.821	0.425	8.1	12.2	-0.7	15.2	-3.7	13.5
B	375	67.150	0.130	222.711	0.378	3.9	14.8	2.0	28.7	8.8	13.2
C	450	70.244	0.362	219.697	0.382	1.4	19.6	7.6	42.3	35.0	13.3
D	525	194.916	0.979	568.191	0.073	0.52	11.6	13.9	44.9	171.5	126.3
E	600	165.706	1.507	433.597	0.133	0.34	8.7	22.7	49.7	234.5	56.6
F	700	147.247	1.758	405.612	0.244	0.29	4.7	18.7	58.4	174.2	30.8
G	800	68.049	1.868	152.443	0.267	0.27	2.2	34.0	67.9	147.6	15.1
H	900	94.109	1.996	115.267	0.101	0.26	2.3	63.9	71.5	361.5	38.4
I	1050	140.835	1.548	145.021	0.073	0.33	4.2	69.6	74.2	556.7	61.9
J	1200	248.362	1.332	549.627	0.057	0.38	4.3	34.6	76.2	496.8	151.9
K	1300	115.616	0.350	243.432	0.071	1.5	5.0	37.8	78.7	269.1	73.1
L	1400	65.365	0.248	149.517	0.214	2.1	5.8	32.4	86.4	135.5	18.7
M	1500	109.929	0.199	251.479	0.087	2.6	5.5	32.4	89.5	222.3	58.8
N	1600	198.816	0.240	487.858	0.077	2.1	6.3	27.5	92.2	330.8	105.2
O	1800	217.242	0.251	566.416	0.218	2.0	6.6	23.0	100.0	304.1	43.0
total gas age			n=15		2.800	2.6				144.7	33.2
plateau			n=5	steps K-O	0.666	2.1			23.8	175.5	37.2
W3F tube:91, Crushed Quartz 93.19 mg, J=0.003690117±0.09%, D=1.00253±0.00119, NM-91,											
A	300	754.785	0.058	2639.141	0.048	8.8	20.8	-3.3	8.7	-175.4	936.4
B	375	347.103	0.282	1205.122	0.057	1.8	15.6	-2.6	19.1	-61.0	345.0
C	450	132.017	0.130	402.340	0.060	3.9	18.4	9.9	30.0	85.2	115.8
D	525	169.574	0.652	415.119	0.031	0.78	16.9	27.7	35.7	288.3	226.4
E	600	248.608	0.747	527.829	0.034	0.68	15.4	37.3	41.9	530.8	247.5
F	700	229.838	0.888	421.027	0.051	0.57	7.4	45.9	51.3	593.3	142.8
G	800	215.510	1.202	266.302	0.053	0.42	1.9	63.5	60.9	738.1	114.8
H	900	427.252	2.125	403.949	0.028	0.24	1.1	72.1	66.0	1371.0	276.6
I	1050	320.336	0.836	329.901	0.043	0.61	2.2	69.6	73.9	1083.3	162.7
J	1200	386.635	0.099	709.834	0.049	5.2	0.9	45.7	82.8	906.4	207.7
K	1300	251.976	0.255	763.985	0.024	2.0	1.6	10.4	87.3	166.6	480.2
L	1400	312.310	0.466	1028.874	0.016	1.1	4.9	2.7	90.2	54.4	995.4
M	1500	561.209	0.259	1744.997	0.009	2.0	5.6	8.1	91.8	280.4	2713.
N	1600	586.996	0.486	1924.728	0.013	1.0	5.3	3.1	94.1	117.6	2238.
O	1800	777.300	0.208	2545.097	0.032	2.5	6.5	3.2	100.0	160.5	1145.
total gas age			n=15		0.547	2.4				425.7	441.8
plateau			n=5	steps K-O	0.094	1.9			17.2	149.2	394.6
W3C64T, 297.20 mg, J=0.00350826±0.09%, D=1.0035±0.00098, NM-64, Lab#=7680-01											
A	0	8006.100	1.391	27332.980	0.013	0.4	2.1	-0.9	0.5	-514.9	8530.
B	0	2947.653	0.221	9798.542	0.201	2.3	3.3	1.8	8.7	303.3	311.1
C	0	3103.774	0.756	10102.420	0.034	0.7	3.0	3.8	10.1	627.6	916.0
D	0	168.284	0.289	514.921	0.184	1.8	3.2	9.6	17.5	99.3	14.1

Table A-13 con.

ID	Temp	$^{40}Ar/^{39}Ar$	$^{37}Ar/^{39}Ar$	$^{36}Ar/^{39}Ar$	$^{39}Ar_K$	K/Ca	Cl/K	$^{40}Ar^*$	^{39}Ar	Age	±1s
	(°C)			(x 10^{-3})	(x 10^{-16} mol)			(%)	(%)	(Ma)	(Ma)
E	0	684.021	0.264	2133.852	0.121	1.9	3.7	7.8	22.4	310.2	79.9
F	0	452.555	0.252	1358.844	0.343	2.0	3.5	11.3	36.3	297.1	22.9
G	0	482.335	0.322	1365.287	0.222	1.6	3.8	16.4	45.2	440.9	26.3
H	400	473.478	0.032	1587.930	0.458	15.7	7.0	0.9	63.8	26.5	44.4
I	450	64.329	0.130	183.821	0.317	3.9	7.4	15.5	76.6	62.1	9.4
J	500	90.771	0.170	211.318	0.101	3.0	6.9	31.2	80.6	170.6	20.2
K	550	135.346	0.670	280.814	0.050	0.8	10.7	38.7	82.7	304.1	43.4
K	625	103.875	0.517	212.830	0.068	1.0	7.7	39.5	85.4	242.1	25.8
L	725	102.207	0.797	201.188	0.071	0.6	4.3	41.9	88.3	252.1	27.9
M	825	152.644	1.778	275.258	0.031	0.3	0.7	46.8	89.5	403.2	57.7
N	925	119.566	2.716	151.018	0.021	0.2	0.6	62.8	90.4	422.1	74.6
O	1025	164.915	5.967	287.030	0.014	0.1	1.2	48.8	91.0	449.8	104.0
P	1125	277.969	4.998	760.143	0.024	0.1	1.1	19.3	91.9	311.9	122.0
Q	1225	102.071	23.450	250.718	0.027	0.0	2.1	29.2	93.0	181.5	53.8
R	1325	87.728	16.694	202.648	0.043	0.0	4.0	33.2	94.8	176.9	32.2
S	1425	212.186	1.679	602.570	0.021	0.3	4.4	16.1	95.6	204.5	139.0
T	1700	176.442	0.326	525.344	0.108	1.6	5.0	12.0	100.0	129.3	28.9
total gas age			n=21		2.472	4.5				200.6	113.3
plateau			n=21	steps A-T	2.472	4.5			100.0	149.9	25.5
MTEC64T, 204.22 mg, J=0.00351267±0.09%, D=1.0035±0.00098, NM-64, Lab#=7683-01											
A	0	1821.218	0.277	5901.671	0.066	1.8	5.4	4.2	1.3	433.3	381.0
B	0	802.798	0.364	2591.371	0.084	1.4	4.0	4.6	3.0	220.8	130.6
C	0	1081.541	0.297	3581.137	0.147	1.7	4.1	2.2	5.9	142.0	133.9
D	0	760.463	0.279	2497.201	0.246	1.8	4.2	3.0	10.8	137.5	56.1
E	0	423.570	2.034	1375.060	0.003	0.3	4.9	4.1	10.9	107.0	1427.
F	0	613.368	0.521	2008.289	0.530	1.0	4.7	3.2	21.4	122.1	33.3
G	0	460.955	0.582	1528.287	0.192	0.9	4.2	2.0	25.2	58.4	38.7
H	0	992.052	0.308	3260.615	0.180	1.7	4.0	2.9	28.8	172.4	73.4
I	0	194.281	0.410	669.887	0.083	1.2	4.2	-1.9	30.5	-23.4	34.8
J	0	310.093	0.373	1001.692	0.301	1.4	4.2	4.5	36.4	87.2	18.4
K	0	336.202	0.444	1088.356	0.134	1.1	4.8	4.3	39.1	90.3	36.0
L	0	1483.542	0.333	5032.968	0.207	1.5	3.9	-0.2	43.2	-23.6	130.7
M	0	80.275	0.273	232.238	0.091	1.9	4.3	14.5	45.0	72.3	17.5
N	0	338.124	0.253	1132.805	0.130	2.0	4.3	1.0	47.6	21.3	38.4
O	0	119.136	0.364	372.270	0.095	1.4	5.0	7.7	49.5	57.0	23.5
P	0	67.327	0.273	231.995	0.121	1.9	5.3	-1.8	51.9	-7.8	14.2
Q	0	121.679	0.453	432.739	0.055	1.1	5.6	-5.1	53.0	-39.6	35.8
R	0	64.954	0.646	211.602	0.064	0.8	6.3	3.8	54.3	15.5	18.8
S	0	99.544	0.343	337.933	0.064	1.5	5.6	-0.3	55.6	-2.0	26.0
T	0	56.285	0.477	171.549	0.077	1.1	5.2	10.0	57.1	35.2	16.9
U	0	160.230	0.243	416.071	0.063	2.1	5.6	23.3	58.4	222.0	29.8
V	0	148.830	0.830	482.061	0.024	0.6	6.6	4.3	58.8	40.3	70.7
W	0	44.959	0.100	119.938	0.054	5.1	6.2	21.1	59.9	59.2	17.4
X	0	91.605	0.036	247.809	0.048	14.0	6.6	20.0	60.9	112.7	24.7
Y	0	92.990	0.009	345.495	0.026	54.5	5.6	-9.8	61.4	-58.8	49.8
Z	550	758.811	0.210	2509.851	1.148	2.4	7.5	2.3	84.2	105.5	33.7
AA	625	174.539	0.950	526.985	0.121	0.5	2.1	10.8	86.7	115.8	32.8
AB	700	103.384	1.020	304.565	0.194	0.5	0.8	13.0	90.5	83.3	14.1
AC	775	98.670	1.492	286.393	0.152	0.3	0.2	14.3	93.5	87.5	17.0

Table A-13 con.

ID	Temp	$^{40}Ar/^{39}Ar$	$^{37}Ar/^{39}Ar$	$^{36}Ar/^{39}Ar$	$^{39}Ar_K$	K/Ca	Cl/K	$^{40}Ar^*$	^{39}Ar	Age	±1s
	(°C)			(x 10^{-3})	(x 10^{-16} mol)			(%)	(%)	(Ma)	(Ma)
AD	850	108.138	2.538	259.231	0.075	0.2	0.2	29.3	95.0	190.8	29.3
AE	925	183.666	2.983	471.169	0.031	0.2	0.4	24.3	95.6	263.3	99.6
AF	1000	273.979	2.468	613.768	0.017	0.2	0.8	33.9	96.0	509.6	190.2
AG	1075	260.909	0.925	424.094	0.015	0.6	1.2	52.0	96.3	703.3	121.1
AH	1150	93.840	0.169	256.894	0.080	3.0	0.3	19.1	97.9	110.1	24.3
AI	1225	471.431	0.766	1360.603	0.011	0.7	3.2	14.7	98.1	393.8	413.2
AJ	1300	139.102	0.425	428.072	0.014	1.2	4.1	9.1	98.4	78.2	137.5
AK	1400	222.179	0.060	469.632	0.012	8.6	4.8	37.5	98.6	463.5	159.4
AL	1700	215.344	0.046	720.370	0.071	11.1	3.7	1.1	100.0	15.5	50.0
total gas age			n=38		5.025	2.1				100.5	49.4
plateau			n=38	steps A-AL	5.025	2.1			100.0	65.8	11.3
Isotopic ratios corrected for blank, radioactive decay, and mass discrimination, not corrected for											
Individual analyses show analytical error only; mean age errors also include error in J and irradiation											
Analyses in italics are excluded excluded from mean age calculations.											
Correction factors:											
$(^{39}Ar/^{37}Ar)_{Ca}$ = 0.00065±0.00005											
$(^{36}Ar/^{37}Ar)_{Ca}$ = 0.00026±0.00002											
$(^{38}Ar/^{39}Ar)_K$ = 0.0119											
$(^{40}Ar/^{39}Ar)_K$ = 0.0265±0.0024											
MTEC64, 204.22 mg, J=0.00351267±0.09%, D=1.0035±0.00098, NM-64, Lab#=7683-01											
A	0	1821	0.2772	5901.67	0.664	1.8	5.4	4.2	2.2	433.3	381
B	0	802.8	0.3637	2591.37	0.838	1.4	4.0	4.6	4.9	220.8	131
C	0	1082	0.2972	3581.14	1.47	1.7	4.1	2.2	9.6	142.0	134
D	0	760.5	0.2795	2497.20	2.46	1.8	4.2	3.0	17.6	137.5	56
E	0	423.6	2.034	1375.06	0.030	0.25	4.9	4.1	17.7	107.0	1427
F	0	613.4	0.5211	2008.29	5.30	0.98	4.7	3.2	34.9	122.1	33
G	0	461.0	0.5819	1528.29	1.92	0.88	4.2	2.0	41.1	58.4	39
H	0	992.1	0.3076	3260.62	1.80	1.7	4.0	2.9	46.9	172.4	73
I	0	194.3	0.4102	669.89	0.826	1.2	4.2	-1.9	49.6	-23.4	35
J	0	310.1	0.3730	1001.69	3.01	1.4	4.2	4.5	59.4	87.2	18
K	0	336.2	0.4440	1088.36	1.34	1.1	4.8	4.3	63.7	90.3	36
L	0	1484	0.3330	5032.97	2.07	1.5	3.9	-0.2	70.4	-23.6	131
M	0	80.3	0.2732	232.24	0.905	1.9	4.3	14.5	73.4	72.3	17
N	0	338.1	0.2529	1132.81	1.30	2.0	4.3	1.0	77.6	21.3	38
O	0	119.1	0.3644	372.27	0.955	1.4	5.0	7.7	80.7	57.0	23
P	0	67.3	0.2730	231.99	1.21	1.9	5.3	-1.8	84.6	-7.8	14
Q	0	121.7	0.4529	432.74	0.546	1.1	5.6	-5.1	86.4	-39.6	36
R	0	65.0	0.6462	211.60	0.644	0.79	6.3	3.8	88.4	15.5	19
S	0	99.5	0.3433	337.93	0.636	1.5	5.6	-0.3	90.5	-2.0	26
T	0	56.3	0.4772	171.55	0.773	1.1	5.2	10.0	93.0	35.2	17
U	0	160.2	0.2433	416.07	0.632	2.1	5.6	23.3	95.1	222.0	30
V	0	148.8	0.8305	482.06	0.242	0.61	6.6	4.3	95.8	40.3	71
W	0	45.0	0.1000	119.94	0.542	5.1	6.2	21.1	97.6	59.2	17
X	0	91.6	0.0364	247.81	0.484	14.0	6.6	20.0	99.2	112.7	25
Y	0	93.0	0.0094	345.49	0.255	54.5	5.6	-9.8	100.0	-58.8	50
total gas age			n=25		30.8	2.1				90.2	57
plateau			n=25	steps A-Y	30.8	2.1			100.0	49.4	13

Table A-13 con.

ID	Temp	$^{40}Ar/^{39}Ar$	$^{37}Ar/^{39}Ar$	$^{36}Ar/^{39}Ar$	$^{39}Ar_K$	K/Ca	Cl/K	$^{40}Ar^*$	^{39}Ar	Age	±1s
	(°C)			(x 10^{-3})	(x 10^{-16} mol)			(%)	(%)	(Ma)	(Ma)
W3C64, 297.20 mg, J=0.00350826±0.09%, D=1.0035±0.00098, NM-64, Lab#=7680-01											
A	0	8006	1.391	27332.98	0.131	0.37	2.1	-0.9	1.2	-514.9	8530
B	0	2948	0.2209	9798.54	2.01	2.3	3.3	1.8	19.2	303.3	311
C	0	3104	0.7559	10102.42	0.344	0.67	3.0	3.8	22.3	627.6	916
D	0	168.3	0.2887	514.92	1.84	1.8	3.2	9.6	38.7	99.3	14
E	0	684.0	0.2644	2133.85	1.21	1.9	3.7	7.8	49.5	310.2	80
F	0	452.6	0.2523	1358.84	3.43	2.0	3.5	11.3	80.2	297.1	23
G	0	482.3	0.3224	1365.29	2.22	1.6	3.8	16.4	100.0	440.9	26
total gas age			n=7		11.2	1.9				296.2	208
plateau			n=7	steps A-G	11.2	1.9			100.0	205.3	56
MTE Crushed Quartz, Quartz, 197.47 mg, J=0.00351267±0.09%, D=1.0035±0.00098, NM-64,											
A	550	758.811	0.210	2509.85	11.48	2.4	7.46	2.3	59.2	105.5	34
B	625	174.539	0.950	526.98	1.21	0.54	2.09	10.8	65.4	115.8	33
C	700	103.384	1.020	304.56	1.94	0.50	0.77	13.0	75.5	83.3	14
D	775	98.670	1.492	286.39	1.52	0.34	0.21	14.3	83.3	87.5	17
E	850	108.138	2.538	259.23	0.75	0.20	0.21	29.3	87.1	190.8	29
F	925	183.666	2.983	471.17	0.31	0.17	0.40	24.3	88.7	263.3	100
G	1000	273.979	2.468	613.77	0.17	0.21	0.81	33.9	89.6	509.6	190
H	1075	260.909	0.925	424.09	0.15	0.55	1.21	52.0	90.3	703.3	121
I	1150	93.840	0.169	256.89	0.80	3.0	0.29	19.1	94.5	110.1	24
J	1225	471.431	0.766	1360.60	0.11	0.67	3.21	14.7	95.1	393.8	413
K	1300	139.102	0.425	428.07	0.14	1.2	4.08	9.1	95.8	78.2	138
L	1400	222.179	0.060	469.63	0.12	8.6	4.79	37.5	96.4	463.5	159
M	1700	215.344	0.046	720.37	0.71	11.1	3.67	1.1	100.0	15.5	50
total gas age			n=13		19.40	2.2	4.89			116.9	37
plateau			n=4	steps J-M	1.07	8.5	3.79		5.5	62.0	85
W3-3 Crushed Quartz, Quartz, 144.37 mg, J=0.00350249±0.09%, D=1.0035±0.00098, NM-64,											
A	400	473.478	0.032	1587.93	4.58	15.7	7.04	0.9	33.8	26.5	44
B	450	64.329	0.130	183.82	3.17	3.9	7.39	15.5	57.2	62.1	9
C	500	90.771	0.170	211.32	1.01	3.0	6.89	31.2	64.7	170.6	20
D	550	135.346	0.670	280.81	0.50	0.76	10.74	38.7	68.4	304.1	43
E	625	103.875	0.517	212.83	0.68	0.99	7.72	39.5	73.4	242.1	26
F	725	102.207	0.797	201.19	0.71	0.64	4.26	41.9	78.6	252.1	28
G	825	152.644	1.778	275.26	0.31	0.29	0.67	46.8	80.9	403.2	58
H	925	119.566	2.716	151.02	0.21	0.19	0.62	62.8	82.5	422.1	75
I	1025	164.915	5.967	287.03	0.14	0.086	1.18	48.8	83.5	449.8	104
J	1125	277.969	4.998	760.14	0.24	0.10	1.14	19.3	85.3	311.9	122
K	1225	102.071	23.450	250.72	0.27	0.022	2.08	29.2	87.3	181.5	54
L	1325	87.728	16.694	202.65	0.43	0.031	4.00	33.2	90.5	176.9	32
M	1425	212.186	1.679	602.57	0.21	0.30	4.37	16.1	92.0	204.5	139
N	1700	176.442	0.326	525.34	1.08	1.6	4.95	12.0	100.0	129.3	29
total gas age			n=14		13.54	6.7	6.32			121.6	35
plateau			n=4	steps K-N	1.99	0.9	4.30		14.7	155.8	25
MTE Crushed Quartz, Quartz, 197.47 mg, J=0.00351267±0.09%, D=1.0035±0.00098, NM-64, Lab#=7683-02											
A	550	758.811	0.210	2509.85	11.48	2.4	7.46	2.3	59.2	105.50	33.73
B	625	174.539	0.950	526.98	1.21	0.54	2.09	10.8	65.4	115.81	32.83
C	700	103.384	1.020	304.56	1.94	0.50	0.77	13.0	75.5	83.27	14.07

Table A-13 con.

ID	Temp	$^{40}Ar/^{39}Ar$	$^{37}Ar/^{39}Ar$	$^{36}Ar/^{39}Ar$	$^{39}Ar_K$	K/Ca	Cl/K	$^{40}Ar^*$	^{39}Ar	Age	±1s
	(°C)			(x 10^{-3})	(x 10^{-16} mol)			(%)	(%)	(Ma)	(Ma)
D	775	98.670	1.492	286.39	1.52	0.34	0.21	14.3	83.3	87.48	17.03
E	850	108.138	2.538	259.23	0.75	0.20	0.21	29.3	87.1	190.80	29.27
F	925	183.666	2.983	471.17	0.31	0.17	0.40	24.3	88.7	263.26	99.65
G	1000	273.979	2.468	613.77	0.17	0.21	0.81	33.9	89.6	509.61	190.22
H	1075	260.909	0.925	424.09	0.15	0.55	1.21	52.0	90.3	703.28	121.09
I	1150	93.840	0.169	256.89	0.80	3.0	0.29	19.1	94.5	110.12	24.32
J	1225	471.431	0.766	1360.60	0.11	0.67	3.21	14.7	95.1	393.78	413.24
K	1300	139.102	0.425	428.07	0.14	1.2	4.08	9.1	95.8	78.24	137.53
L	1400	222.179	0.060	469.63	0.12	8.6	4.79	37.5	96.4	463.45	159.38
M	1700	215.344	0.046	720.37	0.71	11.1	3.67	1.1	100.0	15.48	49.99
total gas age			n=13		19.40	2.2	4.89			116.91	37.17
plateau			n=4	steps J-M	1.07	8.5	3.79		5.5	61.98	85.27
W3-3 Crushed Quartz, Quartz, 144.37 mg, J=0.00350249±0.09%, D=1.0035±0.00098, NM-64, Lab#=7681-01											
A	400	473.478	0.032	1587.93	4.58	15.7	7.04	0.9	33.8	26.49	44.40
B	450	64.329	0.130	183.82	3.17	3.9	7.39	15.5	57.2	62.08	9.41
C	500	90.771	0.170	211.32	1.01	3.0	6.89	31.2	64.7	170.61	20.22
D	550	135.346	0.670	280.81	0.50	0.76	10.74	38.7	68.4	304.07	43.39
E	625	103.875	0.517	212.83	0.68	0.99	7.72	39.5	73.4	242.15	25.83
F	725	102.207	0.797	201.19	0.71	0.64	4.26	41.9	78.6	252.07	27.88
G	825	152.644	1.778	275.26	0.31	0.29	0.67	46.8	80.9	403.18	57.69
H	925	119.566	2.716	151.02	0.21	0.19	0.62	62.8	82.5	422.07	74.64
I	1025	164.915	5.967	287.03	0.14	0.086	1.18	48.8	83.5	449.80	103.98
J	1125	277.969	4.998	760.14	0.24	0.10	1.14	19.3	85.3	311.88	122.02
K	1225	102.071	23.450	250.72	0.27	0.022	2.08	29.2	87.3	181.51	53.78
L	1325	87.728	16.694	202.65	0.43	0.031	4.00	33.2	90.5	176.95	32.25
M	1425	212.186	1.679	602.57	0.21	0.30	4.37	16.1	92.0	204.49	139.00
N	1700	176.442	0.326	525.34	1.08	1.6	4.95	12.0	100.0	129.26	28.91
total gas age			n=14		13.54	6.7	6.32			121.63	35.41
plateau			n=4	steps K-N	1.99	0.9	4.30		14.7	155.79	24.56

Isotopic ratios corrected for blank, radioactive decay, and mass discrimination, not corrected for interferring reactions.

Individual analyses show analytical error only; mean age errors also include error in J and irradiation parameters.

Analyses in italics are excluded excluded from mean age calculations.

Correction factors:
$(^{39}Ar/^{37}Ar)_{Ca}$ = 0.00065±0.00005
$(^{36}Ar/^{37}Ar)_{Ca}$ = 0.00026±0.00002
$(^{38}Ar/^{39}Ar)_K$ = 0.0119
$(^{40}Ar/^{39}Ar)_K$ = 0.0250±0.0050

Figure A- 3 Additional Crushing Age Spectra

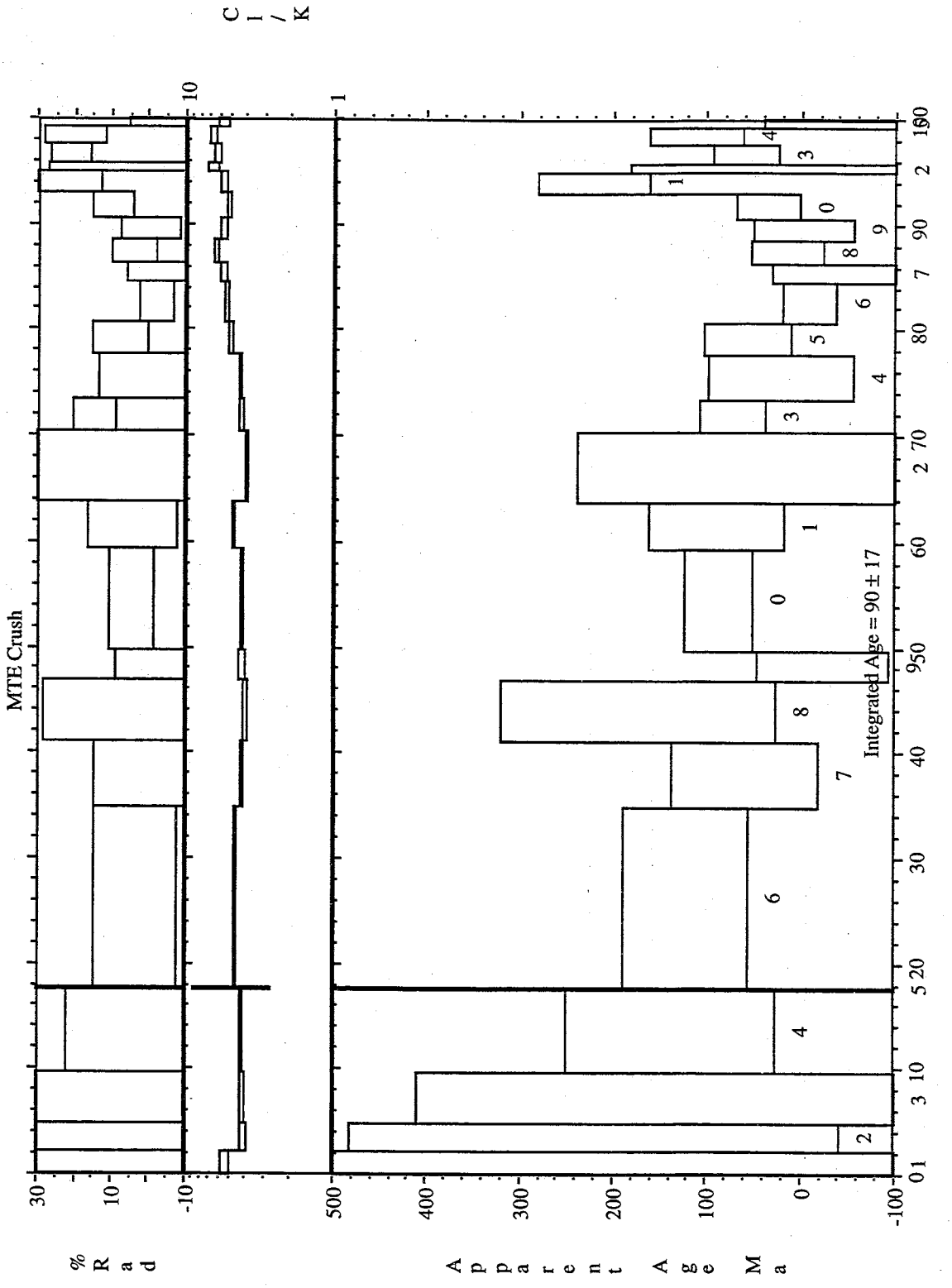

FigureA3 A

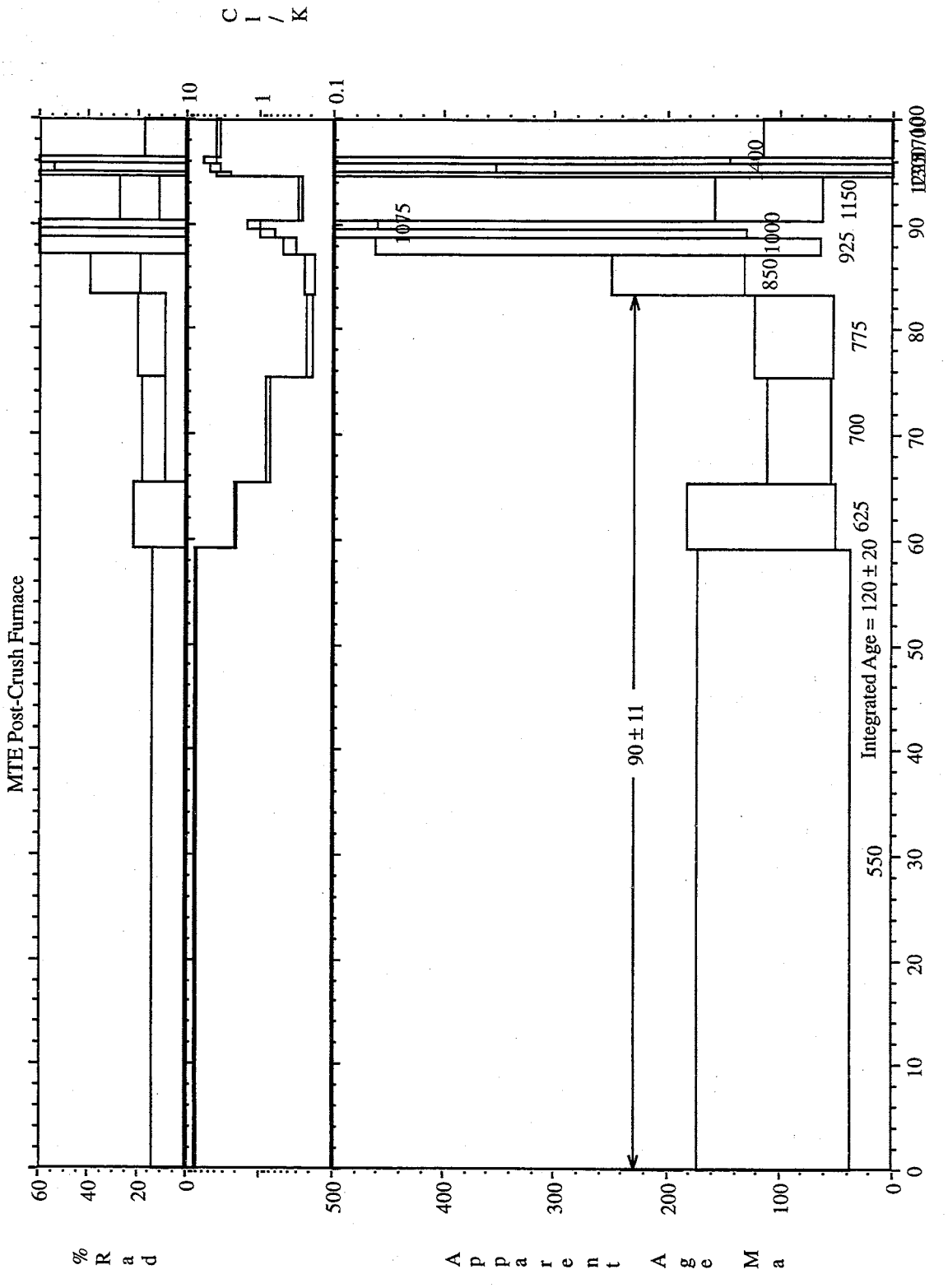
MTE Post-Crush Furnace
Integrated Age = 120 ± 20
90 ± 11
% Rad
Apparent Age Ma
Ca/K
10
1
0.1
1075
1000
925
850
775
700
625
550
400
1150

FigureA3 B

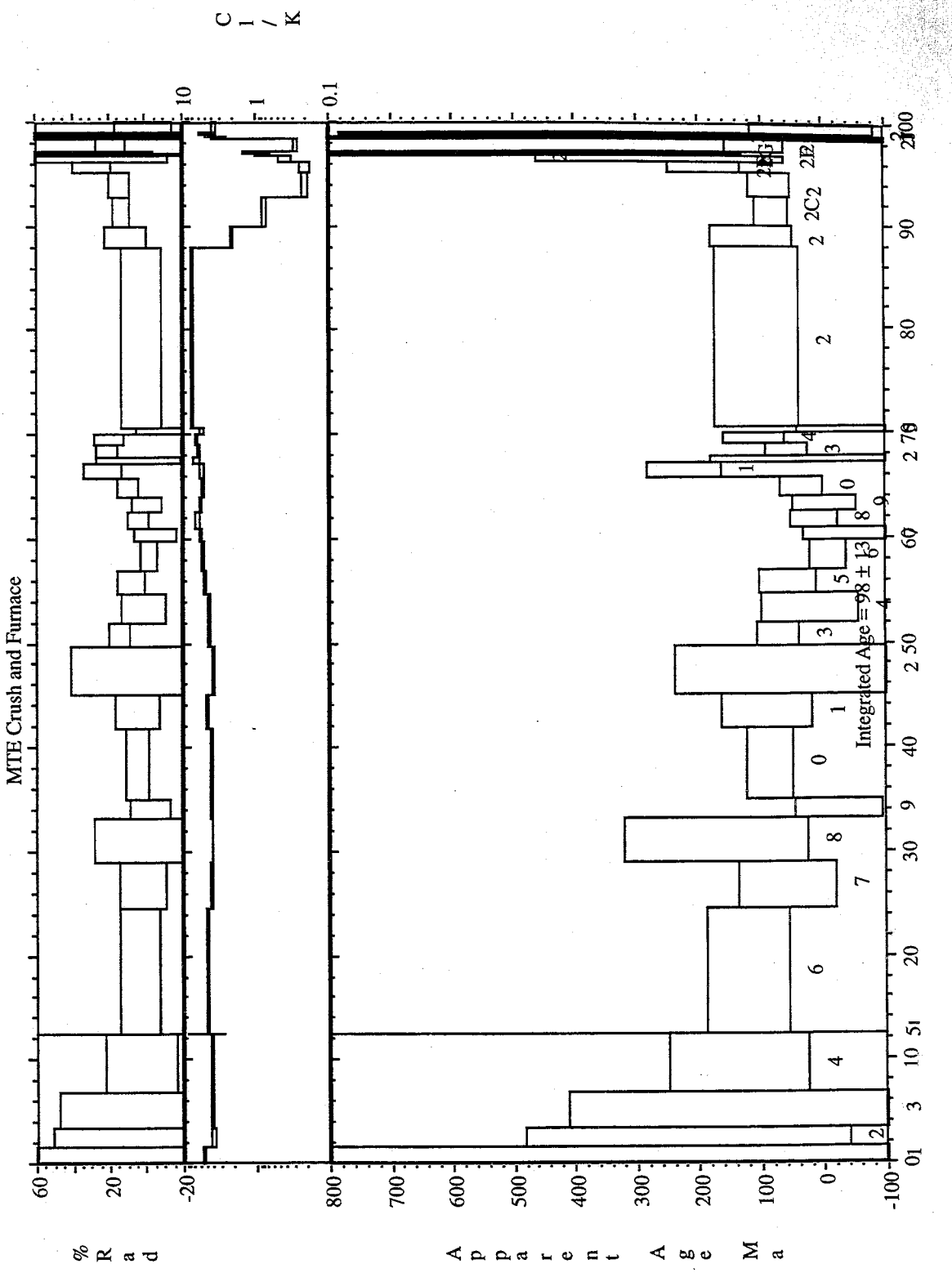
MTE Crush and Furnace
Integrated Age = 98 ± 13
% Rad
Apparent Age Ma
C 1 / K
60
20
-20
800
700
600
500
400
300
200
100
0
-100
10
1
0.1

FigureA3 C

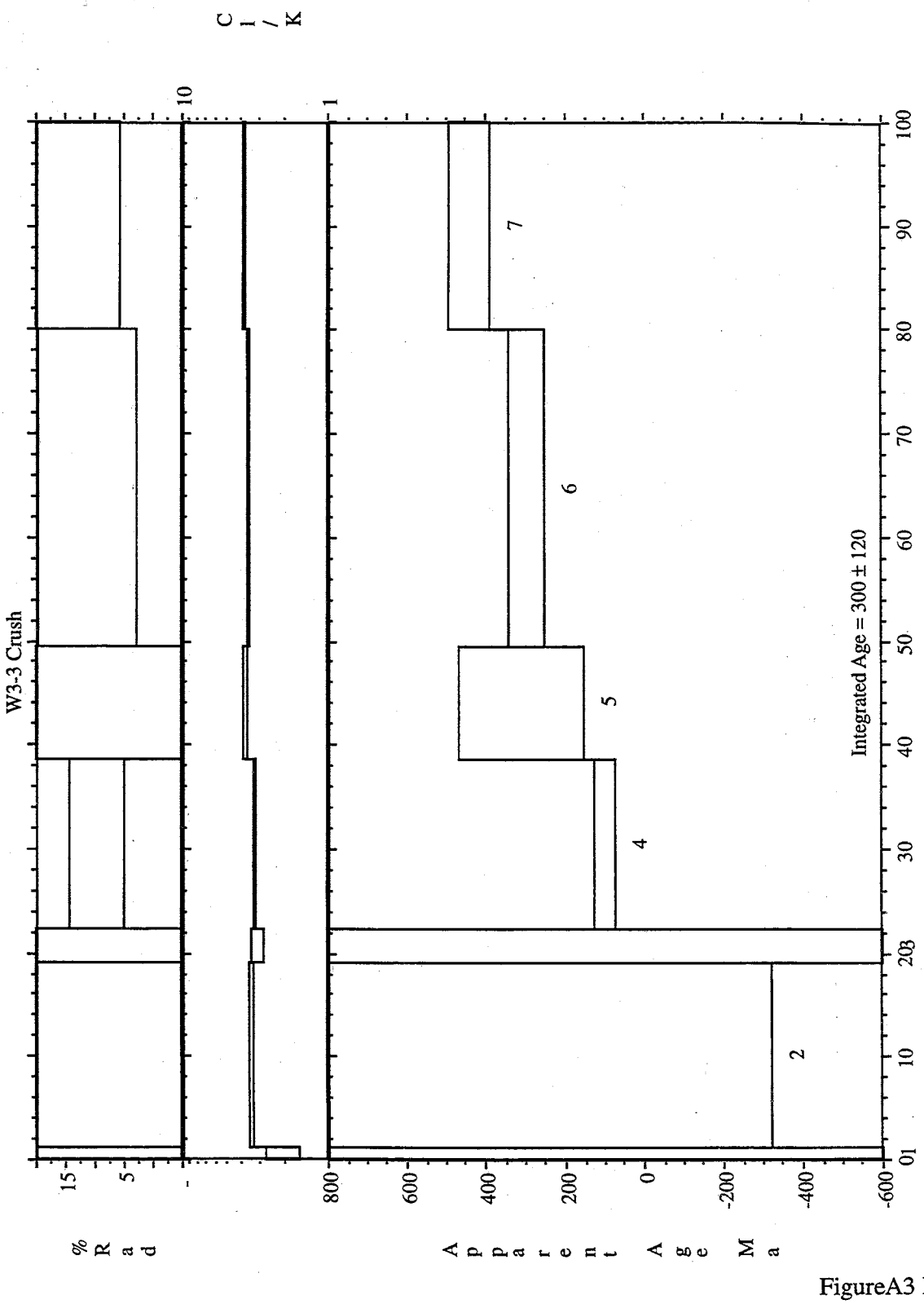
W3-3 Crush
Integrated Age = 300 ± 120
Ca/K
% Rad
Apparent Age Ma
2
4
5
6
7

FigureA3 D

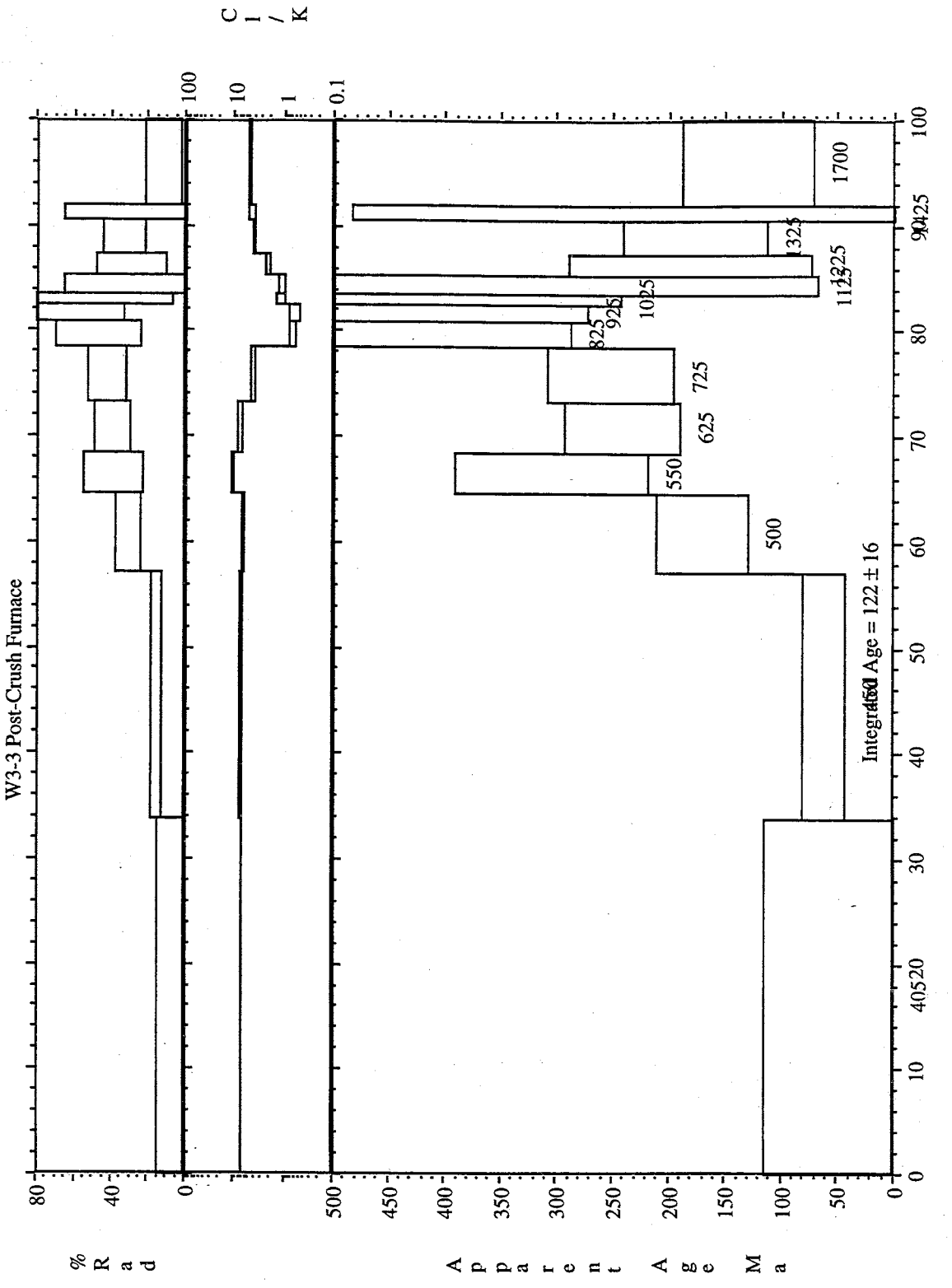
W3-3 Post-Crush Furnace
Integral Age = 122 ± 16
% Rad
Apparent Age Ma
Ci/K
1700
1325
1125
1025
925
825
725
625
550
500

FigureA3 E

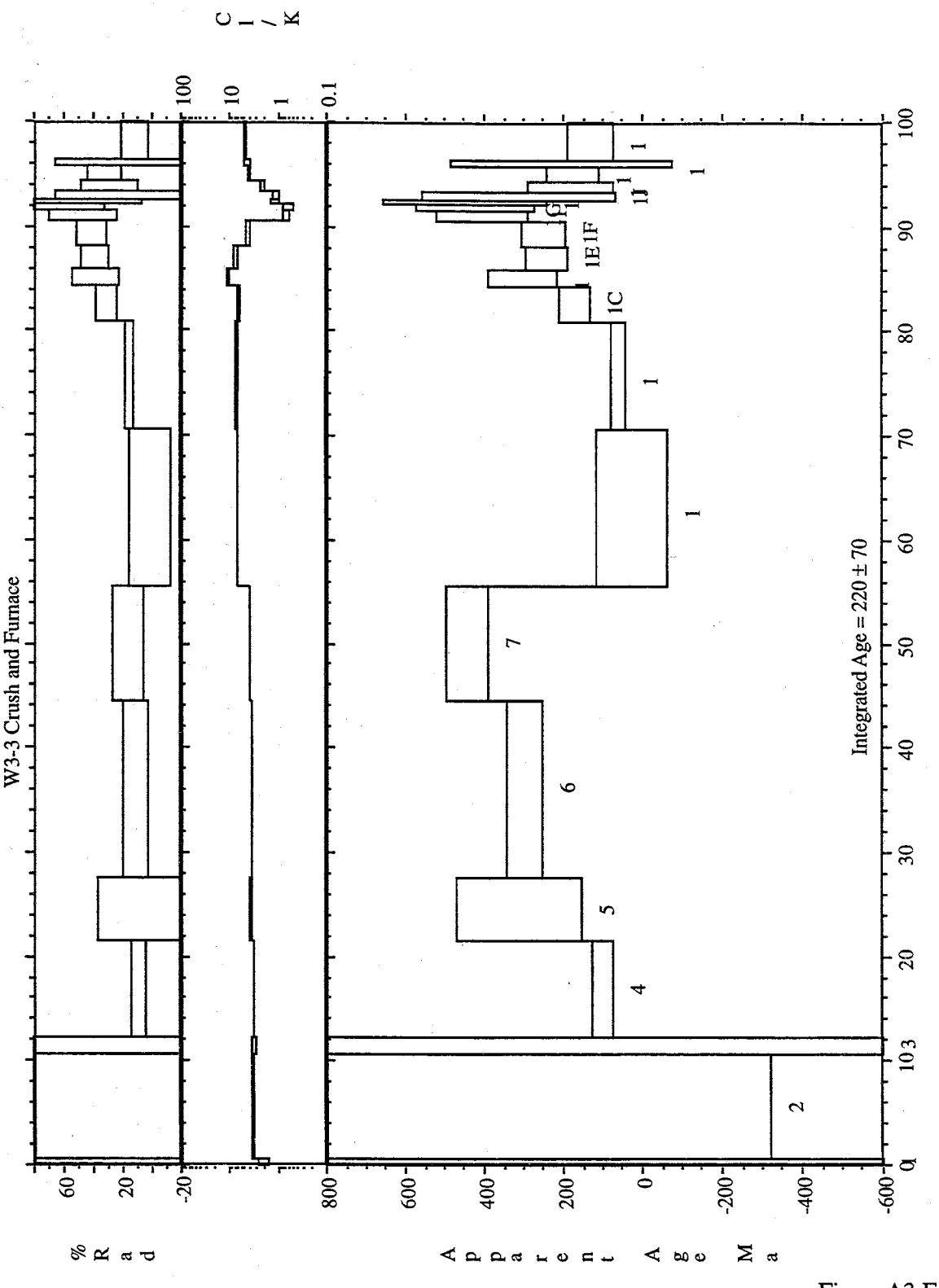
W3-3 Crush and Furnace
Integrated Age = 220 ± 70
% Rad
Ca/K
Apparent Age Ma
1E1F
1C
1
2
4
5
6
7

FigureA3 F

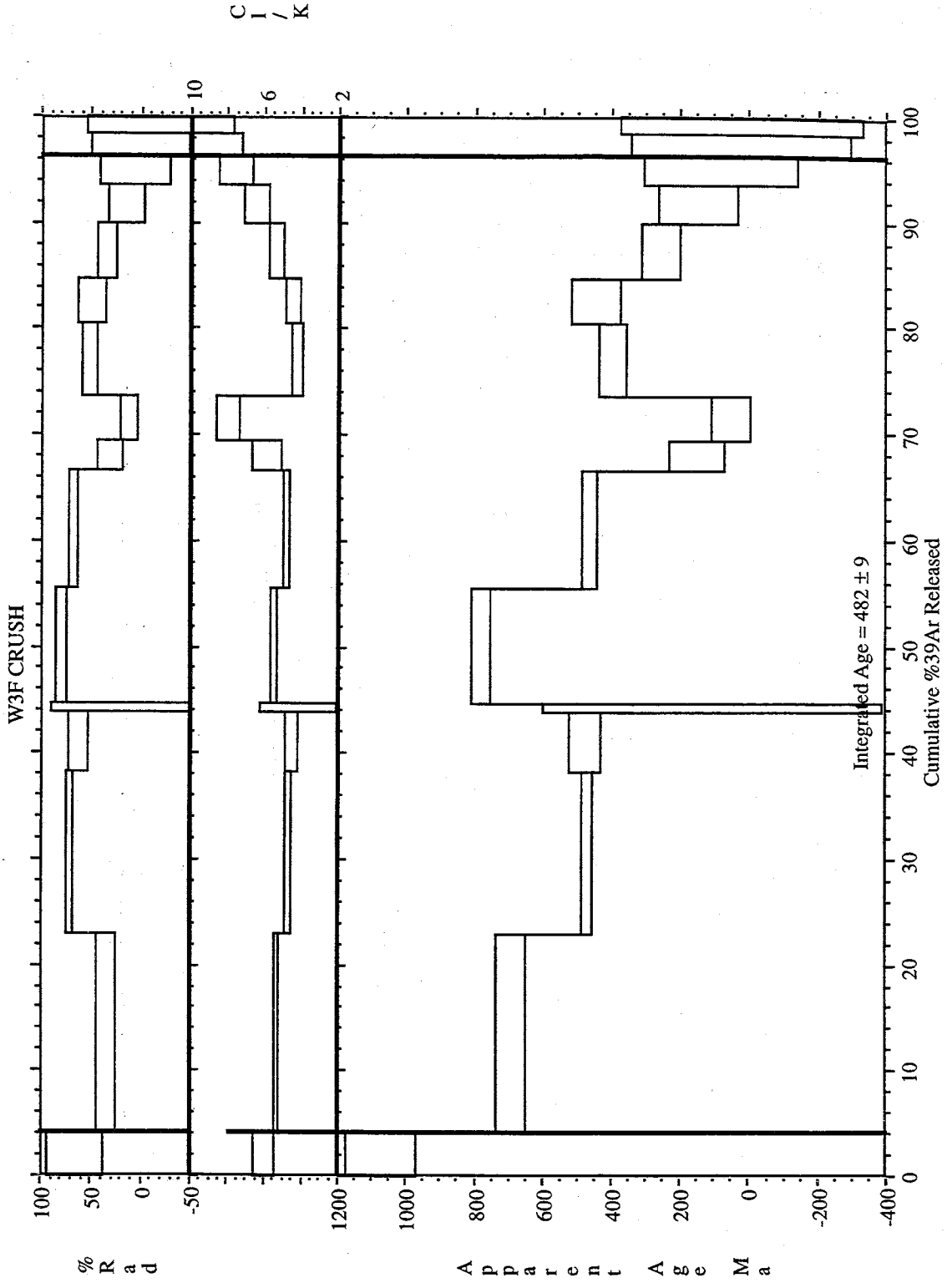
W3F CRUSH
Integrated Age = 482 ± 9
Cumulative %39Ar Released
Apparent Age Ma
%Rad
Ca/K

FigureA3 G

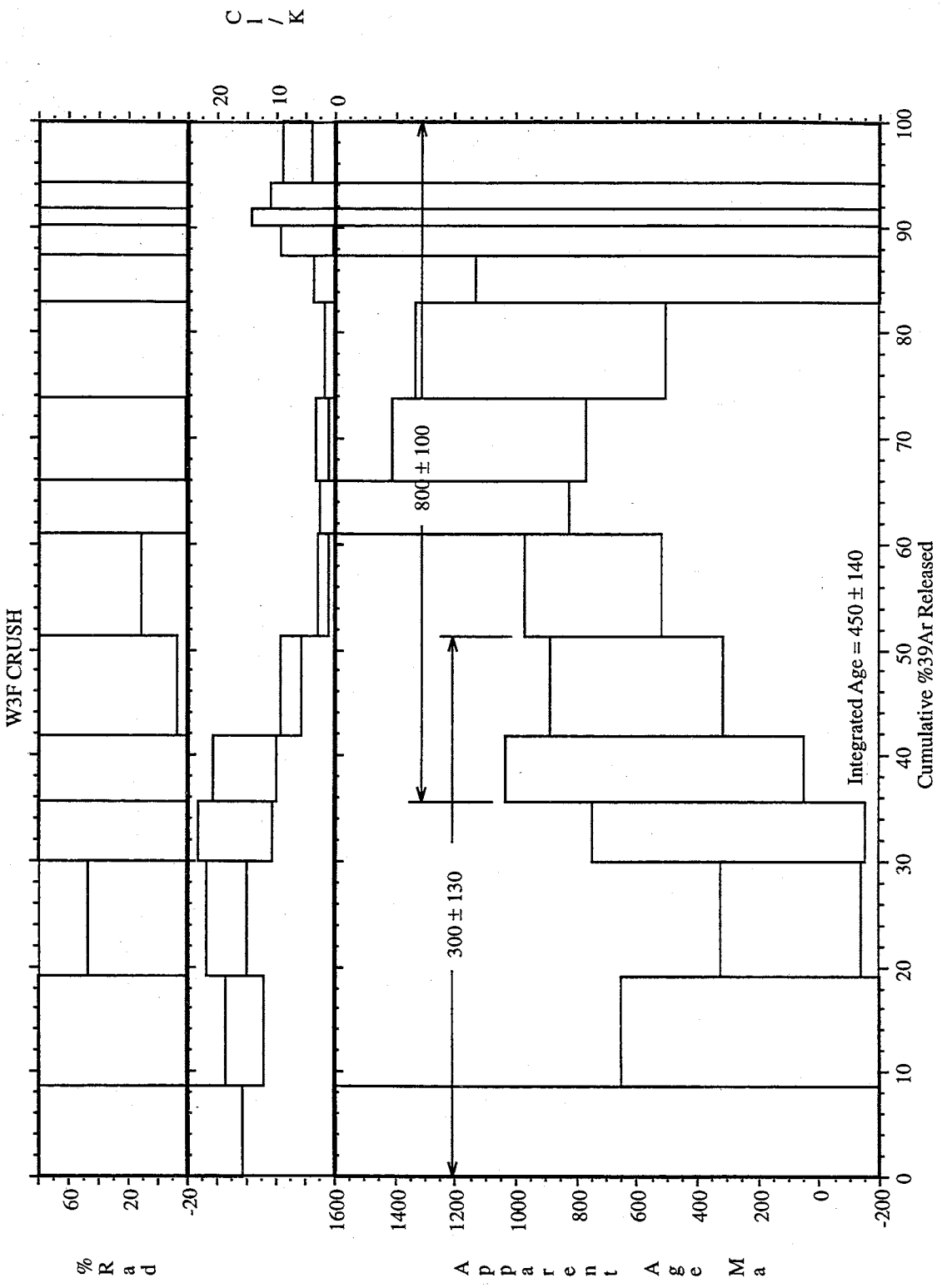
W3F CRUSH
Integrated Age = 450 ± 140
800 ± 100
300 ± 130
Cumulative %39Ar Released
Apparent Age Ma
%Rad
Ca/K

FigureA3 H

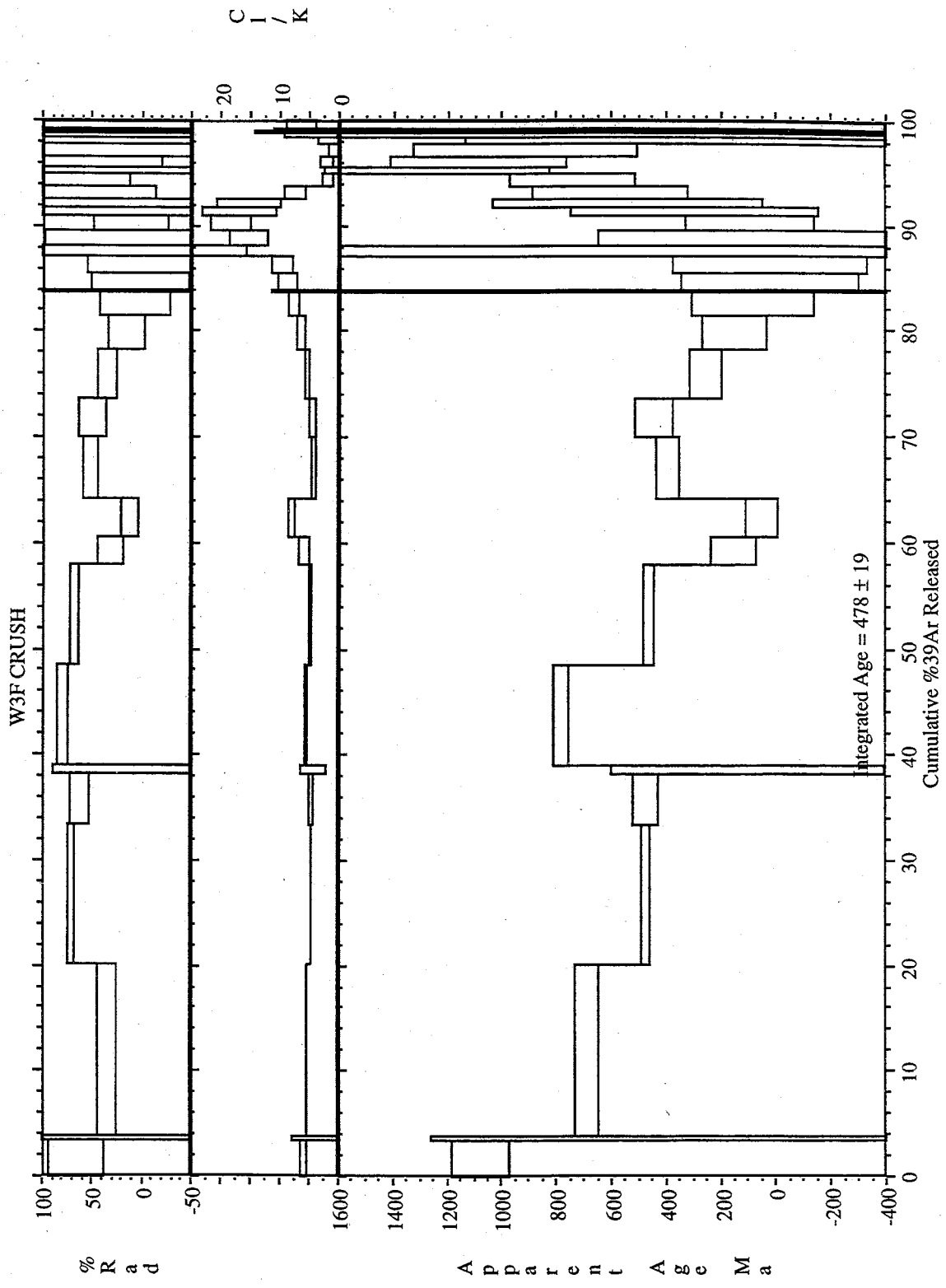
W3F CRUSH
Integrated Age = 478 ± 19
Cumulative %39Ar Released
Ca/K
%Rad
Apparent Age Ma

FigureA3 I

APPENDIX N Laser and furnace fusions data from $^{40}Ar/^{39}Ar$ analysis

Table A- 14 Complete Data Tables from Laser and Furnce Fusions

ID	$^{40}Ar/^{39}Ar$	$^{37}Ar/^{39}Ar$	$^{36}Ar/^{39}Ar$ (x 10^{-3})	$^{39}Ar_K$ (x 10^{-15} mol)	K/Ca	Cl/K	$\%^{40}Ar^*$	Age (Ma)	±1s (Ma)
W3FF1-5, approx 5 mg, J=0.003784168±0.10%, D=1.0035±0.00098, NM-53, Lab#=6854									
02A	20.729	0.0000	65.07	0.342	-	6.5	7.1	10.0	19.9
03A	55.177	0.0000	167.7	0.159	-	4.4	10.1	37.8	44.4
01A	92.232	42.90	280.4	0.029	0.012	4.5	13.7	86.8	285.1
05A	568.049	0.0000	1859.9	0.050	-	6.4	3.2	121.6	618.6
04A	275.772	0.0000	839.3	0.334	-	5.9	10.1	180.0	47.1
weighted mean ± Taylor err			n=5		0.012 ±0.000			36.3	16.9
W3FF6-8, approx 20 mg, J=0.003841047±0.10%, D=1.0045±0.0012, NM-53, Lab#=6898									
02A	26.648	0.1869	85.86	52.5	2.7	0.13	4.7	8.74	0.85
20A	64.688	0.8601	181.1	3.68	0.59	5.6	17.3	76.1	2.5
10A	175.194	1.356	478.1	3.80	0.38	6.4	19.4	221.6	5.6
weighted mean ± Taylor err			n=3		1.2 ±1.3			19.85	0.80
CPU2FF1, 8.00 mg, J=0.00380857±0.10%, D=1.0035±0.00098, NM-53, Lab#=6846									
02A	827.805	2.483	2710.5	0.252	0.21	5.9	3.3	177.0	187.3
CMX2FF1-3, approx 5 mg, J=0.003824535±0.10%, D=1.0035±0.00098, NM-53, Lab#=6852									
04A	164.310	10.34	522.6	0.223	0.049	6.1	6.5	72.5	51.2
03A	432.473	28.32	1412.6	0.034	0.018	4.2	4.0	117.3	701.5
02A	168.052	2.874	494.2	0.408	0.18	6.9	13.2	147.4	30.2
weighted mean ± Taylor err			n=3		0.082 ±0.085			128.0	26.0
W3FF1-9, 7-15 mg, J=0.00351077±0.09%, D=1.0045±0.0012, NM-64, Lab#=7677									
05A	2222.715	0.0000	7640.0	0.019	-	2.1	-1.6	-236.0	10532.7
04A	175.644	0.0000	606.2	0.050	-	2.6	-2.0	-22.3	307.6
09A	104.402	0.1889	341.1	1.000	2.7	5.5	3.4	22.6	11.5
07A	147.818	1.002	483.2	0.606	0.51	5.3	3.4	32.0	22.1
02A	254.591	0.0000	701.8	0.041	-	1.1	18.5	276.5	427.3
03A	181.638	0.1762	252.7	0.559	2.9	5.9	58.9	575.2	17.3
08A	116.491	0.0000	-78.5749	0.033	-	9.7	119.9	719.9	186.5
06A	965.929	0.6525	1834.1	0.049	0.78	1.6	43.9	1645.2	499.8
weighted mean ± Taylor err			n=8		1.7 ±0.9			168.7	8.8
MTELF1-35, approx 5 mg , J=0.00383994±0.10%, D=1.0062±0.0017, NM-53, Lab#=6902									
30	328.358	1.274	1160.6	0.077	0.40	25.6	-4.4	-103.7	106.1
28	46.795	0.0000	205.4	0.199	-	20.9	-29.8	-99.2	11.0
22	343.008	0.9237	1205.0	0.039	0.55	11.5	-3.8	-92.7	208.5
21	212.236	0.5864	741.0	0.165	0.87	12.6	-3.2	-47.1	37.1
29	92.602	1.589	331.2	0.169	0.32	10.1	-5.6	-36.2	19.0
39	170.708	17.45	596.9	0.132	0.029	7.8	-2.6	-30.9	32.7
38	299.621	0.0000	1027.6	0.071	-	9.0	-1.4	-28.3	92.4
27	353.214	0.0000	1204.0	0.042	-	13.8	-0.7	-18.2	186.7
46	30.603	0.0404	111.5	0.073	12.6	8.2	-7.8	-16.6	24.6
37	222.026	0.0125	755.0	0.097	40.8	6.6	-0.5	-7.6	52.6

Table A-14 con.

ID	$^{40}Ar/^{39}Ar$	$^{37}Ar/^{39}Ar$	$^{36}Ar/^{39}Ar$	$^{39}Ar_K$	K/Ca	Cl/K	$\%^{40}Ar^*$	Age	±1s
			(x 10^{-3})	(x 10^{-15} mol)				(Ma)	(Ma)
23	175.007	0.1184	595.2	0.235	4.3	6.7	-0.5	-6.2	22.5
20	53.292	0.0000	179.8	0.189	-	6.6	0.2	0.9	13.1
36	118.601	0.1098	399.0	0.130	4.6	5.6	0.6	4.7	23.8
24	62.546	0.4450	209.2	0.358	1.1	6.8	1.2	5.0	8.0
51	1412.171	0.0000	4770.8	0.007	-	28.9	0.2	16.3	3875.4
32	46.505	0.0000	147.7	0.166	-	7.1	6.1	19.4	12.7
33	64.992	0.4437	210.2	0.038	1.1	6.9	4.4	19.9	53.4
47	770.747	0.0000	2593.1	0.123	-	11.1	0.6	30.7	149.5
50	29.636	0.0863	85.06	0.134	5.9	6.1	15.1	30.8	13.0
35	115.313	0.7408	372.1	0.162	0.69	9.6	4.7	37.0	21.3
26	300.781	0.0000	998.6	0.061	-	10.0	1.9	38.9	108.4
25	34.013	0.2482	94.65	0.759	2.1	6.0	17.7	41.4	3.3
42	184.964	1.123	605.2	0.103	0.45	8.0	3.3	42.4	43.3
40	452.689	0.0000	1501.0	0.008	-	2.7	2.0	62.1	1028.2
48	464.195	0.0000	1538.7	0.342	-	8.6	2.0	64.6	40.7
49	141.567	0.3775	437.5	0.364	1.4	6.2	8.7	83.2	12.1
45	221.973	0.0000	705.1	0.122	-	10.3	6.1	91.8	41.9
44	597.208	3.563	1959.7	0.028	0.14	13.1	3.1	123.3	385.6
34	955.102	0.0000	3145.6	0.021	-	5.0	2.7	168.9	803.5
43	362.005	2.055	1088.8	0.183	0.25	10.3	11.2	260.5	39.9
53	362.169	0.3054	1021.7	0.023	1.7	30.0	16.6	375.6	235.1
31	624.674	5.647	1605.7	0.010	0.090	13.8	24.1	826.0	684.8
52	2099.225	0.0000	6571.1	0.003	-	13.5	7.5	853.0	7501.9
54	1052.910	0.0000	1793.1	0.047	-	8.6	49.7	1987.0	134.0
41	10002.16	0.0000	246.8	0.039	-	1.9	99.3	6615.2	115.7
weighted mean ± Taylor err			n=35		4.0	±6.9		30.2	2.5

Isotopic ratios corrected for blank, radioactive decay, and mass discrimination, not corrected for
Individual analyses show analytical error only; mean age errors also include error in J and irradiation
Analyses in italics are excluded excluded from mean age calculations.

Correction factors:

- $(^{39}Ar/^{37}Ar)_{Ca} = 0.00070 \pm 0.00005$
- $(^{36}Ar/^{37}Ar)_{Ca} = 0.00026 \pm 0.00002$
- $(^{38}Ar/^{39}Ar)_K = 0.0119$
- $(^{40}Ar/^{39}Ar)_K = 0.0270 \pm 0.0020$

APPENDIX O MTEC data from $^{40}Ar/^{39}Ar$ analysis

Table A- 15 Complete Data Tables from Argon analysis of MTEC

ID	Temp	$^{40}Ar/^{39}A$	$^{37}Ar/^{39}Ar$	$^{36}Ar/^{39}Ar$	$^{39}Ar_K$	K/Ca	Cl/K	$^{40}Ar^*$	^{39}Ar	Age	±1s
	(°C)			(x 10^{-3})	(x 10^{-15} mol)			(%)	(%)	(Ma)	(Ma)
MTEC-1 tube:91, Quartz, 6.4 mg, J=0.003743995±0.09%, D=1.00253±0.00119, NM-91, Lab#=9374-01											
A	500	316.887	0.290	981.570	0.270	1.8	7.6	8.5	2.9	172.7	71.3
B	900	20.836	0.112	45.365	3.557	4.6	2.5	35.6	41.2	49.4	1.5
C	1200	6.418	0.173	7.251	3.129	2.9	0.1	66.4	74.8	28.6	1.3
D	1750	20.561	5.047	44.825	2.342	0.10	3.9	37.3	100.0	51.3	2.1
total gas age			n=4		9.299	2.8				46.4	3.6
plateau			n=1	steps D-D	2.342	0.1			25.2	51.3	0.0
MTEC-2 tube:91, Quartz, 78.44 mg, J=0.003743995±0.09%, D=1.00253±0.00119, NM-91, Lab#=9374-02											
A	400	2014.52	0.335	6769.009	0.199	1.5	8.9	0.7	1.6	94.0	561.6
B	500	546.268	0.256	1806.214	0.855	2.0	9.6	2.3	8.6	82.7	42.1
C	600	180.366	0.226	563.560	1.071	2.3	8.6	7.7	17.3	91.1	12.3
D	700	58.622	0.286	170.495	1.818	1.8	8.1	14.0	32.2	54.8	3.6
E	800	25.237	0.452	65.576	0.279	1.1	6.3	23.2	34.5	39.2	11.6
F	900	30.134	0.786	79.815	0.149	0.65	6.2	21.8	35.7	43.9	21.5
G	1000	31.583	6.975	69.521	0.076	0.073	5.9	36.6	36.3	76.7	40.9
H	1100	33.063	22.294	93.416	0.044	0.023	5.9	21.6	36.7	48.3	72.4
I	1200	18.351	29.636	39.332	0.047	0.017	5.2	48.9	37.0	60.8	61.8
J	1300	45.721	1.384	126.618	1.051	0.37	7.6	18.3	45.6	55.8	4.5
K	1400	31.410	0.354	83.461	3.851	1.4	7.2	21.5	77.1	45.0	1.5
L	1500	22.519	0.349	49.991	0.687	1.5	6.8	34.4	82.7	51.6	4.8
M	1600	27.987	0.378	67.219	0.728	1.3	6.9	29.0	88.6	54.1	4.7
N	1700	31.601	0.377	82.160	1.116	1.4	7.0	23.2	97.7	48.8	3.6
O	1800	57.361	0.423	162.866	0.279	1.2	6.9	16.1	100.0	61.4	15.4
total gas age			n=15		12.249	1.5				56.6	17.0
plateau			n=6	steps J-O	7.711	1.3			63.0	47.4	2.1

APPENDIX P Summary of CAKE diagram regressions

Table A- 16 Data from CAKE regressions

All Data						Less than 900°C				
Sample	Data		Intercept		Age	Data		Intercept		Age
MTEECR	y0=	0.003	zint=	0.003	**AGE**					
MTEECR	a=	0.130	xint=	-0.026	**-282.9**					
MTEECR	b=	-0.008	yint=	0.398						
MTEECR	J=	0.004								
MTEECR		Rsqr = 0.61								
CMXECR	y0=	0.003	zint=	0.003	**AGE**					
CMXECR	a=	-0.216	xint=	0.013	**464.7**					
CMXECR	b=	0.008	yint=	-0.325						
CMXECR	J=	0.004								
CMXECR		Rsqr = 0.66								
W3FCR	y0=	0.002	zint=	0.002	**AGE**					
W3FCR	a=	0.030	xint=	-0.062	**-110.7**					
W3FCR	b=	0.001	yint=	-1.509						
W3FCR	J=	0.004								
W3FCR		Rsqr = 0.04								
MTEELC	y0=	0.004	zint=	0.004	**AGE**	y0=	0.004	zint=	0.004	**AGE**
MTEELC	a=	-0.034	xint=	0.102	**65.2**	a=	-0.069	xint=	0.052	**126.1**
MTEELC	b=	-0.001	yint=	6.053		b=	0.000	yint=	33.451	
MTEELC	J=	0.004					0.004			
MTEELC		Rsqr = 0.96				Rsqr = 0.611				
MTEESC	y0=	0.003	zint=	0.003	**AGE**	y0=	0.003	zint=	0.003	**AGE**
MTEESC	a=	-0.044	xint=	0.072	**91.1**	a=	0.052	xint=	-0.056	**-124.9**
MTEESC	b=	0.001	yint=	-4.112		b=	0.000	yint=	7.504	
MTEESC	J=	0.004				J=	0.004			
MTEESC		Rsqr = 0.43				Rsqr = 0.67				
CMXE	y0=	0.002	zint=	0.002	**AGE**	y0=	0.003	zint=	0.003	**AGE**
CMXE	a=	-0.054	xint=	0.044	**145.1**	a=	-0.037	xint=	0.077	**84.1**
CMXE	b=	0.002	yint=	-1.192		b=	0.001	yint=	-2.492	
CMXE	J=	0.004				J=	0.004			
CMXE		Rsqr = 0.47				Rsqr = 0.64				

Table A-16 con.

All Data						Less than 900°C				
Sample	Data		Intercept		Age	Data		Intercept		Age
W3F	y0=	0.003	zint=	0.003	**AGE**	y0=	0.003	zint=	0.003	**AGE**
W3F	a=	-0.488	xint=	0.007	**756.1**	a=	-0.555	xint=	0.006	**833.5**
W3F	b=	0.006	yint=	-0.575		b=	0.007	yint=	-0.508	
W3F	J=	0.004				J=	0.004			
W3F		Rsqr = 0.36				Rsqr = 0.81				
MTED	y0=	0.003	zint=	0.003	**AGE**	y0=	0.003	zint=	0.003	**AGE**
MTED	a=	-0.030	xint=	0.111	**60.0**	a=	0.065	xint=	-0.052	**-135.6**
MTED	b=	0.000	yint=	-7.800		b=	-0.003	yint=	0.990	
MTED	J=	0.004				J=	0.004			
MTED		Rsqr = 0.90				Rsqr = 0.88				
MTEC-2	y0=	0.003	zint=	0.003	**AGE**	y0=	0.003	zint=	0.003	**AGE**
MTEC-2	a=	-0.017	xint=	0.193	**34.7**	a=	-0.048	xint=	0.068	**96.2**
MTEC-2	b=	0.000	yint=	13.836		b=	0.001	yint=	-2.847	
MTEC-2	J=	0.004				J=	0.004			
MTEC-2		Rsqr = 0.86				Rsqr = 0.82				
CMXD	y0=	0.003	zint=	0.003	**AGE**	y0=	0.003	zint=	0.003	**AGE**
CMXD	a=	0.006	xint=	-0.493	**-13.6**	a=	0.014	xint=	-0.201	**-33.6**
CMXD	b=	-0.003	yint=	1.025		b=	-0.002	yint=	1.197	
CMXD	J=	0.004				J=	0.004			
CMXD		Rsqr = 0.46				Rsqr = 0.69				
CMXA	y0=	0.003	zint=	0.003	**AGE**	y0=	0.003	zint=	0.003	**AGE**
CMXA	a=	0.053	xint=	-0.054	**-129.3**	a=	0.018	xint=	-0.165	**-41.5**
CMXA	b=	-0.003	yint=	0.829		b=	-0.002	yint=	1.758	
CMXA	J=	0.004				J=	0.004			
CMXA		Rsqr = 0.59				Rsqr = 0.76				
CMXB	y0=	0.003	zint=	0.003	**AGE**	y0=	0.002	zint=	0.002	**AGE**
CMXB	a=	-0.014	xint=	0.216	**31.0**	a=	0.074	xint=	-0.029	**-248.7**
CMXB	b=	-0.001	yint=	2.556		b=	-0.002	yint=	1.125	
CMXB	J=	0.004				J=	0.004			
CMXB		Rsqr = 0.16023749				Rsqr = 0.681184				
W3G	y0=	0.001	zint=	0.001	**AGE**	y0=	0.002	zint=	0.002	**AGE**
W3G	a=	-0.042	xint=	0.029	**217.9**	a=	-0.044	xint=	0.034	**188.0**
W3G	b=	0.002	yint=	-0.611		b=	0.002	yint=	-0.854	
W3G	J=	0.004				J=	0.004			
W3G		Rsqr = 0.27				Rsqr = 0.39				

Table A-16 con.

All Data						Less than 900°C				
Sample	Data		Intercept		Age	Data		Intercept		Age
W3E	y0=	0.002	zint=	0.002	**AGE**	y0=	0.002	zint=	0.002	**AGE**
W3E	a=	0.046	xint=	-0.040	**-176.1**	a=	0.037	xint=	-0.056	**-123.3**
W3E	b=	-0.003	yint=	0.570		b=	-0.003	yint=	0.666	
W3E	J=	0.004				J=	0.004			
W3E		Rsqr = 0.60				Rsqr = 0.54				
W3CD	y0=	0.002	zint=	0.002	**AGE**	y0=	0.002	zint=	0.002	**AGE**
W3CD	a=	-0.092	xint=	0.017	**343.3**	a=	-0.023	xint=	0.092	**70.2**
W3CD	b=	0.005	yint=	-0.318		b=	0.001	yint=	-1.668	
W3CD	J=	0.004				J=	0.004			
W3CD		Rsqr = 0.86				Rsqr = 0.055				
CMXC	y0=	0.003	zint=	0.003	**AGE**	y0=	0.002	zint=	0.002	**AGE**
CMXC	a=	-0.055	xint=	0.056	**116.2**	a=	-0.066	xint=	0.027	**234.0**
CMXC	b=	-0.001	yint=	2.699		b=	0.002	yint=	-0.829	
CMXC	J=	0.004				J=	0.004			
CMXC		Rsqr = 0.32				Rsqr = 0.42				
MTEC-1	y0=	0.003	zint=	0.003	**AGE**					
MTEC-1	a=	-0.013	xint=	0.246	**27.3**					
MTEC-1	b=	-0.001	yint=	5.237						
MTEC-1	J=	0.004								
MTEC-1		Rsqr = 0.99								
MTEB	y0=	0.003	zint=	0.003	**AGE**	y0=	0.003	zint=	0.003	**AGE**
MTEB	a=	0.004	xint=	-0.755	**-8.9**	a=	0.036	xint=	-0.097	**-70.9**
MTEB	b=	-0.001	yint=	2.303		b=	-0.003	yint=	1.078	
MTEB	J=	0.004				J=	0.004			
MTEB		Rsqr = 0.97				Rsqr = 1.0				
W3A	y0=	0.002	z_{int}=	0.002	**AGE**	y0=	0.001	z_{int}=	0.001	**AGE**
W3A	a=	-0.114	xint=	0.016	**373.9**	a=	-0.150	xint=	0.008	**642.1**
W3A	b=	0.004	yint=	-0.402		b=	0.006	yint=	-0.207	
W3A	J=	0.004				J=	0.004			
W3A		Rsqr = 0.59				Rsqr = 1.0				

APPENDIX Q Isochrons from the HFIDC

Figure A- 4 Isochrons from HDFICs

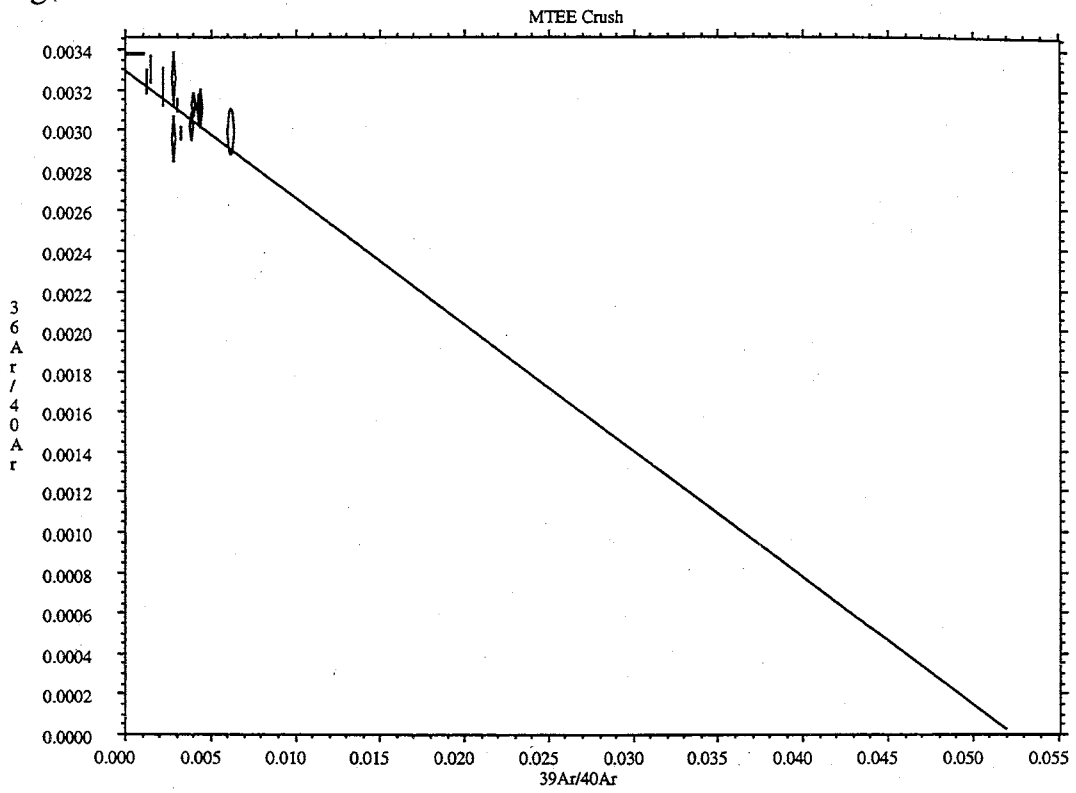

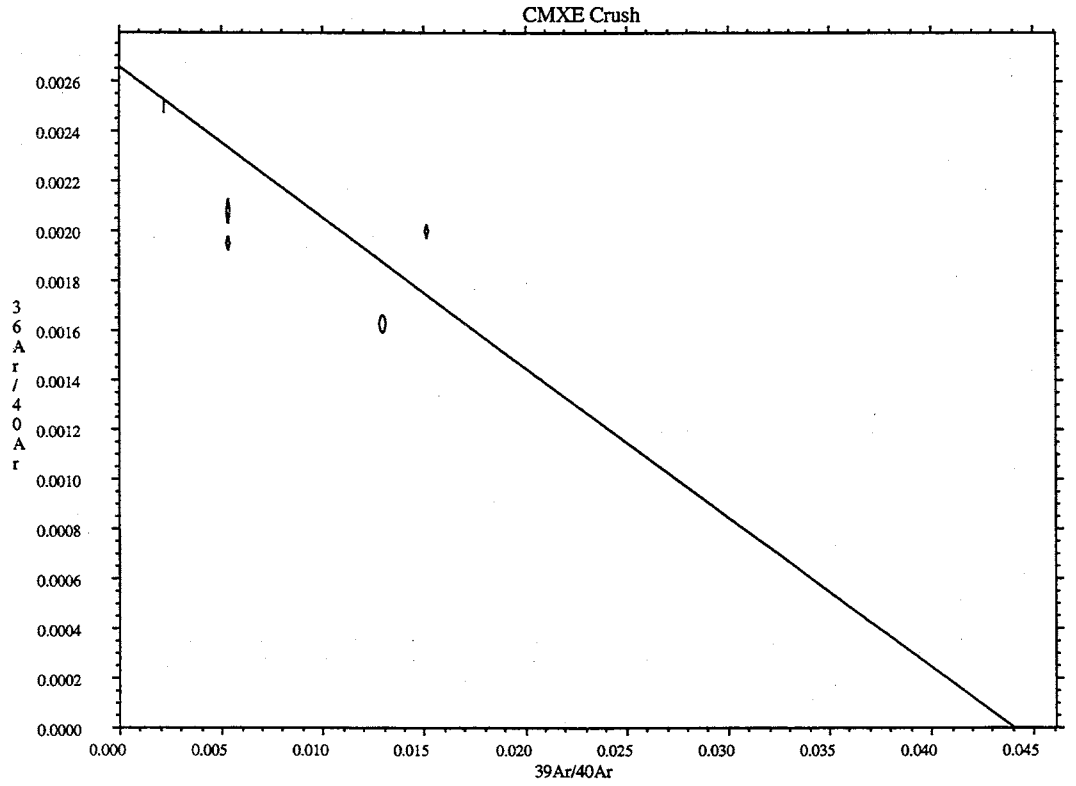

FigureA4 A,B

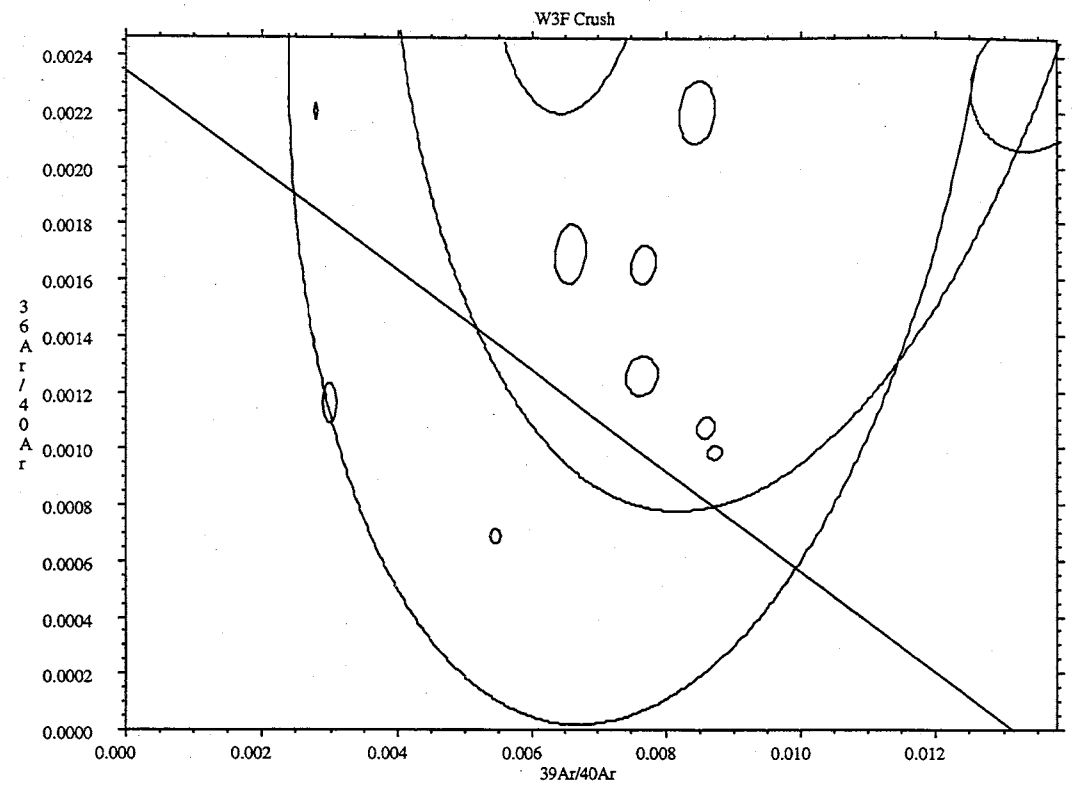
W3F Crush
0.0024
0.0022
0.0020
0.0018
0.0016
0.0014
0.0012
0.0010
0.0008
0.0006
0.0004
0.0002
0.0000
36Ar/40Ar
0.000
0.002
0.004
0.006
0.008
0.010
0.012
39Ar/40Ar

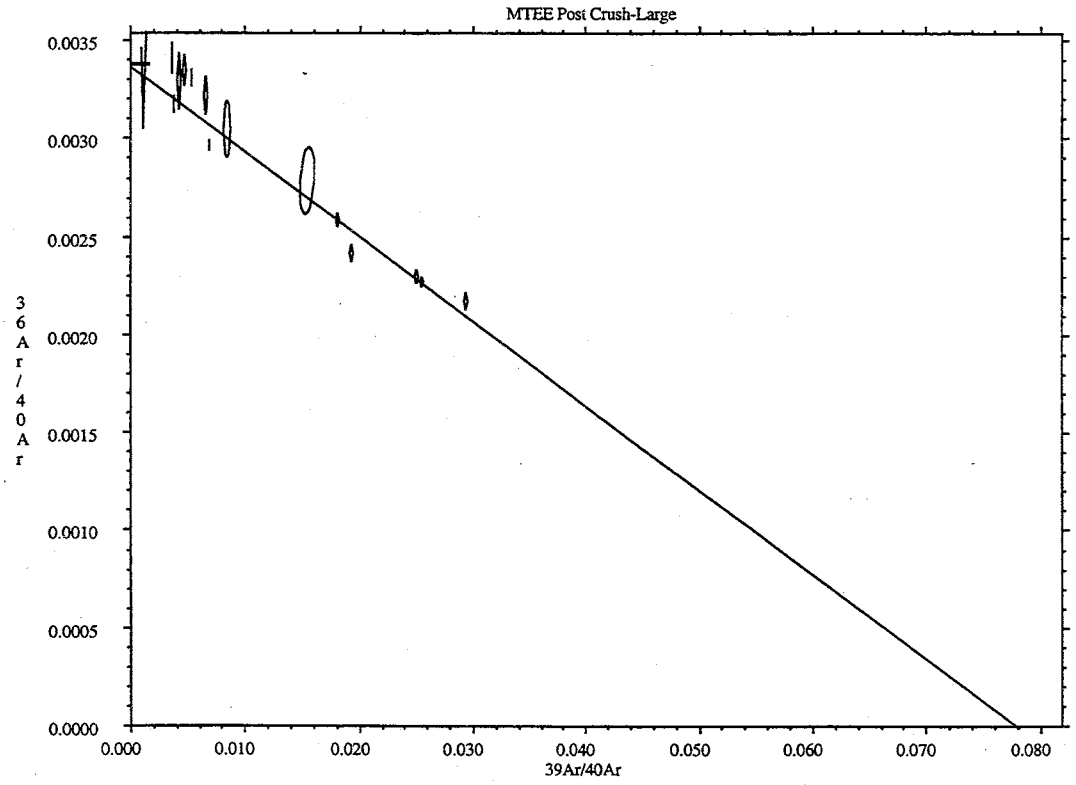
MTEE Post Crush-Large
0.0035
0.0030
0.0025
0.0020
0.0015
0.0010
0.0005
0.0000
36Ar/40Ar
0.000
0.010
0.020
0.030
0.040
0.050
0.060
0.070
0.080
39Ar/40Ar

FigureA4 C, D

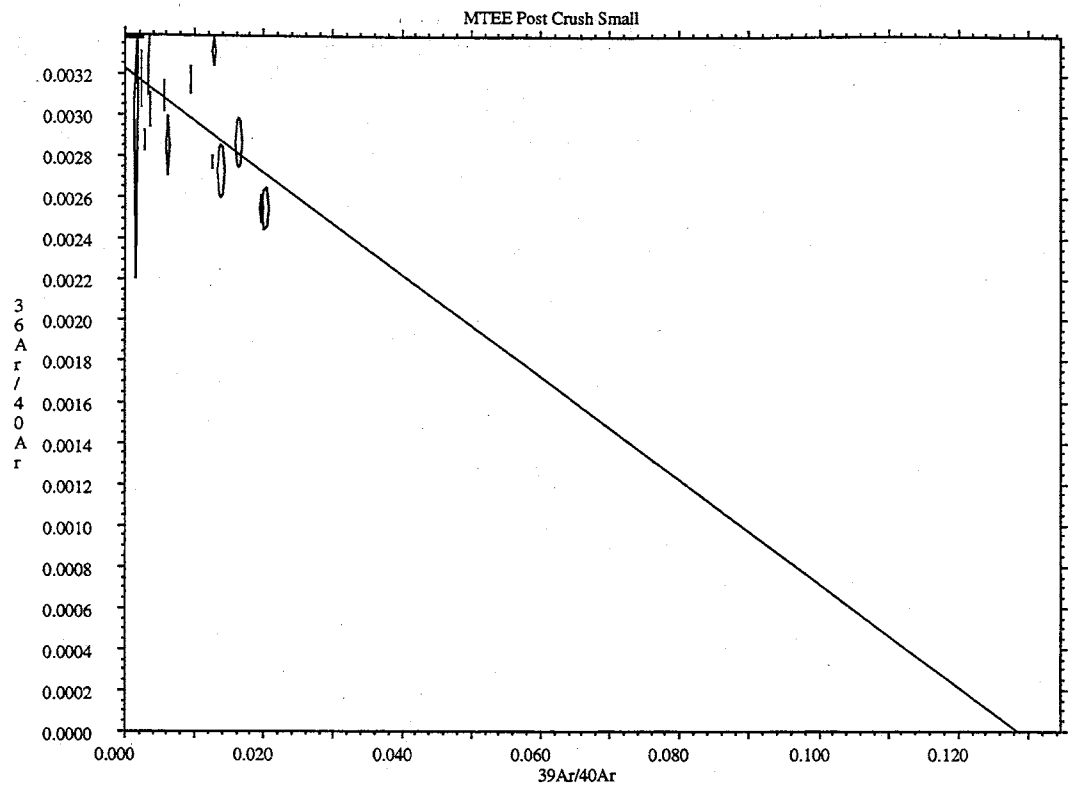
MTEE Post Crush Small
0.0032
0.0030
0.0028
0.0026
0.0024
0.0022
0.0020
0.0018
0.0016
0.0014
0.0012
0.0010
0.0008
0.0006
0.0004
0.0002
0.0000
36Ar/40Ar
0.000
0.020
0.040
0.060
0.080
0.100
0.120
39Ar/40Ar

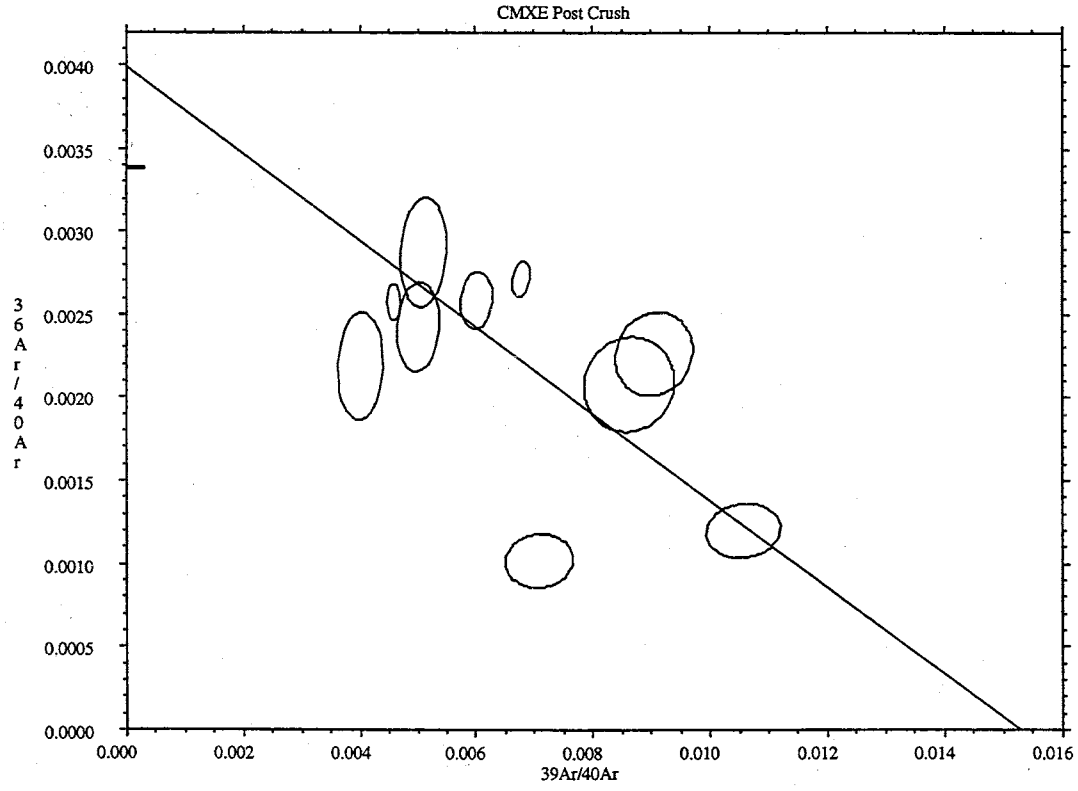
CMXE Post Crush
0.0040
0.0035
0.0030
0.0025
0.0020
0.0015
0.0010
0.0005
0.0000
36Ar/40Ar
0.000
0.002
0.004
0.006
0.008
0.010
0.012
0.014
0.016
39Ar/40Ar

FigureA4 E, F

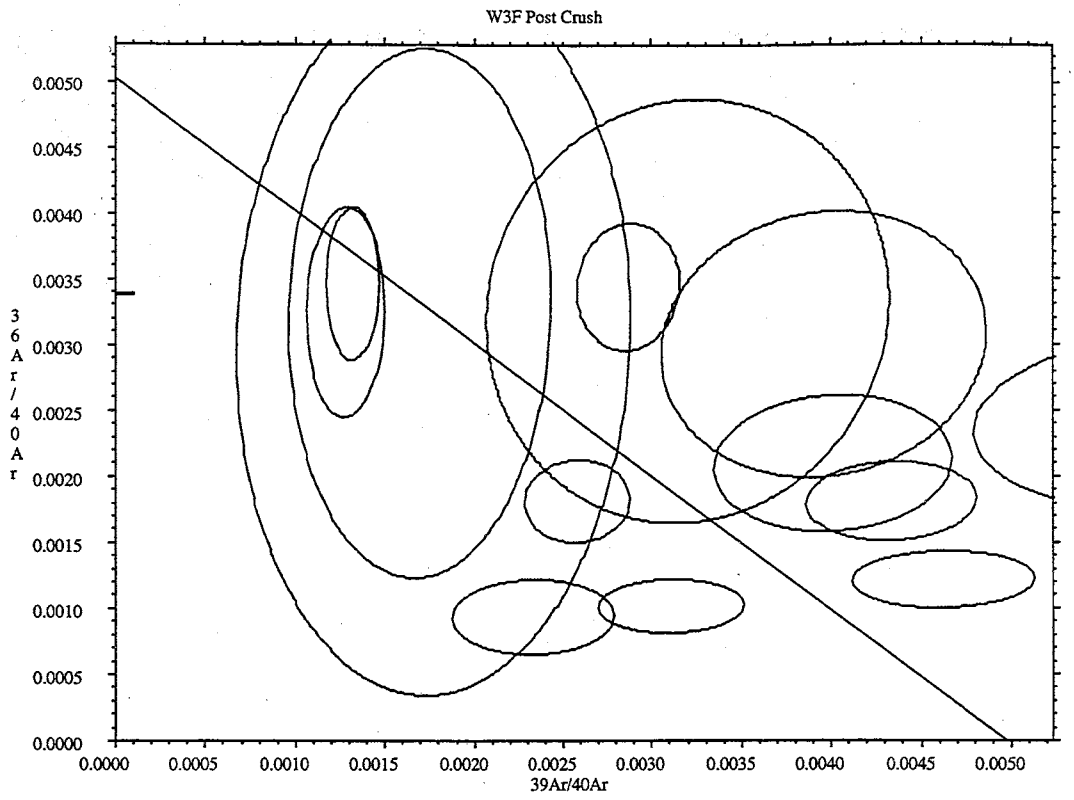
W3F Post Crush
0.0050
0.0045
0.0040
0.0035
0.0030
0.0025
0.0020
0.0015
0.0010
0.0005
0.0000
36Ar/40Ar
0.0000 0.0005 0.0010 0.0015 0.0020 0.0025 0.0030 0.0035 0.0040 0.0045 0.0050
39Ar/40Ar

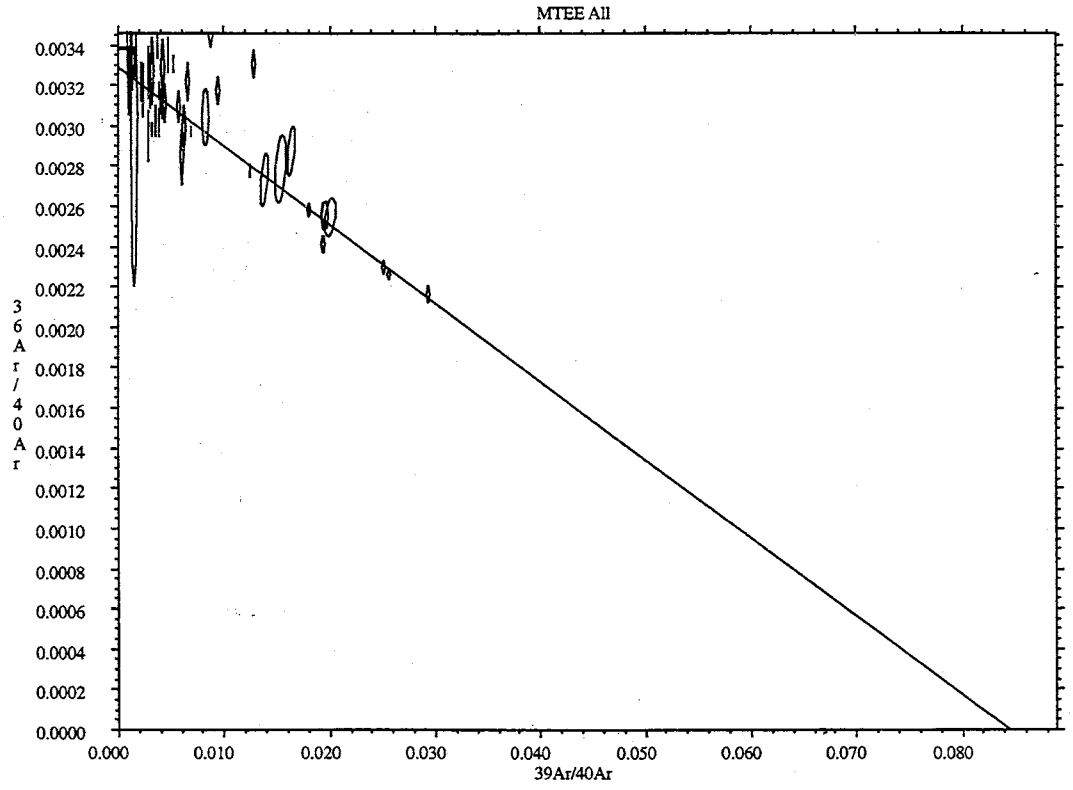
MTEE All
0.0034
0.0032
0.0030
0.0028
0.0026
0.0024
0.0022
0.0020
0.0018
0.0016
0.0014
0.0012
0.0010
0.0008
0.0006
0.0004
0.0002
0.0000
36Ar/40Ar
0.000 0.010 0.020 0.030 0.040 0.050 0.060 0.070 0.080
39Ar/40Ar

FigureA4 G, H

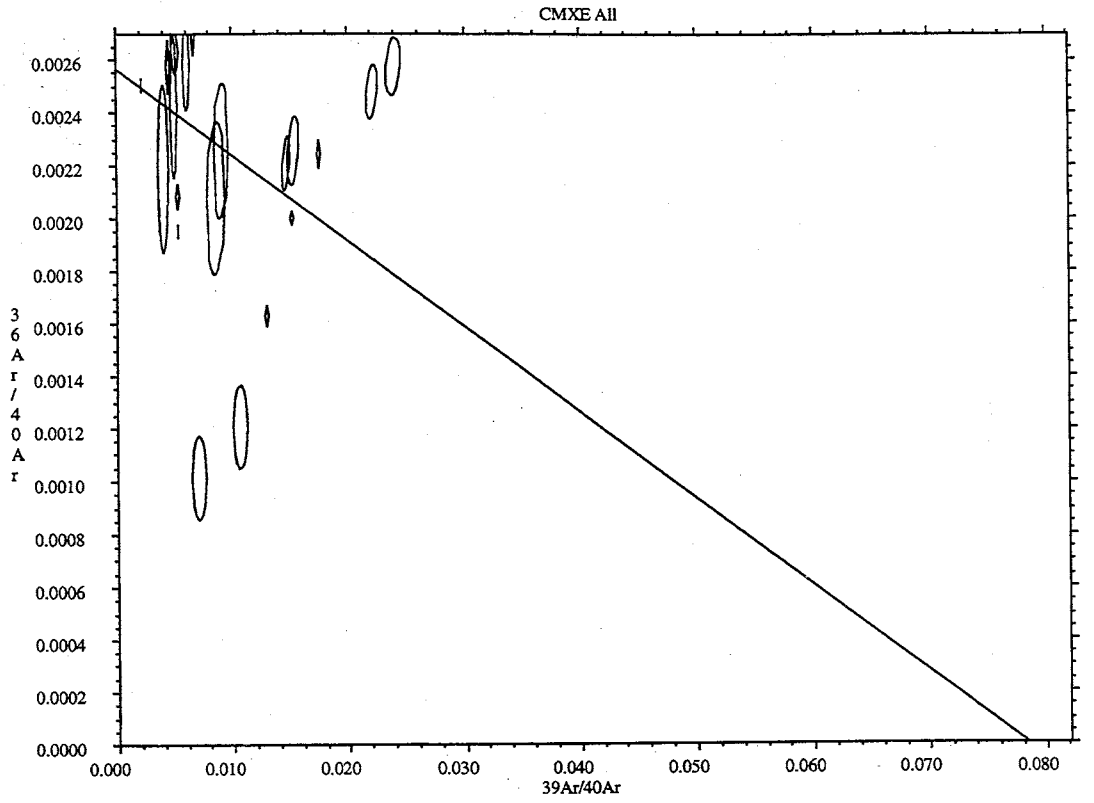
CMXE All
0.0026
0.0024
0.0022
0.0020
0.0018
0.0016
0.0014
0.0012
0.0010
0.0008
0.0006
0.0004
0.0002
0.0000
36Ar/40Ar
0.000
0.010
0.020
0.030
0.040
0.050
0.060
0.070
0.080
39Ar/40Ar

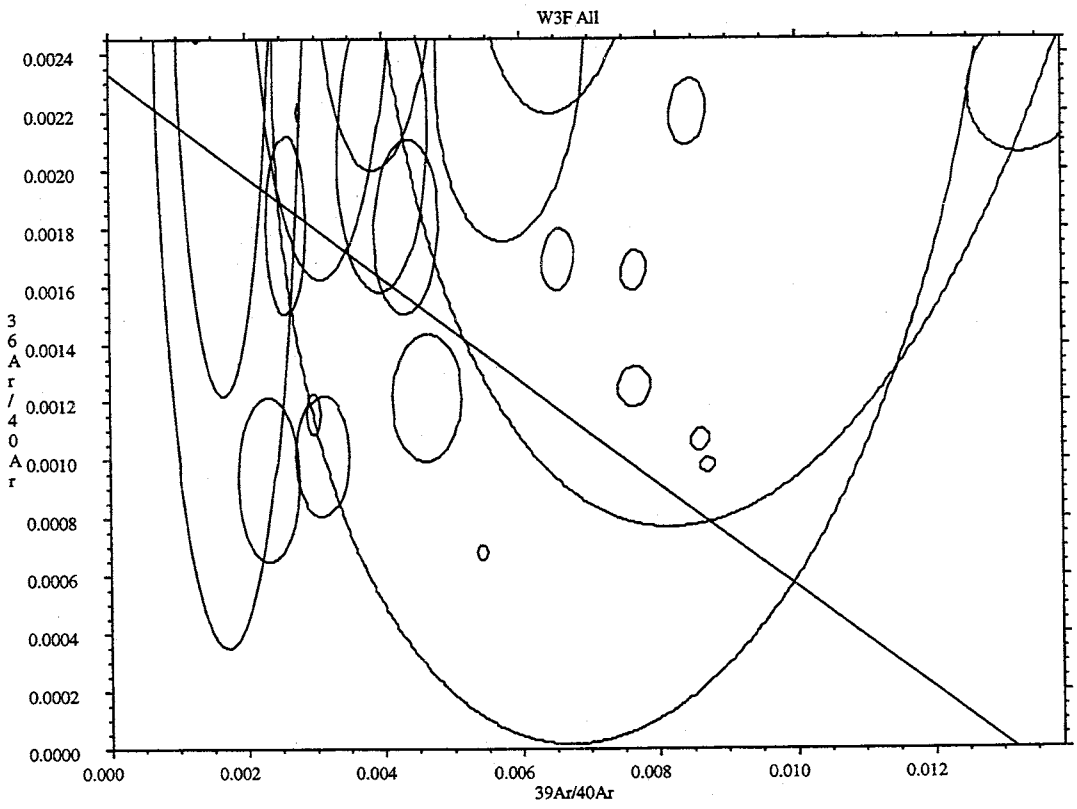
W3F All
0.0024
0.0022
0.0020
0.0018
0.0016
0.0014
0.0012
0.0010
0.0008
0.0006
0.0004
0.0002
0.0000
36Ar/40Ar
0.000
0.002
0.004
0.006
0.008
0.010
0.012
39Ar/40Ar

FigureA4 I, J

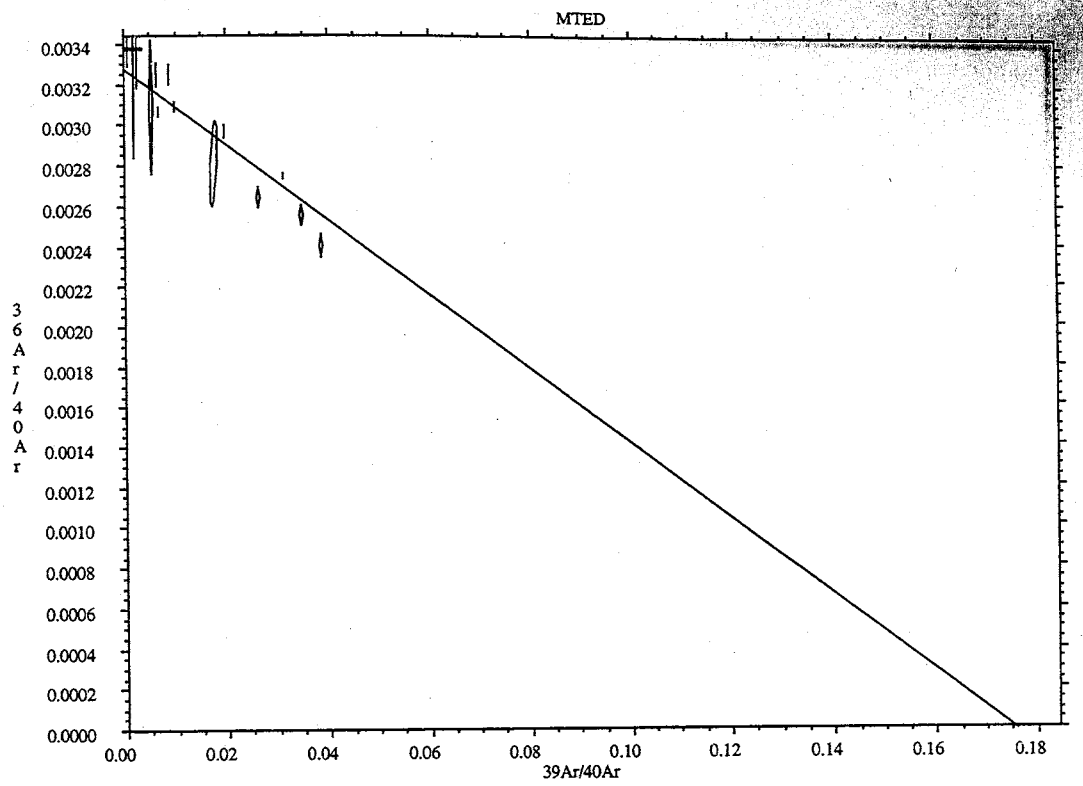
MTED
0.0034
0.0032
0.0030
0.0028
0.0026
0.0024
0.0022
0.0020
0.0018
0.0016
0.0014
0.0012
0.0010
0.0008
0.0006
0.0004
0.0002
0.0000
36Ar/40Ar
0.00
0.02
0.04
0.06
0.08
0.10
0.12
0.14
0.16
0.18
39Ar/40Ar

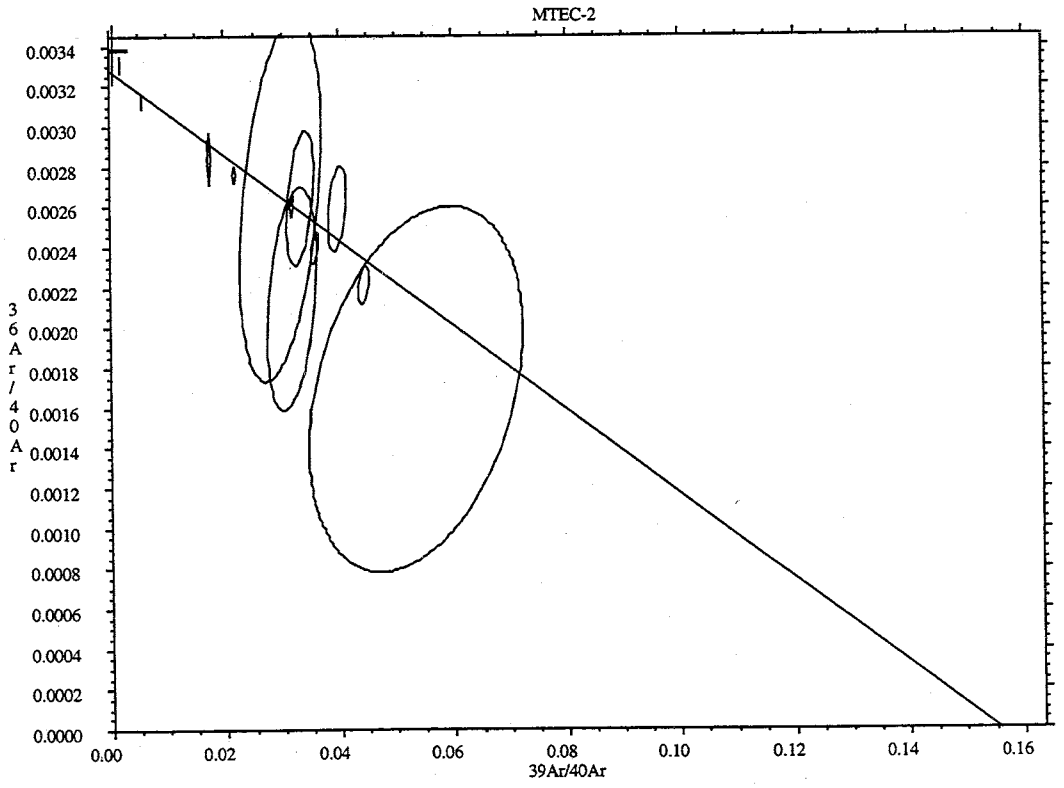
MTEC-2
0.0034
0.0032
0.0030
0.0028
0.0026
0.0024
0.0022
0.0020
0.0018
0.0016
0.0014
0.0012
0.0010
0.0008
0.0006
0.0004
0.0002
0.0000
36Ar/40Ar
0.00
0.02
0.04
0.06
0.08
0.10
0.12
0.14
0.16
39Ar/40Ar

FigureA4 K, L

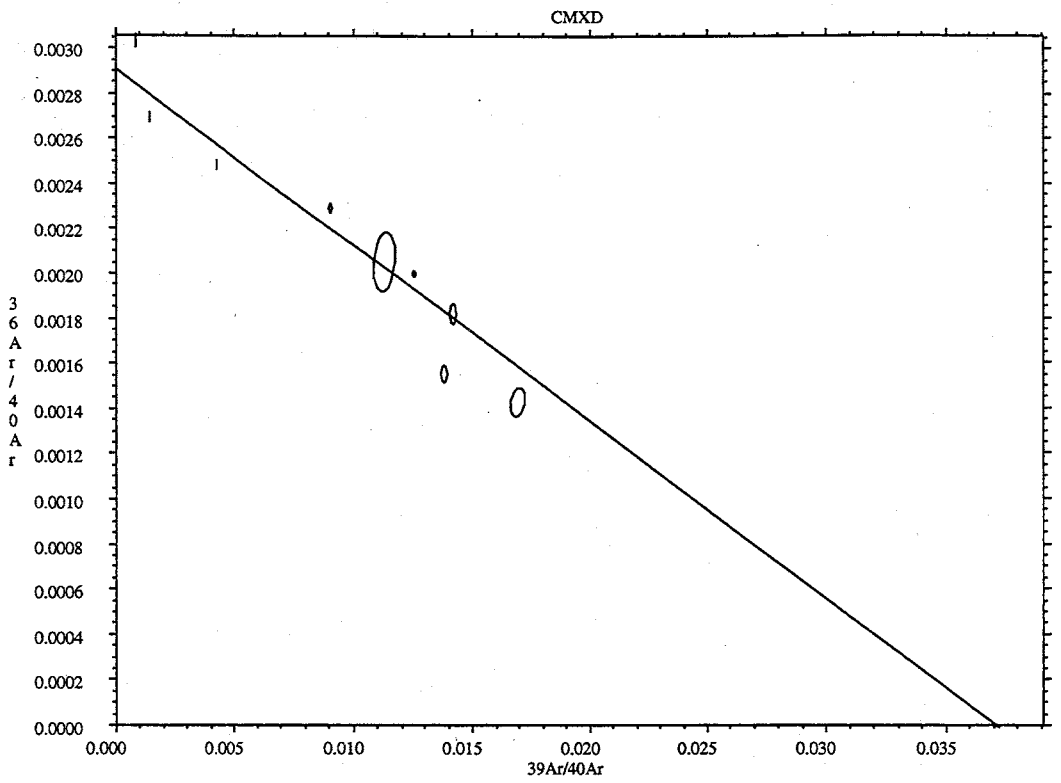
CMXD
0.0030
0.0028
0.0026
0.0024
0.0022
0.0020
0.0018
0.0016
0.0014
0.0012
0.0010
0.0008
0.0006
0.0004
0.0002
0.0000
36Ar/40Ar
0.000
0.005
0.010
0.015
0.020
0.025
0.030
0.035
39Ar/40Ar

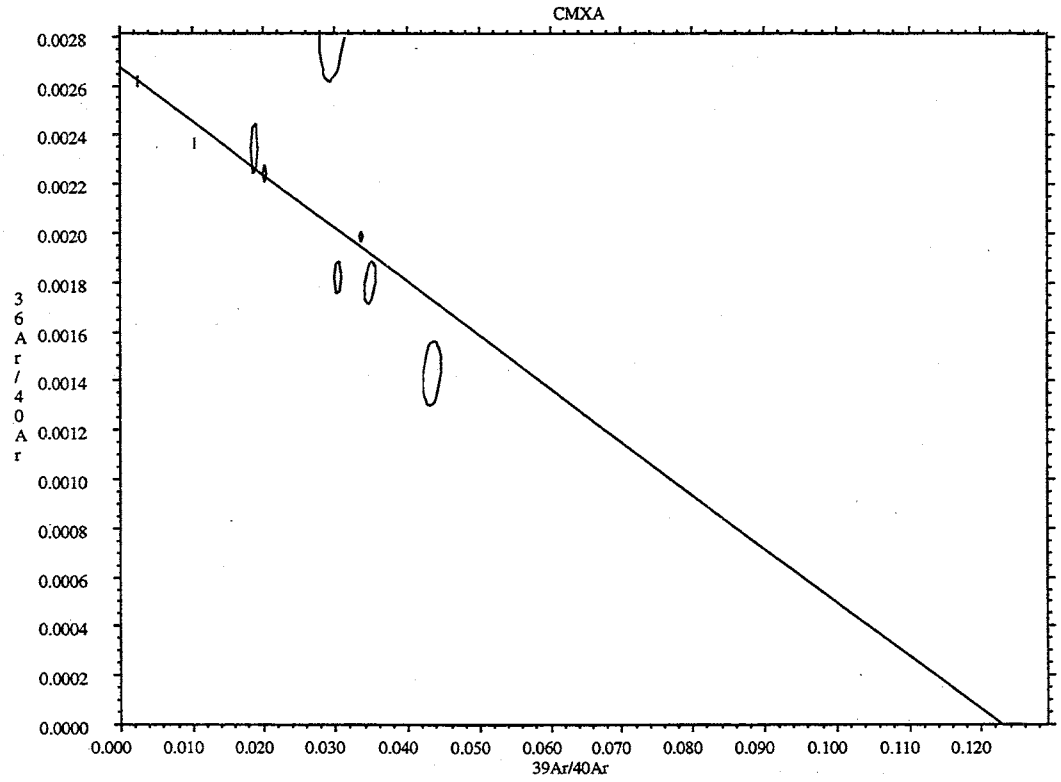
CMXA
0.0028
0.0026
0.0024
0.0022
0.0020
0.0018
0.0016
0.0014
0.0012
0.0010
0.0008
0.0006
0.0004
0.0002
0.0000
36Ar/40Ar
0.000
0.010
0.020
0.030
0.040
0.050
0.060
0.070
0.080
0.090
0.100
0.110
0.120
39Ar/40Ar

FigureA4 M, N

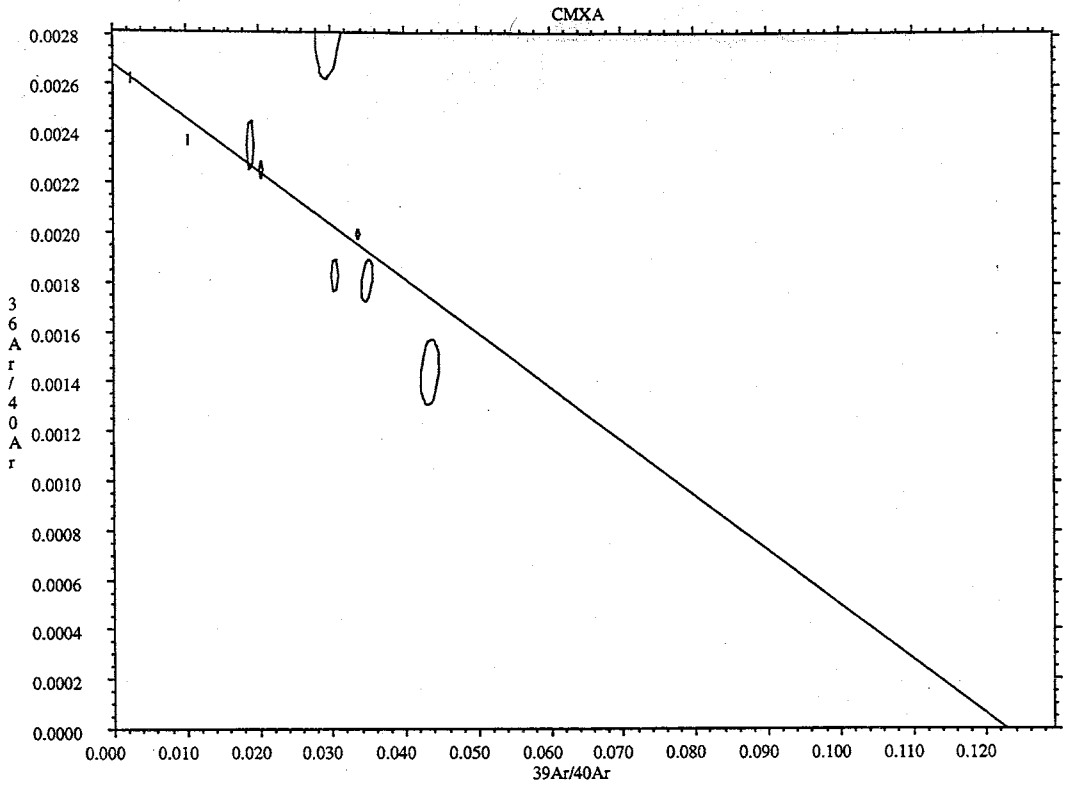
CMXA
0.0028
0.0026
0.0024
0.0022
0.0020
0.0018
0.0016
0.0014
0.0012
0.0010
0.0008
0.0006
0.0004
0.0002
0.0000
36Ar/40Ar
0.000 0.010 0.020 0.030 0.040 0.050 0.060 0.070 0.080 0.090 0.100 0.110 0.120
39Ar/40Ar

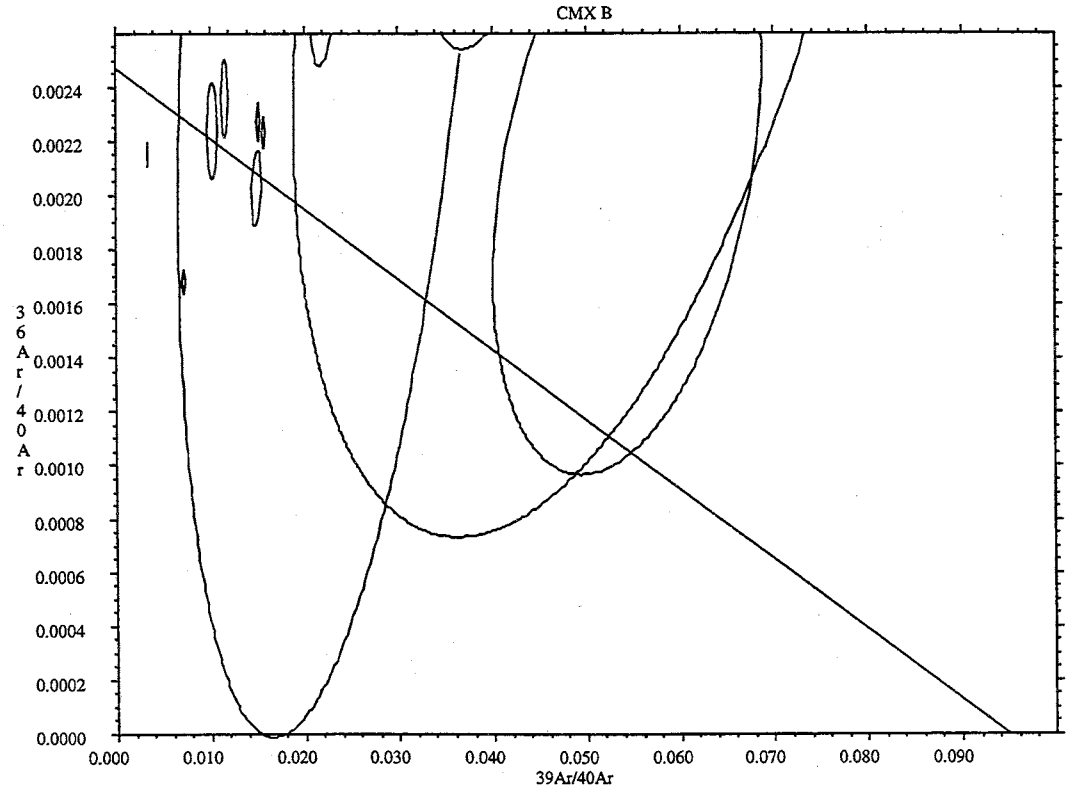
CMX B
0.0024
0.0022
0.0020
0.0018
0.0016
0.0014
0.0012
0.0010
0.0008
0.0006
0.0004
0.0002
0.0000
36Ar/40Ar
0.000 0.010 0.020 0.030 0.040 0.050 0.060 0.070 0.080 0.090
39Ar/40Ar

FigureA4 O, P

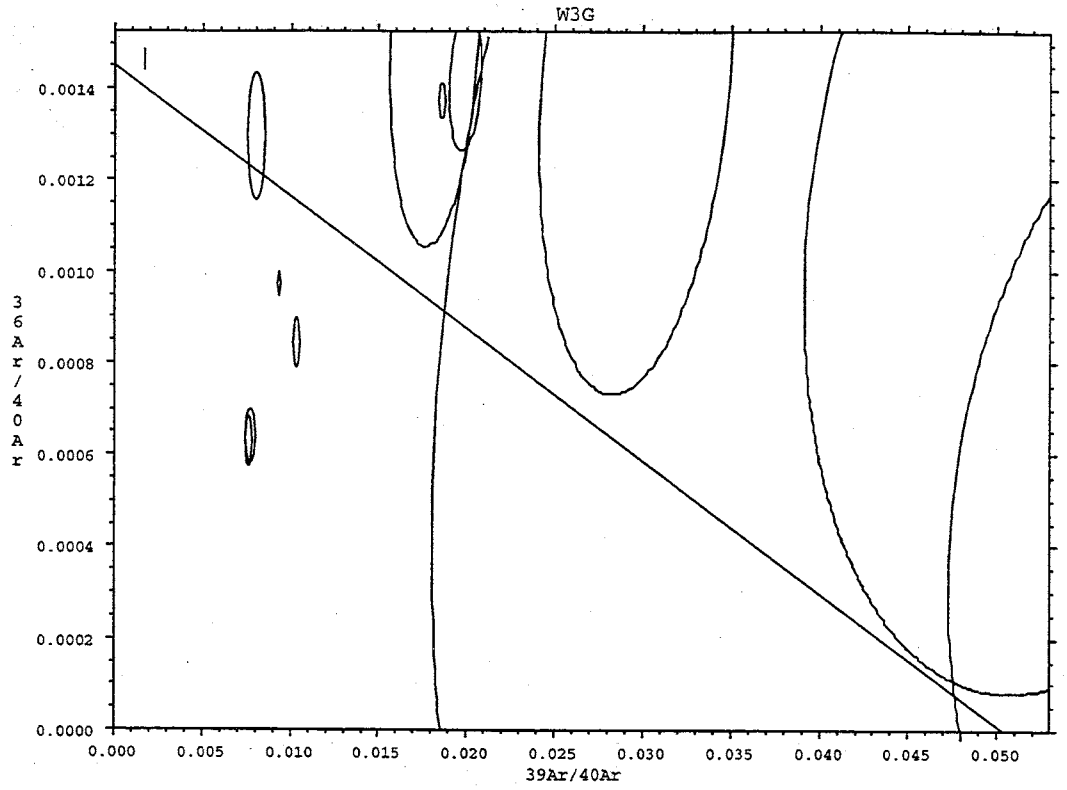
W3G
0.0014
0.0012
0.0010
0.0008
0.0006
0.0004
0.0002
0.0000
36Ar/40Ar
0.000
0.005
0.010
0.015
0.020
0.025
0.030
0.035
0.040
0.045
0.050
39Ar/40Ar

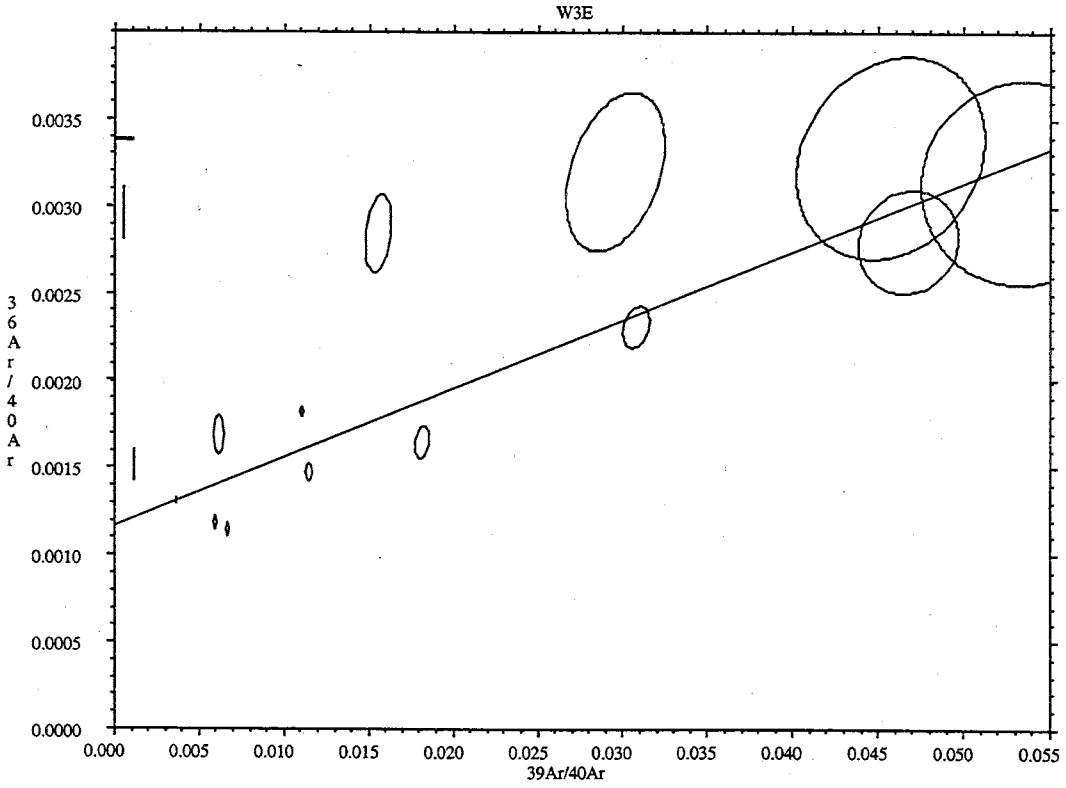
W3E
0.0035
0.0030
0.0025
0.0020
0.0015
0.0010
0.0005
0.0000
36Ar/40Ar
0.000
0.005
0.010
0.015
0.020
0.025
0.030
0.035
0.040
0.045
0.050
0.055
39Ar/40Ar

FigureA4 Q, R

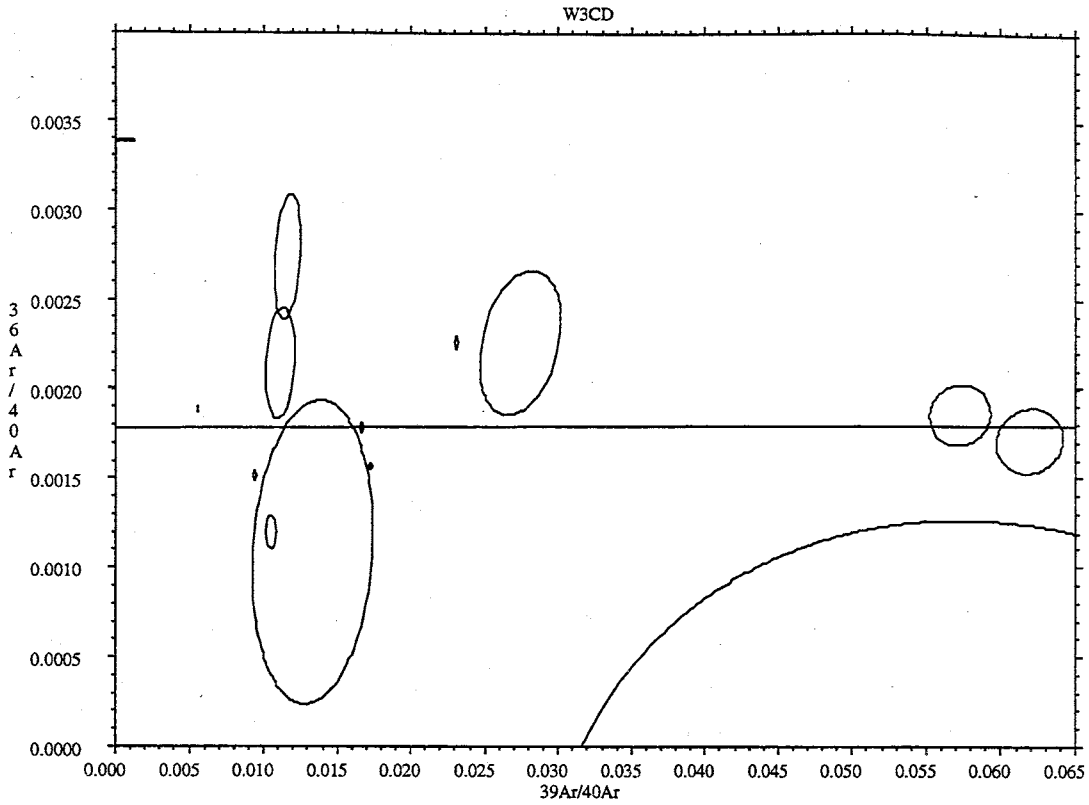
W3CD
0.0035
0.0030
0.0025
0.0020
0.0015
0.0010
0.0005
0.0000
36Ar/40Ar
0.000 0.005 0.010 0.015 0.020 0.025 0.030 0.035 0.040 0.045 0.050 0.055 0.060 0.065
39Ar/40Ar

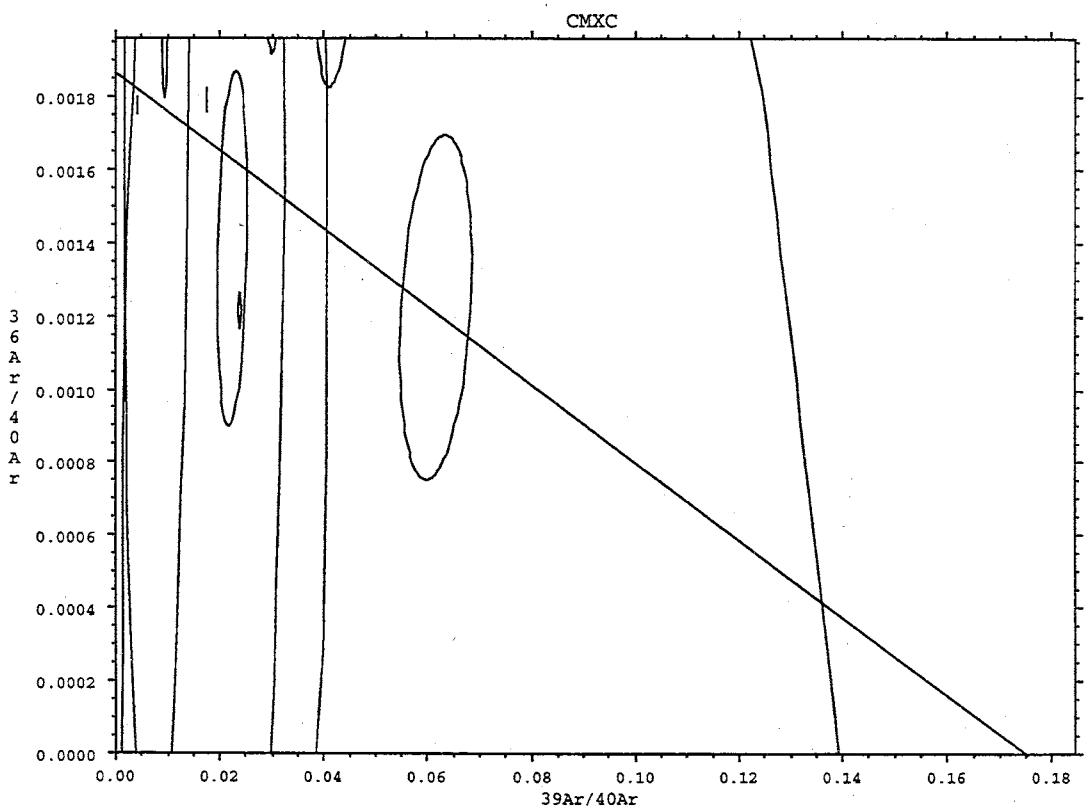
CMXC
0.0018
0.0016
0.0014
0.0012
0.0010
0.0008
0.0006
0.0004
0.0002
0.0000
36Ar/40Ar
0.00 0.02 0.04 0.06 0.08 0.10 0.12 0.14 0.16 0.18
39Ar/40Ar

FigureA S, T

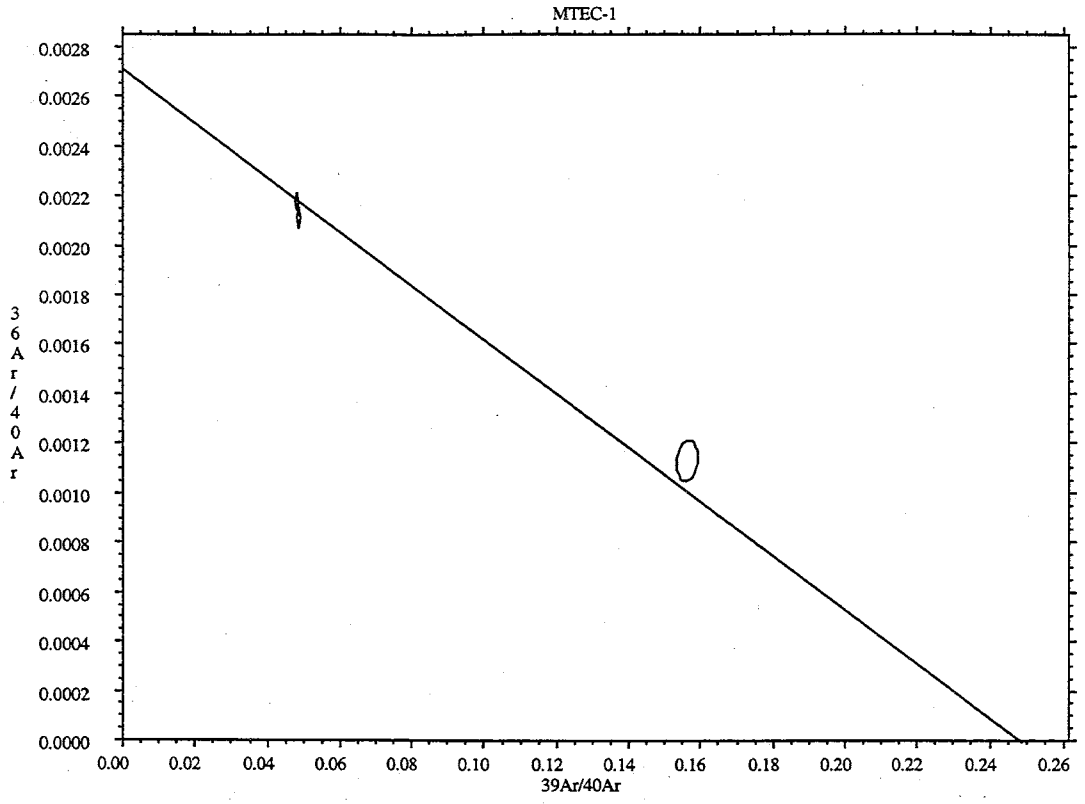
MTEC-1
0.0028
0.0026
0.0024
0.0022
0.0020
0.0018
0.0016
0.0014
0.0012
0.0010
0.0008
0.0006
0.0004
0.0002
0.0000
36Ar/40Ar
0.00
0.02
0.04
0.06
0.08
0.10
0.12
0.14
0.16
0.18
0.20
0.22
0.24
0.26
39Ar/40Ar

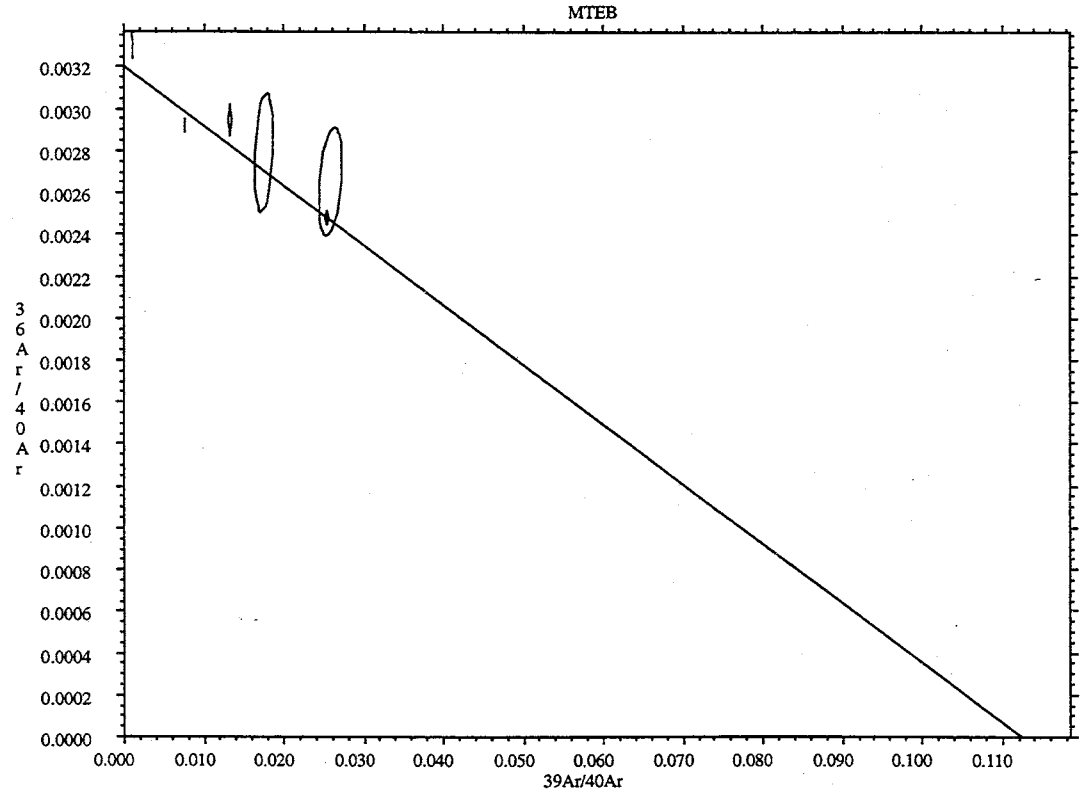
MTEB
0.0032
0.0030
0.0028
0.0026
0.0024
0.0022
0.0020
0.0018
0.0016
0.0014
0.0012
0.0010
0.0008
0.0006
0.0004
0.0002
0.0000
36Ar/40Ar
0.000
0.010
0.020
0.030
0.040
0.050
0.060
0.070
0.080
0.090
0.100
0.110
39Ar/40Ar

FigureA U, V

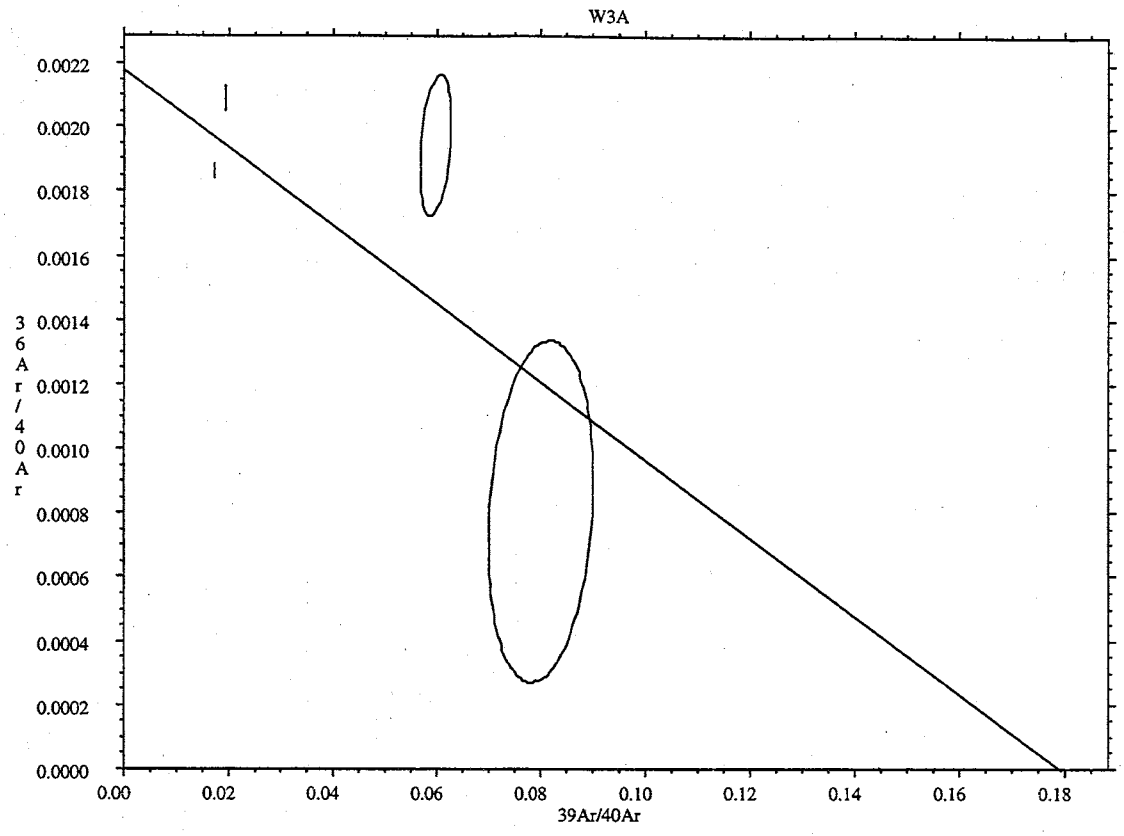
W3A
0.0022
0.0020
0.0018
0.0016
0.0014
0.0012
0.0010
0.0008
0.0006
0.0004
0.0002
0.0000
36Ar/40Ar
0.00
0.02
0.04
0.06
0.08
0.10
0.12
0.14
0.16
0.18
39Ar/40Ar

FigureA W

APPENDIX R Summary of argon ages

Table A-17 Summary of All Argon Ages

Sample		Integrated Age			800-1200° C			< 800° C			> 1200° C		
		Cl/K	Age	±1s	Cl/K	Age	±1s	Cl/K	Age	±1s	Cl/K	Age	±1s
	Irradiatio		(Ma)	(Ma)		(Ma)	(Ma)		(Ma)	(Ma)		(Ma)	(Ma)
CPU<535	53-TB1	0.1	9.1	0.8	0.0	8.5	3.1	0.0	6.7	1.0	0.7	25.3	2.5
CPU>535	53-TB1	0.1	8.9	1.8	0.1	4.6	2.1	0.0	5.5	0.7	0.7	25.3	2.9
MTE<535	53-TB1	0.2	8.7	0.7	0.0	14.0	4.4	0.2	7.3	0.6	0.5	4.8	4.9
MTE>535	53-TB1	0.3	11.0	0.7	0.0	19.5	5.4	0.3	7.3	1.1	0.4	12.9	3.3
MTEE53	53-TB1	6.5	56.6	11.2	6.1	32.0	3.9	6.9	54.6	9.8	6.5	42.6	4.3
MTELF1	53-TB1	25.6	-103.7	106.1									
MTELF2	53-TB1	20.9	-99.2	11.0									
MTELF3	53-TB1	11.5	-92.7	208.5									
MTELF4	53-TB1	12.6	-47.1	37.1									
MTELF5	53-TB1	10.1	-36.2	19.0									
MTELF6	53-TB1	7.8	-30.9	32.7									
MTELF7	53-TB1	9.0	-28.3	92.4									
MTELF8	53-TB1	13.8	-18.2	186.7									
MTELF9	53-TB1	8.2	-16.6	24.6									
MTELF10	53-TB1	6.6	-7.6	52.6									
MTELF11	53-TB1	6.7	-6.2	22.5									
MTELF12	53-TB1	6.6	0.9	13.1									
MTELF13	53-TB1	5.6	4.7	23.8									
MTELF14	53-TB1	6.8	5.0	8.0									
MTELF15	53-TB1	28.9	16.3	3875.4									
MTELF16	53-TB1	7.1	19.4	12.7									
MTELF17	53-TB1	6.9	19.9	53.4									
MTELF18	53-TB1	11.1	30.7	149.5									
MTELF19	53-TB1	6.1	30.8	13.0									
MTELF20	53-TB1	9.6	37.0	21.3									
MTELF21	53-TB1	10.0	38.9	108.4									
MTELF22	53-TB1	6.0	41.4	3.3									
MTELF23	53-TB1	8.0	42.4	43.3									
MTELF24	53-TB1	2.7	62.1	1028.2									
MTELF25	53-TB1	8.6	64.6	40.7									
MTELF26	53-TB1	6.2	83.2	12.1									
MTELF27	53-TB1	10.3	91.8	41.9									
MTELF28	53-TB1	13.1	123.3	385.6									
MTELF29	53-TB1	5.0	168.9	803.5									
MTELF30	53-TB1	10.3	260.5	39.9									
MTELF31	53-TB1	30.0	375.6	235.1									
MTELF32	53-TB1	13.8	826.0	684.8									
MTELF33	53-TB1	13.5	853.0	7501.9									
MTELF34	53-TB1	8.6	1987.0	134.0									
MTELF35	53-TB1	1.9	6615.2	115.7									
W353	53-TB1	0.2	3.8	0.3	7.4	27.8	13.2	-248.8	20.0	3.6	0.1	2.1	1.5
CPU2FF1	53-TR2	5.9	177.0	187.3									
CMX2FF	53-TR2	6.1	72.5	51.2									
CMX2FF	53-TR2	4.2	117.3	701.5									
CMX2FF	53-TR2	6.9	147.4	30.2									
CMX53	53-TR2	0.9	23.5	1.3	0.3	1.0	0.7	4.9	63.0	44.7	0.9	3.9	5.4
CPU253	53-TR2	0.1	36.3	2.9	0.1	28.6	1.1	5.5	263.3	69.3	0.1	28.6	1.2

Table A-17 con.

		Integrated Age			800-1200° C			< 800° C Plateau			> 1200° C Plateau		
		Cl/K	Age	±1s	Cl/K	Age	±1s	Cl/K	Age	±1s	Cl/K	Age	±1s
	Irradiatio		(Ma)	(Ma)		(Ma)	(Ma)		(Ma)	(Ma)		(Ma)	(Ma)
CPU2AD	53-TR2	0.004	28.11	0.09									
HH53	53-TR2	3.0	79.1	5.8	2.2	36.5	3.0	6.9	81.5	24.5	1.9	68.1	11.6
W3ADL	53-TR2	0.005	76.44	0.21									
W3FF1	53-TR2	6.5	10.0	19.9									
W3FF2	53-TR2	4.4	37.8	44.4									
W3FF3	53-TR2	4.5	86.8	285.1									
W3FF4	53-TR2	6.4	121.6	618.6									
W3FF5	53-TR2	5.9	180.0	47.1									
W3FF6	53-TR2	0.1	8.7	0.9									
W3FF7	53-TR2	5.6	76.1	2.5									
W3FF8	53-TR2	6.4	221.6	5.6									
HHADL	53-TR2	0.003	26.86	0.22									
FNADL	53-TR2	0.003	27.68	0.10									
ADADL	53-TR2	0.005	28.16	0.18									
CMX2AD	53-TR2	0.033	29.51	2.31									
MTE64	64-TR2	5.0	24.9	135.6	4.1	27.5	29.4	5.0	62.3	12.6	5.2	18.7	37.9
MTEC64	64-TR2	4.6	90.2	57.1									
MTEC64	64-TR2	4.7	100.7	49.3									
MTEPC64	64-TR2	4.9	116.9	37.2	0.4	162.9	52.6	5.6	89.5	11.5	3.8	62.0	85.3
W364	64-TR2	5.7	215.7	51.7	4.3	19.7	23.3	5.9	151.3	94.4	6.1	161.6	36.1
W364FF1	64-TR2	2.1	-236.0	10532.7									
W364FF2	64-TR2	2.6	-200.1	574.0									
W364FF3	64-TR2	5.5	-22.3	307.6									
W364FF4	64-TR2	5.3	22.6	11.5									
W364FF5	64-TR2	1.1	32.0	22.1									
W364FF6	64-TR2	5.9	276.5	427.3									
W364FF7	64-TR2	9.7	575.2	17.3									
W364FF8	64-TR2	1.6	719.9	186.5									
W3C64	64-TR2	3.5	296.2	207.8									
W3C64T	64-TR2	5.2	187.4	100.3									
W3PC64	64-TR2	6.3	121.6	35.4	0.9	405.6	44.6	7.2	112.8	36.3	4.3	155.8	24.6
CMXA	91-TB1	6.2	159.0	10.2	5.8	43.4	5.0	6.5	150.9	46.3	6.1	81.7	4.1
CMXB	91-TB1	6.8	239.4	26.2	6.9	36.2	26.9	6.8	263.9	90.0	6.6	145.1	11.9
CMXC	91-TB1	6.7	253.1	14.3	5.9	61.2	15.3	7.0	195.9	70.5	6.5	166.9	5.1
CMXD	91-TB1	6.7	328.5	14.8	3.8	83.9	7.7	7.7	281.1	65.3	6.3	205.1	14.9
CMXE	91-TB1	5.7	432.7	22.4									
CMXEC	91-TB1	9.6	144.7	33.2	2.7	197.2	65.8	13.1	27.0	23.3	6.0	175.5	37.2
CMXET	91-TB1	6.7	359.3	25.1									
MTEB	91-TB1	7.6	71.7	22.3	6.2	55.0	18.2	8.5	105.1	10.8	7.1	66.0	3.2
MTEC1	91-TB1	2.2	46.4	3.6	1.4	37.2	10.3	7.6	172.7	0.0	3.9	51.3	0.0
MTEC2	91-TB1	7.5	56.6	17.0	6.1	43.0	10.7	8.6	57.9	6.7	7.1	47.4	2.1
MTED	91-TB1	6.9	57.0	15.0	6.1	34.1	11.5	7.9	74.3	10.9	6.5	43.1	2.3
MTEE	91-TB1	7.1	163.9	49.3									
MTEELC	91-TB1	7.4	79.8	13.6	6.6	50.7	17.9	9.2	107.0	15.4	6.9	85.4	2.3
MTEESC	91-TB1	7.4	96.8	26.4	4.0	113.9	29.3	9.4	27.5	31.6	6.6	87.0	6.1
MTEET	91-TB1	7.3	100.9	23.9									
W3A	91-TB1	7.6	213.1	5.6	7.0	48.1	9.6	7.8	214.8	150.9	7.3	125.2	15.1
W3CD	91-TB1	6.1	236.9	7.2	5.1	50.9	6.7	6.3	182.5	61.2	6.1	214.2	32.4
W3E	91-TB1	5.0	416.8	28.0	2.0	47.0	14.0	7.3	342.2	127.9	4.2	346.8	77.0

Table A-17 con.

		Integrated Age			800-1200° C			< 800° C Plateau			> 1200° C Plateau		
		Cl/K	Age	±1s	Cl/K	Age	±1s	Cl/K	Age	±1s	Cl/K	Age	±1s
	Irradiatio		(Ma)	(Ma)		(Ma)	(Ma)		(Ma)	(Ma)		(Ma)	(Ma)
W3F	91-TB1	5.4	488.9	32.5									
W3FC	91-TB1	9.3	425.7	441.8	1.5	906.3	142.7	15.7	290.1	132.6	4.7	149.2	394.6
W3FT	91-TB1	6.2	475.6	118.2									
W3G	91-TB1	7.1	572.7	18.6	6.1	85.9	15.9	7.7	341.5	147.3	5.9	424.2	69.6